COMPLEXOS METÁLICOS NO TRATAMENTO DE INFECÇÕES DE *Toxoplasma gondii IN VITRO*

RENATA VASCONCELOS MOREIRA FREITAS

UNIVERSIDADE ESTADUAL DO NORTE FLUMINENSE
DARCY RIBEIRO - UENF
CAMPOS DOS GOYTACAZES - RJ
SETEMBRO - 2025

COMPLEXOS METÁLICOS NO TRATAMENTO DE INFECÇÕES DE *Toxoplasma gondii IN VITRO*

RENATA VASCONCELOS MOREIRA FREITAS

Tese apresentada ao Centro de Biociências e Biotecnologia da Universidade Estadual do Norte Fluminense Darcy Ribeiro, como parte das exigências para obtenção do título de Doutora em Biociências e Biotecnologia.

Orientador: Prof. Sergio Henrique Seabra

CAMPOS DOS GOYTACAZES - RJ
SETEMBRO - 2025

FICHA CATALOGRÁFICA
UENF - Bibliotecas
Elaborada com os dados fornecidos pela autora.

F866 Freitas, Renata Vasconcelos Moreira.

Complexos metálicos no tratamento de infecções de *Toxoplasma gondii in vitro* / Renata Vasconcelos Moreira Freitas. - Campos dos Goytacazes, RJ, 2025.

132 f. : il.
Inclui bibliografia.

Tese (Doutorado em Biociências e Biotecnologia) - Universidade Estadual do Norte Fluminense Darcy Ribeiro, Centro de Biociências e Biotecnologia, 2025.
Orientador: Sergio Henrique Seabra.

1. *Toxoplasma gondii*. 2. chemotherapy. 3. nickel(II) complex. 4. iron(III) complex. I. Universidade Estadual do Norte Fluminense Darcy Ribeiro. II. Título.

CDD - 570

COMPLEXOS METÁLICOS NO TRATAMENTO DE INFECÇÕES DE *Toxoplasma gondii IN VITRO*

RENATA VASCONCELOS MOREIRA FREITAS

Tese apresentada ao Centro de Biociências e Biotecnologia da Universidade Estadual do Norte Fluminense Darcy Ribeiro, como parte das exigências para obtenção do título de Doutora em Biociências e Biotecnologia.

Aprovada em 02 de setembro de 2025

Comissão examinadora:

gov.br Documento assinado digitalmente
ROSSIANE CLAUDIA VOMMARO
Data: 05/09/2025 09:46:34-0300
Verifique em https://validar.iti.gov.br

Profa. Dra. Rossiane Claudia Vommaro – UFRJ

Prof. Dr. Clóvis de Paula Santos – UENF

Prof. Dr. Milton Masahiko Kanashiro – UENF

Prof. Dr. Sergio Henrique Seabra (Orientador) – UENF

Aos meus filhos Luiza e Davi.

AGRADECIMENTOS

A Deus, pela vida e pelas pessoas e oportunidades que colocou no meu caminho para eu chegar até aqui.

À minha mãe, Rosane, pelo exemplo de amor e coragem. Por ter sido minha rede de apoio incondicional ao longo de toda a jornada acadêmica, me proporcionando segurança e tranquilidade ao cuidar dos meus maiores tesouros: Luiza e Davi.

Ao meu marido, Leonardo, por todo apoio e compreensão, por todo o cuidado e dedicação à nossa família.

À Simone Lessa, que me acompanhou ao longo dessa jornada e, no momento mais difícil, me ofereceu todo o suporte, sendo fundamental para que eu seguisse com confiança e resiliência.

Ao meu orientador, Prof. Sergio Henrique Seabra, por ter me acolhido após sete meses de doutorado. Obrigada por confiar em mim, pelos ensinamentos e por me orientar com leveza e humanidade. Seu otimismo é inspirador.

Ao Prof. Renato Augusto DaMatta, que, mesmo diante de tantas atribuições, se fez presente e participou de cada etapa, me apoiando e tornando possível essa conquista. Gratidão sempre.

A todos os colegas do Laboratório de Biologia Celular e Tecidual – LBCT, minha sincera gratidão pela convivência. Em especial, ao Felipe e ao Marcos Roberto, que me receberam com carinho e estiveram sempre dispostos a me ajudar, agradeço imensamente pelo conhecimento compartilhado. À Taymara, agradeço pela amizade e por tornar meus dias no laboratório mais leves. À Karla, Maike, Eliane, Lara e Amanda, sou grata pelas conversas, trocas e pelos momentos descontraídos.

Aos colaboradores que contribuíram de forma direta ou indireta para a realização deste trabalho, seja com apoio técnico, análises, discussões ou sugestões valiosas, registro aqui minha sincera gratidão.

Às técnicas do LBCT - Adriana, Beatriz e Giovana pela ajuda e disponibilidade.

À Universidade Estadual do Norte Fluminense Darcy Ribeiro – UENF pela oportunidade, pela estrutura oferecida e por fazer parte da minha história acadêmica.

O presente trabalho foi realizado com apoio da Coordenação de Aperfeiçoamento de Pessoal de Nível Superior – Brasil (CAPES) – Código de Financiamento 001. Agradeço à CAPES pelo apoio financeiro durante minha pesquisa de doutorado.

A todas as pessoas que participaram deste processo com amizade, conhecimento e bons pensamentos.

Segue o teu destino,
rega as tuas plantas,
ama as tuas rosas.
O resto é sombra
de árvores alheias.

Fernando Pessoa

RESUMO

A toxoplasmose, causada por *Toxoplasma gondii*, é uma infecção parasitária amplamente disseminada, com impactos significativos na saúde, especialmente em indivíduos imunocomprometidos e gestantes. Terapias atuais, como a associação de pirimetamina (PYR) e sulfadiazina (SDZ), apresentam eficácia limitada, efeitos adversos e contraindicações. Diante disso, a busca por terapias alternativas mais eficazes é urgente. Nos últimos anos, complexos metálicos foram testados pelo nosso grupo contra *T. gondii*, *Trypanosoma cruzi* e *Leishmania* spp. apresentando resultados bastante significativos. Neste trabalho foi avaliado o efeito *in vitro* de complexos metálicos $[Ni(BPAH)(H_2O)_2].2ClO_4$, $[Cu(HL1)Cl_2]$, $[Fe(HL1)Cl_3]$, $[Zn(HL1)Cl_2]$, $[Zn(HL1)(SDZ)Cl]\cdot 2H_2O$ em células hospedeiras LLC-MK2 infectadas com cepa RH de *T. gondii.* O complexo de níquel(II) inibiu a proliferação de taquizoítos com IC_{50} de 0,38 μM (24 h) e 0,36 μM (48 h), sem causar toxicidade significativa em células LLC-MK2 até 700 μM. Microscopia eletrônica de transmissão revelou alteração na membrana plasmática e deformação no conoide, comprometendo a capacidade de invasão celular. Após um screening comparativo dos complexos metálicos, o complexo de Fe(III) destacou-se como o mais promissor, resultando em baixa citotoxicidade para células hospedeiras. Por outro lado, inibiu significativamente o crescimento do parasito, com valores de IC_{50} de 12,4 nM e 56,0 nM após 24 h e 48 h de tratamento, respectivamente. O complexo apresentou efeito irreversível mesmo após a retirada do composto por 48 h. Células infectadas tratadas mostraram redução no número de parasitos, que apresentaram um formato arredondado. Análise ultraestrutural do parasito após o tratamento com o complexo revelou blebs na membrana plasmática, fendas no citoplasma e ruptura da membrana plasmática e do complexo membranar interno (IMC), confirmada por ensaio de imunofluorescência utilizando anticorpo anti-IMC1. Análises biofísicas por calorimetria diferencial de varredura e ressonância de spin eletrônico em vesículas multilamelares artificiais demonstraram que o complexo interrompe o empacotamento lipídico em membranas semelhantes às de parasitos, enquanto aumenta a ordenação lipídica em membranas semelhantes às de mamíferos. Os resultados apresentados destacam o potencial dos complexos de níquel(II) e de ferro(III) com eficácia semelhante ou superior à PYR e SDZ. No entanto, o complexo de ferro(III) destacou-se por sua elevada potência, seletividade e efeito irreversível, abrindo perspectivas para estudos *in vivo*.

Palavras - chave: *Toxoplasma gondii*, quimioterapia, complexo de níquel(II), complexo de ferro(III).

ABSTRACT

Toxoplasmosis, caused by *Toxoplasma gondii*, is a widespread parasitic infection with significant health impacts, especially in immunocompromised individuals and pregnant women. Current therapies, such as the combination of pyrimethamine (PYR) and sulfadiazine (SDZ), have limited efficacy, adverse effects, and contraindications. Therefore, the search for more effective alternative therapies is urgent. In recent years, our group has tested metal complexes against *T. gondii*, *Trypanosoma cruzi*, and *Leishmania* spp., yielding highly significant results. In this work, the *in vitro* effect of metal complexes [Ni(BPAH)(H2O)2].2ClO4, [Cu(HL1)Cl_2], [Fe(HL1)Cl_3], [Zn(HL1)Cl_2], [Zn(HL1)(SDZ)Cl]·2H_2O was evaluated in LLC-MK2 host cells infected with RH strain of *T. gondii*. The nickel(II) complex inhibited the proliferation of tachyzoites with an IC_{50} of 0.38 μM (24 h) and 0.36 μM (48 h), without causing significant toxicity in LLC-MK2 cells up to 700 μM. Transmission electron microscopy revealed alterations in the plasma membrane and deformation in the conoid, compromising the cell invasion capacity. After a comparative screening of the metal complexes, the iron(III) complex stood out as the most promising, resulting in low cytotoxicity to host cells. On the other hand, it significantly inhibited parasite growth, with IC_{50} values of 12.4 nM and 56.0 nM after 24 h and 48 h of treatment, respectively. The complex showed an irreversible effect even after withdrawal of the compound for 48 h. Treated infected cells showed a reduction in the number of parasites, which presented a rounded shape. Ultrastructural analysis of the parasite after treatment with the complex revealed blebs in the plasma membrane, clefts in the cytoplasm, and rupture of the plasma membrane and inner membrane complex (IMC), confirmed by immunofluorescence assay using anti-IMC1 antibody. Biophysical analyses using differential scanning calorimetry and electron spin resonance in artificial multilamellar vesicles demonstrated that the complex disrupts lipid packing in parasite-like membranes while enhancing lipid ordering in mammalian-like membranes. The results presented highlight the potential of nickel(II) and iron(III) complexes, with efficacy similar to or superior to PYR and SDZ. However, the iron(III) complex stood out for its high potency, selectivity, and irreversible effect, opening prospects for *in vivo* studies.

Keywords: *Toxoplasma gondii*, chemotherapy, nickel(II) complex, iron(III) complex.

SUMÁRIO

1. INTRODUÇÃO

1.1 *Toxoplasma gondii*

Toxoplasma gondii é um protozoário intracelular obrigatório, agente etiológico da toxoplasmose, uma zoonose caracterizada por alta prevalência global de indivíduos soropositivos (Bigna *et al.*, 2020). Esse parasito foi descoberto de forma independente e simultânea em 1908: por Nicolle e Manceaux, na Tunísia, em um roedor (*Ctenodactylus gundii*), e por Splendore, no Brasil, em coelho (*Oryctolagus cuniculus*) (Dubey, 2008).*T. gondii* pertence ao filo Apicomplexa, que estima-se conter milhares de espécies de parasitos intracelulares; algumas espécies têm importância médica e veterinária, incluindo *Plasmodium* spp., *Cryptosporidium* spp., agentes causadores da malária e de doenças gastrointestinais graves, respectivamente. Os apicomplexas são caracterizados pela presença de um complexo apical, composto por organelas secretoras especializadas e, em alguns casos, por elementos do citoesqueleto baseados em tubulina (Tell I Puig & Favre, 2024).

Ao longo de seu ciclo biológico, *T. gondii* apresenta três formas infectantes: taquizoítos, bradizoítos e esporozoítos. Taquizoítos (do grego *tachos* = rápido) representam o estágio em que o parasito se multiplica rapidamente nas células do hospedeiro, sendo característico da fase aguda da infecção. Bradizoítos (do grego *brady* = devagar) se replicam lentamente e estão presentes em cistos teciduais na fase crônica da infecção. Já os esporozoítos são as formas infectantes encontradas nos oocistos esporulados no ambiente, eliminados por felídeos (Dubey & Frenkel, 1973; Dubey *et al*., 1998).

O ciclo biológico de *T.gondii* envolve um hospedeiro definitivo, os felídeos, e hospedeiros intermediários, como aves e mamíferos. Nos felídeos, o ciclo inicia-se com a ingestão de oocistos provenientes da reprodução sexuada. Esses oocistos contêm esporozoítos, que são liberados no lúmen intestinal e invadem as células epiteliais, diferenciando-se em esquizontes. A infecção intestinal também pode ocorrer pela ingestão de cistos teciduais contendo bradizoítos, que, ao serem liberados, invadem as células epiteliais. Ao final do processo de esquizogonia, formam-se merozoítos, que rompem as células hospedeiras e infectam novas células. Parte desses merozoítos se diferencia em gametócitos — microgametas e macrogametas —, que se fundem originando o zigoto, que evolui para oocisto e é eliminado nas fezes. Após a eliminação, esses oocistos esporulam, formando dois esporocistos, cada um contendo quatro esporozoítos.

A reprodução assexuada ocorre quando os oocistos ou cistos teciduais liberam as formas infectantes — esporozoítos ou bradizoítos, respectivamente — que invadem as células epiteliais intestinais. Uma vez no interior do hospedeiro, diferenciam-se em taquizoítos, que se multiplicam por endodiogenia, atravessam tecidos e se disseminam pelo organismo. Com a resposta imunológica do hospedeiro, os taquizoítos convertem-se em bradizoítos, formando cistos teciduais. Este processo de conversão das formas taquizoítos para bradizoítos é extremamente importante na perpetuação da infecção, caracterizando a fase aguda e crônica da doença, respectivamente (Dubey & Frenkel, 1976; Ferguson, 2004) **(Figura 1)**.

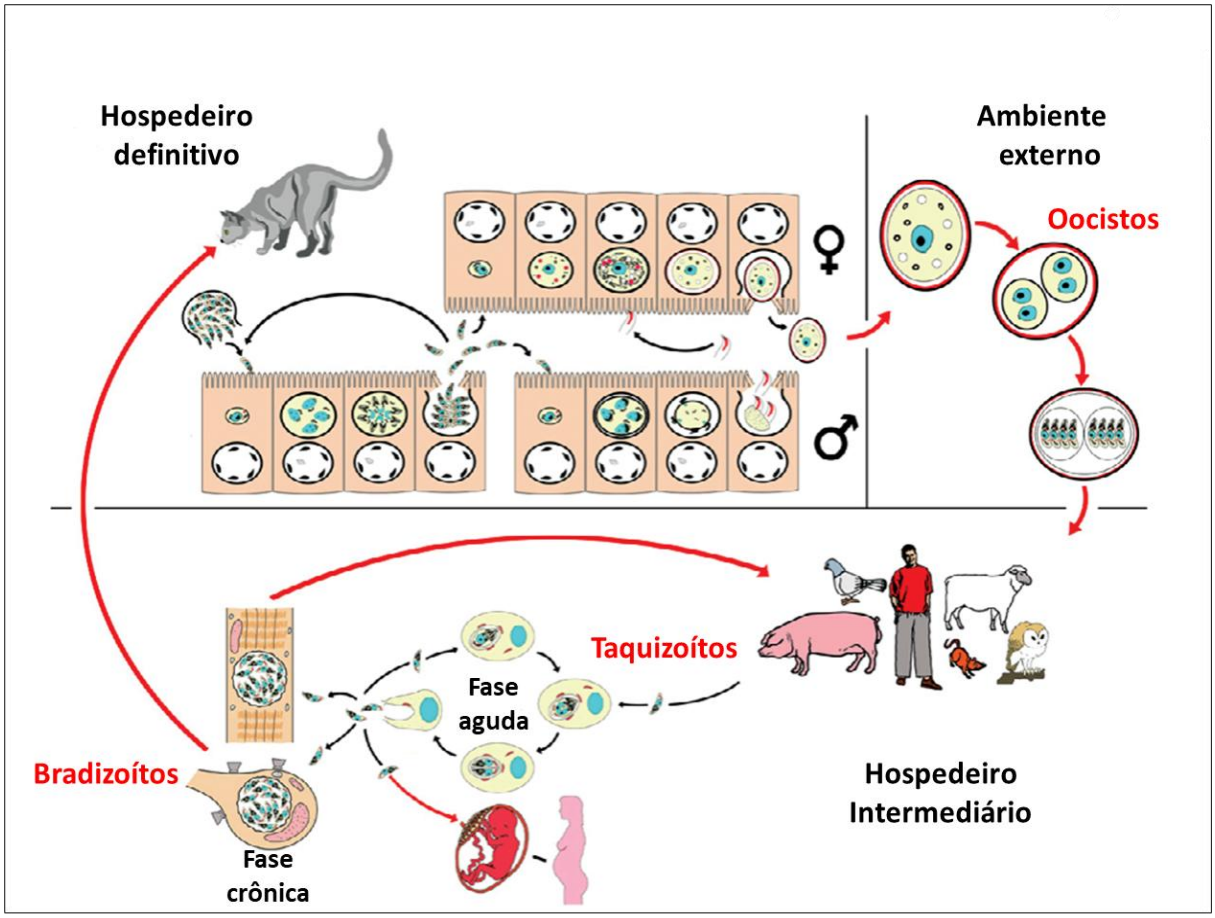

Figura 1. Ciclo biológico de *Toxoplasma gondii*. O gato atua como hospedeiro definitivo, onde ocorre a reprodução sexuada no intestino delgado, resultando na formação de oocistos eliminados pelas fezes. Após esporulação no ambiente, esses oocistos tornam-se infectantes para diversos hospedeiros intermediários, por meio da ingestão de água ou alimentos contaminados. Nos hospedeiros intermediários, o parasito multiplica-se assexuadamente, iniciando uma fase aguda seguida por uma fase crônica, caracterizada pela formação de cistos teciduais, principalmente no cérebro e nos músculos. Esses cistos podem transmitir a infecção a outros hospedeiros intermediários ou ao gato, por meio do carnivorismo. A infecção congênita pode ocorrer quando a fase aguda se desenvolve durante a gestação. Setas grossas indicam o deslocamento do parasito entre os hospedeiros; setas finas representam o desenvolvimento do parasito dentro dos hospedeiros. (Adaptado de Ferguson, 2009).

1.1.1 Taquizoítos

Todas as formas infectantes de *T. gondii* apresentam uma organização geral semelhante e são células altamente polarizadas, com formato alongado (Sanchez & Besteiro, 2021). Dentre elas, os taquizoítos destacam-se por serem formas infectivas de rápida proliferação, associadas à fase aguda da toxoplasmose. Medindo aproximadamente 6 μm de comprimento por 2 μm de largura, essas formas apresentam uma extremidade apical afilada e uma extremidade posterior arredondada, o que lhes confere um formato característico de meia-lua ou crescente (Dubey *et al*., 1998) **(Figura. 2)**.

Os taquizoítos são envoltos por uma estrutura trilaminar denominada película. Essa película é composta pela membrana plasmática e pelo complexo membranar interno (IMC) (Ouologuem & Roos, 2014). A composição lipídica da membrana de *T. gondii* revela uma diversidade de fosfolipídeos, com predominância de fosfatidilcolina (62%), seguida de fosfatidiletanolamina (11,2%) e fosfatidilserina (8,4%). Além disso, a presença de esfingomielina (8%) e fosfatidilinositol (6,6%) aponta para uma estrutura de membrana complexa e dinâmica (Gallois *et al*., 1988).

T. gondii apresenta um metabolismo lipídico endógeno altamente especializado, fundamental para sua sobrevivência, replicação e patogenicidade. Tal metabolismo pode ser classificado em três grandes vias: a síntese de ácidos graxos, o metabolismo de fosfolipídios e o metabolismo de lipídios neutros, constituindo uma complexa rede bioquímica que sustenta as estruturas celulares do parasito e sua adaptação ao ambiente intracelular (He *et al*., 2024). Na via de síntese de ácidos graxos, o parasito emprega três rotas distintas. A via FAS II, localizada no apicoplasto, é responsável pela síntese de ácidos graxos de cadeia curta, como o ácido mirístico (C14:0) e o ácido palmítico (C16:0), a partir de precursores derivados da glicólise, como o piruvato e o acetil-CoA. Posteriormente, esses ácidos graxos são elongados no retículo endoplasmático pela via de elongação (FAE), por meio das elongases ELO-A, ELO-B e ELO-C, gerando ácidos graxos de cadeia longa e muito longa (C18:1, C22:1, C26:1) (He *et al*., 2024). A terceira via, FAS I, ocorre no citoplasma e está envolvida tanto na síntese de C16:0 quanto na elongação de ácidos graxos, por meio de uma enzima multimodular. É relevante destacar que, ao contrário dos mamíferos, que dependem exclusivamente da via FAS I, *T. gondii* possui as três rotas, o que evidencia uma plasticidade metabólica superior (Amiar *et al*., 2020; Liu *et al*., 2021; Bisio *et al*., 2022). O metabolismo de fosfolipídios está estreitamente interligado à biossíntese de ácidos graxos. A enzima TgATS1 catalisa a ligação entre ácidos graxos e glicerol-3-fosfato, originando o ácido lisofosfatídico (LPA), precursor de diversos

fosfolipídios, como fosfatidilcolina (PC), fosfatidiletanolamina (PE), fosfatidilserina (PS) e fosfatidilinositol (PI) (Chen *et al*., 2023). Esses componentes são essenciais para a estrutura e funcionalidade das membranas, além de atuarem como mediadores em processos de sinalização intracelular, secreção e evasão imunológica (He *et al*., 2024).

No que se refere ao metabolismo de lipídios neutros, destaca-se a dependência de *T. gondii* da captação de colesterol das células hospedeiras, uma vez que o parasito não possui vias endógenas para sua síntese (Fraser *et al*., 2023). O colesterol é obtido do hospedeiro por meio de estruturas especializadas, como os túbulos de sequestro de organelas (HOST), e é internalizado e esterificado pelas enzimas ACAT1 e ACAT2, formando ésteres de colesterol que são armazenados em gotículas lipídicas (Nyonda *et al*., 2022). Estudos utilizando lipídios ou precursores marcados com radioisótopos e lipídios fluorescentes demonstraram que o parasito é capaz de importar ativamente lipídios do hospedeiro, direcionando-os às suas organelas, como a membrana plasmática e o sistema endomembranar (Shunmugam *et al.*, 2022). Inicialmente, esses estudos mostraram que o parasito pode importar ácidos graxos (AG), fosfolipídios (PLs) e colesterol. Esfingolipídios — essenciais para a replicação — constituem outra classe importante de lipídios adquiridos por meio de vesículas derivadas do complexo de Golgi do hospedeiro, apesar da existência de uma esfingomielina sintase não essencial em *T. gondii* (Romano *et al.*, 2013; Pratt *et al.*, 2013). Diversas enzimas envolvidas nessas vias metabólicas, como FabI (via FAS II), DGK e LIPIN (metabolismo de fosfolipídios), ACAT (esterificação de colesterol) e DGAT1 (formação de triglicerídeos), são específicas de *T. gondii* e não possuem homólogos funcionais diretos em células humanas. Isso as torna alvos particularmente atrativos para o desenvolvimento de novos fármacos com ação seletiva contra o parasito, minimizando a toxicidade ao hospedeiro (He *et al*., 2024). Além disso, pesquisas mais recentes destacam que o metabolismo lipídico de *T. gondii* é fundamental para a formação e manutenção de estruturas membranosas, como o IMC (Dass *et al*., 2024; Charital *et al*., 2024).

O IMC, componente essencial da película dos Apicomplexas, é formado por alvéolos, sacos de membrana achatados localizados sob a membrana plasmática. Esses alvéolos são sustentados na face citoplasmática por uma estrutura altamente organizada denominada rede subpelicular (SPN). A SPN é composta por dois principais elementos: os microtúbulos subpeliculares, formados por polímeros de tubulina, e uma matriz proteica associada, rica em proteínas alveolinas. Os microtúbulos percorrem longitudinalmente o corpo do parasito, conferindo forma e rigidez, enquanto as alveolinas desempenham papel estrutural semelhante

ao dos filamentos intermediários em células eucarióticas, garantindo resistência mecânica e integridade da arquitetura cortical (Gould *et al*., 2008; Tosetti *et al*., 2019).

Embora tanto a membrana plasmática quanto o IMC dos taquizoítos de *T. gondii* sejam constituídos por bicamadas lipídicas, estudos indicam diferenças marcantes em suas composições e funções. A membrana plasmática, em contato direto com o ambiente extracelular, é rica em fosfolipídios, além de conter proteínas envolvidas em transporte e sinalização. Em contraste, o IMC é formado por alvéolos justapostos à face citoplasmática da membrana plasmática e apresenta uma composição lipídica mais especializada. Estudos com sondas lipofílicas e abordagens proteo-lipídicas demonstram que o IMC possui menor fluidez e uma composição lipídica distinta da observada na membrana plasmática (Anderson-White *et al*., 2011; Harding *et al*., 2019). O IMC desempenha funções essenciais à biologia do parasito, incluindo a motilidade, o armazenamento de cálcio, a invasão da célula hospedeira e a replicação intracelular. Sua face externa atua como ponto de ancoragem para o motor actina-miosina, responsável pelo deslocamento e pela penetração do parasito nas células hospedeiras (Harding & Meissner, 2014). Além disso, o IMC funciona como arcabouço estrutural durante a formação das células-filhas no processo de reprodução assexuada. Em *T. gondii*, essa reprodução ocorre por endodiogenia, mecanismo no qual duas células-filhas se desenvolvem no interior de cada célula-mãe (Ouologuem & Roos, 2014). Dessa forma, o IMC se destaca não apenas por suas características estruturais e composicionais distintas da membrana plasmática, mas também por sua importância funcional nos diversos estágios do ciclo de vida do parasito.

Além da película, outro componente essencial na arquitetura celular dos taquizoítos é o complexo apical. O complexo apical compreende o conoide, uma estrutura citoesquelética formada por fibras dispostas em espiral, que se originam dos anéis pré-conoidais localizados na extremidade distal do complexo. Também fazem parte dessa estrutura o anel polar, do qual se originam 22 microtúbulos subpeliculares, e dois microtúbulos intraconoidais curtos (Hu *et al.*, 2006; Dos Santos *et al.*, 2020). O complexo apical está intimamente associado a dois tipos distintos de organelas secretoras apicais especializadas: os micronemas (Dubois & Soldati, 2019) e as róptrias (Sparvoli & Lebrun, 2021; Ben Chaabene *et al*., 2021) responsáveis pela secreção de fatores de virulência essenciais (Sanchez & Besteiro, 2021), assim como a adesão e penetração na célula hospedeira (Dubey *et al.,* 1998; Carruthers *et al.*, 1999). Além dessas, os grânulos densos constituem outro tipo de organela secretora especializada, que libera, em um momento posterior, fatores importantes para o estabelecimento intracelular do parasito (Mercier

& Cespron, 2015). Diferentemente das demais, essas vesículas não estão restritas à região apical (Heaslip *et al*., 2016) **(Figura 2)**.

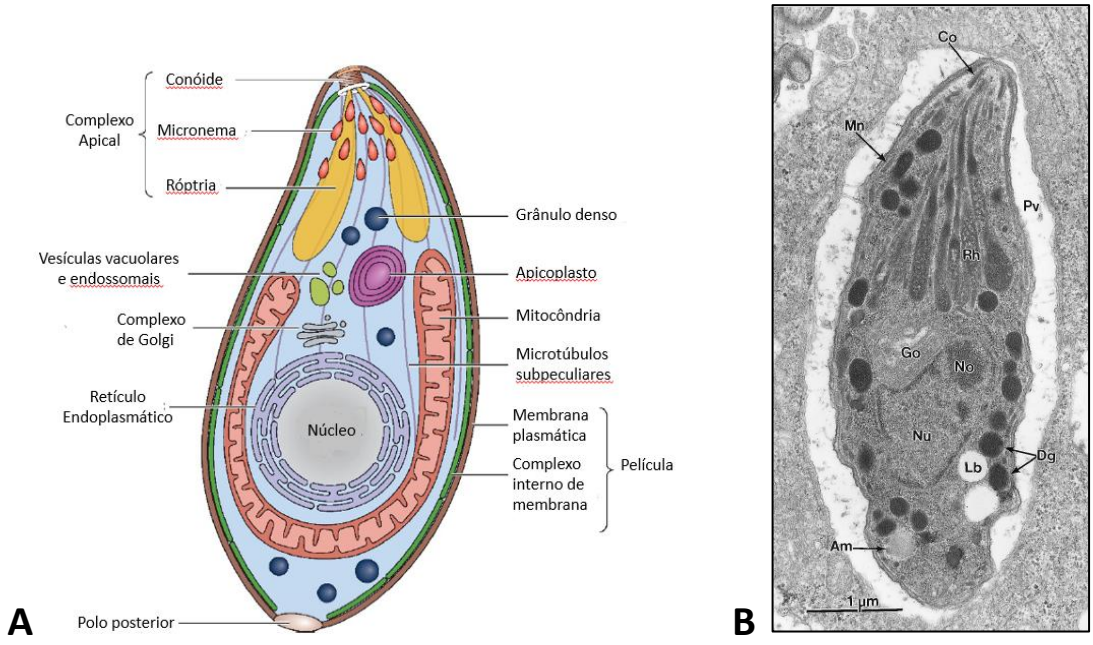

Figura 2. Representação esquemática da ultraestrutura do taquizoíto de *T.gondii* (A) (Adaptado de Sanchez & Besteiro, 2021). **(B)** Micrografia do taquizoíto por MET **Am**, grânulo de amilopectina; **Co**, conoide; **Dg**, grânulo eletrodenso; **Go**, complexo de Golgi; **Mn**, micronema; **No**, nucléolo; **Nu**, núcleo; **Pv**, vacúolo parasitóforo; **Rh**, róptria (Dubey *et al*, 1998).

Por se tratar de uma célula eucariótica, o parasito apresenta organelas comuns de células eucarióticas clássicas, como núcleo, retículo endoplasmático e complexo de Golgi. No entanto, também possui características originais. Por exemplo, taquizoítos de *T. gondii* possuem duas organelas de origem endossimbiótica: mitocôndria, geralmente presente como uma organela única que se ramifica por todo citoplasma (Melo *et al*., 2000), embora sua morfologia seja intrinsecamente dinâmica (Ovciarikova *et al*., 2017); e um plastídio não fotossintético denominado apicoplasto, derivado de um evento endossimbiótico secundário, o que justifica sua delimitação por quatro membranas (van Dooren & Striepen, 2013) **(Figura 2)**. Ambas as organelas exercem funções metabólicas essenciais para o parasito (Sheiner *et al*., 2013).

Taquizoítos apresentam ainda outras organelas, como o acidocalcissomo, envolvido na regulação de cálcio e outros íons, osmorregulação e na regulação do pH intracelular (Docampo *et al.*, 2011). Já os corpos lipídicos têm função na aquisição de lipídios da célula hospedeira pelo parasito (Charron & Sibley, 2002).

1.1.2 Mecanismos de invasão e desenvolvimento dos taquizoítos

T. gondii é capaz de invadir e estabelecer infecção em praticamente todas as células nucleadas. A eficiência no processo de invasão é essencial para sua sobrevivência e para a proliferação no interior da célula hospedeira, constituindo um fator determinante para o sucesso do parasito (Zhu *et al*., 2019).

O estágio inicial do processo de internalização tem início com a interação entre o pólo apical de *T. gondii* e a superfície da célula hospedeira **(Figura 3)**. A adesão e o reconhecimento entre as moléculas de superfície do parasito e da célula hospedeira ocorrem por meio de ligações de baixa afinidade com moléculas expostas na face externa da membrana do parasito, as quais estão ancoradas por glicosil-fosfatidil-inositol (GPI). Entre essas moléculas, destacam-se os SAGs (antígenos de superfície), que reconhecem uma ampla gama de receptores presentes em diferentes tipos celulares, como heparan sulfato, proteoglicanos e laminina (Haas e Plow, 1994; Ortega-Barria & Boothroyd, 1999; Carruthers *et al*., 2000; revisado por Carruthers & Boothroyd, 2007).

Micronemas são organelas em forma de bastonetes agrupadas no polo apical dos parasitos. Elas contêm uma grande variedade de proteínas (MICs), muitas das quais são importantes para o processo de invasão. Diversas MICs secretadas por taquizoítos extracelulares são adesinas, que podem se ligar a diferentes componentes da superfície da célula hospedeira, incluindo proteínas e carboidratos (Carruthers & Tomley, 2008). Essa ligação intermedia uma etapa inicial essencial de adesão do parasito à superfície da célula hospedeira e fornece um ponto de ancoragem para a motilidade deslizante, conhecida como *gliding*, crucial para o processo de invasão (Whitelaw *et al*., 2017). MICs também parecem desempenhar um papel importante no controle da exocitose das róptrias (Kessler *et al.*, 2008), que são organelas secretoras apicais que atuam em etapas subsequentes da invasão.

O *gliding* é considerado um mecanismo conservado do filo Apicomplexa (Heintzelman, 2006), sendo essencial para a migração do parasito através de tecidos, barreiras biológicas e principalmente para invasão e egresso do parasito das células hospedeiras (Sibley, 2010). Esse processo envolve a secreção e liberação de proteínas de superfície do parasito sobre o substrato (tecido ou células do hospedeiro) acopladas a um motor dependente de actina e miosina. Durante esse processo, o conoide se estende e retrai repetidamente ao longo da superfície da célula hospedeira, possibilitando sua movimentação. A projeção desta estrutura durante a motilidade ou a invasão é evidente em *T. gondii*, *Eimeria* e *Sarcocystis* – espécies de apicomplexas que iniciam a infecção através do intestino (Carey *et al*., 2004).

As róptrias são organelas em forma de clava, cujo conteúdo proteico está localizado em subcompartimentos distintos: a parte dilatada (bulbosa), que contém proteínas chamadas ROPs**,** envolvidas na subversão das funções da célula hospedeira; e o pescoço, que contém proteínas chamadas RONs, mais especificamente associadas ao processo de invasão da célula hospedeira (Ben Chaabene *et al*., 2021). Tanto as róptrias quanto os micronemas estão envolvidos na secreção de fatores que constituem a junção móvel (JM) **(Figura 3)**, uma estrutura formada por uma ligante MIC e um complexo de proteínas RON receptoras, secretadas pelo parasito na membrana plasmática da célula hospedeira, permitindo sua firme ancoragem antes da entrada (Besteiro *et al*., 2011). A JM também atua como uma barreira física, provavelmente restringindo a incorporação de proteínas da membrana plasmática da célula hospedeira à membrana do vacúolo parasitóforo (PVM) em formação durante a entrada do parasito (Mordue *et al*., 1999; Charron & Sibley, 2004). Essa incorporação seletiva de material da célula hospedeira é crucial para tornar o vacúolo parasitóforo (PV) não fusogênico com o sistema endolisossomal da célula hospedeira, impedindo, assim, a degradação do parasito pela acidificação lisossomal (Mordue *et al*., 1999).

Posteriormente, durante o processo de invasão ou já no interior da célula hospedeira, os parasitos secretam outros fatores que ajudam a modificar a célula hospedeira a fim de facilitar a replicação (Coppens & Romano, 2018). Esses fatores incluem proteínas ROPs e efetores dos grânulos densos (GRAs), que são secretados no espaço vacuolar ou além, como na PVM, no citosol ou até mesmo no núcleo da célula hospedeira (Rastogi *et al*., 2019). Alguns GRAs estão envolvidos na formação de uma rede de membranas intravacuolares (Sibley *et al*., 1995), já nos primeiros 10–20 minutos após a invasão, ou na criação de poros na PVM que funcionam como peneiras moleculares (Gold *et al*., 2015). Essas modificações são importantes para o crescimento intracelular dos parasitos, pois permitem a captação de nutrientes essenciais da célula hospedeira. *T. gondii* é auxotrófico para diversos metabólitos importantes, incluindo aminoácidos, precursores de nucleotídeos, cofatores essenciais e lipídios. Portanto, para sobreviver e garantir sua divisão, o parasito deve adquirir essas moléculas do hospedeiro (Blume & Seeber, 2018).

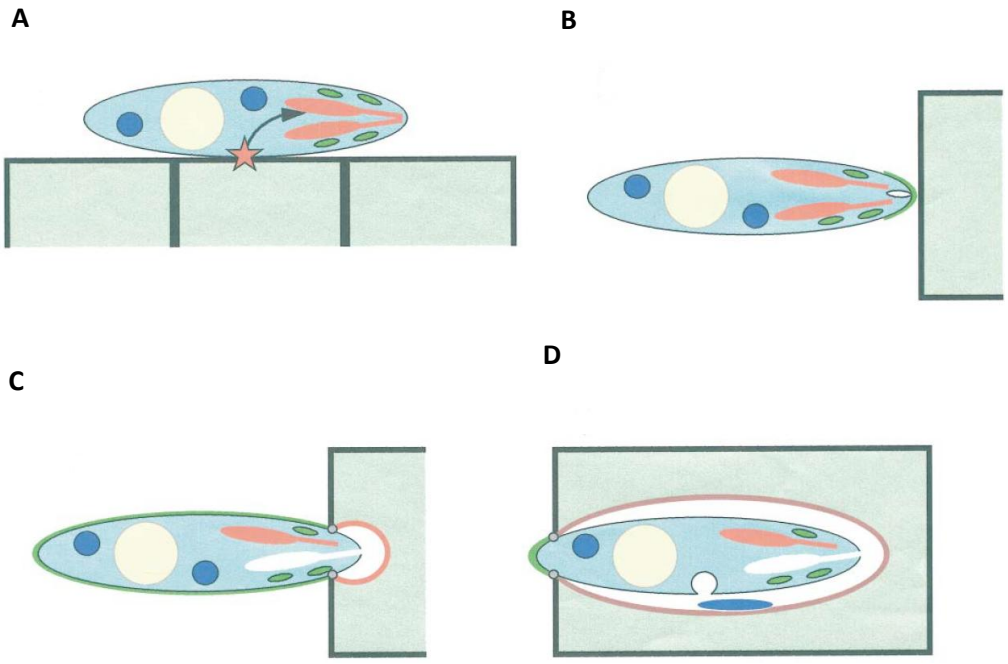

Figura 3. Desenho esquemático das etapas sucessivas da invasão de um Apicomplexa. (A) Um taquizoíto entra em contato com a superfície da célula hospedeira, um sinal é transduzido da superfície (estrela, seta) até o ápice **(B)** O sinal induz a reorientação, a exocitose de micronemas, a ligação apical à célula hospedeira e formação da junção móvel **(C)** As róptrias são exocitadas enquanto a junção móvel desliza para trás e o vacúolo parasitóforo começa a se expandir. O material das róptrias é integrado à membrana do vacúolo. O material liberado dos micronemas se expande na superfície do taquizoíto e é acumulado atrás da junção móvel **(D)** O vacúolo continua a se expandir obtendo a maior parte de seus lipídios da membrana plasmática da célula hospedeira. A junção atinge a extremidade posterior do parasito e eventualmente sela o vacúolo. Grânulos densos são exocitados no espaço vacuolar. (Adaptado de Dubremetz *et al.*, 1998).

Uma característica marcante que ocorre logo após a invasão é o recrutamento de organelas da célula hospedeira ao redor do PV que contém o parasito. Entre essas organelas recrutadas estão partes do retículo endoplasmático, mitocôndrias, corpos multivesiculares, vesículas de transporte, minipilhas do complexo de Golgi e gotículas lipídicas (Nolan *et al*., 2017), sendo que os GRAs desempenham um papel fundamental nesse processo. Por exemplo, a ancoragem das mitocôndrias da célula hospedeira à PVM é mediada por uma proteína GRA chamada MAF1 (fator de associação mitocondrial 1) (Pernas *et al*., 2014). O recrutamento de organelas hospedeiras pelo parasito pode ter diversos propósitos, como a captação de nutrientes e a neutralização de funções celulares prejudiciais. Curiosamente, assim como outras características relacionadas ao hospedeiro que são controladas pelos efetores GRA e ROP, a capacidade de recrutamento de organelas varia entre diferentes cepas (Pernas *et al*., 2014), o que pode explicar também diferenças cepa-específicas na patogênese.

Dentro do VP, taquizoítos se replicam assexuadamente por endodiogenia **(Figura 4)**. Nesse tipo particular de replicação, o brotamento das células-filhas e a replicação do DNA ocorrem de forma coordenada. Enquanto algumas organelas são sintetizadas de novo (como as róptrias e os micronemas), outras, como o apicoplasto e o complexo de Golgi, são duplicadas e segregadas para os brotos das células-filhas em um processo coordenado pelos centrossomos (Hu *et al*., 2002; Nishi *et al*., 2008). Após sucessivas rodadas de divisão (geralmente 5 ou 6, pelo menos *in vitro*) (Radke *et al*., 2001), taquizoítos, então, deixam ativamente o PV e a célula hospedeira (Moudy *et al*., 2001; Caldas *et al*., 2018).

Assim como a invasão, a saída (egresso) é altamente dependente da secreção de micronemas, a qual é regulada pela liberação de cálcio (Biosio & Soldati, 2019; Vella *et al*., 2021), que por sua vez depende de uma cascata de sinalização sensível à concentração local de ácido fosfatídico (Bisio *et al*., 2019; Jia *et al*., 2021). Entre os fatores dependentes de micronemas importantes para o egresso estão aqueles que controlam a motilidade do parasito (Frénal *et al*., 2017). Embora algumas linhagens adaptadas em laboratório apresentem certa sobrevivência de curto prazo (algumas horas) no ambiente extracelular, uma vez que egridem, os taquizoítos extracelulares precisam invadir uma nova célula hospedeira para sobreviver e iniciar um novo ciclo lítico.

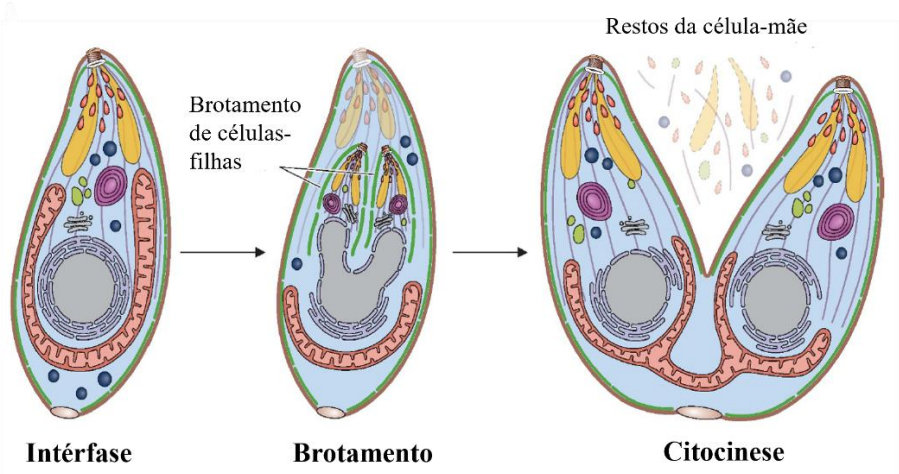

Figura 4. Representação esquemática da endodiogenia. Esse processo envolve a montagem coordenada e o brotamento interno de duas células-filhas dentro de uma célula-mãe (Adaptado de Sanchez & Besteiro, 2021).

1.1.3 Diferentes cepas de *Toxoplasma gondii*

A maioria das cepas de *T. gondii* isoladas na Europa e América do Norte pertence a um dos três genótipos clássicos: tipos I, II e III. Esses genótipos ocorrem tanto em humanos quanto

em animais e são classificados de acordo com a virulência e a ocorrência epidemiológica (Sibley & Boothroyd, 1992; Howe & Sibley, 1995). As ROPs, liberadas da organela apical secretória do parasito, as róptrias, são determinantes para a virulência das cepas de *T. gondii* em camundongos (Saeij *et al*., 2006; Taylor *et al*., 2006).

As cepas RH e GT-1 são exemplos do tipo I, altamente virulentas, com dose letal de 100% (LD_{100}) em camundongos mesmo com inóculos muito baixos, de até um único parasito (Saeij *et al*., 2005). As cepas do tipo I, conhecidas por sua virulência aguda, expressam altos níveis de ROP18. Nesses parasitos, a ROP18 atua de forma cooperativa com a principal variante da pseudocinase ROP5 do tipo I, promovendo a fosforilação das IRGs (*Immunity-Related GTPases*) do hospedeiro. Essa ação inibe o recrutamento dessas proteínas na PVM, bloqueando, assim, a eliminação do parasito em células ativadas por IFN-γ (Hunter & Sibley, 2012).

Essa elevada virulência pode aumentar o risco de transmissão transplacentária e agravar a infecção fetal (Howe & Sibley, 1995). Já a cepa ME49 representa o tipo II, enquanto a cepa VEG é um exemplo do tipo III; ambas são menos virulentas, apresentando LD_{50} com inóculos a partir de 1×10^5 parasitos (Saeij *et al*., 2005; Sibley & Boothroyd, 1992).

Os tipos I e III são comuns em todo o mundo, enquanto o tipo II predomina na Europa Ocidental e nos Estados Unidos da América. Diferentemente das cepas norte-americanas e europeias, as cepas de *T. gondii* encontradas na América do Sul apresentam grande diversidade genética, indicando uma frequência mais elevada de recombinação. Essa diversidade tem levado à identificação de cepas com maior potencial patogênico, em que diversos casos de toxoplasmose grave foram relatados em pacientes imunocompetentes. Essas cepas não arquetípicas parecem não estar bem adaptadas ao hospedeiro humano, o que pode explicar a maior gravidade da infecção (Gilbert *et al.*, 2008).

Novos genótipos vêm sendo classificados como atípicos, exóticos, recombinantes ou não arquetípicos, com base na composição alélica (Ajzenberg *et al.*, 2004; Grigg *et al.,* 2001). Considera-se uma cepa atípica quando ela apresenta ao menos um alelo não característico entre os 11 marcadores genotípicos. Já cepas com perfis mistos, contendo alelos dos tipos I, II ou III em diferentes marcadores, são denominadas recombinantes (Brito *et al.*, 2023). No Brasil, os genótipos BrI (ToxoDB #6), BrII (#11), BrIII (#8) e BrIV (#17) são amplamente distribuídos e mais prevalentes em animais de áreas urbanas, como São Paulo, Rio de Janeiro e Belo Horizonte, e possivelmente também entre humanos nessas regiões, conforme indicado por estudo em casos de toxoplasmose congênita (Silva *et al.*, 2014). No entanto, dada a dimensão territorial do país e sua elevada diversidade ecológica, é possível que populações de outras

regiões, como Amazônia, Nordeste e Sul, apresentem perfis genotípicos bastante distintos. A grande variedade de hospedeiros presentes no país é um dos fatores que contribuem para essa diversidade genética (Gilbert *et al.*, 2008).

1.2 Toxoplasmose

1.2.1 Transmissão

A toxoplasmose é uma antropozoonose de amplo espectro que afeta cerca de um terço da população mundial (Ybañes *et al*., 2020). A infecção pelo *T. gondii* pode ocorrer tanto em hospedeiros definitivos quanto intermediários por meio de duas vias principais: transmissão horizontal, através da ingestão de oocistos presentes no ambiente contaminado (solo, água ou alimentos crus), ou pela ingestão de cistos teciduais encontrados em carnes cruas ou malcozidas de hospedeiros intermediários (Dubey & Thulliez,1993; Dubey *et al*., 1998).

Outra forma relevante de transmissão é a vertical, ou congênita, na qual taquizoítos atravessam a placenta e infectam o feto. Isso ocorre, principalmente, como consequência de uma infecção aguda da mãe durante a gestação (Jones *et al*., 2001). Em mulheres com toxoplasmose crônica, a transmissão transplacentária também pode ocorrer, especialmente em casos de imunossupressão que levam à reativação da fase aguda da doença (Wong e Remington, 1994). A infecção transplacentária ocorre em aproximadamente 30% dos casos quando a mulher adquire a infecção primária durante a gravidez. O risco de transmissão para o feto varia conforme o estágio gestacional: é menor logo após a concepção (<1%) e aumenta progressivamente, podendo atingir quase 90% se a infecção materna ocorrer próximo ao parto (Ribeiro *et al.*, 2025).

Casos menos frequentes de transmissão envolvem transplantes de órgãos, transfusões sanguíneas e acidentes laboratoriais (Jones & Dubey, 2014). Apesar de *T. gondii* já ter sido isolado do sangue periférico de pacientes com sintomas agudos, a transmissão por transfusão sanguínea é considerada rara. Outras formas de infecção incluem o contato direto com fezes de gatos infectados — como durante a limpeza de suas caixas de areia — e, ainda que pouco comum, a exposição ocupacional em ambientes laboratoriais, por meio de acidentes com agulhas ou manipulação de materiais contaminados. Além disso, há relatos de transmissão de taquizoítos pelo leite materno (Camossi *et al*., 2011).

1.2.2 Epidemiologia

Estudos epidemiológicos demonstram que a infecção causada por *T. gondii* é amplamente difundida (Maenz *et al*., 2014). Apesar de ter distribuição mundial, a soroprevalência de *T. gondii* na população humana pode variar de acordo com diferentes regiões geográficas. Soroprevalência de aproximadamente 30% foi observada na América do Norte, Europa, Ásia e mais de 60% no continente africano, uma maior soroprevalência também foi observada em países da América Latina em relação aos EUA e Canadá, com alguns mostrando mais de 50% de infecção (Bigna *et al*., 2020). Essas flutuações resultam de diferentes práticas culturais, condições ambientais ou status socioeconômico da população (Molan *et al*., 2019). Embora fatores socioeconômicos influenciem a prevalência da toxoplasmose, a infecção congênita pode afetar todos os grupos demográficos, tornando-se uma preocupação universal na saúde materna (Montoya & Remington, 2008). Ao contrário dos países do Hemisfério Norte, na América do Sul, *T. gondii* apresenta uma estrutura populacional geneticamente diversificada, com maior gravidade da doença, indicando que a infecção tende a ser mais alta em áreas com climas quentes, úmidos e altitudes mais baixas, onde os oocistos sobrevivem melhor (Gilbert *et al*., 2008; Robert-Gangneux & Dardé, 2012).

No Brasil, a notificação de surtos e a investigação epidemiológica são atividades obrigatórias da vigilância em saúde (Reingold, 1998). Desde 1967, quando o primeiro surto de toxoplasmose foi registrado em Bragança Paulista, São Paulo, mais de 35 surtos foram registrados globalmente, com a maioria desses casos ocorrendo no Brasil (da Costa *et al*., 2020; Pinto-Ferreira *et al*, 2019). As principais vias de transmissão identificadas foram a água (de Moura *et al*., 2006), vegetais, frutas, carnes malcozidas (Masur *et al*., 1978), carnes cruas (Pomares, 2011) e leite de cabra não pasteurizado (Chiari & Neves, 1984). O maior surto de toxoplasmose já registrado no mundo ocorreu em 2018, em Santa Maria, Rio Grande do Sul, afetando mais de 900 pessoas, com a água como principal suspeita de via de transmissão (Arquilla *et al*., 2019). Este evento superou o surto de 2001-2002 em Santa Isabel do Ivaí, Paraná, onde foram registrados 426 casos, com *T. gondii* isolado na rede de abastecimento de água (de Moura *et al*., 2006). Em Campos dos Goytacazes, no estado do Rio de Janeiro, a prevalência sorológica de *T. gondii* atingiu 84%, um valor alto, devido à contaminação por oocistos na água de reservatórios (Bahia-Oliveira *et al*., 2003).

Segundo Salari *et al*. (2025), a soroprevalência global de *T. gondii* em mulheres grávidas foi de 36,6%, sendo mais alta na América do Sul, 52,8% e na África, 46,8%. A menor prevalência foi observada na América do Norte 19,7% e na Europa 24,6% . O estudo também

destacou que a soroprevalência entre mulheres grávidas varia conforme fatores como idade, estilo de vida e nível de conscientização sobre a toxoplasmose. Por isso, programas de conscientização pública e de saúde são essenciais para prevenir e diagnosticar precocemente a doença.

No Brasil, um estudo epidemiológico utilizando dados do Sistema de Informações de Agravos de Notificações (DATASUS) analisou a incidência de toxoplasmose congênita entre 2019 e 2022. Durante o período, foram notificados 40.732 novos casos, representando um aumento de 43,66% na frequência de casos. Em 2019, foram registrados 8.436 casos (20,71%), em 2020, 9.126 casos (22,40%), em 2021, 11.050 casos (27,12%) e em 2022, 12.120 casos (29,75%). A maior incidência absoluta ocorreu na região Sudeste (12.800 casos, 31,42%), seguida pelo Nordeste (11.561 casos, 28,38%). Esses dados são cruciais para estratégias de vigilância epidemiológica, especialmente no Sudeste, onde, apesar da maior riqueza, ainda são necessárias ações de saúde pública para ampliar os recursos das equipes de saúde e garantir a detecção precoce da doença. A possibilidade de subnotificação também deve ser considerada, já que os dados dependem da notificação durante o pré-natal e pós-parto (Prata *et al.*, 2023). A infecção primária por *T. gondii* em mulheres grávidas pode resultar em: aborto espontâneo, natimorto, hidropisia fetal não imune, parto prematuro, restrição de crescimento intrauterino, lesões permanentes no sistema nervoso e na visão, e ainda morte fetal pós-parto (Milewska-Bobula *et al*., 2015).

Embora a infecção por *T. gondii* geralmente seja assintomática em indivíduos imunocompetentes, ela pode causar sintomas inespecíficos, como febre, linfadenopatia e doença ocular, principalmente uveíte posterior. Em casos raros, a toxoplasmose pode evoluir para miocardite, hepatite e doença disseminada em um pequeno número de pessoas imunocompetentes (Layton *et al*., 2023).

Entretanto, a infecção primária ou a reativação de *T. gondii* em pacientes com imunossupressão profunda pode ser fatal. Esse grupo inclui indivíduos com HIV/AIDS, transplantados de órgãos sólidos (SOT), transplantados de células-tronco hematopoéticas (HSCT) e pacientes em tratamento quimioterápico, que podem desenvolver toxoplasmose tanto por infecção primária, por meio da ingestão de alimentos contaminados, quanto por transplante de órgãos contendo cistos latentes (Robert-Gangneux *et al*., 2018). Em pacientes com HIV/AIDS, os fatores de risco para toxoplasmose são semelhantes aos da população geral; contudo, o risco de infecção oportunista, especialmente toxoplasmose cerebral, é aumentado

devido à reativação do parasito latente, particularmente quando a contagem de linfócitos CD4 cai abaixo de 100 células/μL (Vidal, 2019).

Pacientes submetidos a transplante de órgãos sólidos ou de células-tronco hematopoéticas podem apresentar manifestações graves, como doenças do sistema nervoso central, coriorretinite e infecção disseminada, tanto em casos de infecção primária quanto de reativação (Aguirre *et al*., 2019; Elsheikha *et al*., 2020; Rauwolf *et al*., 2021). Estudos indicam que a soroprevalência de toxoplasmose em pacientes com HSCT é variável e pode atingir até 70%, sendo comparável à de indivíduos saudáveis da mesma faixa etária no mesmo país (Gangneux *et al*., 2018; Rauwolf *et al*., 2021). Nesses casos, a realização de rastreamento sorológico para imunoglobulina G ou o uso da reação em cadeia da polimerase (PCR) para detecção de *T. gondii* são estratégias importantes para avaliar infecções prévias e orientar decisões quanto à profilaxia. Com isso, a ausência de profilaxia adequada, associada à imunossupressão profunda, pode resultar em desfechos desfavoráveis (Aerts *et al*., 2024).

1.2.3 Tratamento

A quimioterapia anti-toxoplasmose consiste em diversos medicamentos que podem ser utilizados individualmente ou em combinação. O tratamento convencional utiliza uma combinação de pirimetamina (PYR) e sulfadiazina (SDZ) (Konstantinovic *et al*., 2019; Cerutti *et al*., 2020). No entanto, estudos recentes descreveram muitas desvantagens relacionadas a esses medicamentos, como intolerância, má absorção, toxicidade, hipersensibilidade, resposta alérgica, supressão da medula óssea, teratogenicidade e desenvolvimento de resistência, especialmente durante o uso prolongado. Ambas as drogas podem controlar a toxoplasmose na fase aguda, mas não apresentam bom comportamento sinérgico para pacientes crônicos, pois os cistos não são eliminados (Silva *et al*., 2019).

A PYR é um antagonista do ácido fólico, pois inibe a enzima dihidrofolato redutase (DHFR), bloqueando a síntese de purinas e pirimidinas, essenciais para a síntese de DNA e multiplicação celular. A ação dessa droga é potencializada quando utilizada em conjunto a SDZ, que é capaz de interferir na síntese de ácido fólico de *T. gondii*, inibindo competitivamente a enzima dihidropteroato sintetase (DHPS) (Montoya & Remington, 2008; Dunay *et al*., 2018). Para reduzir os efeitos colaterais, administra-se PYR/SDZ com ácido folínico, leucovorina (LV), que é um metabólito ativo do ácido fólico e uma coenzima essencial para a síntese de ácidos nucleicos (Dunay *et al*., 2018). Apesar disso, os efeitos adversos podem permanecer, incluindo neutropenia, trombocitopenia, leucopenia, e potencial teratogênico. Casos raros de agranulocitose, necrólise epidérmica tóxica e necrose hepática também podem se manifestar

(Ardabili *et al*., 2021; Shamma *et al*., 2021).

Esses efeitos adversos consideráveis e a terapia de longo prazo contribuem para as altas taxas de abandono do tratamento (Deng *et al*., 2019).

Em casos de intolerância à SDZ, a substituição desta por clindamicina (CLI) é recomendada, pois a combinação PYR - CLI é tão efetiva quanto à PYR - SDZ durante a fase aguda da doença (Katlama *et al*., 1996). Em gestantes com suspeita de toxoplasmose, a espiramicina (SPI) é administrada profilaticamente (Konstantinovic *et al*., 2019). A SPI é um antibiótico macrolídeo que atua inibindo a síntese proteica em micro-organismos. Este fármaco apresenta passagem limitada pela barreira placentária. No entanto, sua ação contra o parasito é considerada menos eficaz e o uso em doses elevadas (35 mg/kg) pode provocar vasoespasmo, calafrios, vertigem, hiperemia facial, náuseas, vômitos, diarreia, anorexia e arritmias cardíacas (Stramba-Badiale *et al*., 1997). Além disso, quando o diagnóstico confirma a infecção do feto ou neonato, o tratamento com SPI deve ser interrompido e substituído pelo tratamento convencional PYR/SDZ/LV (Paquet *et al*., 2018).

Pacientes imunocomprometidos requerem terapia de manutenção de longo prazo após o tratamento inicial de 6 semanas, uma vez que os cistos teciduais não são eliminados por nenhum dos tratamentos atuais (Smith *et al*., 2021). Nesses pacientes, a encefalite toxoplasmática é a principal manifestação clínica e leva à fatalidade se não tratada (Luft & Remington, 1992). O tratamento de indução com PYR/SDZ resultou em taxas de resposta de 80%. No entanto, efeitos adversos graves foram encontrados, variando de febre a erupções cutâneas e complicações hematológicas (leucopenia e trombocitopenia). Assim, a leucovorina foi usada para amenizar esses efeitos colaterais (Porter & Sande, 1992). A terapia antirretroviral aumentou a sobrevida e diminuiu a mortalidade e as taxas de recaída em pacientes com HIV e infecções oportunistas, incluindo reativação da toxoplasmose (Hajj *et al*., 2021).

Em pacientes transplantados, a toxoplasmose disseminada ocorre com frequência (Gangneux & Dardé, 2012; Rajapakse *et al*., 2017). Portanto, recomenda-se a profilaxia ou mesmo o início do tratamento nos casos suspeitos, antes da confirmação do diagnóstico. Em um estudo foi demonstrado que a combinação de PYR/SDZ melhorou marginalmente a sobrevida no transplante de células-tronco hematopoéticas (Mele *et al*., 2002).

Em pacientes imunocompetentes, a toxoplasmose aguda geralmente é assintomática. Portanto, não requer nenhuma intervenção terapêutica. No entanto, foi relatado em pacientes imunocompetentes de certas áreas, incluindo a América do Sul, que cepas atípicas causaram complicações graves com envolvimento multivisceral e resultado potencialmente fatal (Demar

et al., 2012). Estes pacientes sintomáticos, que apresentaram sintomas graves após contato ocular, mesmo que raro, ou ainda após uma infecção adquirida no laboratório, são tratados com PYR/SDZ/LV (revisto em Dunay *et al*., 2018).

As modalidades de tratamento mencionadas acima poupam a toxoplasmose crônica e visam apenas à forma aguda da infecção (Montazeri *et al*., 2018). A reativação de cistos teciduais, que são a marca registrada da toxoplasmose crônica, ocorre quando a imunidade do hospedeiro é suprimida (Matta *et al*., 2021). Assim, as estratégias terapêuticas para esta parasitose variam de acordo com o estado da doença e o sistema imunológico do hospedeiro (Hajj *et al*., 2021).

Além das limitações clínicas, como toxicidade, intolerância e baixa eficácia frente à forma crônica da doença, estudos *in vitro* têm demonstrado uma grande variabilidade nos valores de IC_{50} (concentração inibitória do crescimento do parasito em 50%) para fármacos clássicos, como SDZ e PYR. A SDZ apresenta um IC_{50} altamente variável dependendo da célula hospedeira (Portes *et al*., 2015). Por exemplo, para a cepa RH de *T. gondii* na forma de taquizoíto, os valores relatados variam de 7.00 mM em células HeLa após 24 h de tratamento (Jin *et al.,* 2009), 0.30 mM em células Vero após 72 h de tratamento (Doliwa *et al*., 2013), e 2.60 mM em células HEp2 após 90 h de tratamento (van der Ven *et al.,* 1996).

Em estudos mais recentes, Huffman *et al*. (2022) investigaram a ação da SDZ em células hTERT tratadas por 24 e 48 h, observando valores de IC_{50} entre 1.28 e 1.55 μM. Węglińska *et al*. (2022), por sua vez, utilizaram células Hs27 nas mesmas condições de tratamento e relataram IC_{50} de 3.3 μM. Em contraste, Trotsko *et al*. (2019), também com células Hs27 após 24 h de tratamento, identificaram um valor muito inferior, de 0.512 μM.

Com relação à PYR, uma tendência similar de variabilidade é observada. Qiu *et al*. (2025) avaliaram a eficácia da PYR em células Hs27 tratadas por períodos entre 24 e 72 h, encontrando valores de IC_{50} entre 2.42 e 3.59 μM. Huffman *et al*. (2022), utilizando células hTERT tratadas por 24 a 48 h, observaram IC_{50} entre 3.18 e 3.52 μM. Novamente, Trotsko *et al*. (2019) relataram um valor inferior, de 0.326 μM, em células Hs27 após 24 h de tratamento. Essas diferenças enfatizam a variabilidade na suscetibilidade do *T. gondii* a medicamentos padrão e destacam a necessidade de explorar novos agentes terapêuticos com potência e seletividade aprimoradas.

Por fim, as opções quimioterápicas atuais para toxoplasmose são limitadas (Dunay *et al*., 2018), a longa duração do tratamento e a incapacidade de eliminar a infecção, combinados

com a frequência dos efeitos colaterais, tornam esses quimioterápicos não ideais para o tratamento da toxoplasmose (Smith *et al*., 2021). Não obstante, tem sido feito um esforço na última década com estratégias de triagem de alto rendimento, a fim de descobrir novos compostos químicos, incluindo naturais, com atividade anti-*Toxoplasma* ou reaproveitar/melhorar medicamentos existentes e aprovados (Deng *et al*., 2019). A partir disso, um composto anti-*Toxoplasma* ideal teria as seguintes propriedades: menor toxicidade em comparação com medicamentos existentes; seguro para uso durante a gravidez; eficácia aprimorada em comparação com medicamentos existentes; capacidade de atingir os taquizoítos tratando infecções agudas; capacidade atingir bradizoítos eliminando cistos teciduais e a capacidade de atingir concentrações suficientes no Sistema Nervoso Central para eliminar parasitos no cérebro e nos olhos (Smith *et al*., 2021).

Novas pesquisas sobre os impactos da toxoplasmose destacam a necessidade de aumentar a conscientização institucional sobre as vias de infecção e implementar ações abrangentes e interdisciplinares para controlar a transmissão e otimizar o tratamento (dos Santos *et al*., 2023).

A **Tabela 1** mostra os principais medicamentos utilizados no tratamento da toxoplasmose com seus respectivos mecanismos de ação e efeitos colaterais. Logo abaixo, na **Tabela 2** temos as doses e o tempo utilizado durante o tratamento:

Tabela 1- Principais medicamentos utilizados no tratamento da toxoplasmose.

Drogas	Mecanismo de Ação	Efeitos Colaterais	Referências
Pirimetamina	Inibe a diidrofolato redutase, bloqueando a síntese de ácido fólico necessária para a replicação do DNA do parasito.	Supressão da medula óssea (anemia, leucopenia), náuseas, vômitos, hepatotoxicidade. Necessita de suplementação com ácido folínico.	Montoya & Liesenfeld, 2004
Sulfadiazina	Inibe a diidropteroato sintase, interferindo na síntese de ácido fólico do parasito.	Náuseas, vômitos, reações alérgicas, leucopenia, anemia aplástica.	Montoya & Liesenfeld, 2004
Espiramicina	Inibe a síntese proteica ao se ligar à subunidade 50S do ribossomo.	Náuseas, diarreia, reações alérgicas leves.	Robert-Gangneux & Dardé, 2012
Clindamicina	Inibe a síntese proteica ao se ligar à subunidade 50S do ribossomo, bloqueando a replicação.	Diarreia, colite pseudomembranosa, náuseas, erupções cutâneas.	McAuley, 2014
Trimetoprima-Sulfametoxazol	Inibe sequencialmente enzimas da via do ácido fólico (dihidrofolato redutase e diidropteroato sintase).	Náuseas, vômitos, supressão da medula óssea, reações de hipersensibilidade, erupções cutâneas.	Hill & Dubey, 2002

Tabela 2- Doses utilizadas e tempo de tratamento em pacientes imunocompetentes, imunocomprometidos, gestantes e recém-nascidos (Adaptado de Dunay *et al*., 2018).

Nos 3 primeiros dias		Do 4º dia em diante	Tempo
Pacientes imunocompetentes			
Pirimetamina	100 mg	25-50 mg /dia	4 a 6 semanas
Sulfadiazina	1 g	1g 4x ao dia	
Ácido folínico	10-20 mg	10-20 mg /dia	
Pacientes imunocomprometidos			
Pirimetamina	200 mg	75 mg / dia	6 semanas
Sulfadiazina	1,5 g	1 g 4x ao dia	
Ácido folínico	10-50 mg	10-25 mg / dia	
Gestantes			
Espiramicina 1g a cada 8h. Até o final da gestação, ou até confirmação da infecção fetal			
Recém-nascidos			
Pirimetamina	1mg/kg/dia	1 mg/ kg a cada 2 dias	1 ano
Sulfadiazina		50 mg/kg 2x ao dia	
Ácido folínico		10 mg 3x na semana	

1.3 Complexos metálicos

Atualmente, os metais têm sido amplamente utilizados no tratamento de diversas doenças, abrindo novas perspectivas terapêuticas (Carver, 2019). Um dos exemplos mais clássicos é a utilização de metalofármacos como agentes anticancerígenos eficazes. Dentre eles, destaca-se a cisplatina, atualmente o quimioterápico mais utilizado no tratamento de 18 tipos de câncer, incluindo carcinomas testiculares e ovarianos, linfoma, melanoma e neuroblastoma. A atividade desse fármaco e seus derivados como carboplatina, oxaliplatina, foi historicamente atribuída à danos no DNA, interferindo na transcrição e levando à apoptose celular (Dasari & Tchounwou, 2014; Lalita Chopra *et al.*, 2023).

De maneira semelhante, fármacos à base de metais têm sido investigados para outras aplicações terapêuticas, incluindo doenças infecciosas, virais e neurológicas. Nessas condições, os íons metálicos podem inibir enzimas ou modular vias biológicas específicas (Cardoso *et al*, 2025). Uma nova abordagem vem sendo utilizada, em que medicamentos antidiabéticos, como insulina, dapagliflozina, entre outros, apresentam melhor farmacodinâmica como complexos metálicos do que medicamentos isolados e têm sido escolhidos farmacologicamente para atuarem como ligantes. Dessa forma, os metalofármacos podem representar avanços

significativos não apenas no tratamento do diabetes, mas também na farmacoterapia de diversas doenças e distúrbios. (Venkatasubramaniam & Rajappa, 2025).

Estudos têm mostrado que a coordenação de fármacos a íons metálicos resulta em complexos mais ativos e eficazes. Por exemplo, a coordenação de antibióticos a metais pode melhorar significativamente sua farmacologia geral e eficácia, além de atenuar a resistência ao medicamento observada em algumas células-alvo (Guerra *et al*., 2005; Ronconi & Sadler, 2007). A formação do complexo pode ainda reduzir toxicidade, hipersensibilidade e resistência ao promover rearranjos estruturais da molécula (Cassini, 2012). Os metais podem aumentar a lipofilicidade da molécula, facilitando sua difusão através das membranas celulares (Bruijnincx & Sadler, 2010).

Relatos na literatura demonstram que complexos metálicos podem ser uma alternativa interessante como terapia antiparasitária. Por exemplo, complexos contendo íons de cobre ou cobalto, são ativos contra *Leishmania infantum e Leishmania braziliensis*, afetando as membranas das organelas que desencadeia a morte celular (Ramírez-Macías *et al*., 2011). Esses complexos também são ativos contra *Trypanosoma cruzi in vitro e in vivo*, resultando em menor toxicidade para a célula hospedeira. Isso torna esses compostos mais seguros do que a droga atual, benzonidazol, que é usado para tratar a doença de Chagas (Caballero *et al*., 2011).

Estudos anteriores relataram atividade anti-*Toxoplasma* de dois complexos de cobre(II) (Portes *et al*., 2017). Ambos os complexos, controlam irreversivelmente o crescimento de *T. gondii in vitro*, resultando em valores de IC_{50} de 0.78 e 3.57μM, respectivamente, após 48 horas de incubação. Observou-se que esses compostos induzem a conversão de parte dos parasitos da forma taquizoíto para bradizoíto. Além disso, foi visualizado que o composto de cobre causou a morte dos parasitos por dois mecanismos distintos, necrose e apoptose, caracterizadas através de alterações ultraestruturais: necrose foi observado extração do conteúdo citoplasmático dos parasitos, vesiculação do citoplasma e rompimento na membrana; apoptose: parasitos apresentaram *blebs* de membrana e alterações no núcleo e cromatina, além de inúmeras vesículas semelhantes a corpos apoptóticos. Com isso a comparação entre os valores de IC_{50} para os compostos sob investigação indica melhor eficiência quando comparado com SDZ sozinhocom os fármacos, sugerindo um efeito da natureza do metal e do ligante na atividade anti-*Toxoplasma*.

Complexos de zinco e ferro(III), contendo SDZ coordenado ao centro metálico, também exibiram atividade anti-*Toxoplasma in vitro*. Após 48h de tratamento com complexos de zinco contendo SDZ, observou-se a formação de pseudocistos, indicando que os compostos

promovem a conversão de taquizoítos a bradizoítos. No estudo com complexos de Fe(III), além da redução da capacidade de proliferação do parasito com IC_{50} de 1.66 μM e 5.3 μM, respectivamente, observou-se que o Fe(III) provocou a morte do parasito por autofagia: os parasitos apresentaram intensa degradação citoplasmática e perfis de membrana semelhantes a mielina, além de marcação positiva para vesículas autofágicas (Batista *et al*., 2015; Portes *et al*., 2018). O estudo ainda conclui que houve aumento na produção de espécies reativas de oxigênio (ROS) após o tratamento com o complexo de Fe(III), reduzindo os níveis de metaloenzimas que são importantes para a proteção antioxidante do parasito (Portes *et al*., 2018).

Assim, considerando a importância do estudo de novos compostos contra *T. gondii* e conhecendo a severidade da toxoplasmose, doença com terapia atual restrita a poucos medicamentos e severos efeitos adversos, o objetivo do presente trabalho é avaliar o efeito *in vitro* de novos complexos metálicos, coordenados ou não à SDZ, fármaco atualmente utilizado para tratar infecções por *T. gondii*. Com estes novos complexos, buscam-se resultados mais eficazes em concentrações baixas, com o objetivo de reduzir os efeitos tóxicos ao organismo hospedeiro e otimizar a atividade contra o parasito.

2. OBJETIVOS

2.1 Objetivo geral

Avaliar o efeito anti-*Toxoplasma* de novos complexos metálicos *in vitro* e estudar os possíveis mecanismos de ação dos complexos com melhor desempenho.

2.2 Objetivos específicos

2.2.1 Determinar o índice de infecção (I.I) em células hospedeiras LLC-MK2 infectadas com *T.gondii* após tratamento com os complexos $[Ni(BPAH)(H_2O)_2].2ClO_4$, $[Cu(HL1)Cl_2]$, $[Fe(HL1)Cl_3]$, $[Zn(HL1)Cl_2]$, $[Zn(HL1)(SDZ)Cl]\cdot 2H_2O$, selecionando os complexos com melhor desempenho.

2.2.2 Determinar a concentração inibitória de 50% do crescimento do parasito (IC_{50}) em células hospedeiras LLC-MK2 infectadas com *T. gondii* após tratamento com os complexos selecionados.

2.2.3 Avaliar a viabilidade das células hospedeiras LLC-MK2 após tratamento com os complexos selecionados.

2.2.4 Analisar alterações morfológicas e ultraestruturais de *T. gondii* durante a interação com células LLC-MK2 após tratamento com os complexos selecionados.

2.2.5 Avaliar taxa de invasão e reversibilidade da infecção por *T. gondii* em células LLC-MK2 após tratamento com os complexos selecionados.

2.2.6 Investigar, por meio de imunofluorescência, os possíveis mecanismos de ação dos complexos selecionados.

2.2.7 Examinar o impacto do complexo de ferro(III) no comportamento térmico de diferentes modelos lipídicos.

2.2.8 Investigar como o complexo de ferro(III) influencia a dinâmica, fluidez e organização dos modelos lipídicos estudados.

3. MATERIAL E MÉTODOS E RESULTADOS

Os materiais e métodos, assim como os resultados, serão apresentados na forma de artigos científicos:

3.1 A new water-soluble Ni(II) complex as a prototype of metallodrug to treat toxoplasmosis - Em processo de submissão para o Journal of Inorganic Chemistry Frontiers.

3.2 Development, structural, spectroscopic and *in silico* investigation of new complexes relevant as anti-toxoplasma metallopharmacs - Publicado em Journal of Molecular Structure / 2022.

3.3 Iron(III) complex impacts *Toxoplasma gondii* growth by altering the plasma membrane and inner membrane complex - Submetido na ACS Omega / agosto de 2025.

3.1 A new water-soluble Ni(II) complex as a prototype of metallodrug to treat toxoplasmosis

Wagner S. Terra[a], Renata V. M. Freitas[c], Eduardo da S. Neves,[b] Christiane Fernandes[b], Adailton J. Bortoluzzi[b], Lino Meurer,[b] Bruno Szpoganicz,[b], Felipe F. Moreira[c], Pedro S. Rodrigues[c], Sergio H. Seabra,[c] Renato A. DaMatta[c*], and Adolfo Horn Jr[b*]

[a]Instituto Federal Fluminense, Campus Campos Centro, Campos dos Goytacazes, RJ, Brazil
[b]Departamento de Química, Universidade Federal de Santa Catarina, Florianópolis, Santa Catarina, Brasil.
[c]Laboratório de Biologia Celular e Tecidual, Universidade Estadual do Norte Fluminense Darcy Ribeiro, Campos dos Goytacazes, Rio de Janeiro, Brasil.
* Corresponding authors (adolfo.junior@ufsc.br, renato@uenf.br)

ABSTRACT

The synthesis, characterization and anti-toxoplamosis activity of the new mononuclear $[Ni(BPAH)(H_2O)_2].2ClO_4$ compound is described. The complex was synthesized with the tetradentate ligand 1,4-bis(propanamide)homopiperazine (BPAH) and thoroughly characterized in the solid state (x-ray diffraction, elemental analysis) and in solution (UV-Vis, ESI-(+)-MS, potentiometric titration). Biological investigation revealed that the complex effectively reduced the growth of *Toxoplasma gondii* infecting LLC-MK2 host cells, with an IC_{50} of 0.38 and 0.36 μM after 24 h and 48 h incubation, respectively, and avoided reinfection of healthy cells. Moreover, the compound exhibited no toxicity to host cell at a concentration of 700 μM. Transmission electron microscopy showed that treatment with $[Ni(BPAH)(H_2O)_2].2ClO_4$ induced aberrant deformation of the parasite's conoid structure, which plays a crucial role in the cellular invasion process. As a result of this treatment, the parasites were unable to invade host cells. This study indicates that Ni(II) compounds may be a promising candidates for the development of metallodrugs to treat toxoplasmosis, providing new opportunities for researchers on parasitic diseases.

Introduction

Toxoplasma gondii is an apicomplexan parasite related to *Plasmodium* spp., the agent of malaria. *T. gondii* is a cosmopolitan pathogen that causes Toxoplasmosis, a chronic infection that affects over one-third of the world´s human population as well as many intermediate hosts (birds and mammals)[1]. Toxoplasmosis can cause loss of motor and cognitive function, sight, hearing, and fatal encephalitis. This disease can infect the fetus, causing extensive problems, even abortion. Immunosuppressed patients (such as HIV and organ transplants), also suffer from acquired toxoplasmosis or may experience reactivation of the infection during their live[2]. *T. gondii* can exist in three different forms: (i) bradyzoites, which is the latent form found in tissue cysts; (ii) tachyzoites, is the acute form of the infection; (iii) sporozoites, is found in sporulated oocysts shed by Felidae[3].

Unfortunately, there is no cure for toxoplasmosis. The drugs employed at the moment are not able to control the bradyzoites found in tissue cysts[4]. These drugs just induce the conversion of the tachyzoite form to bradyzoite. The most employed treatment involves mainly the use of pyrimethamine and/or sodium sulfadiazine (IC_{50} 600-700 mg kg^{-1})[5]. The large quantity of these drugs employed in the treatment has resulted in several side effects, such as hypersensibility, hematological toxicity, teratogenicity, allergic responses, bone marrow suppression, and the development of resistance[6].

Based on these points, the development of new therapeutic alternatives is necessary to treat this pathogen[7]. At the moment, the majority of compounds with anti-toxoplasma activity are synthetic or natural organic molecules[8,9]. Only recently, coordination compounds have emerged as a promising class of chemicals with the potential to be applied in the chemotherapy of toxoplasmosis. A few examples reported in the literature include the metals Ru, Fe, Co, Cu, and Zn[10–15]. Previous studies by our group investigated coordination compounds with anti-toxoplasma activity *in vitro*. A dinuclear Fe compound demonstrated potent activity against *T. gondii* tachyzoites, inducing cyst formation and ultrastructural changes typical of bradyzoites. This compound triggered apoptosis and autophagy of the parasites while disrupting redox balance and increasing reactive oxygen species[13]. A binuclear Co(II) complex inhibited *T. gondii* growth in LLC-MK2 host cells, reducing parasite proliferation by 55%[12]. In 2017, two Cu(II) complexes were reported to damage *T. gondii* growth irreversibly, causing both necrosis and apoptosis of the parasite[14]. Additionally, Zn complexes containing sulfadiazine induced cyst formation after 48 h, promoting the conversion of tachyzoites to bradyzoites[15]. Recently, new coordination compounds ($[Cu(HL1)Cl_2]$ (1), $[Fe(HL1)Cl_3]$ (2), $[Zn(HL1)Cl_2]$

(3), [Zn(HL1)(SDZ)Cl]. $2H_2O$ (4)) were synthesized and their anti-toxoplasma activity was evaluated. After 48 h, complexes (2), (3) and (4) inhibited the growth of *T. gondii* with activities superior to the SDZ, with compound (2) showing the highest reduction in the infection index. Light microscopy images of LLC-MK2 cells infected with *T. gondii* suggest that, due to the small number of parasites and morphology alteration, complex (2) had the best capacity to promote the death of the parasite[16].

Ni is a trace element found in natural metalloenzymes[17], such as glyoxalase I, which plays a role in detoxifying methylglyoxal[18]; urease, which promotes the hydrolysis of urea[19]; and superoxide dismutase, which catalyzes the breakdown of superoxide[20]. Despite this, nickel coordination compounds have been poorly studied as potential metallodrugs for treating parasitic diseases[21,22]. A few studies have explored their effects on Chagas disease [23,24], malaria[25], and leishmaniosis[26,27]. However, to the best of our knowledge, there are currently no nickel coordination compounds that demonstrate significant activity against *T. gondii.*

Aiming to contribute to the development of new compound candidates to treat toxoplasmosis, we are reporting herein the synthesis, X-ray crystal structure, and the antiproliferative effect against *T. gondii* of the first mononuclear Ni(II) complex containing the ligand 1,4-bis(propanamide)homopiperazine (BPAH) on its structure **(Figure 1)**.

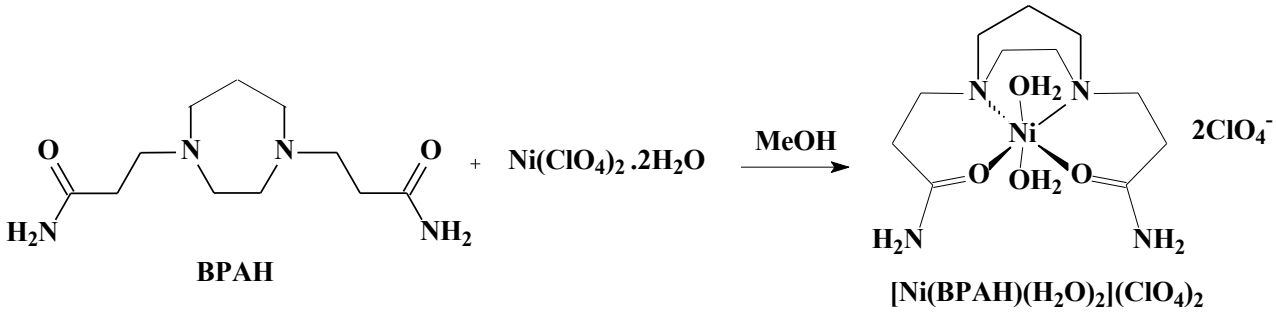

Figure 1. Scheme of synthesis for the complex $[Ni(BPAH)(H_2O)_2](ClO_4)_2$.

Materials and methods

All reagents and solvents were used as received from the commercial sources without further purification. Infrared analyses were performed in KBr disk on a Shimadzu IRAffinity-1. The UV-Vis spectra were obtained in a Cary 50 Bio Varian spectrophotometer. CHN elemental analysis was carried out on a Thermo Scientific Flash 2000 CHN analyzer, and the melting point was obtained on a 430 Fisatom melting point apparatus. The electrical

conductivity of the complex was measured in DMSO with a Biocristal conductivity meter at a concentration of $1x10^{-3}$ mol dm^{-3}. Mass spectrometry (ESI-(+)-MS/MS) was performed in a Bruker MicroTOF spectrometer with MeOH/H_2O (1:1) as the solvent. The NMR (^1H and ^{13}C) spectra were recorded on an Ascend 500 Advance III HD Bruker instrument operating at 500 MHz for ^1H and 125 MHz for ^{13}C in DMSO-D_6. X-ray analysis was carried out with a single crystal Bruker APEX II DUO diffractometer using graphite-monochromated MoKα radiation (λ = 0.71073 Å). Temperature of the sample was set at 200 (± 2) K with an Oxford Instruments Cryostream 700 series device. All frames were recorded with φ and ω scans method using APEX2 software[10]. All data were corrected for Lorentz and polarization effects and for absorption using SADABS semi-empirical multi-scan method[10]. The structure was solved by direct methods and refined applying the full-matrix least-squares method using SHELXS and SHELXL2014 programs[11], respectively. ORTEP plot was drawn with the PLATON software[12]. All non-hydrogen atoms were refined with anisotropic displacement parameters. Hydrogen atoms were placed at their idealized positions with distances of 0.97 Å for C-H_2 and its Uiso were fixed at 1.2 times Ueq of the carrier atom (C). Hydrogen atoms of the amide groups and coordinated water molecules were found from Fourier difference map and treated with riding model. Crystal data are shown in Table SI1 (see supporting information material).

In addition, a XRPD analysis of the Ni(II) complex was carried out with a D2-Phaser diffractometer using filtered Cu radiation. Frames in a 2Theta range from 7º to 45º with an increment of 0.04º/s. The potentiometric titration studies were carried out with a Corning 350 digital pH meter fitted with a blue-glass and Ag/AgCl reference electrodes calibrated to read -log[H^+] directly, designated as pH. Bidistilled water in the presence of $KMnO_4$ was used to prepare the solutions. For the ligands, the study was performed in ethanol–water (70:30) solution. The electrode was calibrated using the data obtained from the potentiometric titration of a known volume of a standard 0.100 mol L^{-1} HCl solution with a standard 0.100 mol L^{-1} KOH solution. The ionic strength of the HCl solution was maintained at 0.100 mol L^{-1} by the addition of KCl. The measurements were carried out in a temperature-controlled cell containing the compound or ligand solution (0.5 mmol/50 mL). The experiments were performed under argon flow to eliminate the presence of CO_2. The samples were titrated by the addition of fixed volumes of a standard CO_2-free KOH solution (0.100 mol L^{-1}). Computations were carried out with the BEST7 program, and species distribution diagrams were obtained with SPE and SPEPLOT programs[28,29].

Syntheses

The ligand BPAH was synthesized according to the methodology described previously, through the reaction between acrylamide and homopiperazine[30]. The Ni(II) complex was prepared by the reaction between the ligand BPAH (1 mmol, 242 mg) and $[Ni(H_2O)_6]2ClO_4$ (1 mmol, 366 mg) in 40 cm^3 of methanol **(Figure 1)**, which resulted in a blue solution. After 20 min under stirring, a blue solid was obtained, which was filtered under vacuum. The solution was allowed to stand for some days, resulting in monocrystals suitable for X-ray diffraction. Yield: 0.42 g (78 %); m.p. > 250 ºC. Anal. Calcd. for $C_{11}H_{26}Cl_2N_4NiO_{12}$ (MW= 535.94 g mol^{-1}): C, 24.65; H, 4.89; N, 10.45. Found: C, 24.43; H, 5.07; N, 10.68.

Biological studies

Toxoplasma gondii: Tachyzoites of *T. gondii* (RH strain) were maintained in Swiss mice. After 48 h of infection, the parasites were collected by a peritoneal cavity wash with phosphate-buffered saline (PBS), pH 7.2, that was centrifuged at 1000g for 10 min, the pellet was washed with PBS and DMEM. The parasites were used within 30 - 40 min of their removal from the peritoneal cavity. All animal studies were reviewed and approved by the ethics committee of animal use of UENF (Universidade Estadual do Norte Fluminense Darcy Ribeiro, code: 600).

Culture of host cells: LLC-MK2 kidney epithelial cells (Rhesus monkey, *Macaca mulata*) were grown in 25 cm^2 culture flasks (SPL Life Sciences) containing DMEM supplemented with 10% fetal bovine serum (FBS) at 37°C in a 5% CO_2 atmosphere. Infection of the cells by the parasite was performed in subconfluent cultures in flasks or on coverslips in 24-well tissue culture plates (SPL Life Sciences).

Anti-proliferative assays: Approximately 2×10^5 LLC-MK2 cells were seeded per well onto coverslips in a 24-well plate 1 day before the assay. The cells were infected with parasites using a 5:1 parasite/host cell ratio. Tachyzoites interacted with the host cells for 1 h. The cells were then washed, and the Ni(II) complex was added to the cells at different concentrations (1- 100 μM) in DMEM supplemented with FBS and further cultured. After 24 and 48 h of treatment, cells were washed, fixed with freshly prepared 4% formaldehyde in PBS, stained with Giemsa, and observed by bright field microscopy at the light microscope Axioplan-ZEISS. Images were captured with an MRc5 AxioCam digital camera and processed with the Axiovision program. Parasite growth was evaluated using the infection index (calculated by multiplying the mean

number of internalized *T. gondii* per host cell by the percentage of infected cells). These values were obtained by counting parasites and host cells on two separate coverslips in at least three independent experiments. To determine the drug concentration that inhibited parasite growth by 50% (IC_{50}), the percentage of growth inhibition was plotted as a function of the drug concentration, and the values were fitted in a non-linear curve. Logarithmic regression analyses were performed using Microsoft Excel software. Data were plotted using the GraphPad Prism 6.0® software. Results were represented as the means ± standard deviation of at least three independent experiments. Statistical analysis were performed using one-way ANOVA and two-way ANOVA followed by Tukey´s post hoc test.

Cell viability assay: The effect of Ni(II) complex on host cells were evaluated based on the reduction of MTT (3-(4,5-dimethyl-thiazol-2-yl)-2,5-diphenyltetrazolium bromide). For this assay, 1×10^5 cells were seeded per well into 96-well plates and cultured with DMEM supplemented with 5% FBS. After 24 h, the cells were incubated with the Ni(II) complex (300-700 µM) in DMEM supplemented with 5% FBS. As a negative control, some cells were also cultured in DMEM supplemented with 5% FBS without the addition of the Ni(II) complex. As a positive control, cells were incubated with 10% Triton X-100 in DMEM. After 24h or 48 h of treatment, the cells were incubated with 15 µL of MTT (5 mg/mL) solution in DMEM for 4 h at 37°C protected from light. The formazan crystals were solubilized by adding 100 µl of DMSO per well and the absorbance was measured in the Versamax microplate reader (Molecular Devices) at 570 nm using the 6.0 SoftMax Pro® software.

Transmission electron microscopy: Cells were infected in culture flasks, treated or not for 48 h with 10 µM of Ni(II) complex, and fixed for 1 h in a solution containing 2.5% glutaraldehyde in 0.1 mol L^{-1} sodium cacodylate buffer, pH 7.4. Cells were scraped off the flasks using a rubber policeman, washed with sodium cacodylate buffer, and post-fixed for 1 h in the dark in a solution containing 1% osmium tetroxide in 0.1 M sodium cacodylate buffer. Cells were washed, dehydrated in acetone, and embedded in Epon. Ultrathin sections were stained with uranyl acetate and lead citrate and observed under a Jeol 1400 Plus.

Invasion rate after treatment with Ni(II) complex: LLC-MK2 cells were grown in 25 cm^2 culture flasks ($2x10^5$/flask) and infected with tachyzoites as described above. After 1 h of interaction, cells were washed and the Ni(II) complex was added at concentrations of 2 and 5 µM. After 48 h, cells were scraped off the flasks using a rubber policeman and centrifuged for 300g, 10 min, 20° C to obtain the parasites that were quantified. LLC-MK2 cells previously cultured in a 24-well plate were infected (5:1) with the recovered parasites. After 1h of

interaction, coverslips were fixed and prepared for immunofluorescence. Cells were also stained with Giemsa as before for counting and the calculation of the infective index.

Imunofluorescence assays: LLC-MK2 cells over coverslips were infected with tachyzoites, treated or not with the Ni(II) complex for 48 h, washed with PBS and fixed with 4% freshly prepared formaldehyde in PBS. After fixation, the cells were washed, permeabilized with 0.5% Triton X-100 in PBS for 15 min, incubated with 100 mM NH_4Cl for 30 min and with PBS containing 1.5% bovine serum albumin (PBS- BSA) for 30 min at room temperature. Cells were incubated for 1 h in the presence of a mouse polyclonal antibody anti-*Toxoplasma* (1:3000 dilution in PBS-BSA) obtained from chronically infected mice. Cells were washed with PBS, incubated with PBS-BSA, and further incubated for 1 h with anti-mouse conjugated with Alexa-488 (1:400 dilution in PBS-BSA) from Invitrogen. Cells were washed with PBS and the coverslips were mounted with ProLong® Gold antifade (Invitrogen) with DAPI and observed under a fluorescence microscope Axioplan-ZEISS. Images were captured as before.

Results and discussions

The aforementioned BPAH ligand was synthesized through the reaction between acrylamide and homopiperazine as described previously by us. The molecule was characterized by ^{1}H and ^{13}C NMR (Figure 1SM, Table 1SM). The data agree with those reported in the literature[31].

The nickel compound was initially characterized by spectroscopic methods. The IR spectrum of the complex exhibits bands at 3362 and 3179 (ν N-H), 2997 and 2856 (ν C-H), 1651 (ν C=O), 1456 and 1424 (ν C-N and C-C) and an intense bands in the range 1145-1082 cm^{-1} (ν_{as} ClO_4^-) and 623 cm^{-1} (νs ClO_4^-) (Figure 2SM)[32]. Two low intensity bands at 459 and 419 cm^{-1} are tentatively assigned as νNi-N and νNi-O[33,34].

The UV-Vis spectrum (Figure 3SM) of $[Ni(BPAH)(H_2O)_2](ClO_4)_2$ is an uncommon example in which five d-d absorption bands are clearly visible, showing absorption bands at 891 (ε = 25 dm^3 mol^{-1} cm^{-1}), 752 (ε = 11 dm^3 mol^{-1} cm^{-1}), 604 (ε = 7 dm^3 mol^{-1} cm^{-1}), 449 (ε = 17 dm^3 mol^{-1} cm^{-1}) and 368 nm (ε = 23 dm^3 mol^{-1} cm^{-1}). The Tanabe-Sugano diagram is not suitable to explain the absorptions, since it is applied to compounds showing Oh symmetry and the described nickel compound shows a C_{2V} symmetry. According to Lever[35,36], under a C_2v symmetry, the spectroscopic terms observed under Oh field ($^3F \rightarrow {}^3A_2g$, ^3T_2g, ^3T_1g) undergo the following splitting: $^3A_2g \rightarrow {}^3A_1$; $^3T_2g \rightarrow {}^3A_2$, $^3B_1$, $^3B_2$; $^3T_1g \rightarrow {}^3A_2$, $^3B_1$, $^3B_2$,

indicating that six allowed d-d transitions are possible, considering the $^3A_1$ as the ground state. So, considering the five absorptions bands, four of them may be classified as d-d allowed transitions (891, 604, 449 and 368 nm).The band at 752 nm is very narrow, which is a typical feature of forbidden transition, as described for other hexacoordinated Ni(II) complexes[37].

The conductivity data in methanol (160.5 Ω^{-1} cm^2 mol^{-1}) support that the complex is a dication in solution, since this value is typical for a 2:1 electrolyte type (160–220 Ω^{-1} cm^2 mol^{-1})[38] in agreement with the X-ray data (see below) that revealed the presence of two perchlorate anions. Therefore, in methanol solution, and considering the CHN elemental analysis and spectroscopic data, a mononuclear compound with composition $[Ni(BPAH)(H_2O)_2](ClO_4)_2$ is proposed, as presented in **Figure 1**.

Crystallographic analysis **(Figure 2)** agrees with the structure suggested in **Figure 1** (Crystallographic data presented as Supplementary Information – Table 2SM) and confirmed the formation of a mononuclear hexacoordinated Ni(II) complex with distorted octahedral geometry. The main bond lengths and angles are shown in **Table 1**.

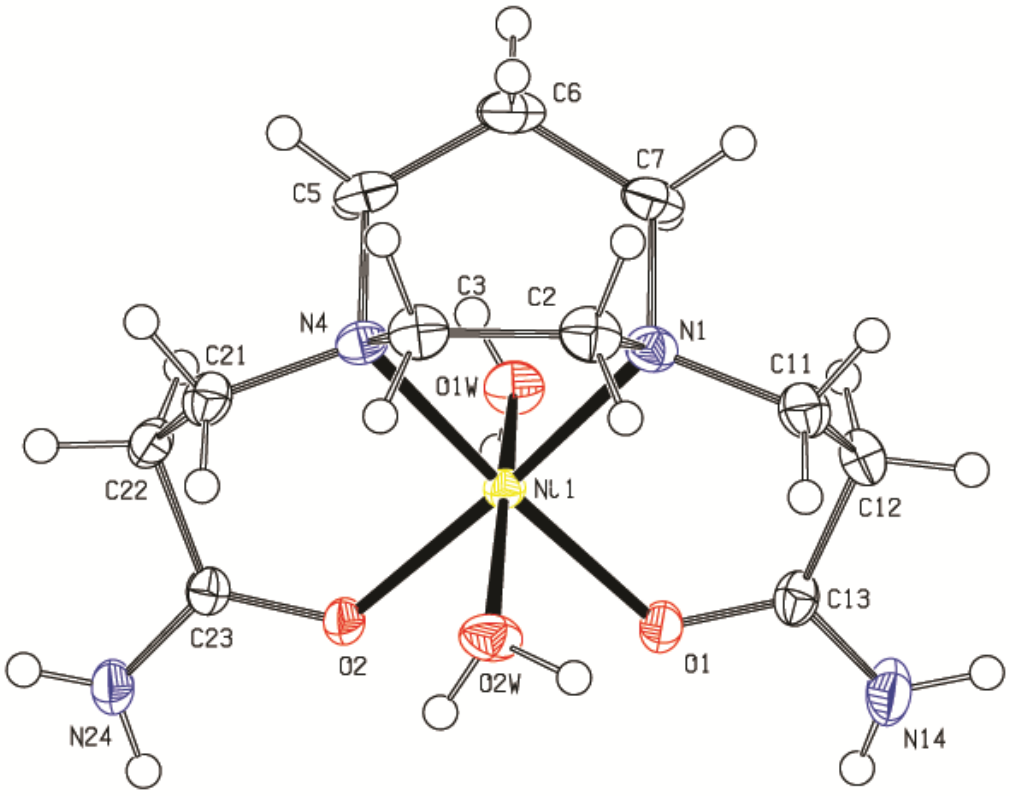

Figure 2. ORTEP plot with labelling scheme of the dication $[Ni(BPAH)(H_2O)_2]^{2+}$, thermal ellipsoid plot at 50 % probability level.

Table 1. Selected bond lengths [Å] and angles [°] for Ni(II) complex.

Ni(1)-O(2)	2.0413(11)
Ni(1)-O(1)	2.0469(11)
Ni(1)-N(1)	2.0791(13)
Ni(1)-N(4)	2.0800(13)
Ni(1)-O(2W)	2.1217(12)
Ni(1)-O(1W)	2.1222(12)
O(2)-Ni(1)-O(1)	88.75(4)
O(2)-Ni(1)-N(1)	173.61(5)
O(1)-Ni(1)-N(1)	96.65(5)
O(2)-Ni(1)-N(4)	96.57(5)
O(1)-Ni(1)-N(4)	174.03(5)
N(1)-Ni(1)-N(4)	77.87(5)
O(2)-Ni(1)-O(2W)	83.32(5)
O(1)-Ni(1)-O(2W)	87.17(5)
N(1)-Ni(1)-O(2W)	93.51(5)
N(4)-Ni(1)-O(2W)	90.77(5)
O(2)-Ni(1)-O(1W)	86.04(5)
O(1)-Ni(1)-O(1W)	83.44(5)
N(1)-Ni(1)-O(1W)	97.93(5)
N(4)-Ni(1)-O(1W)	99.57(5)
O(2W)-Ni(1)-O(1W)	165.95(5)
C(13)-O(1)-Ni(1)	125.00(10)
C(23)-O(2)-Ni(1)	125.69(10)

Symmetry transformations used to generate equivalent atoms:
#1 -x+1,-y+1,-z+1 #2 x-1,-y+3/2,z-1/2 #3 -x+1,y-1/2,-z+3/2
#4 -x,-y+1,-z+1 #5 x,-y+3/2,z-1/2

The coordination environment (N_2O_4) is composed of a molecule of the ligand BPAH coordinated in the equatorial plane and two water molecules (in trans position to each other) in the axial axis. Two perchlorate anions are acting as counterions. The bond distances in the plane (Ni-N1,4 and Ni-O1,2) are similar (~2.06 Å) and slightly shorter than the Ni-OH_2 bonds [average = 2.1220(12) Å]. For the Cu(II) complex synthesized with the same ligand, the bond lengths are smaller (Cu-N 2.0057(8), Cu-O 1.9640(7) Å)[31]. The angle O1W-Ni-O2W [165.95(5)º] deviates from the linearity, probably due to the steric hindrance caused by the

homopiperazine ring. A powder X-ray analysis was also carried out and confirmed the phase purity (Figure 4SM).

In solution studies using potentiometric titration allowed us to determine the pKas associates with the ligand and the complex protonation/deprotonation equilibria in the pH range 2-12, as well as the formation constant of the complex. Four pkas were observed for the ligand **(Table 2)**. The two amine groups showed different pKa values (8.41 and 4.70), indicating that the ligand is found predominantly in the unprotonated form (L) only at pH higher than 8.41. The ligand is monoprotonated (HL^+) in the pH range 8.41-4.70. Below 4.70, the two amines are protonated and the ligand is a dicationic (H_2L^{2+}) species. Furthermore, the two amide groups undergo protonation at pH 2.06 and 0.80. The potentiometric titration data support that the molecular structure of the complex observed in the solid state (X-ray diffraction) remains stable in the pH range 6.06 to 8.57. The formation constant is $3.31x10^8$. The pKa 6.06 is related to the protonation of one amine group present in the structure of the ligand. On the other hand, the pKa observed at 8.57 is attributed to the deprotonation of one of the water molecules coordinated to the Ni^{2+} ion. It is important to highlight that the species $[Ni(BPAH)(H_2O)_2]^{2+}$ reached ~90% at pH 7.29, being responsible for the biological activity.

Table 2. Thermodynamic data obtained by potentiometric titration of the ligand BPAH (L) and the complex $[Ni(BPAH)(H_2O)_2]2ClO_4$ (NiL).

Quotient	Log K
$[HL]/[H][L]$	8.41
$[H_2L]/[HL][H]$	4.70
$[H_3L]/[H_2L][H]$	2.06
$[H_4L]/[H_3L][H]$	0.80
$[NiL]^{2+}/[Ni]^{2+}[L]$	8.52
$[NiHL]^{3+}/[NiL]^{2+}[H]^+$	6.06
$[NiL(OH)]^{1+}/[NiL]^{2+}[OH]^-$	8.57
$[NiL(OH)_2]/[NiL(OH)]^{1+}[OH]^-$	16.97

ESI-(+)-MS and ESI-(+)-MS/MS data for the complex $[Ni(BPAH)(H_2O)_2]ClO_4$ (Figures SM5-SM8) present a characteristic set of isotopologue ions due mainly to the presence of Ni(II) ion. The base peak is observed at m/z 399.1 and is ascribed to the species $[Ni(BPAH)(ClO_4)]^+$ (see Figure 6SM). Another peak of relevance is observed at m/z 899.1. According to the isotopic pattern, the peak with m/z 899.1 is attributed to the overlay of two cationic species: $[Ni_2(BPAH)_2(ClO_4)_3]^+$ and $[Ni_4(BPAH)_4(ClO_4)_6]^{2+}$ (Figures 7SM). Such species are clusters that may be formed in the gas phase. The MS/MS data of this peak yields

the cation with m/z 399.1, by the loss of a neutral molecule of 500 Da, described as $[Ni(BPAH)(ClO_4)_2]$ (Figure 8SM). The dicationic species $[Ni(BPAH)(H_2O)_2]^{2+}$, identified by X-ray study, was not detected; only the monocation $[Ni(BPAH)(ClO_4)]^{+}$ was observed, due to its higher stability after the ionization process.

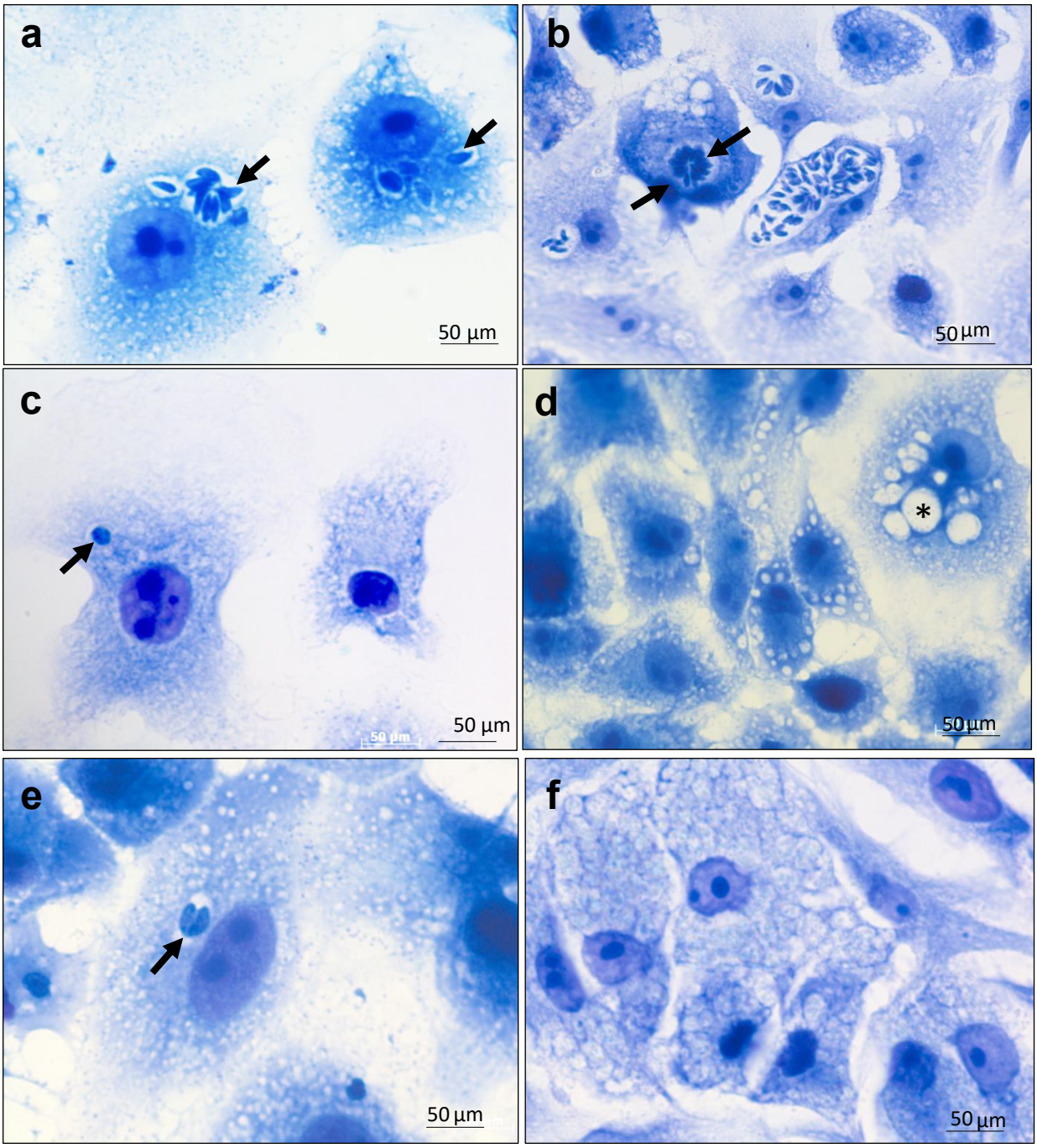

Figure 3. Bright field images of LLC-MK2 cells infected with *Toxoplasma gondii* treated or not with Ni(II) complex for 24 h and 48 h, stained with Giemsa. a. Tachyzoites in the parasitophorous vacuoles (arrows) after 24 h without treatment. b. Tachyzoites forming rosettes (arrows) after 48 h without treatment. c. LLC-MK2 cells infected with *T. gondii* treated with

50 μM of Ni(II) complex for 48h showed unusually shaped tachyzoites (arrow). d, e, f. LLC-MK2 cells infected with *T. gondii* treated with 100 μM of Ni(II) complex. d. LLC-MK2 cells presented expanded vacuoles (*) without parasites after treatment for 24 h. e. Swollen-shaped tachyzoites (arrow) after 24 h of treatment. f. Absence of tachyzoites in treated cells for 48 h. Scale bars: 50 μm.

T. gondii tachyzoites infected and grew well in host cells (LLC-MK2) **(Figure 3a, b)**. However, treatment with the Ni(II) complex controlled the *T. gondii* growth **(Figure 3c, d, e, f)**. Quantification of the infective index showed that the Ni(II) complex inhibits the parasite growth **(Figure 4)**, presenting an IC_{50} of 0.38 μM at 24 h and 0.36 μM at 48 h, causing changes at the morphology **(Figure 3c, e)** of the parasite. The complex was found to be non-toxic to host cells, maintaining over 90% cell viability when a concentration of 700 μM was used for 48 h **(Figure 5)**. Due to this favorable response, we could not calculate an exact selective index. However, the complex exhibits remarkable selectivity against the parasite (SI > 1800). This characteristic emphasizes its potential as a safe and effective therapeutic option, as the low IC_{50} value against the parasite indicates that the Ni(II) complex is highly effective in inhibiting the growth of *T. gondii*, even with short exposure times.

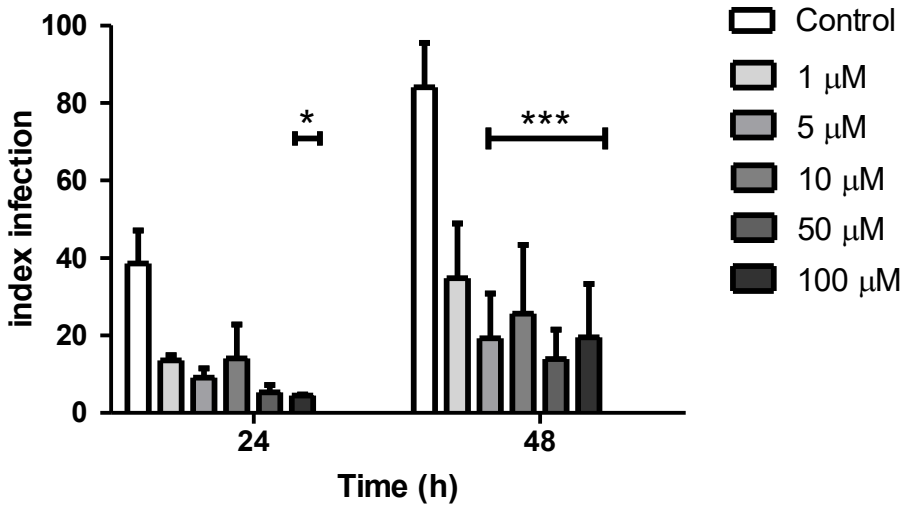

Figure 4. Infection index of *Toxoplasma gondii* in LLC-MK2 cells after 24 h and 48 h of treatment with different concentrations of the Ni(II) complex. Control cells were untreated. Mean and standard deviation of three independent experiments. * $P \leq 0.05$, *** $P \leq 0.001$ in relation to the control.

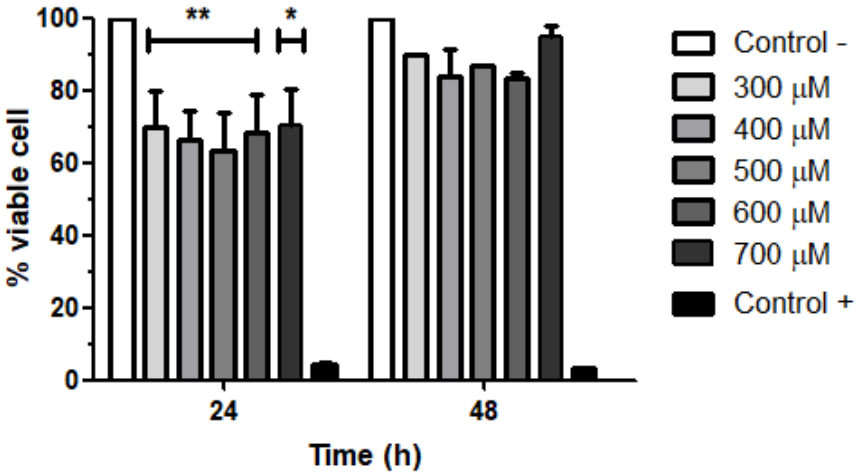

Figure 5. Viability of LLC-MK2 cells after treatment with different concentrations of the Ni(II) complex for 24 h and 48 h. The toxicity of the Ni(II) complex to the LLC-MK2 cells was evaluated based on the reduction of MTT [3-(4,5-dimethylthiazol-2-yl)-2,5-diphenyltetrazolium bromide]. Negative control cells were cultured in DMEM with FBS without complex. Positive control cells were cultured with 10% Triton X-100 in DMEM. * $P \leq 0.05$ and ** $P \leq 0.01$ in relation to the negative control.

Because of the morphological changes observed after treatment of *T. gondii* infected host cells **(Figure 3c, e)**, ultrastructural analyses were performed using transmission electron microscopy. Non-treated cells exhibited a normal ultrastructure characterized by a typical conoid structure **(Figure 6a)**. However, treatment with the Ni(II) complex caused significant alterations in the plasma membrane structure of the parasite and resulted in a distinct rounding of the conoid **(Figure 6b, c, d)**. The conoid, which is crucial for the parasite's invasion, was notably impacted by this treatment.

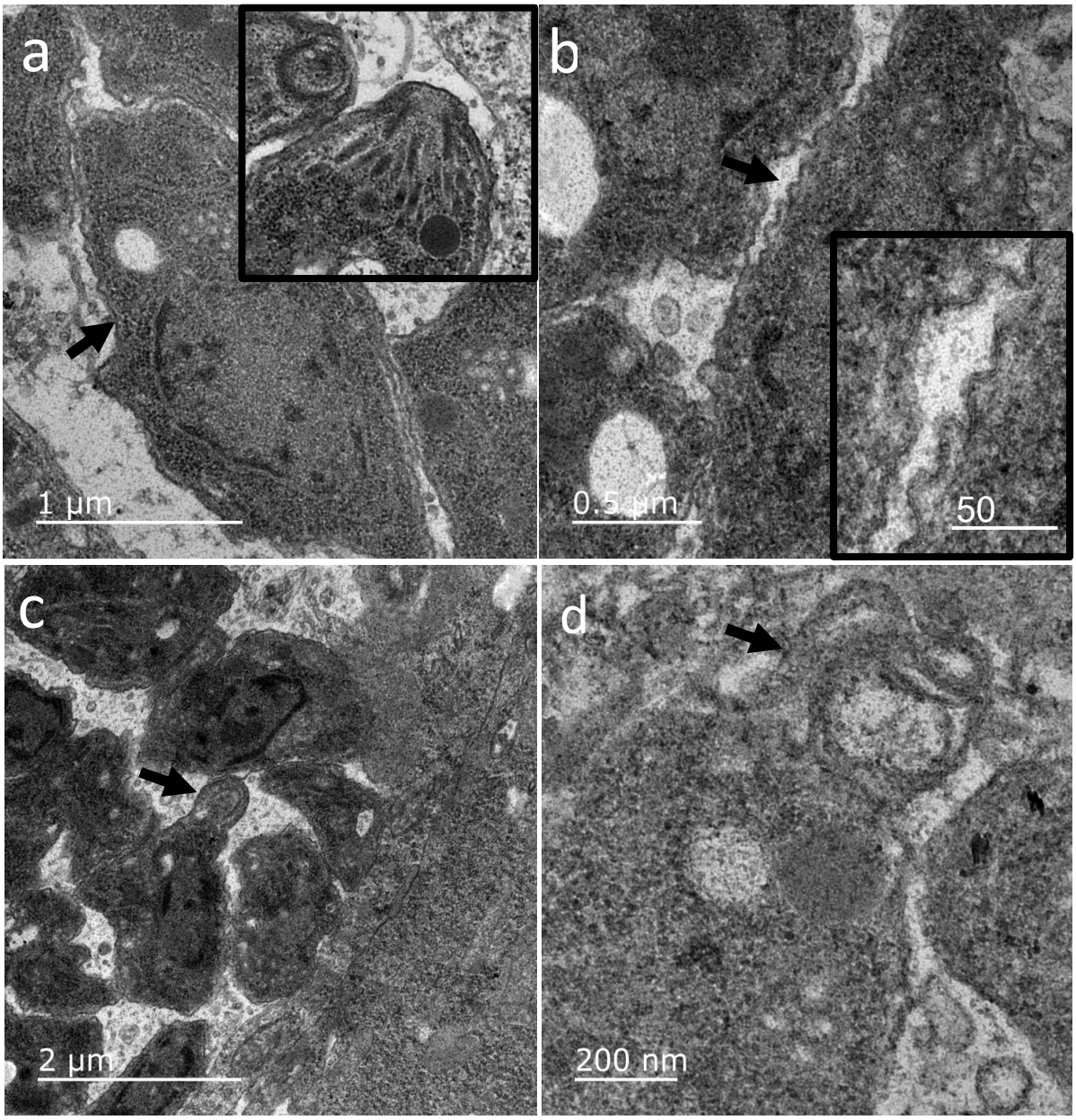

Figure 6. Transmission electron microscopy images of LLC-MK2 cells infected with *Toxoplasma gondii* treated or not for 48 h with 10 µM of Ni(II) complex. a *T. gondii* inside LLC-MK2 cells without treatment after 48 h of infection (arrow). Note the well-preserved typical apical structure of the tachyzoite (inset). b Treatment caused alteration of membrane structure. Note the altered membrane structure (inset). c and d treatment alters the structure of the conoid (arrow). Scale bar values are in the figures.

In subsequent experiments, infected host cells were treated, and parasites were then used to infect another batch of host cells. Data from immunofluorescence microscopy clearly demonstrated that untreated parasites successfully infected other host cells **(Figure 7a)**.

Conversely, cells treated with 2.5 μM of the Ni(II) complex resulted in a much lower amount of infected host cells **(Figure 7b)**. Total prevention of the infection was reached by doubling the concentration of the Ni(II) complex (5 μM) **(Figure 7c)**. Quantification of the assay confirmed the result, showing only a residual infection after treatment **(see Figure 8)**. This suggests that the Ni(II) complex altered the structure, hindering the parasite's ability to infect new host cells.

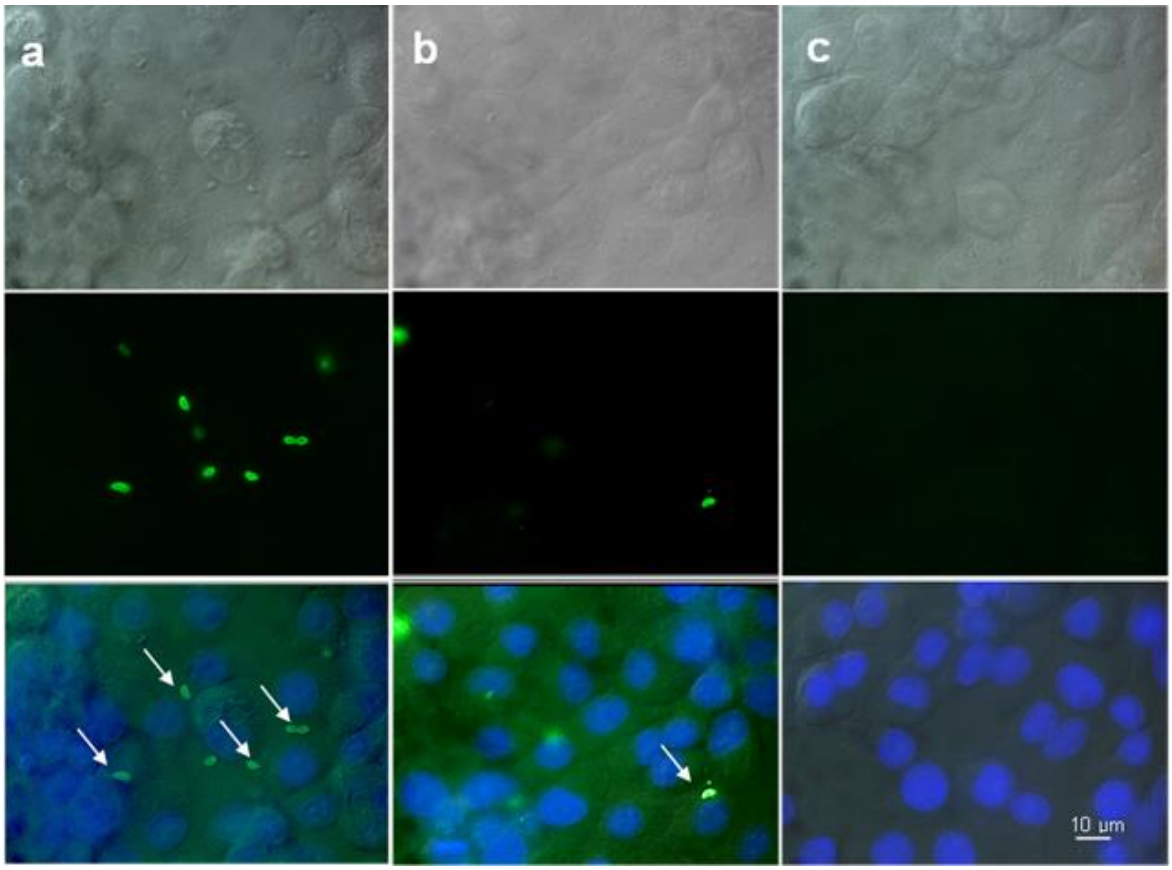

Figure 7. Differential interferential contrast, immunofluorescence, and merged images of LLC-MK2 cells infected with *Toxoplasma gondii* treated or not for 48 h with 2.5 and 5 μM of Ni(II) complex. (a) Control, LLC-MK2 cells infected with *T. gondii* that were untreated. Note the presence of many parasites (arrows). (b) LLC-MK2 cells infected with *T. gondii* that were treated with 2.5 μM of Ni(II) complex. Note the reduced number of parasites infecting the host cells (arrow). (c) LLC-MK2 cells infected with *T. gondii* that were treated with 5 μM of Ni(II) complex. Note the absence of parasites.

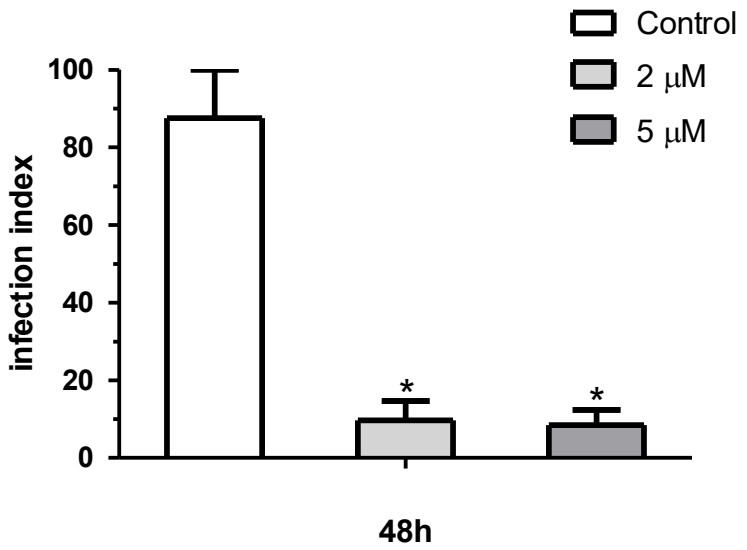

Figure 8. Invasion capacity of *Toxoplasma gondii* tachyzoites in LLC-MK2 cells after 48h of treatment with Ni(II) complex. Tachyzoites infecting LLC-MK2 cells were treated with Ni(II) complex, recovered by mechanical disruption, and used to reinfect cells. Control tachyzoites were not treated. *$P \leq 0.05$ in relation to the control.

$[Ni(BPAH)(H_2O)_2](ClO_4)_2$ has controlled *T. gondii* growth with an IC_{50} value lower than other complexes reported in the literature, including a Co(II)[12], iron(III) (IC_{50} = 3.6 μM after 48 h) and Cu(II) complexes (IC_{50} = 0.78 μM and 3.57 μM after 48 h) reported previously by us[13,14]. Furthermore, the simplicity associated with the synthesis of the ligand BPAH and its respective Ni(II) compound is an advantage over other compounds. Another benefit is the high solubility in water of the $[Ni(BPAH)(H_2O)_2](ClO_4)_2$ species, which reached 5 mmol L^{-1}, as demonstrated in the UV-Vis study carried out in pure water (Figure 3SM). Solubility is a crucial physicochemical property in both drug discovery and development. More than 75% of drug candidates and 40% of marketed drugs have low aqueous solubility[39], making this a critical factor that influences drug dissolution and oral bioavailability[40].

Conclusions

The data presented here mark the development of a promising molecule for medical application, a mononuclear Ni(II) complex. Unprecedented in the literature, this Ni(II) complex demonstrates remarkable activity against *T. gondii*, indicating that Ni(II) compounds can have a crucial role in developing metallodrugs for treating this parasite. Furthermore, it shows two

important features related to drug development: high selectivity for the parasite (SI > 1800) and excellent water solubility. Ultrastructure analysis clearly demonstrates that the conoid structure, crucial for the parasite's invasion of host cells, undergoes significant abnormal morphological changes. These changes are likely a direct consequence of the action of the Ni(II) complex on such an important structure. This investigation is pivotal in advancing the search for metallodrugs to combat this widespread disease, toxoplasmosis, opens new possibilities for compounds synthesized with this cheap metal ion (Ni^{2+}). Encouraged by these promising findings, we are in the process of producing a range of similar Ni(II) complexes with the aim of enhancing their activity and gaining a better understanding of their mechanisms of action.

Conflicts of interest

There are no conflicts of interest to declare.

Acknowledgements

The authors are grateful to the financial support received from FAPERJ (Fundação Carlos Chagas de Amparo à Pesquisa do Estado do Rio de Janeiro) and CNPq (Conselho Nacional de Desenvolvimento Científico e Tecnológico). This work was also financed in part by the Coordenação de Aperfeiçoamento de Pessoal de Nível Superior - Brasil (CAPES) - Finance Code 001.

Notes and references

‡ Perchlorate salts are potentially explosive and should be handled carefully. CCDC 1486373 contains the supplementary crystallographic data for this paper. These data can be obtained free of charge at www.ccdc.cam.ac.uk.conts/retrieving.html/ or from the Cambridge Crystallographic Data Centre (CCDC), 12 Union Road, Cambridge CB2 IEZ, UK; fax: + 44(0) 1223-336033; e-mail: deposit@ccdc.cam.ac.uk.

References

[1] F. Robert-Gangneux, M.L. Dardé, Epidemiology of and diagnostic strategies for toxoplasmosis, Clin. Microbiol. Rev. (2012). https://doi.org/10.1128/CMR.05013-11.

[2] C. Paquet, M.H. Yudin, V.M. Allen, C. Bouchard, M. Boucher, S. Caddy, E. Castillo, D.M. Money, K.E. Murphy, G. Ogilvie, J. van Schalkwyk, V. Senikas, Toxoplasmosis

in Pregnancy: Prevention, Screening, and Treatment, J. Obstet. Gynaecol. Canada. (2013). https://doi.org/10.1016/S1701-2163(15)31053-7.

[3] D.E. Hill, S. Chirukandoth, J.P. Dubey, Biology and epidemiology of *Toxoplasma gondii* in man and animals, Anim. Heal. Res. Rev. (2005). https://doi.org/10.1079/ahr2005100.

[4] M. Antczak, K. Dzitko, H. Długońska, Human toxoplasmosis–Searching for novel chemotherapeutics, Biomed. Pharmacother. (2016). https://doi.org/10.1016/j.biopha.2016.05.041.

[5] H.X. Wei, S.S. Wei, D.S. Lindsay, H.J. Peng, A systematic review and meta-analysis of the efficacy of anti-*Toxoplasma gondii* medicines in humans, PLoS One. (2015). https://doi.org/10.1371/journal.pone.0138204.

[6] A.J.A.M. Van Der Ven, E.M.E. Schoondermark-van De Ven, W. Camps, W.J.G. Melchers, P.P. Koopmans, J.W.M. Van Der Meer, J.M.D. Galama, Anti-toxoplasma effect of pyrimethamine, trimethoprim and sulphonamides alone and in combination: Implications for therapy, J. Antimicrob. Chemother. (1996). https://doi.org/10.1093/jac/38.1.75.

[7] M. Montazeri, M. Sharif, S. Sarvi, S. Mehrzadi, E. Ahmadpour, A. Daryani, A systematic review of *in vitro* and *in vivo* activities of anti-toxoplasma drugs and compounds (2006-2016), Front. Microbiol. (2017). https://doi.org/10.3389/fmicb.2017.00025.

[8] S.A. Abdullahi, N.Z. Unyah, N. Nordin, R. Basir, W.M. Nasir, A.A. Alapid, Y. Hassan, T. Mustapha, R.A. Majid, Therapeutic Targets on *Toxoplasma gondii* Parasite in Combatting Toxoplasmosis, Annu. Res. Rev. Biol. (2019). https://doi.org/10.9734/arrb/2019/v32i230081.

[9] N. Konstantinovic, H. Guegan, T. Stäjner, S. Belaz, F. Robert-Gangneux, Treatment of toxoplasmosis: Current options and future perspectives, Food Waterborne Parasitol. 15 (2019) e00036. https://doi.org/https://doi.org/10.1016/j.fawpar.2019.e00036.

[10] A.P. Basto, J. Müller, R. Rubbiani, D. Stibal, F. Giannini, G. Süss-Fink, V. Balmer, A. Hemphill, G. Gasser, J. Furrer, Characterization of the Activities of Dinuclear Thiolato-Bridged Arene Ruthenium Complexes against Toxoplasma gondii, Antimicrob. Agents Chemother. 61 (2017) e01031-17. https://doi.org/10.1128/AAC.01031-17.

[11] F. Barna, K. Debache, C.A. Vock, T. Küster, A. Hemphill, *In Vitro* effects of novel ruthenium complexes in Neospora caninum and *Toxoplasma gondii* tachyzoites, Antimicrob. Agents Chemother. (2013). https://doi.org/10.1128/AAC.02446-12.

[12] V.M. De Assis, L.C. Visentin, F.S. De Souza, R.A. DaMatta, A. Horn, C. Fernandes, Synthesis, crystal structure and relevant antiproliferative activity against *Toxoplasma gondii* of a new binuclear Co(II) complex, Inorg. Chem. Commun. 67 (2016). https://doi.org/10.1016/j.inoche.2016.02.017.

[13] J.A. Portes, T.G. Souza, T.A.T. Dos Santos, L.L.R. Da Silva, T.P. Ribeiro, M.D. Pereira, A. Horn, C. Fernandes, R.A. DaMatta, W. De Souza, S.H. Seabra, Reduction of *Toxoplasma gondii* development due to inhibition of parasite antioxidant enzymes by a dinuclear iron(III) compound, Antimicrob. Agents Chemother. 59 (2015). https://doi.org/10.1128/AAC.00057-15.

[14] J.A. Portes, C.S. Motta, N.F. Azeredo, C. Fernandes, A. Horn, W. De Souza, R.A. DaMatta, S.H. Seabra, *In vitro* treatment of *Toxoplasma gondii* with copper(II) complexes induces apoptosis-like and cellular division alterations, Vet. Parasitol. 245 (2017) 141–152. https://doi.org/10.1016/j.vetpar.2017.04.002.

[15] L.C. Batista, F.S. De Souza, V.M. De Assis, S.H. Seabra, A.J. Bortoluzzi, M.N. Rennó, A. Horn, R.A. DaMatta, C. Fernandes, Antiproliferative activity and conversion of tachyzoite to bradyzoite of *Toxoplasma gondii* promoted by new zinc complexes containing sulfadiazine, RSC Adv. 5 (2015). https://doi.org/10.1039/c5ra17690e.

[16] A.P. Cardoso, L.M.P. Madureira, B.B. Segat, J. do N.C. Menezes, R. Cargnelutti, D.R.S. Candela, D.L. Mariano, R.L.T. Parreira, A. Horn, S.H. Seabra, R.A. DaMatta, F.F. Moreira, R. V. Moreira, G.F. Caramori, C. Fernandes, Development, structural, spectroscopic and in silico investigation of new complexes relevant as anti-toxoplasma metallopharmacs, J. Mol. Struct. 1265 (2022) 133380. https://doi.org/10.1016/j.molstruc.2022.133380.

[17] J.L. Boer, S.B. Mulrooney, R.P. Hausinger, Nickel-dependent metalloenzymes, Arch. Biochem. Biophys. 544 (2014) 142–152. https://doi.org/10.1016/j.abb.2013.09.002.

[18] J.W. Peters, Determination of the structure of Escherichia coli glyoxalase I suggests a structural basis of differential metal activation, Chemtracts. 15 (2002) 7–11.

[19] E. Jabri, M.B. Carr, R.P. Hausinger, P.A. Karplus, The crystal structure of urease from Klebsiella aerogenes, Science (80-.). 268 (1995) 998–1004.

https://doi.org/10.1126/science.7754395.

[20] D.P. Barondeau, C.J. Kassmann, C.K. Bruns, J.A. Tainer, E.D. Getzoff, Nickel superoxide dismutase structure and mechanism, Biochemistry. 43 (2004) 8038–8047. https://doi.org/10.1021/bi0496081.

[21] Y.C. Ong, S. Roy, P.C. Andrews, G. Gasser, Metal Compounds against Neglected Tropical Diseases, Chem. Rev. 119 (2019) 730–796. https://doi.org/10.1021/acs.chemrev.8b00338.

[22] D. Gambino, L. Otero, 13. Metal Compounds in the Development of Antiparasitic Agents: Rational Design from Basic Chemistry to the Clinic, Essent. Met. Med. Ther. Use Toxic. Met. Ions Clin. (2019) 331–358. https://doi.org/10.1515/9783110527872-019.

[23] C.R. Maldonado, C. Marín, F. Olmo, O. Huertas, M. Quirós, M. Sánchez-Moreno, M.J. Rosales, J.M. Salas, *In vitro* and *in vivo* trypanocidal evaluation of nickel complexes with an azapurine derivative against *Trypanosoma cruzi*, J. Med. Chem. 53 (2010) 6964–6972. https://doi.org/10.1021/jm100581z.

[24] F.C. De Alcantara, V.F. Lozano, A.S. Vale Velosa, M.R.M. Dos Santos, R.M.S. Pereira, New coumarin complexes of Zn, Cu, Ni and Fe with antiparasitic activity, Polyhedron. 101 (2015) 165–170. https://doi.org/10.1016/j.poly.2015.09.010.

[25] S. Savir, Z.J. Wei, J.W.K. Liew, I. Vythilingam, Y.A.L. Lim, H.M. Saad, K.S. Sim, K.W. Tan, Synthesis, cytotoxicity and antimalarial activities of thiosemicarbazones and their nickel (II) complexes, J. Mol. Struct. 1211 (2020) 128090. https://doi.org/10.1016/j.molstruc.2020.128090.

[26] I. Ramírez-Macías, C.R. Maldonado, C. Marín, F. Olmo, R. Gutiérrez-Sánchez, M.J. Rosales, M. Quirós, J.M. Salas, M. Sánchez-Moreno, *In vitro* anti-leishmania evaluation of nickel complexes with a triazolopyrimidine derivative against *Leishmania infantum* and *Leishmania braziliensis*, J. Inorg. Biochem. 112 (2012) 1–9. https://doi.org/10.1016/j.jinorgbio.2012.02.025.

[27] D.O. Maia, V.F. Santos, C.R.S. Barbosa, Y.N. Fróes, D.F. Muniz, A.L.E. Santos, M.H.C. Santos, R.R.S. Silva, C.G.L. Silva, R.O.S. Souza, J.C.S. Sousa, H.D.M. Coutinho, C.S. Teixeira, Nickel (II) chloride schiff base complex: Synthesis, characterization, toxicity, antibacterial and leishmanicidal activity, Chem. Biol. Interact. 351 (2022). https://doi.org/10.1016/j.cbi.2021.109714.

[28] A.E. Martell, R.M. Smith, R.J. Motekaitis, in: NIST Critical Stability Constants; of Metal Complexes, NIST Database 46, 2001.

[29] A.E. Martell, R.J. Motekaitis, Determination and Use of Stability Constants, 1992.

[30] W.S. Terra, S.S. Ferreira, R.O. Costa, L.L. Mendes, R.W.A. Franco, A.J. Bortoluzzi, J.A.L.C. Resende, C. Fernandes, A. Horn, Evaluating the influence of the diamine unit (ethylenediamine, piperazine and homopiperazine) on the molecular structure, physical chemical properties and superoxide dismutase activity of copper complexes Dedicated to Prof. Ademir Neves on the occasion of, Inorganica Chim. Acta. 450 (2016) 353–363. https://doi.org/10.1016/j.ica.2016.06.024.

[31] W.S. Terra, S.S. Ferreira, R.O. Costa, L.L. Mendes, R.W.A. Franco, A.J. Bortoluzzi, J.A.L.C. Resende, C. Fernandes, A. Horn, Evaluating the influence of the diamine unit (ethylenediamine, piperazine and homopiperazine) on the molecular structure, physical chemical properties and superoxide dismutase activity of copper complexes Dedicated to Prof. Ademir Neves on the occasion of, Inorganica Chim. Acta. 450 (2016). https://doi.org/10.1016/j.ica.2016.06.024.

[32] A. Jayamani, N. Sengottuvelan, S.K. Kang, Y.I. Kim, Studies on nucleic acid/protein interaction, molecular docking and antimicrobial properties of mononuclear nickel(II) complexes of piperazine based Schiff base, Inorg. Chem. Commun. (2014). https://doi.org/10.1016/j.inoche.2014.08.029.

[33] S. Eğlence-Bakır, S. Celik, M. Şahin, A.E. Ozel, S. Akyuz, B. Ülküseven, Synthesis, molecular modelling, FT-IR, Raman and NMR characterization, molecular docking and ADMET study of new nickel(II) complex with an N4-tetradentate thiosemicarbazone, J. Biomol. Struct. Dyn. (2020). https://doi.org/10.1080/07391102.2020.1775128.

[34] K. Nakamoto, Infrared and Raman Spectra of Inorganic and Coordination Compounds: Part B: Applications in Coordination, Organometallic, and Bioinorganic Chemistry, 2008. https://doi.org/10.1002/9780470405888.

[35] J.C. Donini, B.R. Hollebone, A.B.P. Lever, The Derivation and Application of Normalized Spherical Harmonic Hamiltonians, in: 2007. https://doi.org/10.1002/9780470166239.ch2.

[36] J.C. Hempel, J.C. Donini, B.R. Hollebone, A.B.P. Lever, Symmetry Adapted Functions and Normalized Spherical Harmonic (NSH) Hamiltonians for the Point Groups Oh, Td, D4h, D2d, C4v, D2h, C2v, J. Am. Chem. Soc. (1974).

https://doi.org/10.1021/ja00813a009.

[37] E. González, A. Rodrigue-Witchel, C. Reber, Absorption spectroscopy of octahedral nickel(II) complexes: A case study of interactions between multiple electronic excited states, Coord. Chem. Rev. (2007). https://doi.org/10.1016/j.ccr.2006.08.011.

[38] W.J. Geary, The use of conductivity measurements in organic solvents for the characterisation of coordination compounds, Coord. Chem. Rev. 7 (1971) 81–122. https://doi.org/10.1016/S0010-8545(00)80009-0.

[39] S.Z. Asghar, R. Kaviani, A. Shayanfar, Solubility of Some Drugs in Aqueous Solutions of Choline Chloride-Based Deep Eutectic Solvent Systems: Experimental Data, Modeling, and the Impact of Solution pH, Iran. J. Pharm. Res. 22 (2023) 1–9. https://doi.org/10.5812/ijpr-137011.

[40] S. Onoue, New Drug Delivery Systems for Stable Oral Absorption: Theory, Strategies, and Applications, Biol. Pharm. Bull. 47 (2024) 1797–1803. https://doi.org/10.1248/bpb.b24-00566.

3.2 Development, structural, spectroscopic and *in silico* investigation of new complexes relevant as anti-toxoplasma metallopharmacs

Journal of Molecular Structure 1265 (2022) 133380

Contents lists available at ScienceDirect

Journal of Molecular Structure

journal homepage: www.elsevier.com/locate/molstr

Development, structural, spectroscopic and *in silico* investigation of new complexes relevant as anti-toxoplasma metallopharmacs

Ana Paula Cardoso[a], Letícia M.P. Madureira[a], Bruna B. Segat[a], Jennifer do N.C. Menezes[b], Roberta Cargnelutti[c], Dalber R.S. Candela[d], Davor L. Mariano[d], Renato L.T. Parreira[e], Adolfo Horn Jr[a], Sérgio H. Seabra[f], Renato A. DaMatta[f], Felipe F. Moreira[f], Renata V. Moreira[f], Giovanni F. Caramori[a,*], Christiane Fernandes[a,*]

[a] *Departamento de Química, Universidade Federal de Santa Catarina, 88040-900, Florianópolis, SC, Brazil*
[b] *Laboratório de Ciências Químicas, Universidade Estadual do Norte Fluminense, 28013-602, Campos dos Goytacazes, RJ, Brazil*
[c] *Departamento de Química, Universidade Federal de Santa Maria, 97105-900, Santa Maria, RS, Brazil*
[d] *Departamento de Física, Universidade Federal Fluminense, 24220-900, Niterói, RJ, Brazil*
[e] *Núcleo de Pesquisas em Ciências Exatas e Tecnológicas, Universidade de Franca, 14404600, Franca, SP, Brazil*
[f] *Laboratório de Biologia Celular e Tecidual, Universidade Estadual do Norte Fluminense, 28013-602, Campos dos Goytacazes, RJ, Brazil*

ARTICLE INFO

Article history:
Received 18 November 2021
Revised 11 April 2022
Accepted 24 May 2022
Available online 26 May 2022

Keywords:
Toxoplasmosis
Coordination compounds
Sodium Sulfadiazine (NaSDZ)
DFT
X-ray crystallography
ESI(+)-MS

ABSTRACT

Toxoplasmosis is an endemic neglected disease spread throughout the southern hemisphere, affecting a large part of the population concentrated in these countries. Aiming to develop new coordination compounds with anti-toxoplasma activity, we report herein the reactions between the mononuclear complexes $[Cu(HL1)Cl_2]$ **(1)**, $[Fe(HL1)Cl_3]$ **(2)**, and $[Zn(HL1)Cl_2]$ **(3)** (HL1 is the ligand N-2[(pyridine-2-ylmethyl)amino)ethanol)) and sodium sulfadiazine (NaSDZ), one of the current drugs used to treat toxoplasmosis. DFT data suggested that complexation reactions between complexes **(1)-(3)** and NaSDZ result in stable complexes **(4)-(6)**, containing SDZ^- in their coordination spheres, based on EDA (Energy Decomposition Analysis), which indicate favorable interaction between the metallic centers of the complexes and the anion SDZ^-. The EDA results also suggest that the SDZ^- anion donates negative charge to the metal, weakening the M-Cl interaction, present in complexes **(1)-(3)**, and making the coordination with SDZ^- anion easier. However, the reactions of **(1)** and **(2)** with NaSDZ were indeed ineffective, then complexes **(4)** and **(5)** were not obtained. Only the formation of $[Zn(HL1)(SDZ)Cl]\cdot 2H_2O$ **(6)** was achieved, the product of the reaction between complex **(3)** and NaSDZ. Further analysis of DFT calculations and EDA data were carried out to understand the lack of the reactivity of compounds **(1)** and **(2)**. The data revealed higher lability for the chloro ligand present in complex **(3)** and better stabilization of complex **(6)**'s HOMO. Steric and stacking effects could also justify these experimental data. This parallel theoretic-experimental study allowed us to conclude that complex **(6)** is the most probable to be obtained synthetically, in agreement with the experimental behavior. Furthermore, a complete characterization employing spectroscopic and electrochemical is presented for all the complexes, with and without SDZ^- anion, including X-ray diffraction studies for complexes **(1)** and **(6)**. The cytotoxic effects on *T. gondii* infecting LLC-MK2 host cells are presented and indicate that all the complexes reduced the parasiteś ability to proliferate. These results suggest that these compounds are promising, especially complex **(2)**, which causes the death of the parasite.

1. Introduction

Toxoplasmosis is a broad spectrum anthropozoonosis that affects about one-third of the world population [1]. The protozoan responsible for this infection *(Toxoplasma gondii)* is an intracellular parasite that can contaminate various tissues of birds and mammals, including humans and domestic animals, especially felids. In general, the disease is silent and usually asymptomatic in healthy individuals. In the case of immunosuppressed organisms, the consequences of contamination are severe, causing abortion, triggering a series of neurological and congenital problems, such as retinochoroiditis, encephalitis and schizophrenia [2,3]. Recently,

* Corresponding authors.
E-mail addresses: giovanni.caramori@ufsc.br (G.F. Caramori), christiane.horn@ufsc.br (C. Fernandes).

https://doi.org/10.1016/j.molstruc.2022.133380
0022-2860/

T Nayeri and co-workers reported a possible relationship between *T.gondii* and spontaneous abortion [4].

In general, the treatment of toxoplasmosis uses a combination of sulfadiazine (SDZ^-) and pyrimethamine (PYR). [5–7] However, recent debates and studies have described many drawbacks related to this medication such as drug intolerance [8], malabsorption and side effects, especially during long-term use. Both drugs can control this disease in the acute phase but do not show good synergistic behavior for chronic patients because cysts and inactive etiologic agents are not eliminated by these drugs [9]. Side effects can lead to the temporary or permanent suspension of therapy, or reduction of dosage, depending on the extent of the damage caused by the use of SDZ^- and PYR [10].

Sulfadiazine, a sulfonamide antibiotic, is a competitive inhibitor of the bacterial enzyme dihydropteroate synthetase (DHPS), in bacteria and in some protozoa. This is an essential enzyme in the biosynthesis of dihydrofolate in microorganisms and plants, and is sequentially involved in the folate pathway of nucleic acids. Mammals get folate from their diet, but bacteria must synthesize this vitamin. Folate synthesis is obtained from the reaction between DHPP (7,8-dihydropterin pyrophosphate) and PABA (p-aminobenzoic acid), which is catalyzed by DHPS. Sulfa antibiotics work because they fit into the DHPP active site and take PABA's place [11].

Our group has been developing coordination compounds and investigating the anti-toxoplasma activity *in vitro* [12–14]. In 2017, we reported anti-toxoplasma activity of two copper(II) complexes and ultrastructural analyzes [14]. These complexes had also exhibited relevant antitumoral activity, reported previously [15]. Both complexes, which do not present SDZ^- coordinated to the copper(II) center, irreversibly control the growth of the parasite *T. gondii in vitro*, resulting in IC_{50} values of 3.57 and 0.78 μmol L^{-1}, respectively, after 48h of incubation. It was observed that these compounds induce conversion of part of the parasites from the tachyzoite form to bradyzoite, with their subsequent death. The comparison between the IC_{50} values for the compounds under investigation indicates better efficiency when compared with SDZ^- alone, suggesting an effect of the nature of the metal and the ligand on the anti-toxoplasma activity. Zinc and iron(III) complexes, containing SDZ^- coordinated to the metal center, also exhibited anti-toxoplasma activity *in vitro* [16,17].

Recently, Y. Deng and co-workers reported in a review the design, synthesis and screening of more than 100 compounds, as anti-Toxoplasma drugs [18] The authors pointed out that the potency of transition metal complexes against *T. gondii* has not been explored. Therefore, we report herein the results obtained by the utilization of Energy Decomposition Analysis (EDA) to evaluate the strength and to shed light on the physical nature of the M–L bonding in two situations: i) when transition metal cations as Cu(II), Fe(III) and Zn(II) interact with the N,O-donor groups present in the ligand HL1 (N-2[(pyridine-2-ylmethyl)amino)ethanol), resulting in the starting complexes; ii) when the starting complexes interact with the anion SDZ^-. So, these results can guide us to carry out the more favorable reactions.

Thus, aiming to synthesize new coordination complexes with the anion SDZ^-, reactions between complexes $[Cu(HL1)Cl_2]$ **(1)** [19], $[Fe(HL1)Cl_3]$ **(2)**, and $[Zn(HL1)Cl_2]$ **(3)** [20] and NaSDZ were carried out. We present herein a new complex $[Zn(HL1)(SDZ)Cl]\cdot 2H_2O$ **(6)**, which was characterized by ^1H NMR, ESI(+)-MS and X-ray diffraction studies. DFT findings support our experimental data. In addition, initial results of the anti-toxoplasma activity of these complexes are presented.

2. Experimental

2.1. Materials and methods

The ligand and their respective complexes were synthesized using commercial grade reagents. UV-Vis, electrochemical and ESI-(+)-MS investigations were carried out employing spectroscopic, HPLC or MS grade solvents. All chemicals and reagents were purchased from Sigma-Aldrich and used as such. ^1H and ^{13}C NMR spectra were recorded with NMR AS 400 spectrometer. Chemical shifts (δ) are given in ppm, and the spectra were recorded in deuterated solvents, as indicated. TMS (0 ppm) was employed as standard. The elemental analysis (CHN) for the complexes was performed with a Perkin Elmer 2400 CHN analyzer. Infrared spectra were recorded with a Shimadzu FT-IR 8300 spectrophotometer. The solid samples were prepared in a KBr pellet and the spectra were recorded over the frequency range of 400-4000 cm^{-1}. UV-Vis spectra of the ligands and complexes were recorded in DMSO, in a UV-Vis Varian, Cary 50 Bio. Full scan mass spectra (MS mode) were obtained with a MicroTOF LC Bruker Daltonics spectrometer equipped with an electrospray source operating in positive ion mode. Samples were dissolved in a $MeOH/H_2O$ (50/50) solution and were injected into the apparatus by direct infusion. The determination of melting points was made in the Microquimica MQAPF – 307 apparatus. The electrical conductivity of a 1×10^{-3} mol dm^{-3} solution of each complex was measured with a MS Tecnopon mCA-150 apparatus. Cyclic voltammograms (CVs) were carried out with an Autolab PGSTAT 10 potentiostat/galvanostat in acetonitrile containing 0.1 mol dm^{-3} tetrabutylammonium perchlorate ($TBAClO_4$) as supporting electrolyte under argon atmosphere at room temperature. The electrochemical cell employed was a standard three-electrode configuration: a glassy carbon working electrode, a platinum wire auxiliary electrode and a commercial Ag/AgCl electrode immersed in a salt bridge containing 0.1 mol dm^{-3} $TBAClO_4$. The formal potential of the ferrocenium/ferrocene couple was 0.426 V *vs* the reference electrode Ag/AgCl, being established as 0.400 V *vs* NHE [21]. Single-crystal X-ray diffraction data were carried out with a Bruker D8 Venture diffractometer equipped with a Photon 100 detector, Incoatec microfocus Montel optic X-ray tube with Mo-Kα radiation ($\lambda = 0.71073$ Å) or Ag-Kα radiation ($\lambda = 0.56086$ Å). The structures were solved and refined with the SHELX program package [22,23]. Non-hydrogen atoms were refined anisotropically. The molecular structure was drawn with Diamond program (version 4.6.0) [24]. The crystallographic information file (CIF) for the complexes **(2)** and **(6)** were deposited at the Cambridge Crystallographic Data Centre (CCDC) under identification number 2095336–2095337, respectively. These data can be obtained free of charge via http://www.ccdc.cam.ac.uk/conts/retrieving.html (or from the Cambridge Crystallographic Data Centre, 12, Union Road, Cambridge CB2 1EZ, UK; fax: +44 1223 336033). Crystal data and more details of the data collection and refinement of the complexes **(2)** and **(6)** are provided in Table 1S (supporting information material). The Mössbauer spectroscopy of ^{57}Fe was performed at room temperature in transmission geometry. The spectra were taken with the Co-57 Rh-matrix source and the powdered sample maintained at the same temperature, moving in a sinusoidal mode. The isomer shift (δ) values are in relation to metallic iron. All the spectra were fitted with only one paramagnetic component (doublet) and the quadrupole splitting ΔEQ, isomer shift δ, the linewidth Γ and the absorption area were the free fitting parameters. Electron Paramagnetic Resonance (EPR) spectra were obtained using a Bruker EMX micro-9.5/2.7/P/L system using

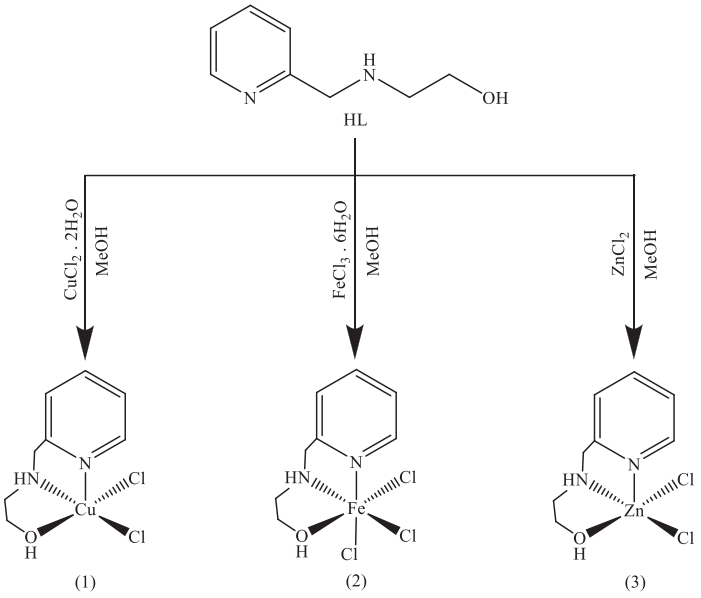

Scheme 1. Synthetic route of complexes **(1), (2)** and **(3).**

Table 1
Selected bond lengths [Å] and angles [°] for complexes **(2)** and **(6)**.

[Fe(HL)Cl_3] **(2)**		[Zn(HL)(SDZ)Cl]·$2H_2O$ **(6)**	
Bond lengths		Bond lengths	
Fe1–N1	2.149(3)	Zn1–N3	2.031(2)
Fe1–O1	2.164(3)	Zn1–N1	2.096(2)
Fe1–N2	2.186(3)	Zn1–N2	2.115(2)
Fe1–Cl3	2.262(2)	Zn1–O1	2.220(2)
Fe1–Cl2	2.266(2)	Zn1–Cl1	2.2922(11)
Fe1–Cl1	2.349(2)	S1–N5	1.581(2)
Angles		S1–O2	1.4491(17)
N1–Fe1–O1	82.68(13)	S1–O3	1.4553(17)
N1–Fe1–N2	77.54(13)	Angles	
O1–Fe1–N2	75.00(13)	N3–Zn1–N1	143.00(8)
N1–Fe1–Cl3	94.76(11)	N3–Zn1–N2	101.17(8)
O1–Fe1–Cl3	87.97(11)	N1–Zn1–N2	80.47(8)
N2–Fe1–Cl3	161.99(8)	N3–Zn1–O1	88.97(8)
N1–Fe1–Cl2	90.79(11)	N1–Zn1–O1	78.16(8)
O1–Fe1–Cl2	166.18(7)	N2–Zn1–O1	155.50(8)
N2–Fe1–Cl2	91.74(11)	N3–Zn1–Cl1	104.61(6)
Cl3–Fe1–Cl2	104.76(8)	N1–Zn1–Cl1	111.54(7)
N1–Fe1–Cl1	165.78(8)	N2–Zn1–Cl1	99.93(6)
O1–Fe1–Cl1	89.23(10)	O1–Zn1–Cl1	98.95(6)
N2–Fe1–Cl1	89.11(11)	O2–S1–O3	113.22(11)
Cl3–Fe1–Cl1	96.62(8)	O2–S1–N5	113.26(11)
Cl2–Fe1–Cl1	94.51(8)	O3–S1–N5	112.99(11)

a highly sensitive cylindrical cavity, operating in X-band (9 GHz), at 120 K, with 5 mW microwave power, 5 G modulation amplitude and 100 kHz modulation frequency. The spectra were simulated using the Qpow program and a MgO:Cr(III) (g = 1.9797) marker.

2.2. Synthesis

2.2.1. Synthesis of the ligand

The ligand HL1 (N-2[(pyridine-2-ylmethyl)amino)ethanol)) was synthesized and characterized as previously described by us, in 2014 [20]. In order to obtain high purity grade, to perform NMR analysis of the zinc(II) complexes, with and without SDZ^- anion, the ligand was purified using silica chromatographic column and chloroform as eluent, increasing the polarity slowly, until 20% of EtOH, to obtain the ligand HL1 as a pure light yellow oil. Yield: 80%. This ligand was employed in the synthesis of new coordination compounds of Cu(II), Fe(III) and Zn(II), as shown in Scheme 1.

2.2.2. Synthesis of complexes [Cu(HL1)Cl_2] (1), [Fe(HL1)Cl_3] (2) and [Zn(HL1)Cl_2] (3)

The synthesis of complexes **(1)-(3)** is described in Scheme 1. Complex **(1)**, was obtained through a reaction between the ligand HL1 (1 mmol, 152 mg) and $CuCl_2{\cdot}2H_2O$ (1 mmol, 170 mg) in methanol, resulting in a blue microcrystalline solid. Yield: 230mg (82%). m.p.: 175°C. Anal. Calcd for $C_8H_{12}Cl_2CuN_2O$; MW = 286.64g.mol^{-1}: C, 33.52; H, 4.21; N 9.77. Found: C, 33.66; H, 4.19; N, 9.60. Complex **(2)**, was obtained by reacting 1 mmol (152 mg) of the ligand HL1, with $FeCl_3{\cdot}6H_2O$ (1 mmol, 270 mg) in methanol, under reflux. Light yellow crystals were obtained after a few days. Yield: 87 mg (26%). m.p.: 240°C. Anal. Calcd for $C_8H_{12}Cl_2FeN_2O$; MW = 314.5 g.mol^{-1}: C, 30.55; H, 3.84; N 8.94. Found: C, 30.53; H, 3.83; N, 8.94. Complex **(3)**, was obtained as previously described as colorless crystals [20]. Yield: 280mg (65%). This complex was characterized by elemental analysis and melting point determination in order to attest its purity. m.p.: 173°C (literature: 175°C). Anal. Calcd for $C_8H_{12}Cl_2ZnN_2O$; MW = 288.48 g.mol^{-1}: C, 33.31; H, 4.19; N 9.71. Found: C, 33.47; H, 4.21; N, 9.98.

Crystal data and more details of the data collection and refinement of complex **(2)** are provided in Table 1S.

2.2.3. Synthesis of complexes containing SDZ^- anion: [Zn(HL1)(SDZ)(Cl)].2H2O (6)

Complex **(6)**, was obtained through a reaction between complex **(3)** (1 mmol, 288 mg) and NaSDZ (1 mmol, 270 mg). The reactins between complexes **(1)** and **(2)** with NaSDZ were ineffective and then complexes **(4)** and **(5)** were not obtained. Scheme 2 describes the synthetic route employed. An aqueous solution of NaSDZ was added to a methanol/water solution (8:2) of the complex **(3)** and then refluxed at 65°C for 2 h. Colorless crystals were obtained. Yield.: 140 mg (50%). m.p.: 255°C. Anal. Calcd for $C_{18}H_{25}ClN_6O_5SZn$, MW = 503.30g.mol^{-1}: C, 40.16; H, 4.68; N 15.61. Found: C, 40.08; H, 4.68; N, 15.38. Crystal data and more details of the data collection and refinement of complex **(6)** are provided in Table 1S.

2.3. Computational Methods

The structures obtained were previously optimized using semi-empirical xTB(extended Tight Binding) [25,26], developed by

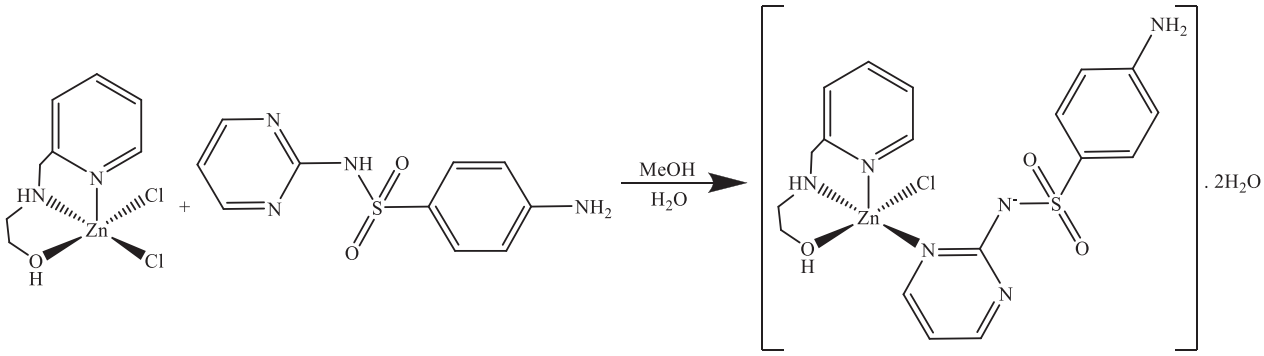

Scheme 2. Synthetic route of complex **(6)**, a Zn(II) complex containing the anion SDZ^{-}.

Grimme et al [27], the parameters are incorporated considering essential physics to describe properties of interest, at GFNn-xTB level of theory. Then, conformational searches based on pre-optimized geometries were performed with CREST (Conformer-Rotamer Ensemble Sampling Tool), an utilitary of xTB, using iMTD-GC, an extensive metadynamics selection (MTD) and an additional GC step at the end of the calculation [28]. These calculations had been performed to find a better arrangement to the complex in which the input structure of DFT optimization could converge more easily, even though the complexes reported herein are compounds with so many degrees of freedom and coordination forms. That is, with stable conformational geometries, the interaction sites of interaction between ligands and the metal must be clearly obtained.

The lowest energy conformers were then optimized using Density Functional Theory [29] (DFT), Generalized Gradient Approximation (GGA) [30] for exchange and correlation (BP86 basis set) with a ZORA-def2-TZ2P (Zero Order Regular Approximation) [31] for relativistic corrections. The most stable electronic states were determined for complexes containing copper(II) (complexes **(1)** and **(4)**) and iron(III) (complexes **(2)** and **(5)**). For Cu(II) the most stable electronic state is a doublet. In the case of complexes containing Fe(III), two different electronic states (doublet and sextuplet) have been taken into account. All calculated geometries have been confirmed to correspond to minima on the potential energy surface by the absence of imaginary eigenvalues in the hessian matrix. Hartree-Fock geometry optimizations and DLPNO-CCSD(T) [32,33] single-points calculations were applied, with the same basis set as used in DFT calculations [34], to verify geometries and energy values attributed to compounds **(1)-(6)** from DFT.

The metal-ligand bonding situations were analyzed in the light of canonical EDA (Energy Decomposition Analysis), as implemented in ADF (Amsterdam Density Functional) code [35], by employing the same functional BP86 (Becke Perdew) and a triple-zeta quality Slater-type basis set, TZ2P. Hirshfeld charges of ligands and transition metal cations were also determined. The EDA is a quantitative analysis, developed by Ziegler and Rauk to classify the interactions between two or more interacting fragments, with chemical predictability. The total interaction energy, ΔE^{int}, is decomposed according to Eq. (1):

$$\Delta E^{\text{int}} = \Delta E^{elstat} + \Delta E^{Pauli} + \Delta E^{orb} + \Delta E^{disp} \quad (1)$$

where ΔE^{elstat} is a quasiclassic electrostatic interaction between the densities of fragments with a fixed charge, ΔE^{Pauli} is a repulsion generated by electron of the same spin moment, ΔE^{orb} orbital interactions between occupied and empty states of each fragment, which, as consequence also include polarization effects. The ΔE^{disp} is the dispersion contribution, obtained when dispersion corrected density functionals are employed.

The EDA decomposes the interaction energy, which is the instantaneous interaction energy between two or more prepared fragments (A and B), considering that A and B are fragments of the same compound. Parameters like geometries and electronic states for A and B, are the same as those found in the compound AB. Therefore, the instantaneous interaction energy is given by (Eq. (2)).

$$\Delta E^{\text{int}} = E^{AB} - (E^{A} + E^{B}) \quad (2)$$

Since chemical bonds, or bonding interactions are not physical observables, it becomes crucial to access some experimental quantity, capable of providing binding strength; in this case, the bonding dissociation energy, ΔE^{tot} (Eq. (3)). It is intuitive that adding the energies of interaction ΔE^{int} and preparation ΔE^{prep}, the opposite of ΔE^{tot} is obtained, which can also be determined experimentally. The latter is given by the sum of the differences between electronic energies of the prepared E^{i} and relaxed fragments E^{i}_{o} (isolated) (Eq. (4)).

$$-\Delta E^{tot} = \Delta E^{\text{int}} + \Delta E^{prep} \quad (3)$$

$$\Delta E^{prep} = E^{A} - E^{A}_{o} + E^{B} - E^{B}_{o} = \sum_{i}^{n} \left(E^{i} - E^{i}_{o}\right) \quad (4)$$

2.4. In vitro *investigations of anti-toxoplasma activity*

Complexes and sodium sulfadiazine. For *in vitro* studies, complexes **(1), (2), (3)** and **(6)** were dissolved in RPMI 1640 medium (aqueous medium), and then stored at -22°C. NaSDZ (Sigma), used as positive control of experiments, was solved in distilled water and stored a -22°C.

Toxoplasma gondii. Tachyzoites used in this study were from the virulent RH strain of *T. gondii*, maintained via intraperitoneal infections of Swiss mice. After 48 h of infection, the parasites were collected by a peritoneal wash with phosphate-buffered saline (PBS), pH 7.2, and then centrifuged at 1000 g for 10 min. The pellet was washed with PBS and RPMI-1640 medium. The parasites were used within 30 - 40 min of their removal from the peritoneal cavity. All animal studies were reviewed and approved by the ethics committee of animal use of the UENF (Universidade Estadual do Norte Fluminense, code: 318).

Culture of LLC-MK2 cells. The LLC-MK2 kidney epithelial cells (Rhesus monkey, *Macaca mulata*) were grown in 25 cm^2 culture flasks (SPL Life Sciences) containing RPMI 1640 medium supplemented with 10% fetal bovine serum (FBS) at 37°C in a 5% CO_2 atmosphere. Infection by the parasite was conducted in subconfluent cultures in flasks or over coverslips in 24-well tissue culture plates (SPL Life Sciences).

Anti-proliferative assays. These studies were performed as described by us, in the literature [17].

Light microscopy imagens of Giemsa-stained LLC-MK2 cells infected with T. gondii. After methanol fixation, cells were washed, stained with Giemsa (diluted in distilled water), dehydrated in a series of acetonexylene solution, mounted on Entellan and observed under Fig. 14. Results are from two independent experiments with 6 animals per group, obtained at optical microscope Axioplan-ZEISS. Images were captured with an MRc5 AxioCam digital camera and processed with the Axiovision program.

3. Results and discussion

The starting complexes ((**1**)-(**3**)), due to the presence of labile ligands (chloro) or free coordination position, were selected to react with the current drug (anion sulfadiazine SDZ^-) to obtain complexes with this active molecule, aiming to investigate their anti-toxoplasma activity.

The reaction between complex **(3)** and the drug NaSDZ has resulted in complex **(6)**, a new complex, which was obtained as colorless crystals: $[Zn(HL1)(SDZ)Cl]\cdot 2H_2O$. This complex presents one SDZ^- anion coordinated to the Zn(II) center by the N atom of the pyrimidine ring.

Although DFT data suggested that complexation reactions between complexes **(1), (2)** and **(3)** (starting materials) and sodium sulfadiazine (NaSDZ) lead to the formation of stable complexes, the reactions between complexes **(1)** and **(2)** and NaSDZ resulted in a mixture of complexes and low yields. As the reactions between complexes **(1)** and **(2)** and SDZ were ineffective, as well as the complete characterization of these complexes, we report herein only the complexation of complex **(3)** and SDZ^-, which resulted in complex **(6),** which was obtained as colorless crystals and characterized by X-ray diffraction, ESI(+)-MS and ^1H NMR analysis.

For complex **(6)**, where the X-ray structure is available, the direct comparison between the X-ray crystal and DFT calculated structures shows that the calculations are in close agreement. Therefore, the calculations are expected to reliably characterize the coordination spheres for complexes with and without the anion SDZ^-. All four complexes reported herein ((**1**), **(2), (3)** and **(6)**) are stable in air and soluble in polar solvents such as water, DMF, DMSO and slightly soluble in CH_3CN, ethanol, MeOH and chloroform. Preliminary anti-toxoplasma studies were carried out in aqueous medium.

3.1. Description of crystal structure of complexes (2) and (6)

3.1.1. Description of crystal structure of complexes (2) and (6)

The single-crystal X-ray data obtained for complex **(2)** reveals the formation of a mononuclear hexacoordinated iron(III) complex containing a molecule of HL1 ligand and three chloride anions: $[Fe(HL)Cl_3]$. The molecular formula is $FeC_8H_{12}Cl_3N_2O$ with a molecular weight of 314.4 $g\cdot mol^{-1}$. The crystallographic data for complex **(2)** are presented in Table 1S and the most relevant bond lengths and angles are shown in Table 1. The molecular structure of the complex **(2)** reveals the formation of a mononuclear iron(III) complex (Fig. 1), which adopts a distorted octahedral geometry. The equatorial positions are occupied by N1, O1, Cl1 and Cl2 atoms, and the axial positions are occupied by N2 and Cl3 atoms. Thus, the Fe(III) ion coordinates to the HL1 ligand via the pyridinic nitrogen atom (N1), aminic nitrogen atom (N2) and by the alcohol group (O1), similarly observed for the Zn(II) complex, reported by us previously [20]. Three chloride anions (Cl1, Cl2 and Cl3) are also bound to the Fe(III) center, resulting in a N_2OCl_3 coordination environment. The bond distances [Å] for the coordination sphere of iron(III) center are: Fe1–N2 = 2.186(3), Fe1–N1 = 2.149(3), Fe1–O1 = 2.164(3), Fe1–Cl1 = 2.349(2), Fe1–Cl2 = 2.266(2), and Fe1–Cl3 = 2.262(2). The two five-membered rings observed in the complex have bite angles of 75.00(13)° in O1–Fe1–N2 and 77.54(13)° for N1–Fe1–N2. The iron atom shows a deviation of -0.2461 Å out of the N1/O1/Cl1/Cl2 equatorial plane.

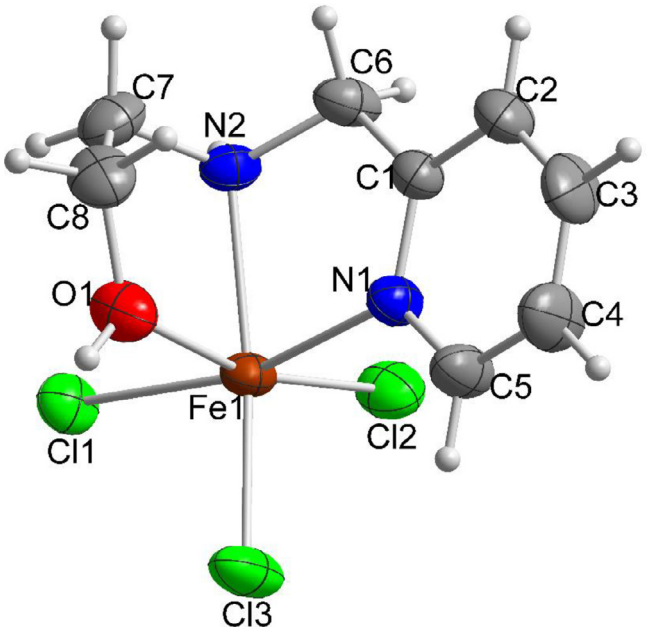

Fig.1. Ellipsoid representations (50% probability) of $[Fe(HL1)Cl_3]$ (**2**), obtained by X-ray crystallography.

The reaction between $[Zn(HL)Cl_2]$ and NaSDZ has resulted in colorless crystals, suitable for crystallographic analysis. A new Zn(II) complex was obtained, showing the presence of SDZ^- anion coordinated to the zinc. A perspective view of complex **(6)** is displayed in Fig. 2. Bond lengths and angles for complex **(6)** are listed in Table 1. The crystallographic data reveals that complex **(6)** consists of a neutral mononuclear zinc(II) complex, which is coordinated to three nitrogen (amine, pyridine and to the pyrimidine ring N atom of SDZ^- anion), one oxygen (alcohol group) and to one chloride anion. The zinc ion is pentacoordinated and the polyhedron around the metal ion can be described as slightly distorted square pyramidal geometry, which is confirmed by the calculation of the τ parameter for five-coordinated metal complexes. The formula used for the calculation is $\tau_5 = (\beta-\alpha)/60°$, resulting in $\tau_5 = 0.21$ [35]. The coordination mode for SDZ^- anion in complex **(6)** is the same previously observed in the complex [(SDZ)Zn(m-BPA)Zn(SDZ)], (BPA^- is the deprotonated ligand HBPA= N-(2-hydroxybenzyl)-N-(pyridin-2-ylmethyl)amine), reported by us in 2015 [16] The pyrimido nitrogen atom is coordinated to the Zn(II) center, in complex (**6**), and the sulfonamidic nitrogen atom is deprotonated. There is one anion chloride coordinated to the Zn(II) center, resulting in a neutral complex.

Similar coordination mode for the SDZ^- anion was reported in the complexes $[Zn(SDZ)_2(H_2O)(NH_3)]$ and $[Zn(SDZ)(Erx)(ErxH)](ClO_4)$, (ERx= enrofloxacin), reported by Tommasino and co-workers, in 2018 [36]. Complex containing both antibiotics (sulfadiazine and enrofloxacin) exhibited greater efficiency toward the bacteria *E.coli, S. aureus* and *E. Faecalis.* In addition, recently, R. P. Dubey reported crystallographic, DFT, antibacterial and antifungal activity of a new octahedral Cd(II) complex, containing sulfadiazine and picoline as ligands: $[Cd(SDZ)_2(PIC)_2]$ [37] Cadmium is coordinated to two sulfonamidic nitrogen atoms, one pyrimido nitrogen atom and two β-picoline molecules via N atoms.

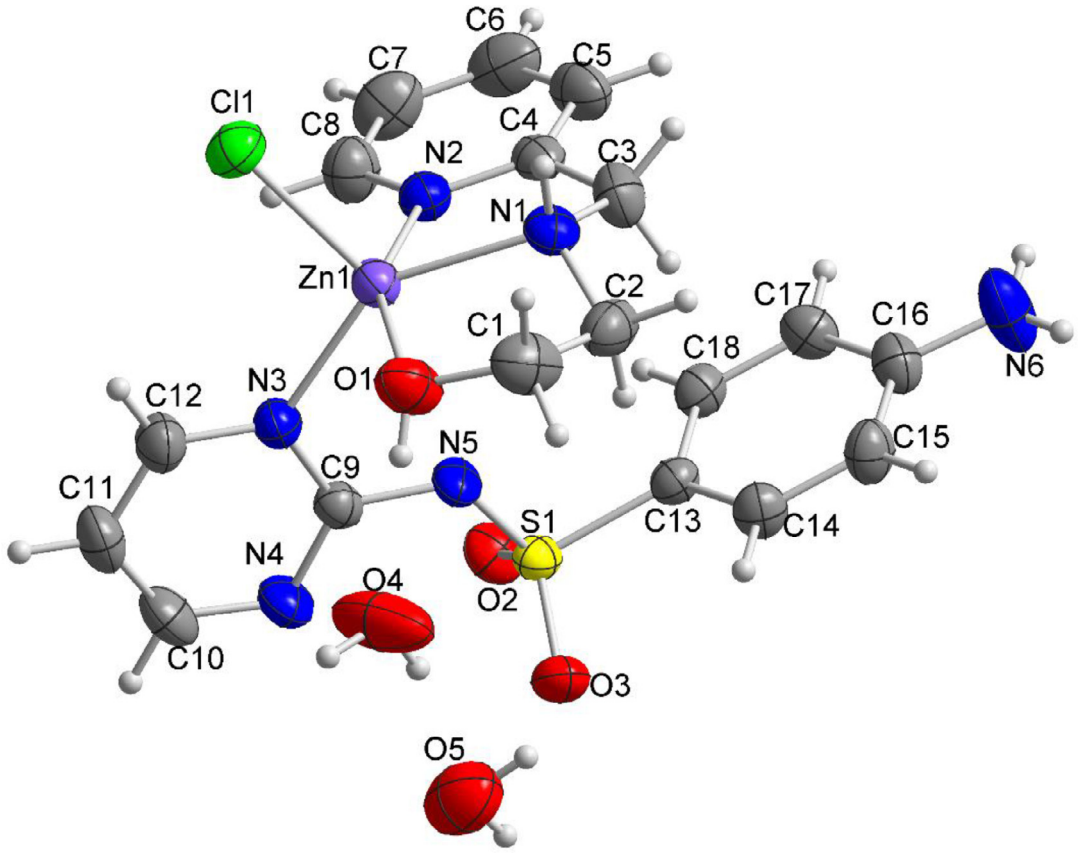

Fig. 2. Ellipsoid representations (50% probability) of [Zn(HL1)(SDZ)Cl]·2H_2O (**6**), obtained by X-ray crystallography.

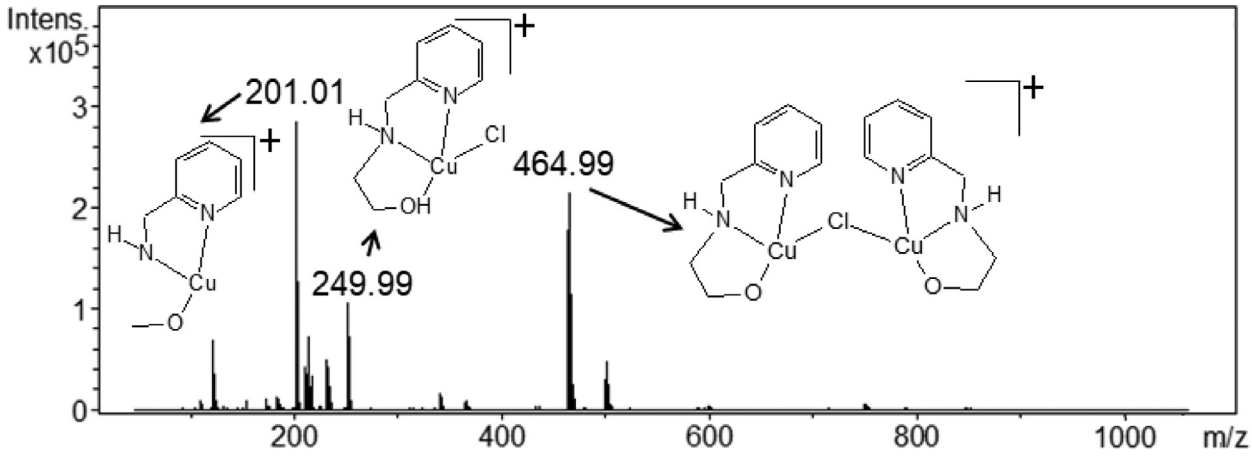

Fig. 3. ESI-(+)-MS in water/methanol (1:1) for complex **(1)**, in H_2O/MeOH (1:1) with proposals of structures for the main peaks observed.

3.2. NMR spectra for Zn(II) complexes (3) and (6)

Figs. 1S and 2S show the ^{1}H NMR and ^{13}C NMR spectra of HL1. The ^{1}H NMR spectra of complex **(3)** (Fig. 3S and Table 2) presents aromatic hydrogens signals (H1, H2, H3 and H4) between 8.57 and 7.50 ppm. A shift to higher ppm values is observed when compared to HL1 (8.49 – 7.24 ppm), this shift can be explained by the coordination of the ligand HL1 with Zn(II). The singlet at 4.00 ppm is attributed to H5 of methylene. The triplet at 2.73 ppm is attributed to H6, which is coupled with H7, also presenting as a triplet (3.45 ppm). The signal at 3.33 ppm is attributed to water from the solvent used in the analysis and another signal at 2.52 is observed, referring to residual protons present in the deuterated solvent. Fig. 4S shows the ^{13}C NMR of complex **(3)**.

Table 2
^{1}H NMR and ^{13}C NMR multiplicity and chemical shift of complex **(3)**.

	Multiplicity (*J*/*Hz*)	δH/ppm	δC/ppm
H1	d (*J*=5.2)	8.51	147.67
H2 and H4	Multiplet	7.51	124.52 and 123.80
H3	td (*J*=7.7, 1.7)	7.99	140.67
H5	Singlet	4.00	58.38
H6	t (*J*=5.4)	2.73	50.57
H7	t (*J*=5.4)	3.45	51.39

The signals shown on ^{1}H NMR spectra of NaSDZ (Fig. 5S and Table 3) are mainly attributed to aromatic hydrogens. H1 and H3 are observed as a duplet at 7.97 ppm, which is a result of coupling

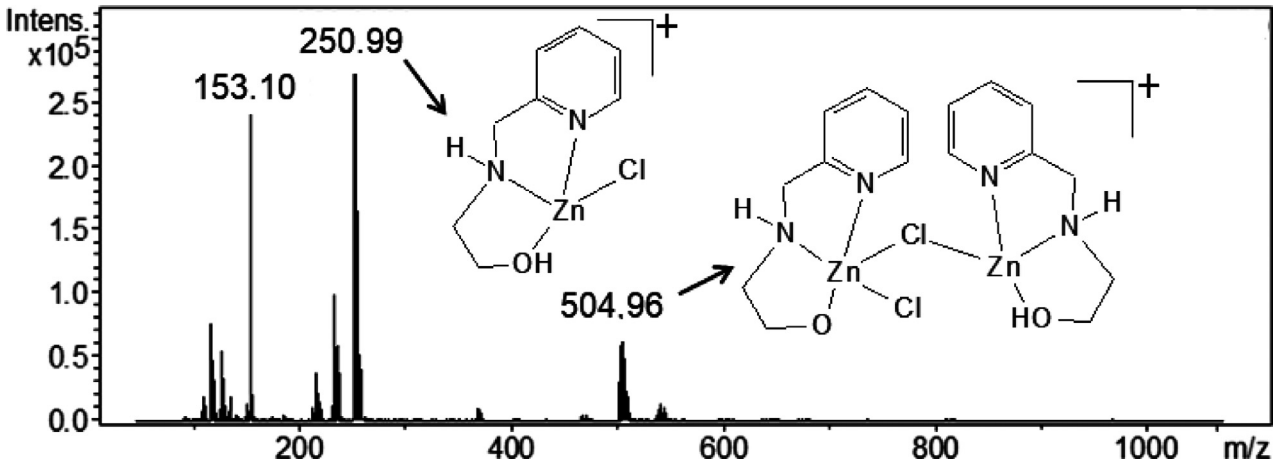

Fig. 4. ESI(+)-MS in water/methanol (1:1) for complex **(3)**, in H_2O/MeOH (1:1) with proposals of structures for the main peaks observed.

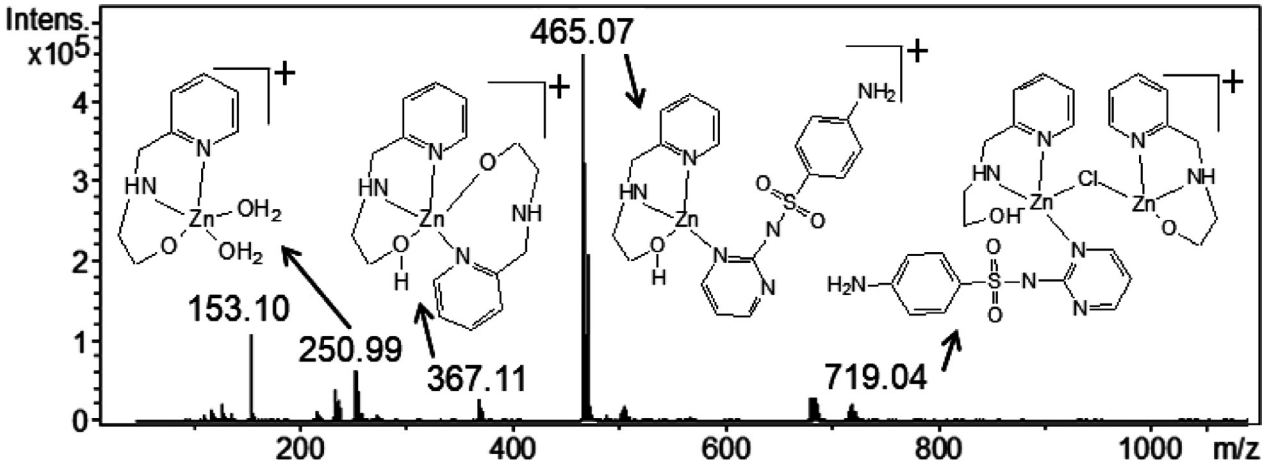

Fig. 5. ESI(+)-MS in water/methanol (1:1) for complex **(6)**, in H_2O/MeOH (1:1) with proposals of structures for the main peaks observed.

Table 3
^{1}H NMR and ^{13}C NMR multiplicity and chemical shift of NaSDZ.

	Multiplicity (J/Hz)	δH/ppm	δC/ppm
H1 and H3	d (*J*=4,7)	7.97	157.75
H2	t (*J*=4,7)	6.23	109.57
H4 and H4'	Multiplet	7.33	128.66
H5 and H5'	Multiplet	6.31	112.35

Table 4
^{1}H NMR and ^{13}C NMR multiplicity and chemical shift of complex **(6)**.

	Multiplicity (J/Hz)	δH/ppm	δC/ppm
H1, H3	d (J = 4.9)	8.25	158.36
H2	t (J = 4.91)	6,64	111.5
H4	d (*J* = 8.31))	7,23	129.36
H5	d (*J*=8.41)	6,30	112.27
H7	d (J = 5.02)	8.51	147.85
H8	Multiplet	7.47	124.43
H9	d (*J*=7.76, 7.77, 1,74))	7.99	140.35
H10	d (*J*=7.89)	7.55	123.65
H11 and H11'	Singlet	4.25	50.49
H12 and H12'	Singlet	2.92	50.99
H13	t (J=5.37)	3.57	58.61

with H2 that is observed as a triplet at 6.23 ppm. Signals at 7.33 and 6.31 ppm are attributed to H4 and H5 respectively. The signal at 3.33 ppm is attributed to water from the solvent used in the analysis and another signal at 2.52 is observed, referring to residual protons present in the deuterated solvent.

^{1}H NMR spectrum of complex **(6)** shows well defined signals typical of the compound **(3)** and SDZ^- (Fig. 5S and Table 4), with just one more signal due to the splitting of H8 and H10, that now appears at 7.47 and 7.55 (multiplets), respectively. The broad signal (duplet) at 8.51 ppm is attributed to H7. At 8.25 ppm a duplet is observed, referring to H1 and H3, which are coupled with H2, shown in the spectra as a triplet (6.64 ppm). The triplet observed at 7.99 ppm is attributed to H9. H4 and H4'' are coupling with H5 and H5', which can be observed as duplets in 7.23 and 6.30 respectively. The signals referring to amine hydrogens were observed at 5.50 ppm, while the signals for aliphatic hydrogens (H11, H12 and H13) were observed at 4.25, 2.92 and 3.57 ppm respectively. The signal at 3.33 ppm is attributed to water from the solvent used in the analysis and another signal at 2.52 is observed, referring to residual protons present in the deuterated solvent. Fig. 6S shows ^{13}C NMR spectra of anion SDZ^- and complex **(6)**.

In order to detect any changes in the structures of complex **(6)**, in solution, ^{1}H NMR spectra were obtained, after 0, 24 and 48h (Fig. 5S). Thus, it can be concluded that the structure of compound **(6)** is maintained in solution. This confirms that, at the time of 48h, the sulfadiazine anion remains coordinated to the metallic center.

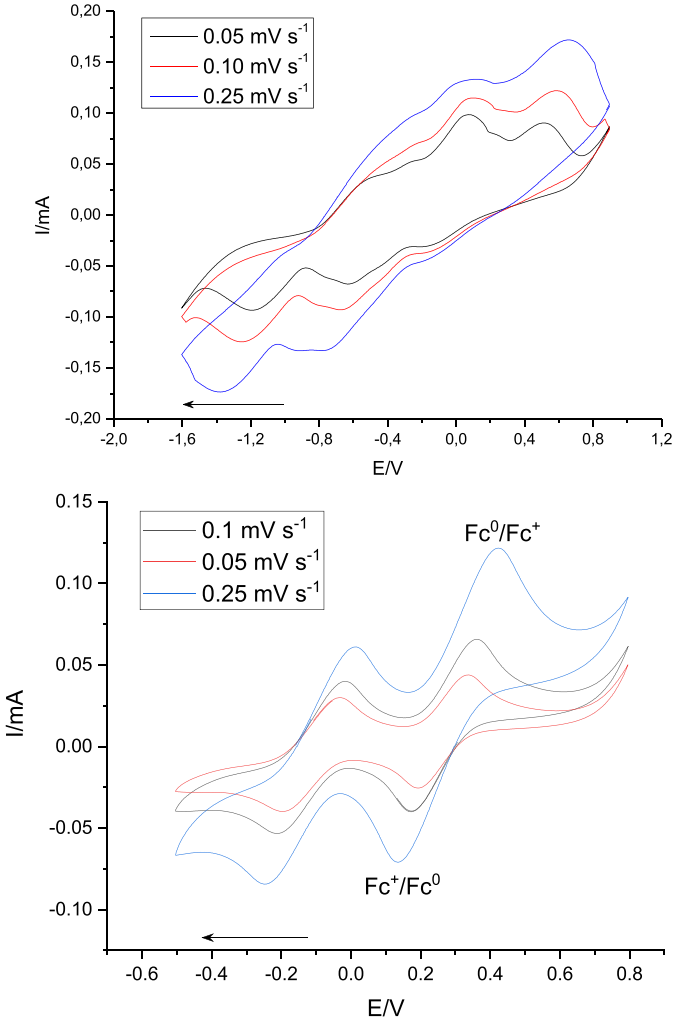

Fig. 6. Cyclic voltammogram of complexes **(1)** (top) and **(2)** (bottom) respectively. Working electrode: platinum. Pseudo-reference electrode: Ag/Ag^{+}. Counter electrode: platinum. Support electrolyte: tetrabutylammonium hexafluorophosphate 0.1 $mol.dm^{-3}$. Solvent: DMSO. Internal reference: Fc/Fc^{+}.

3.3. Spectroscopic characterization: Infrared and electronic spectroscopies

IR spectra for complexes **(1), (2)** and **(3)** shows similar bands: 3427, 3356 and 3411 (νOH), 3180, 3251 and 3229 (νNH), 3123, 3107 and 3072 (νCHarom), from 2985 to 2890 (νCH_2), from 1610 to 1440 ($\nu C{=}C_{py}$, $C{=}N_{py}$),1285, 1289 and 1297 (νC-O), 1100, 1091 and 1102 (νC-N), 769, 767 and 781 cm^{-1} (δCH) respectively. IR spectra of complexes **(1), (2), (3), (6)** and NaSDZ are presented in Figs. 7 and 8S. The drug sulfadiazine exhibits characteristic absorptions related to the amino group (NH_2), pyrimidine (N heterocyclic) and sulfonamide oxygen (SO_2). The IR spectrum of NaSDZ presents the amino group $\nu as(NH_2)$ and $\nu sy(NH_2)$ at 3419 and 3300 cm^{-1}, the group $\nu as(SO_2)$ and $\nu sy(SO_2)$ appear at 1326 and 1157 cm^{-1} and ν(N-S) at 995 cm^{-1}. IR spectrum of complex **(6)**, which contains SDZ^{-} coordinated to the Zn(II) center, presents characteristic IR bands assignments of SDZ^{-}. Most of the absorption bands observed in complex **(6)** are displaced to higher wavenumbers compared to the NaSDZ spectrum. The $\nu as(SO_2)$ and $\nu sy(SO_2)$ appear at the same region in complex **(6)** suggesting that the sulfonamide oxygen is not taking part in the coordination with the metal. The band for (N-H) group is absent in complex **(6)**, confirming the deprotonation of the $-SO_2NH-$ moiety in complex **(6)** as well as in the NaSDZ. Electronic spectra for complex **(1)**, presents a transition at 704 nm (ε= 120 L mol^{-1} cm^{-1}), attributed to d-d transitions of Cu(II), a transition at 283 nm (ε= 5811 L mol^{-1} cm^{-1}), attributed to LMCT Cl → Cu(II), and a transition at 267 nm (ε= 6574 L mol^{-1} cm^{-1}) attributed to intraligand π-π^{*}. Complex **(2)** presents two transitions at 328 and 264 nm (ε= 2227 and 3563 L mol^{-1} cm^{-1} respectively), attributed to LMCT Cl → Fe(III) and intraligand π-π^{*}, respectively. The electronic spectra for complexes **(1)** and **(2)** are displayed in Figs. 9 and 10S.

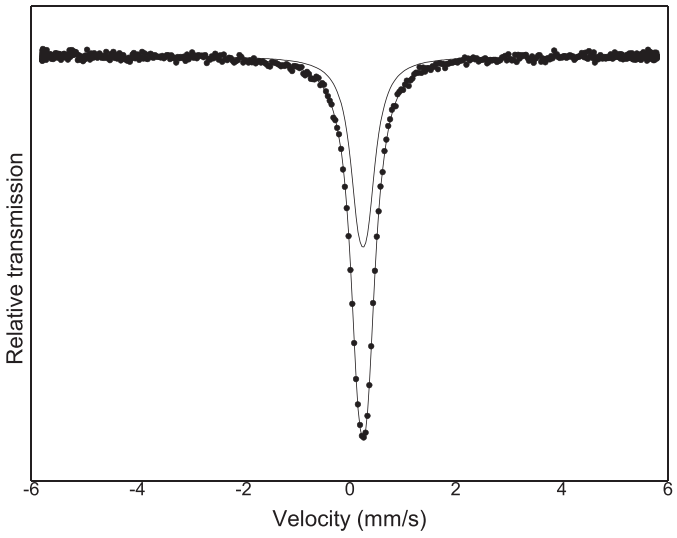

Fig. 7. Mössbauer spectrum of complex **(2)**, at 298K.

3.4. ESI(+)-MS and ESI(+)-MS/MS

ESI-(+)-MS data for complex **(1)** and **(3)** indicates the presence of mononuclear and binuclear species in $MeOH/H_2O$ (1:1) solution. Complex **(2)** did not show peaks corresponding to the metallic complex, only to the ligand HL1, which can be explained by the low solubility of the complex in the solvents used and also by its neutral charge. Figs. 3-5 present the ESI(+)-MS spectra of complexes **(1), (3)** and **(6)**.

ESI(+)-MS spectrum of complex **(2)** presents peaks at *m/z* 249 and at *m/z* 469, corresponding to the cations with composition $[Cu(HL1)Cl]^{+}$ and $[Cu(L)(\mu\text{-}Cl)Cu(L)]^{+}$, respectively. For complex **(3)**, the main peaks are attributed to the cations $[Zn(HL1)Cl]^{+}$ at *m/z* 250.99 and $[Zn(Cl)(L)(\mu\text{-}Cl)Zn(HL1)]+$ at *m/z* 504.96. Peaks at *m/z* 249.99 (complex **(1)** and 250.99 (complex **(3)** correspond to the proposed structure of these complexes, at solid state, with small divergences due to the ionization of the originally neutral complexes.

ESI-(+)-MS spectrum of complex **(6)** (see Fig. 5) presents a characteristic set of isotopologue ions due to mainly the presence of metal ions. Complex **(6)** presents six cations in $MeOH{:}H_2O$ (1:1) solution, with peaks at *m/z* 153, 233, 251, 367, 465 and 719. The proposal for each peak, based on isotopic distribution is: $[HL1]^{+}$ (*m/z* 153), $[Zn(L)(H_2O)]^{+}$ (*m/z* 233), $[Zn(L)(H_2O)_2]^{+}$ (*m/z* 251), $[Zn(HL1)(L)]^{+}$ (*m/z* 367), $[Zn(HL1)(SDZ)]^{+}$ (*m/z* 465) and $[Zn(HL1)(SDZ)(\mu\text{-}Cl)Zn(HL1)]^{+}$ (*m/z* 719). MS/MS data for the species with *m/z* 719 yields a cation with *m/z* 468 $[(L)Zn(\mu\text{-}Cl)Zn(L)]+$ by the loss of a neutral [HSDZ] (*m/z* 250), and the cation with *m/z* 567 $[(SDZ)Zn(\mu\text{-}Cl)Zn(L)]^{+}$, by the loss of a neutral [HL1] (*m/z* 152).

Figs. 11-25S present the isotopic profile assignments for the main peaks observed in the ESI-(+)-MS and ESI(+)-MS/MS of the ligand HL1, complexes **(1), (2), (3)** and **(6)**.

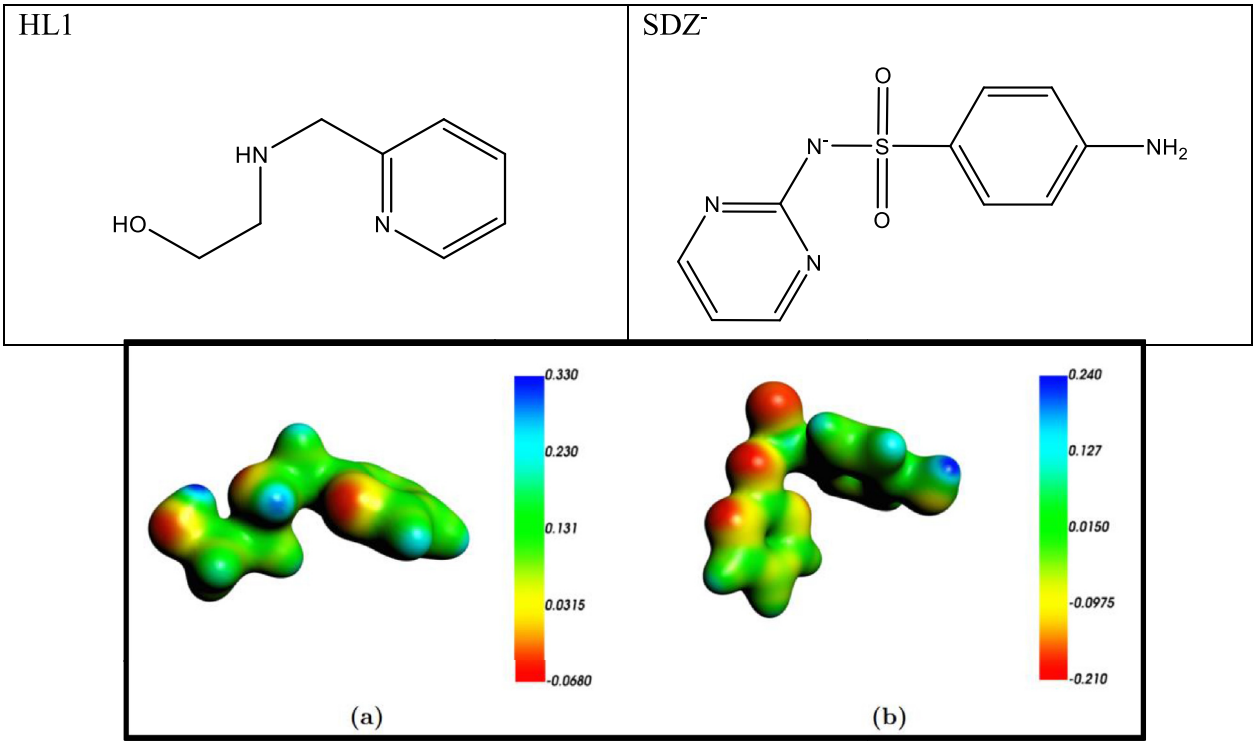

Fig. 8. Molecular electrostatic potential plots of HL1 (a) and SDZ^- (b), scale shown in a.u (hartree). Surface contour value of 0.01 a.u

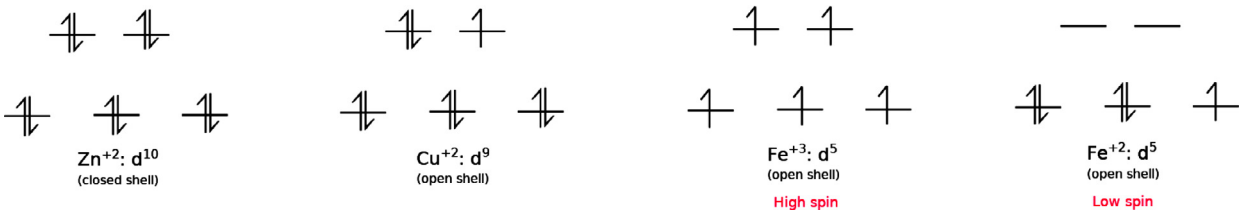

Fig. 9. Scheme of electronic distribution of d orbitals in metallic cations present in the complexes under investigation.

3.5. Characterization of complex (1) by EPR

The EPR spectrum of the complex **(1)** was recorded in frozen CH_3CN solution and at room temperature. The spectrum (Figure 26S) of the copper(II) complex shows typical features of a Cu(II) center, electron configuration $3d^9$, electron spin S = ½ and nuclear spin 3/2. Of the four hyperfine lines expected for the parallel region due to the interaction electron-nuclei, only three are observed. The fourth line is superimposed on the perpendicular component. Such behavior suggests the formation of a compound with square pyramidal geometry [38].

The computational simulation of the EPR spectrum of **(1)**, measured in frozen solution CH_3CN (Figure 26S), was carried out by solving the spin Hamiltonian and afforded $g_{//}$ = 2.27266, $g_{\perp}$ = 2.06766 (g_x = 2.05036, g_y = 2.08497), $A_{//}$ = 16788.5 cm^{-1} and $A_{\perp}$ = 18.8307 cm^{-1} (A_x= 2247.07 cm^{-1}, A_y = 1519.075 cm^{-1}). Such data indicates the presence of a copper(II) center with axial symmetry elongated in the axis z due to Jahn-Teller effect and its ground state is d_{x2-y2}, since $g_{//}>g_{\perp}>2.0023$ and $A_{//}>A_{\perp}$ [39]. The presence of covalent bonds metal-ligand is confirmed by the observation that the $g_{//}$ value is lower than 2.3.

3.6. Electrochemical studies

Conductimetry and cyclic voltammetry were employed for the electrochemical characterization of complexes.

The conductivity measurements of solutions of complexes **(1), (2), (3)** and **(6)**, in DMSO, were obtained for fresh solutions (0 h), and after 24 and 48h, in order to detect any changes in the structures of the complexes, in solution. The values obtained in DMSO indicate that all the complexes are neutral: 28.46, 31.41 and 30.06 μΩ/cm (complex **(1)**), 13.55, 32.80 and 37.01 μΩ/cm (complex **(2)**), 5.77, 6.06 and 5.87 μΩ/cm (complex **(3)**), and 5.89, 6.12 and 6.03 μΩ/cm (complex **(6)**). The range in DMSO for 1:1 electrolyte is 0-46 μΩ/cm. [40] According to X-ray crystal data, complexes **(3)** and **(6)** are neutral in solid state. Thus, these complexes generate some cationic species in DMSO, suggesting that some chloride ions are displaced from the coordination sphere, mainly for complexes **(1)** and **(2)**.

The cyclic voltammetry for complex **(1)** shows two cathodic and two anodic processes at – 0.664 and -1.254 V vs Fc^+/Fc, respectively, in DMSO (Fig. 6). The presence of two cathodic processes can be attributed to two events: i) formation of a hexacoordinated copper(II) complex, due to the coordination of DMSO to the Cu(II) center, in complex **(1)**, resulting in the observed color change from blue to green; ii) formation of cationic species in solution, suggesting the loss of the chloride ligand, resulting in a tetracoordinated Cu(II) complex, as indicated by conductivimetry measurements. Complex **(2)** exhibits one *quasi*-reversible redox process, with cathodic peak at -0.247 and -0.0592 V vs Fc^+/Fc, attributed to the Fe(III)/Fe(II) redox couple (Fig. 6). The presence of only one redox process for complex **(2)** indicates the maintenance

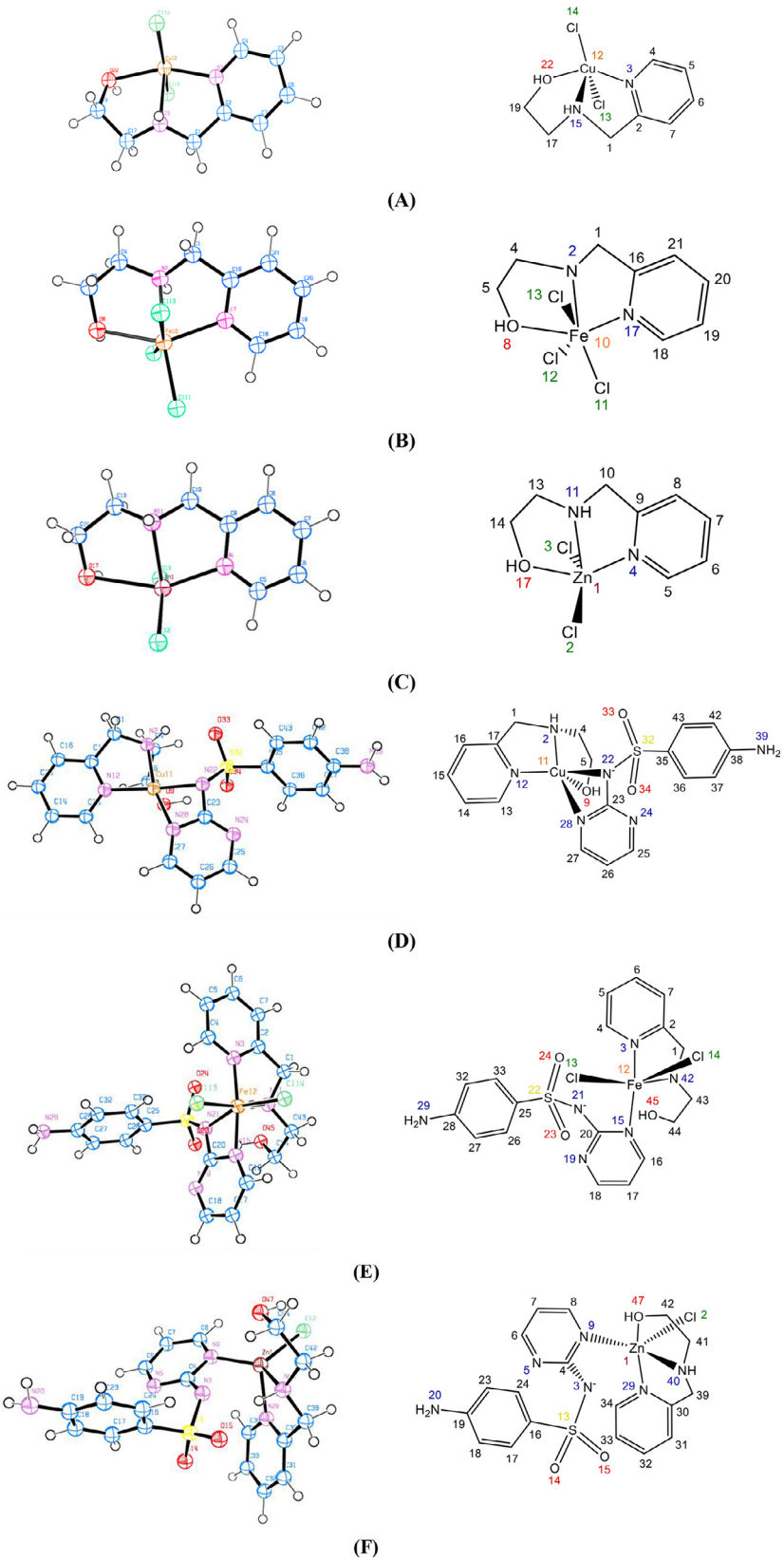

Fig. 10. Optimized structures of complexes **(1)-(6)** at BP86-D3BJ ZORA-TZVP-def2(-f) level of theory, where A) $[Cu(HL1)(Cl)_2]$ **(1)**, B) $[Fe(HL1)(Cl)_3]$ **(2)**, C) $[Zn(HL1)(Cl)_2]$ **(3)**, D) $[Cu(HL1)(SDZ)]^+$ **(4)**, E) $[Fe(HL1)(SDZ)(Cl)_2]$ **(5)** and F) $[Zn(HL1)(SDZ)(Cl)]$ **(6)**, based on data presented in Table 2S.

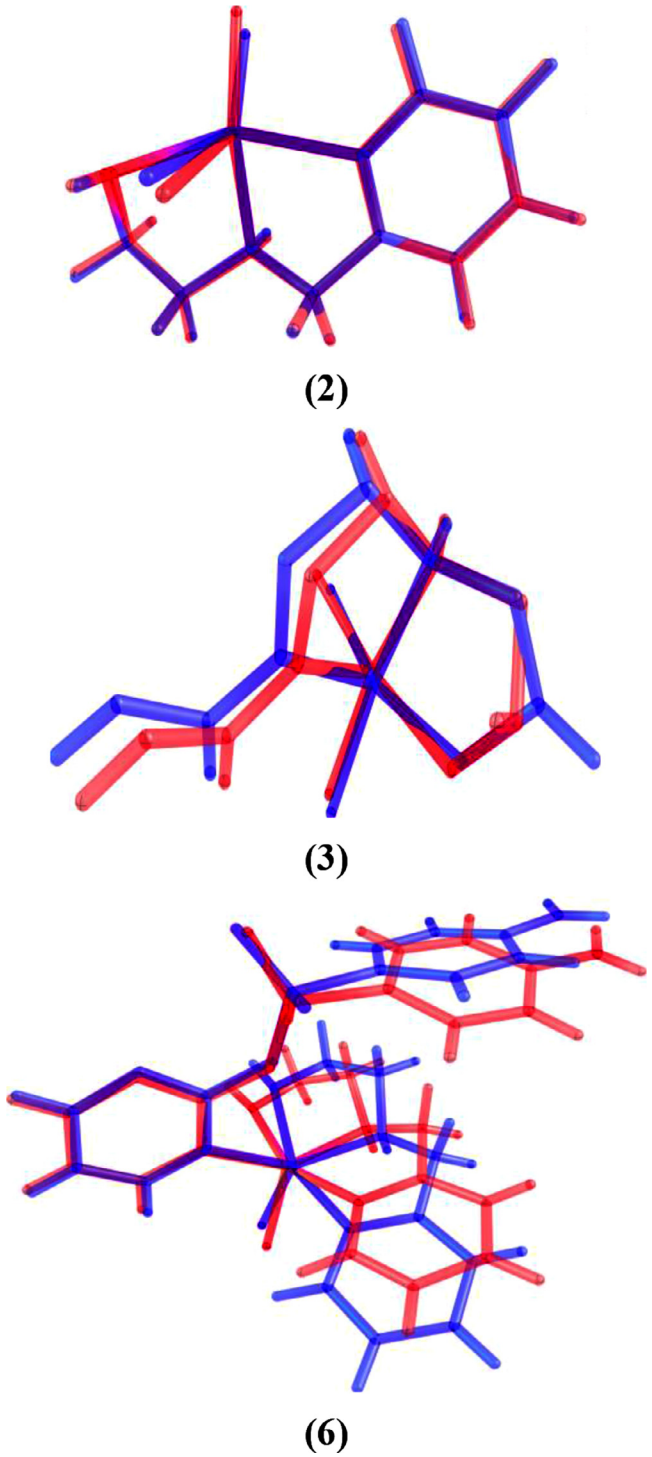

Fig. 11. Superposition between crystallographic data of complexes **(2), (3)** and **(6)** (in red) and DFT optimized geometries (in blue), at BP86-D3BJ ZORA-TZVP-def2(-f) level of theory. Crystallographic data for complexes **(2)** and **(6)** are presented in Tables 1 and 2, Figs. 1 and 2. Structural data for complex **(3)** were reported previously by us [20].

of a mononuclear unit in solution, in accordance with structural data (Fig. 1).

3.7. Mössbauer spectroscopy

The presence of an iron(III) center in complex **(2)** was confirmed by ^{57}Fe Mössbauer spectroscopy. The spectrum is presented in Fig. 7.

The spectrum for complex **(2)** was fitted with a single doublet with parameters δ= 0.365 (relative to alpha-iron) and ΔEq= 0.168 mm/s. The Mössbauer spectrum for complex **(2)** was fitted with a single quadrupole doublet with an isomer shift δ= 0.365 (relative to alpha-iron), a small quadrupole splitting ΔEq= 0.196 mm/s and a linewidth Γ= 0.360 mm/s. The isomer shift parameter is typical of octahedral iron(III) complexes [41]. The average Fe-ligand bond length for complex **(2)** of 2.229 Å (see Table 1) is typical for such bonds where the central ferric ion has a high-spin d^5 electron configuration in a $^6A_1$ ground state [42,43]. As it is well known, the valence electrons belonging to the Mössbauer atom usually make the strongest contribution to the electric field gradient if their charge distribution deviates from spherical symmetry [41]. So, the small quadrupole splitting observed for complex **(2)** reflect the spherical symmetry of the $(t_{2g})^3(e_g)^2$ electron configuration. In this configuration, the valence contribution for the ΔEq is zero and the small value observed for this parameter may arise from the presence of chemically different ligands which produces an inhomogeneous electrical field at the nucleus.

3.8. DFT Calculation

Molecular electrostatic potential surfaces (MEPS) of the ligand HL1 and the anion SDZ^-, which act as ligands in this work, have been plotted in order to identify the most probable coordination sites (Fig. 8). MEPS reveals that the nitrogen atoms in HL1 are less negatively charged than those of the anion SDZ^-. Additionally, HL1 is a tridentate ligand and has an aromatic ring, which makes the electron density more diffuse, besides the presence of a polar hydroxyl group, which is more electronegative than nitrogen. The anion SDZ^- exhibits three coordination points represented in red (N atom form the pyrimidine group- N heterocyclic, oxygen and N atoms from the sulfonamide group) (Fig. 8). Despite the presence of a sulphonamide group (SO_2), the most stable proposed structures for the complexes with Cu(II), Fe(III) and Zn(II) (complexes **(4)-(6)**), do not exhibit any coordination by the oxygen atoms of the sulfonamide group, in good agreement with IR results. The most probable coordination is with the pyrimidine ring N atom of the anion SDZ^-, due the lower hindrance, in this case. In 2015 we reported X-ray data of a zinc(II) complex containing a covalent bond between the metal center and one pyrimidine ring N atom of the anion SDZ^-, as described here for complex **(6)** [16].

Two groups of complexes were considered comparatively, (*i*) the starting complexes formed by the reaction between transition metals ions Cu(II), Fe(III) and Zn(II) and the HL1 ligand [19] (complexes **(1), (2)** and **(3)** [20], and (*ii*) possible complexes obtained from the substitution reaction between the starting coordination compounds (complexes **(1)-(3)**) and the anion SDZ^- (new complexes **(4)-(6)**). The electronic energies (a.u.) of complexes **(1)-(6),** obtained at BP86-D3/TZ2P basis set and DLPNO(CCSD(T)) corrections are displayed in Table 5. They indicate that the stability of the complexes, based on the distribution of the electron in the orbitals. For complex **(3)** the value of electronic energy is -3197.05 hartree or (a.u) or atomic units, considering singlet state and this is the most stable complex. As shown in Fig. 9, Zn(II) cation has closed-shell electronic configuration ($3d^{10}$), while Cu(II) and Fe(III) cations are open-shell systems. The Cu(II) cation ($3d^9$) with an unpaired electron is a doublet state (complexes **(1)** and **(4)**), but Fe(III) cation has two types of possible electronic arrangement, high-spin, with five unpaired electrons (sextuplet) such as complex **(2)**, and low-spin, with one unpaired electron (doublet), such as calculated for complex **(5)**. (Table 5) This changed from high-spin to low-spin, observed for the Fe(III) complexes (**(2)** and **(5)**) should be related to the higher Lewis basicity of the anion SDZ^-, present in complex **(5)**, when compared to the chloro ligand, present in complex **(3)**. The electronic energies calculated for complexes **(1)-**

Table 5
Electronic energies (a.u.) for the structures of complexes **(1)-(6)**, obtained at BP86-D3/TZ2P basis set and DLPNO(CCSD(T)) corrections.

Complex	**2S+1**	DFT	DLPNO-CCSD(T)	**Complex**	2S+1	DFT	DLPNO-CCSD(T)
(**1**)	Doublet	-3058.200	-3051.565	(**4**)	doublet	-3292.002	-3281.567
(**2**)	Doublet	-3141.690	-3135.008	(**5**)	doublet	-3836.080	-3832.039
	Sextuplet	-3141.800	-3135.057		sextuplet	-3836.070	-3832.006
(**3**)	Singlet	-3197.050	-3193.079	(**6**)	singlet	-3920.850	-3915.675

(6), indicate that the most stable configuration for each complex are doublet for complexes **(1), (4)** and **(5)** and sextuplet for complex **(2)**. Based on these values, optimized structures were then obtained. Table 2S presents selected geometric parameters of optimized structures for coordinating bonds observed in complexes **(1)-(6)** (angles (°), bond distances (Å)). DFT and DLPNO-CCSD(T) [44] calculations revealed the same trends for the relative energies, suggesting that the most stable complexes should be those with open-shell electronic states (containing Cu(II) and Fe(III)).

The structural parameters calculated with DFT for complexes **(2), (3)** and **(6)** when compared with the available X-ray diffraction data present good agreement, which attests the quality of the level of theory employed for the study of the complexes considered here.

Optimized DFT structures for complexes **(4)-(6)**, showed in Fig. 10, indicate that the coordination mode for the anion SDZ^- is the same for complexes **(4)** and **(5)**, in which the coordination occurs by the N of the pyrimidine group and by the N of the sulfonamide group, resulting in complexes penta and hexacoordinated, respectively. For complex **(6)** the calculated structure indicates the coordination of the Zn(II) center to only one N atom of the pyrimidine group, resulting in a pentacoordinated Zn(II) complex (Fig. 2 and Table 1).

Then, comparing the environment coordination of complexes **(1)-(3)** to the **(4)-(6)**, it is observed that the bonds between M and the ligand HL1, are shortened by the loss of chloro ligand and the coordination of the anion SDZ^- (Table 2S). In this approach, are taken in account the bonds between the metal and the donor groups present in the ligand HL1 (pyridine, secondary amine and alcohol). The bond lengths calculated at BP86-D3BJ ZORA-TZVP-def2(-f) level of theory (Table 2S), for the starting complexes **(1)-(3)**, reveal that the bond M-Cl (M= Cu(II), Fe(III) and Zn(II)) is much longer than those attributed to those between the groups presented in the ligand HL1 (pyridine, secondary amine and alcohol groups) and the M, being the largest for complex **(2)**: Fe-Cl(11), Fe-Cl(12) and Fe-Cl(13) = 2.21, 2.40 and 2.30Å, respectively. These results are in good agreement with X-ray diffraction data, since similar bond length were observed in complexes **(2)** (Fe1-Cl1 = 2.349(2), Fe1-Cl2= 2.266(2) and Fe1-Cl3= 2.262(2)Å)), and **(3)** (Zn-Cl1= 2.2650(7) and Zn-Cl2=2.2598(7)Å). Complex **(2)** is hexacoordinated while complex **(3)** is pentacoordinated. X-ray data for complex **(1)** are not available since good quality crystals were not obtained.

Analysing the complexation reaction of complex **(2)** to the anion SDZ^-, which results in complex **(5)** (Table 2S), it can be seen that the bond lengths Fe-N15(SDZ^-) and Fe-N21(SDZ-) (N15 and N21 are N pyrimidine ring N atom of the anion SDZ^-) are 1.93 and 1.98 Å, respectively. The bond lengths Fe-N2 (amine)=2.30Å and Fe-N17 (pyridine)= 2.17Å, in complex **(2)**, are shortened, after the coordination of the anion SDZ^- to the Fe(III) center, resulting in the lengths Fe-N41 (amine)= 2.04 and Fe-N3 (pyridine)= 1.97 Å (see Table 2S). This does not occur in complexes **(4)** and **(6)**, since the M-N bond distances in both complexes exhibit the same average length, suggesting that a stronger interaction between the anion SDZ^- and the Fe(III) center, than with Cu(II) and Zn(II). Such behavior may be related to the stabilization of a low spin iron(III) compound in the presence of SDZ^-, as described above.

Fig. 11 presents the superposition between crystallographic data of complexes **(2), (3)** and **(6)** and DFT optimized geometries, aiming to compare these theoretical data with the structural data obtained by X-ray crystallography. New structural data were obtained and are presented herein (Tables 1 and 2,Figs. 1 and 2), for complexes **(2)** and **(6)**. Data for the Zn(II) complex **(3)**, were reported previously by us [20]. Furthermore, this comparison is useful to validate parameters for other complexes for which no crystallographic data were obtained (complexes **(1), (4)** and **(5)**). By comparing the calculated structures with the crystallographic structures, the superposition of the Cartesian coordinates of the atoms present in the observed structures for complexes **(2), (3)** and **(6)** was performed. The RMSDs (Root Mean Square Errors) calculated in this superpositions were 0.0042, 0.0099, 0.0125, respectively. Lower RMSD values represent better agreement between the structures obtained by X-ray diffraction and the optimized geometry. This means that the optimized geometry of compound **(2)** is the one that most closely matches the molecule in the crystal. Also, the blue (optimized) structures are more open than the experimental structures. This is because the theoretical structures are obtained in vacuum, and the crystallographic structures have the full potential of the crystal lattice.

Tables 3S and 4S (supporting information material) present the calculated EDA (Energy Decomposition Analysis) of complexes **(1)-(3)** and **(4)-(6)**, respectively. The EDA findings allow us to infer a general chemical profile: the interaction with the chloro ligands, which remained coordinated to the metal center, after the coordination of the anion SDZ^-, is weakened (this is valid for complexes **(5)** and **(6)**). This can be confirmed by the values of ΔE^{int} M-Cl of both complexes when compared with its precursors **(2)** and **(3)** (ΔE^{int} M-Cl = -157.3, -159.8 and -162.5 for the three chloro fragments in complex **(2)**, -141.4 and -144.2 for complex **(5),** -154.7 and -152.1 for the two chloro fragments in complex **(3)** and 148.4 for complex **(6)**). This occurs because the anion SDZ^- donates electron density towards the metal, weakening the M-Cl interaction (see Table 2S). Such results corroborate the Fe-Cl bond distances observed in **(2)**, which reveal an increase in the bond length Fe-Cl from 2.21 to 2.24, indicating that the bond is weakened by the coordination with SDZ^- (see Table 2S). Concerning complex **(3)**, it exhibits two bonds Zn-Cl, with the following bond lengths, determined by X-ray diffraction studies: 2.2650(7) and 2.2598(7) Å [20], however complex **(6)** presents only one Zn-Cl bond length of 2.2922(11) Å (Table 1). The coordination of the anion SDZ^- through the N from the pypimidine ring to the Zn(II) centre (complex **(6)**) results in weakness of the Zn-Cl bond, confirmed by structural data obtained by X-ray diffraction studies and presented herein (Zn-Cl= 2.2922(11) Å).

These results reveal that there is a competition concerning the substitution reactions between the chloro ligand and the anion SDZ^-. As can be seen in Table 3S, the difference in the labilities of both is around 100 kcal/mol. Then, the resulting complex with the anion SDZ^- coordinated is much more stable than the reactant (less 100 kcal/mol), because the anionic form of sulfadiazine is more strongly bonded to the metallic center than the chloro ligand, which indicates an enormous probability of the chloro ligand leaving the structure before the coordination of the anion SDZ-. For complex **(5)**, which has three chloro ligands, two are kept after the

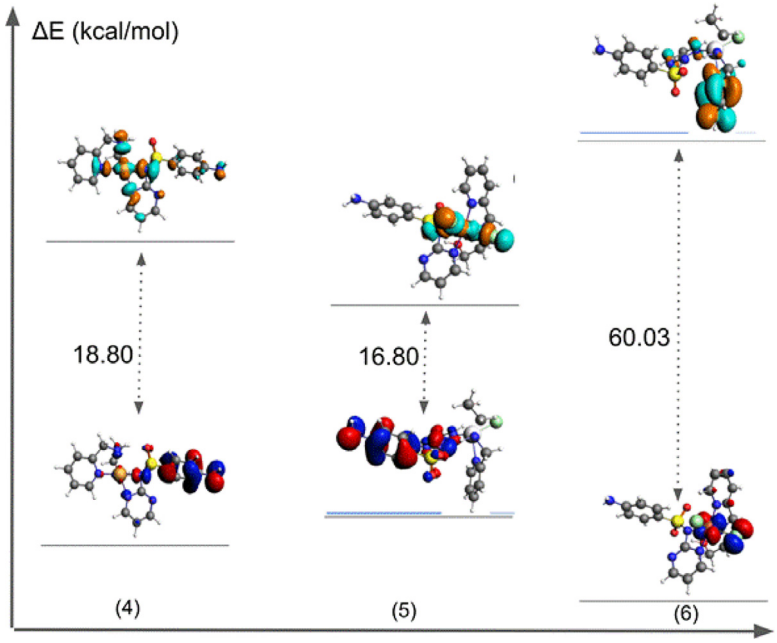

Fig. 12. Molecular orbital scheme of complexes **(4)-(6)**, based on DFT calculations. The HOMO-LUMO gaps are compared and the energies are reported in kcal/mol.

coordination with the anion SDZ^-, resulting in a hexacoordinated iron(III) complex.

According to EDA, for all the complexes, it is possible to infer that the interactions between the ligand (HL1 or anion SDZ^-), and the transition metal, such as M (Cu(II), Fe(III) or Zn(II) are mostly electrostatic, being more significant in complex **(4)**, positively charged (this complex is a cation- see Fig. 10). However, the orbital character is about 30%, indicating a certain degree of covalence in the bonds between the anion SDZ^- and cationic metal, which are mostly ionic. Analyzing the data presented in Table 4S, we can state that the value of ΔE^{orb} for the coordination of SDZ^- in complex **(5)** (-65.10 kcal.mol^{-1}) is much less significant than in **(4)** and **(6)** (-134.5 kcal.mol^{-1} and -141.6 kcal.mol^{-1} respectively), complex **(6)** being the one with the strongest interaction between fragment B ([Zn(HL1)Cl]) and fragment A (SDZ^-). It stems from the highest occupied state (LUMO) of **(6)** as well as its HOMO state are located in fragment B (Fig. 12 and Table 3S) which includes Zn(II), the ligand HL1 and chloro ligands, while complexes **(4)** and **(5)** have the HOMO orbitals mainly localized at the anion SDZ^-. Then, complex **(6)** is more thermodynamically more stable than complexes **(4)** and **(5)**, justifying its formation. The preparation energies of the interacting fragments in relation to the complexes as a whole, it is show that the distortion of the anion SDZ^- and the ligand HL1 when coordinated is small. This demonstrates that the structural changes through the formation of the studied compounds make it probable that the biological activity related to the drug will not change after the coordination.

3.9. In vitro *anti-toxoplasma activity*

The anti-toxoplasma activity of complexes **(1), (2), (3)** and **(6)**, and of the reference pharmac (NaSDZ), were evaluate under the same conditions. Fig. 13 shows the reduction in the infection index, after 48h of treatment, employing two concentrations (10 and 20 µmol/L). Host cell viability was about 90% after treatment with all the complexes, indicating that it had low toxicity.

All the compounds promoted the reduction in the infection index, and the following sequences can be proposed: **(2)** > **(6)** > **(3)** >NaSDZ > **(1)** and **(2)** > **(6)** ≈ **(3)** >NaSDZ ≈ **(1)**, employing at 10 and 20 µmol/L of each complex, respectively, after 48 h of incubation. The results indicate that the complexes **(2), (3)** and **(6)** inhibit the growth of *T. gondii*, after 24 and 48h, with activities superior to the drug NaSDZ. These results suggest that the coordination of the anion SDZ^- to the Zn(II) center in complex **(3)**, which has resulted in the in complex **(6)**, did not significantly alter the anti-toxoplasma activity presented by the complex **(3)**. Compound **(2)**, containing Fe(III), proved to be the most active, motivating further studies.

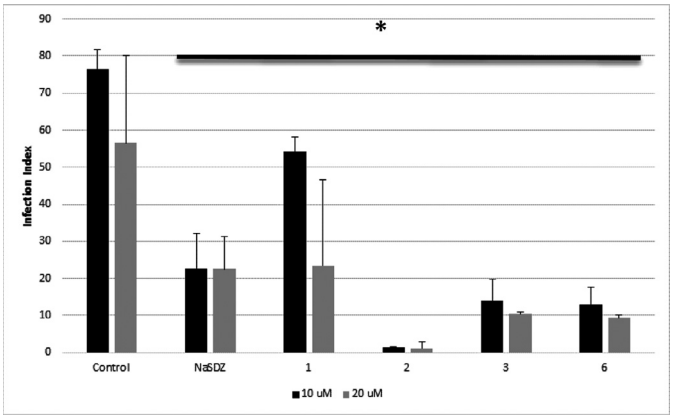

Fig. 13. Infection Index of *T. gondii* interaction with host cells after treatment with complexes **(1), (2), (3), (6)** and NaSDZ (10 and 20 µmol/L) and no treatment (control), for 48h. * Anova one way, P ≤ 0,05.

Light microscopy imagens (Fig. 14) reveals that untreated infected cells displayed parasites organized in rosettes, with normal morphology (Figs. 14A and B), exhibiting very parasites in the parasitophorous vacuoles (arrow). Figs. 14C and D indicate that the treatment with NaSDZ induces the organization of the parasites in structures similar to tissue cysts, resulting in rounded shape parasites (bradyzoites-like forms) (arrows). However, after treatment for 48h with complex **(1)** (Figs. 14E and F), few irregularly shaped parasites were observed and normal parasites (tachyzoite-like forms) and no tissue cysts were observed**.** The treatment with complex **(2)** (Figs. 14G and H)**,** the most active complex, has resulted in few parasites which present degraded shapes (arrows).

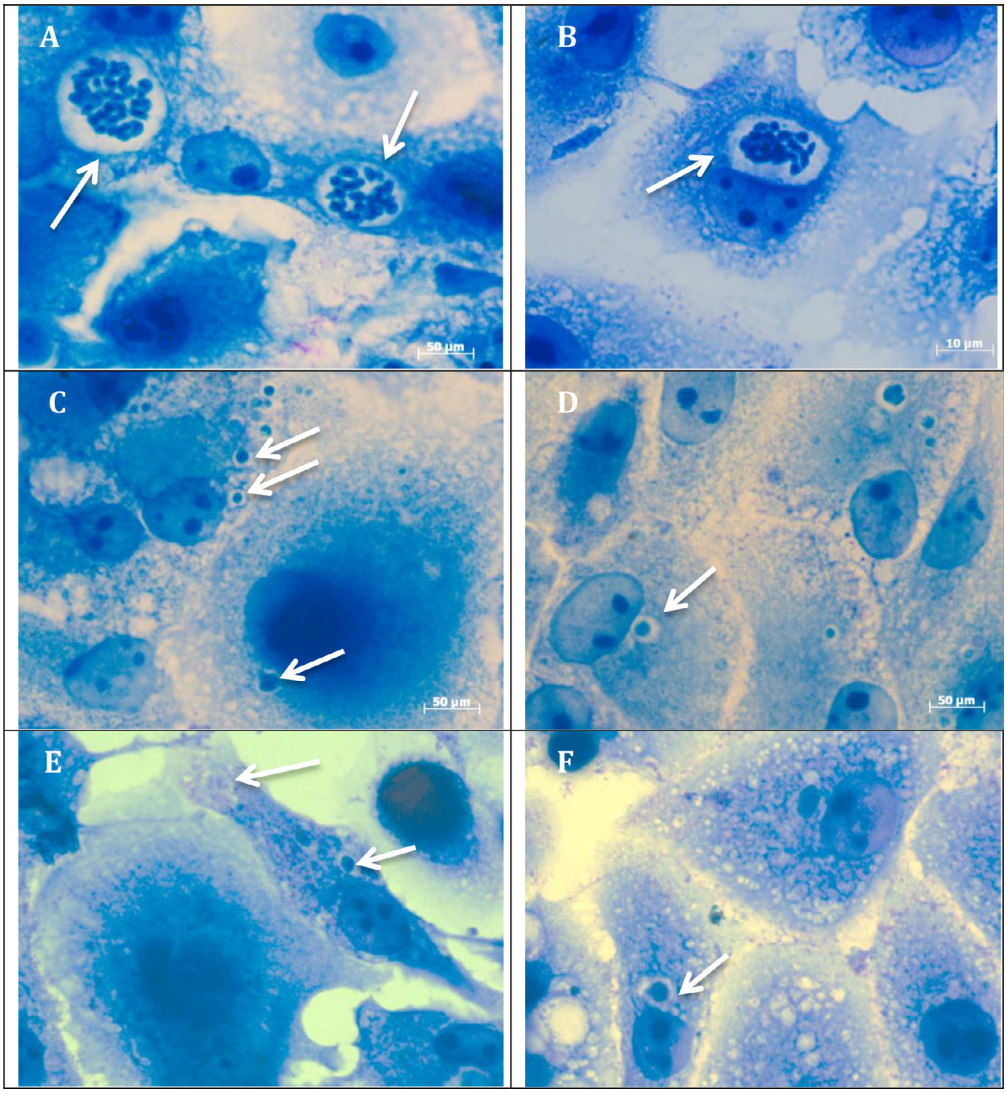

Fig. 14. Light microscopy of interaction *T. gondii* with host cell by 48 h, in presence complexes **(1), (2), (3), (6)** and NaSDZ. A-B: Control or no treatment, rosettes (arrow) inside untreated cells after 48h. C-D: Treatment with NaSDZ, note the rounded shape of the parasite (arrow). E-F: Treatment with complex **(1)**, note few irregularly shaped parasites. G-H: Treatment with complex **(2)**, note degraded parasites (arrows) I-J and K-L: Treatments with complexes **(3)** and **(6)**, note normal (few, arrow head) and degraded parasites (many, arrow).

Treatment with complexes **(3)** and **(6)** (Figs. 14I-L) promote reduction in the number of viable parasites and result in parasites with unusual shapes, indicating degradation of them. Few parasites present intact structure (arrow head- Fig. 14K).

4. Conclusions

Coordination compounds containing Cu(II), Fe(III) and Zn(II) have been prepared and successfully characterized, using the tripodal tridentate ligand HL1. Complexes **(1)-(3)** were employed in the reactions with the anion SDZ-. Only the reaction between complex **(3)** and the anion SDZ^- was effective, resulting in the new complex **(6)**, which was characterized by X-ray diffraction studies.

According to the results, it is possible to conclude that there is a competitive reaction between the chloro coordinated to the metal (M), and the anion SDZ^-, in the reaction between complexes **(1)-(3)**, and the anion SDZ^-, resulting in complexes **(4)-(6)**. The interaction M-SDZ^- is the most favorable, since $\Delta E^{tot}(Cl)$ is less intense than $\Delta E^{tot}(SDZ^-)$.

The data suggests that all three complexes containing the SDZ^- coordinated **(4), (5)** and **(6)** should be obtained. However, this was not observed experimentally, since only the synthesis of **(6)** was effective. Through parallel DFT calculations, we can infer that the chloro ligand of initial complex **(3)** is more labile than in complexes **(1)** and **(2)**. Complex **(6)** also presents a more significant value of Δ^{orb} for the SDZ^- substitution and a higher stabilization of its crystalline field, presenting HOMO orbital in lower energy and bigger gap between its HOMO and LUMO orbitals. These parameters help justify the difficulty in the obtention of complexes **(4)** and **(5)** as pure, crystalline compounds. The results obtained by DFT suggest that complex **(6)** is the most probable to be obtained synthetically.

These initial studies suggest that these water-soluble complexes **(2), (3)** and **(6)** were more effective than NaSDZ against *T. gondii*. Complex **(1)** showed similar anti-toxoplasma activity than the gold standard drug, just at higher concentration (20 µM). All the complexes under investigation act by different mechanisms than the one presented by NaSDZ, since no tissue cysts or bradyzoite-like forms were detected in light microscopy images. However, the coordination of the anion SDZ^-, which might be a promising strategy for increasing the anti-toxoplasma activity of coordination compounds [17], it was not detected in this work. Compound **(6)**,

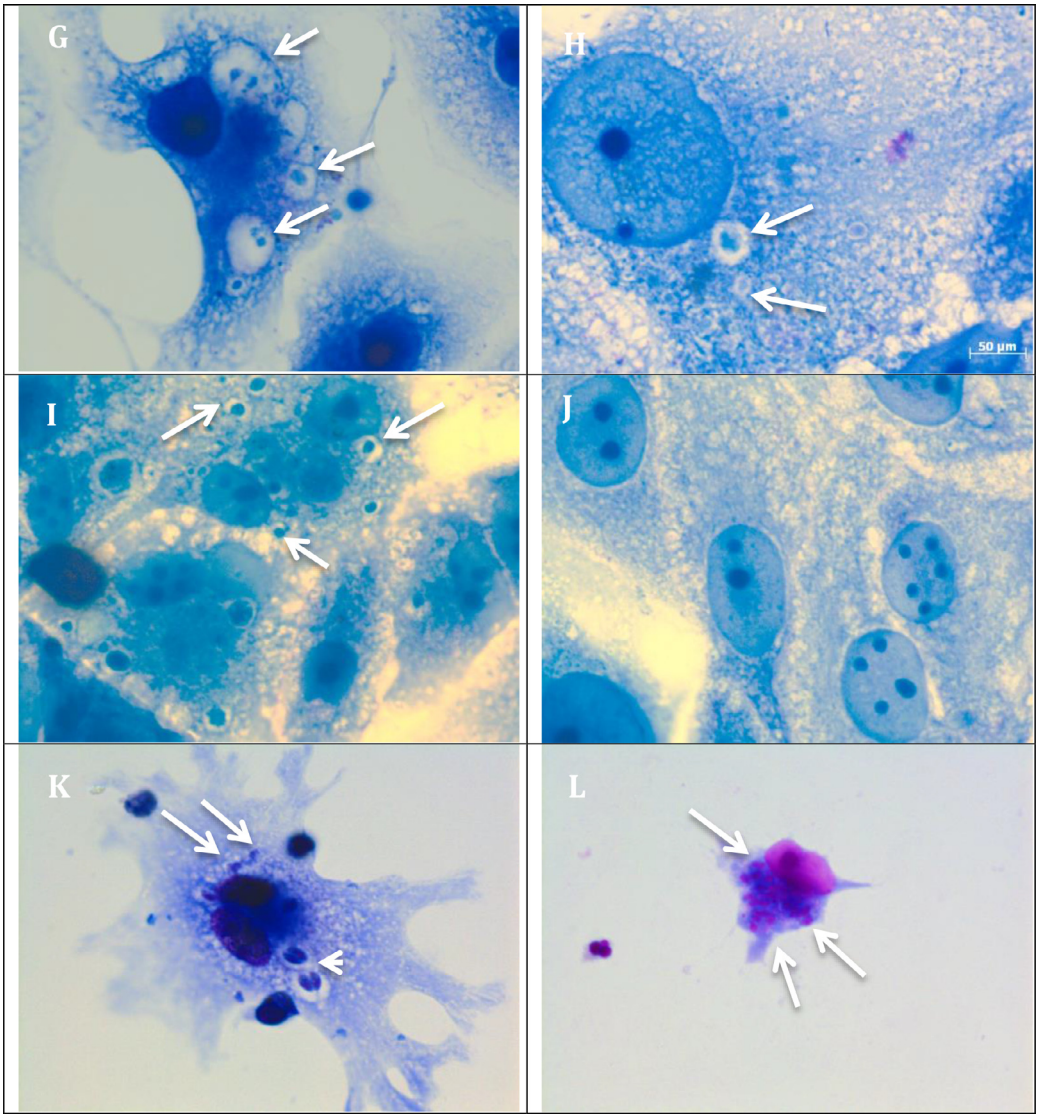

Fig. 14. Continued

which has the SDZ^{-} anion in its structure, showed a high reduction in the infection index, with values very similar to those presented by the complex **(3)**. Among all compounds investigated, compound **(2)** showed the best reduction in the infection index. Light microscopy images of LLC-MK2 cells infected with *T. gondii* suggest that, due to the small amount of parasites, complex **(2)** promotes the death of the parasite.

Credit author statement

Ana Paula Cardoso: synthesis of ligands and coordination compounds, spectrochemical and electrochemical characterization.; Bruna B. Segat: characterization of ligands and coordination compounds by NMR, characterization of compounds by ESI(+)-MS, preparation of tables and supplementary material.; Jennifer do N. C. Menezes: obtaining compound (6) in crystalline form. Initial characterization of the same. Purification of HL1 ligand by column chromatography.; Roberta Cargnelutti: X-ray diffraction studies for complexes (2) and (6).; Dalber R. S. Candela and Davor L. Mariano: characterization of complex (2) by Mössbauer spectroscopy.; Letícia M. P. Madureira, Renato L. T. Parreira and Giovanni F. Caramori: DFT studies, manuscript writing, corrections and implementations according to the suggestions made by the reviewers.; Adolfo Horn Jr.: work design, manuscript writing, obtaining the RPE spectrum for the compound (1).; Sérgio H. Seabra, Renato A. DaMatta, Felipe F. Moreira and Renata V, Moreira: *in vitro* antitoxoplasma activity (infection index and light microscopy images).; Christiane Fernandes: conception of the work, writing of the manuscript, supervision of the students (Bruna, Ana Paula, Jennifer) sending samples for biological studies and others carried out in other institutions, contact with collaborators, organization of the manuscript and coordination of the review stage and acquisition of new experiments.

Declaration of Competing Interest

The authors declare that they have no known competing financial interests or personal relationships that could have appeared to influence the work reported in this paper.

Acknowledgement

G.F.C. thanks National Council for Scientific and Technological Development, CNPq, for his research grant (311132/2020-0). L.M.P.M also thanks CNPq for her scientific initiation scholarship (147153/2021-2).

Supplementary materials

Complementary data as Cartesian coordinates of all optimized structures, geometric parameters, as well as EDA values are available free of charge as supporting information material. Figs. 7S and 8S present the IR spectra of the ligand HL1, of NaSDZ and complexes **(1), (2), (3)** and **(6)**. Figs. 9S and 10S represent the electronic spectra of complexes **(1)** and **(2)**. Figs. 11-24S present the isotopic profiles assignments obtained for the main peak observed in the ESI-(+)-MS spectra of complexes **(2), (3)** and **(6).** Fig. 25S represents the ESI-(+)-MS/MS of the *m/z* 719 (complex **(6)**). Fig. 26S represent the experimental and simulated EPR spectra of complex **(1)**.

Supplementary material associated with this article can be found, in the online version, at doi:10.1016/j.molstruc.2022.133380.

References

[1] R.H.D. Ybañez, A.P. Ybañez, Y. Nishikawa, Review on the current trends of toxoplasmosis serodiagnosis in humans, Front. Cellular Infect. Microbiol. 10 (2020) 204, doi:10.1080/13880200802398002.

[2] L.E. Mboera, C. Kishamawe, E. Kimario, S.F. Rumisha, Mortality patterns of toxoplasmosis and its comorbidities in Tanzania: a 10-year retrospective hospital-based survey, Front. Public Health 7 (2019) 25, doi:10.3389/fpubh.2019.00025.

[3] A. Rostami, S.M. Riahi, Y. Fakhri, V. Saber, H. Hanifehpour, S. Valizadeh, H.R. Gamble, The global seroprevalence of Toxoplasma gondii among wild boars: a systematic review and meta-analysis, Vet. Parasitol. 244 (2017) 12, doi:10.1016/j.vetpar.2017.07.013.

[4] T. Nayeri, S. Sarvi, M. Moosazadeh, A. Amouei, Z. Hosseininejad, A. Daryani, The global seroprevalence of anti-Toxoplasma gondii antibodies in women who had spontaneous abortion: a systematic review and meta-analysis, PLoS Negl.Trop. Dis. 14 (3) (2020) e0008103, doi:10.1371/journal.pntd.0008103.

[5] A. Cerutti, N. Blanchard, S. Besteiro, The bradyzoite: a key developmental stage for the persistence and pathogenesis of toxoplasmosis, Pathogens 9 (3) (2020) 234, doi:10.3390/pathogens9030234.

[6] A.P. Holland, J.S. Doggett, Drugs in development for toxoplasmosis: advances, challenges, and current status. Drug design, Development and Therapy 11 (2017) 273, doi:10.2147/DDDT.S60973.

[7] N. Konstantinovic, H. Guegan, T. Stäjner, S. Belaz, F.R. Gangneux, Treatment of toxoplasmosis: Current options and future perspectives, Food and Waterborne Parasitol. 15 (2019), doi:10.1016/j.fawpar.2019.e00036.

[8] A.V. Fernandes, P. Thota, D. Pellegrino, V. Pasupuleti, V.A. Benites-Zapata, A. Desphpande, A.C. Penalva de Oliveira, J.E. Vidal, A systematic review and meta-analysis of the relative efficacy and safety of treatment regimens for HIV-associated cerebral toxoplasmosis: is trimethoprim-sulfamethoxazole a real option? HIV Med. 18 (2016) 115, doi:10.1111/hiv.12402.

[9] L.A. Silva, M.D. Fernandes, A.S. Machado, J.L. Reis-Cunha, D.C. Bartholomeu, R.W. A.Vitor, Efficacy of sulfadiazine and pyrimetamine for treatment of experimental toxoplasmosis with strains obtained from human cases of congenital disease in Brazil, Exp. Parasitol. 202 (2019) 7, doi:10.1016/j.exppara.2019.05.001.

[10] J.S. Doggett, S. Nilsen, I. Forquer, K.W. Wegmann, L. Jones-Brando, R.H. Yolken, C. Bordon, S.A. Charman, K. Katneni, T. Schultz, J.N. Burrows, D.J. Hinrichs, B. Meunier, V.B. Carruthers, M.K. Riscoe, Endochin-like quinolones are highly efficacious against acute and latent experimental toxoplasmosis, Proc. Natl. Acad. Sci. 109 (39) (2012) 15936, doi:10.1073/pnas.1208069109.

[11] M.K. Yun, Y. Wu, Z. Li, Y. Zhao, M.B. Waddell, A.M. Ferreira, R.E. Lee, D. Bashford, S.W. White, Catalysis and sulfa drug resistance in dihydropteroate synthase, Science 335 (6072) (2012) 1110, doi:10.1126/science.1214641.

[12] J.A. Portes, T.G. Souza, T.A.T. Dos Santos, L.L.R. Da Silva, T.P. Ribeiro, M.D. Pereira, A. Horn Jr, C. Fernandes, R.A. Da Matta, W. de Souza, S.H. Seabra, Reduction of *Toxoplasma gondii* development due to inhibition of parasite antioxidant enzymes by a dinuclear iron (III) compound, Antimicrob. Agents Chemother. 59 (12) (2015) 7374, doi:10.1128/AAC.00057-15.

[13] V.M. de Assis, L.C. Visentin, F.S. de Souza, A.R. DaMatta, A. Horn Jr, A, C. Fernandes, Synthesis, crystal structure and relevant antiproliferative activity against *Toxoplasma gondii* of a new binuclear Co(II) complex, Inorg. Chem. Commun. 67 (2016) 47, doi:10.1016/j.inoche.2016.02.017.

[14] J.A. Portes, C.S. Motta, N.F. Azeredo, C. Fernandes, A. Horn Jr, W. de Souza, R.A. DaMatta, S.H. Seabra, *In vitro* treatment of *Toxoplasma gondii* with copper(II) complexes induces apoptosis-like and cellular division alterations, Vet. Parasitol. 245 (2017) 141, doi:10.1016/j.vetpar.2017.04.002.

[15] C. Fernandes, A. Horn Jr, B.F. Lopes, E.S. Bull, N.F. Azeredo, M.M. Kanashiro, F.V. Borges, A.J. Bortoluzzi, B. Szpoganicz, A.B. Pires, R.W.A. Franco, J.C.A. Almeida, L.L.F. Maciel, J.A.L.C. Resende, G. Schenk, Induction of apoptosis in leukemia cell lines by new copper (II) complexes containing naphthyl groups via interaction with death receptors, J. Inorg. Biochem. 153 (2015) 68, doi:10.1016/j.jinorgbio.2015.09.014.

[16] L.C. Batista, F.S. de Souza, V.M. de Assis, S.H. Seabra, A.J. Bortoluzzi, M.N. Renno, A. Horn Jr, R.A. Da Matta, C. Fernandes, Antiproliferative activity and conversion of tachyzoite to bradyzoite of *Toxoplasma gondii* promoted by new zinc complexes containing sulfadiazine, RSC Adv. 5 (122) (2015) 100606, doi:10.1039/C5RA17690E.

[17] J.D.A. Portes, N.F. Azeredo, P.G. Siqueira, T.G. de Souza, C. Fernandes, A. Horn Jr, D.R.S. Candela, W. de Souza, R.A. DaMatta, S.H. Seabra, A new iron (III) complex-containing sulfadiazine inhibits the proliferation and induces cystogenesis of *Toxoplasma gondii*, Parasitol. Res. 117 (9) (2018) 2795, doi:10.1007/s00436-018-5967-7.

[18] Y. Deng, T. Wu, S.Q. Zhai, C.H. Li, Recent progress on anti-toxoplasma drugs discovery: design, synthesis and screening, Eur. J. Med. Chem. 183 (2019) 111711, doi:10.1016/j.ejmech.2019.111711.

[19] S. Striegler, M. Dittel, A sugar's choice: Coordination to a mononuclear or a dinuclear copper (II) complex? Inorg. Chem. 44 (8) (2005) 2728, doi:10.1021/ic048724p.

[20] C. Fernandes, A. Horn Jr, O.V. da Motta, M.M. Kanashiro, M.R. Rocha, R.O. Moreira, S.R. Morcelli, B.F. Lopes, L. da S. Mathias, F.V. Borges, L.J. Borges, W.R. Freitas, L.C. Visentin, J.C. de A. Almeida, G. Schenk, Synthesis, characterization, antibacterial and antitumoral activities of mononuclear zinc complexes containing tridentate amine based ligands with N_3 or N_2O donor groups, Inorg. Chim. Acta 416 (2014) 35, doi:10.1016/j.ica.2014.02.040.

[21] R.R. Gange, C.A. Koval, G.C. Lisensky, Ferrocene as an internal standard for electrochemical measurements, Inorg. Chem. 19 (1980) 2854, doi:10.1021/ic50211a080.

[22] G.M. Sheldrick, Crystal structure refinement with SHELXL, Acta Crystallogr. Sect. C Struct. Chem. 71 (1) (2015) 3–8, doi:10.1107/S2053229614024218.

[23] G.M. Sheldrick, A short history of SHELXL, Acta Crystallogr. Sect. A Found. Crystallogr. 64 (2008) 112, doi:10.1107/S0108767307043930.

[24] K. Brandenburg, H. Putz, Diamond - Crystal and Molecular Structure Visualization. Crystal Impact GbR- Bonn, Germany.

[25] C. Bannwarth, S. Ehlert, S. Grimme, GFN2-xTB-an accurate and broadly parametrized self-consistent tight-binding quantum chemical method with multipole electrostatics and density-dependent dispersion contributions, J. Chem. Theory Comput. 15 (2019) 1652PMID: 30741547, doi:10.1021/acs.jctc.8b01176.

[26] P. Pracht, E. Caldeweyher, S. Ehlert, S. Grimme, S, A robust non-self-consistent tight-binding quantum chemistry method for large molecules, Chem. RXIV (2019), doi:10.26434/chemrxiv8326202.

[27] S. Grimme, C. Bannwarth, P. Shushkov, A robust and accurate tight-binding quantum chemical method for structures, vibrational frequencies, and noncovalent interactions of large molecular systems parametrized for all spd-block elements (Z= 1–86), J. Chem. Theory Comput. 13 (5) (2017) 1989, doi:10.1021/acs.jctc.7b00118.

[28] P. Pracht, F. Bohle, S. Grimme, Automated exploration of the low-energy chemical space with fast quantum chemical methods, Phys. Chem. Chem. Phys. 22 (14) (2020) 7169, doi:10.1039/C9CP06869D.

[29] M. Orio, D.A. Pantazis, T. Petrenko, F. Neese, Magnetic and spectroscopic properties of mixed valence manganese (III, IV) dimers: a systematic study using broken symmetry density functional theory, Inorg. Chem. 48 (15) (2009) 7251, doi:10.1021/ic9005899.

[30] N. Mardirossian, M.H. Gordon, Thirty years of density functional theory in computational chemistry: an overview and extensive assessment of 200 density functionals, Mol. Phys. 115 (19) (2017) 2315, doi:10.1080/00268976.2017.1333644.

[31] E.V. Van Lenthe, J.G. Snijders, E.J. Baerends, The zero-order regular approximation for relativistic effects: the effect of spin–orbit coupling in closed shell molecules, J. Chem. Phys. 105 (15) (1996) 6505 doi.org/, doi:10.1063/1.472460.

[32] G. Schmitz, C. Hättig, Accuracy of explicitly correlated local PNO-CCSD (T), J. Chem. Theory Comput. 13 (6) (2017) 2623, doi:10.1021/acs.jctc.7b00180.

[33] E. Paulechka, A. Kazakov, Efficient DLPNO–CCSD(T)-based estimation of formation enthalpies for c-, h-, o-, and n-containing closed-shell compounds validated against critically evaluated experimental data, J. Phys. Chem. 121 (2017) 4379 PMID: 28514153, doi:10.1021/acs.jpca.7b03195.

[34] Y. Guo, C. Riplinger, U. Becker, D.G. Liakos, Y. Minenkov, L. Cavallo, F. Neese, Communication: An improved linear scaling perturbative triples correction for the domain based local pair-natural orbital based singles and doubles coupled cluster method [DLPNO-CCSD (T)], J. Chem. Phys. 148 (1) (2018) 011101, doi:10.1063/1.5011798.

[35] G. te Velde, F.M. Bickelhaupt, E.J. Baerends, C. Fonseca Guerra, S.J.A. van Gisbergen, J.G. Snijders, T.J Ziegler, Chemistry with ADF, J. Comput. Chem. 22 (9) (2001) 931, doi:10.1021/ja039770b.

[36] J. Tommasino, G. Pilet, D. Luneau, A. Messai, N. Attik, D. Decoret, F.Z. Cherchali, A. Boughougal, M. Hologne, C. Sanglar, New model of metalloantibiotic: Synthesis, structure and biological activity of a zinc (II) mononuclear complex carrying two enrofloxacin and sulfadiazine antibiotics, New J. Chem. 42 (18) (2018) 1534, doi:10.1039/C8NJ01774C.

[37] R.P. Dubey, U.H. Patel, Crystallography study, Hirshfeld surface analysis and DFT studies of Cadmium complex of the triple sulfa drug constituent sulfadiazine with secondary ligand β-picoline, J. Chem. Crystallogr. 49 (4) (2019) 281, doi:10.1007/s10870-019.

[38] R. Singh, L.V.K.N. Ramlingeswara Rao, Distortion of the coordination polyhedron in mononuclear copper (II) complexes. Optical absorption and electron spin resonance studies on some five-coordinate copper(II) complexes, Polyhedron 3 (2) (1984) 137.

[39] B.Karabulut Kalfaoğlu, Theoretical investigation of EPR and molecular orbital coefficient parameters for $[Cu(hsm)_2(sac)_2]$ complex, Chem. Phys. Lett. 505 (2011) 154.

[40] W.J. Geary, The use of conductivity measurements in organic solvents for the characterisation of coordination compounds, Coord. Chem. Rev. 7 (1971) 81 122, doi:10.1016/S0010-8545(00)80009-0.
[41] P. Gütlich, B. Eckhard, A.X. Trautwein, Mössbauer spectroscopy and transition metal chemistry: fundamentals and applications, Springer Science & Business Media, 2010.
[42] W.M. Reiff, W.A. Baker Jr, N.E. Erickson, Binuclear, oxygen-bridged complexes of iron (III). New iron (III)-2, 2′, 2"-terpyridine complexes, J. Am. Chem. Soc. 90 (18) (1968) 4794, doi:10.1021/ja01020a008.
[43] K. Sundaravel, M. Sankaralingam, E. Suresh, M. Palaniandavar, Biomimetic iron(III) complexes of N_3O and N_3O_2 donor ligands: protonation of coordinated ethanolate donor enhances dioxygenase activity, Dalton Trans. 40 (33) (2011) 8444 doi.org/, doi:10.1039/C1DT10495K.

3.3 Iron(III) complex impacts *Toxoplasma gondii* growth by altering the plasma membrane and inner membrane complex

Renata V.M. Freitas[a], Christiane Fernandes[b], Adolfo Horn Jr[b], Ana Paula Cardoso[b], Gustavo Victor Tissi Batista[c], Iasmim Barreto dos Santos[c], Luis Guilherme Mansor Basso[c], Renato A. DaMatta[a*], Sergio H. Seabra[a*]

[a]Laboratório de Biologia Celular e Tecidual, Universidade Estadual do Norte Fluminense Darcy Ribeiro, Campos dos Goytacazes, Rio de Janeiro, Brasil.

[b]Departamento de Química, Universidade Federal de Santa Catarina, Florianópolis, Santa Catarina, Brasil.

[c]Laboratório de Ciências Físicas, Universidade Estadual do Norte Fluminense Darcy Ribeiro, Campos dos Goytacazes, Rio de Janeiro, Brasil.

* Corresponding authors (seabrash@uenf.br, renato@uenf.br)

Abstract

Therapies for toxoplasmosis are limited, emphasizing the need for treatment options. The *in vitro* effect of the mononuclear iron(III) complex [Fe(HL1)Cl_3](HL = N-2[(pyridine-2-ylmethyl)amino]ethanol) on LLC-MK2 host cells infected with *Toxoplasma gondii* was investigated. Complex showed no cytotoxicity to host cells up to 500 µM but inhibited parasite growth with IC_{50} values of 12.4 and 56.0 nM after 24 h and 48 h, respectively. These values indicate that the complex is more potent than sulfadiazine and pyrimethamine, two clinically used anti-*Toxoplasma* agents. The effect of the complex was irreversible after 48 h of treatment and compound withdrawal. Treated infected cells displayed fewer parasites with a rounded morphology. Ultrastructural analysis revealed severe damage to the parasite, including membrane blebbing, cytoplasmic clefts, and rupture of both the plasma membrane and the inner membrane complex, confirmed by anti-IMC1 immunofluorescence. Biophysical studies demonstrated that the complex disrupts lipid packing in parasite-mimicking membranes while increasing order in mammalian-like membranes. These findings suggest that the complex directly targets and disrupts parasite membranes, leading to potent antiparasitic activity at nanomolar concentrations.

Keywords: *Toxoplasma gondii*, iron(III) complex, chemotherapy, plasma membrane, inner membrane complex.

Introduction

Toxoplasma gondii is an obligate intracellular protozoan parasite of the Apicomplexa phylum, the etiological agent of toxoplasmosis, which can infect warm-blooded animals, including humans [1]. Based on seroepidemiological studies, nearly 30% of the global population has anti-*T. gondii* antibodies, indicating that they were infected with *T. gondii* [2]. Humans can become infected by ingestion of oocyst-contaminated water, vegetables and fruits and/or the ingestion of tissue cysts in undercooked meat [3]. Ingested parasites convert into tachyzoites that spread throughout the body. As the body's immune response builds up, the parasite convert to bradyzoites, which develop into tissue cysts and the infection proceeds to the chronic stage [4]. When cysts are in immunosuppressed or immunocompromised individuals, bradyzoites egress from the cysts, and convert into tachyzoites, causing acute infection [5]. Congenital infections occur with the placental transmission of tachyzoites in early infections during pregnancy [6]. Acute infection is typically asymptomatic in immunocompetent individuals, but cervical lymphadenopathy or ocular disease can occur. Infection of immunocompetent individuals with more virulent strains of *T. gondii*, can result in severe pneumonia and disseminated disease, including death [7]. *T. gondii* is an important opportunistic agent in people with impaired immune function (immunocompromised), especially in patients with AIDS and organ recipients, and is the most common cause of encephalitis in them [8,9]. Furthermore, toxoplasmosis is also a major congenital infection with a wide clinical spectrum, varying from neonatal asymptomatic birth to abortion, stillbirth, and birth of infants with severe cerebral and ocular complications (hydrocephalus or microcephaly, and calcification) [1,10].

The combination of pyrimethamine (PYR) and sulfadiazine (SDZ) is the first line of therapy against *T. gondii* infections [11,12,13]. PYR is a folic acid antagonist and inhibits the dihydrofolate reductase enzyme, blocking the synthesis of purines and pyrimidines, essential for DNA synthesis and cell multiplication. The action of this drug is enhanced when used in conjunction with sulfonamides, such as SDZ, which is capable of interfering with *T. gondii*'s folic acid synthesis by competitively inhibiting the dihydropteroate synthetase enzyme [14-17]. Several *in vitro* studies have reported a wide range of IC_{50} values for these drugs. SDZ has a highly variable IC_{50} depending on the host cell [18]. For *T. gondii* (RH strain, tachyzoite form) in epithelial cell lines such as HeLa [19], Vero [20], and HEp2 [21], the reported IC_{50} values are 7.00 mM in HeLa cells after 24 h of treatment, 0.30 mM in Vero cells after 72h of treatment and 2.60 mM in Hep2 cells after 90 h of treatment. In hTERT cells treated for 24 h and 48 h, Huffman et al. (2022) [22] reported IC_{50} values ranging from 1.28 to 1.55 µM. Similarly,

Węglińska et al. (2022) [23] in Hs27 cells after 24 h and 48 h of treatment observed an IC_{50} of 3.3 µM. In contrast, Trotsko et al. (2019) [24] in Hs27 cells after 24 h of treatment reported a lower IC_{50} of 0.512 µM. For PYR, in Hs27 cells treated for 24 h to 72 h, Qiu et al. (2025) [25] reported IC_{50} values ranging from 2.42 to 3.59 µM. Similarly, Huffman et al. (2022) [22] in hTERT cells after 24 h to 48 h of treatment observed IC_{50} values between 3.18 and 3.52 µM. In contrast, Trotsko et al. (2019) [24] in Hs27 cells after 24 h of treatment reported a much lower IC_{50} of 0.326 µM. These differences emphasize the variability in susceptibility of *T. gondii* to standard drugs and highlight the need to explore new therapeutic agents with improved potency and selectivity.

Unfortunately, the side effects of SDZ and PYR are severe, including bone marrow suppression, hematologic toxicity, and/or life-threatening allergic reactions [3], forcing about 40% of patients to interrupt the treatment [26]. At the same time, prolonged treatment is necessary for immunocompromised patients [27]. Long-term treatment, side effects, and resistance limits the use of these drugs. Therefore, it is necessary to find high-efficiency and low-toxic drugs in the treatment of toxoplasmosis [28].

The interest in the development of therapeutic transition metal complexes is in part driven by the clinical success of the platinum(II) anticancer drug, cisplatin (cis-diamminedichloroplatinum) [29-32]. Metal-based drugs are attractive due to their great versatility in terms of metal center, oxidation state, coordination number, in addition to the nature and geometric orientation of the ligands [33]. Along with platinum, other transition metals including gold, titanium, rhodium, iridium, ruthenium and osmium, as well as essential metals as iron, copper, zinc, and cobalt, inspired the development of numerous compounds as potential anticancer candidates due to their variable coordination modes, redox activity and reactivity towards biomolecules [34-39]. Studies have also been focused on the identification of other pharmacological applications, e.g., diagnostic tools such as biomolecular and cellular probes [40-42] or antibacterial, antifungal, and antiparasitic therapeutics [43-48].

Concerning the use of first row transition metal compound to treat parasites, iron(III) complexes showed potent activity against epimastigotes of *Trypanosoma cruzi,* presenting half maximal inhibitory concentration (IC_{50}) values in the nanomolar range, acting on mitochondria and reservosomes, essential organelles for the survival of the parasite [49]. Previous studies by our group investigated coordination compounds with anti-*Toxoplasma* activity *in vitro* [18,50-54]. In 2017, the anti-*Toxoplasma* activity and ultrastructural alterations of the parasite after treatment with two copper(II) complexes were reported. Both complexes irreversibly control the growth of *T. gondii in vitro*, resulting in IC_{50} values of 0.78 and 3.57 µM, after 48 h of

treatment. It was observed that these copper compounds caused the death of the parasites by two distinct mechanisms, necrosis and apoptosis. In addition, copper(II) complex interfered with the correct disposition of the inner membrane complex (IMC) of the parasite, affecting cell division [51]. The IMC is a parasite structure involved in cell shape maintenance, motility, and division, all of which are disturbed when the IMC is disrupted [55,56,57].

Recently, coordination compounds synthesized with the ligand HL = N-2[(pyridine-2-ylmethyl)amino)ethanol) (1- $[Cu(HL1)Cl_2]$, 2- $[Fe(HL1)Cl_3]$, 3- $[Zn(HL1)Cl_2]$, 4- $[Zn(HL1)(SDZ)Cl]. 2H_2O$) had their anti-*Toxoplasma* activity evaluated [54]. After 48 h, at concentrations of 10 µM and 20 µM, the water-soluble complexes (2), (3), and (4) inhibited the growth of *T. gondii* with activities superior to the SDZ, with compound (2) showing the highest reduction in the infection index. Light microscopy images of LLC-MK2 cells infected with *T. gondii* suggest that, due to the small number of parasites and morphology alteration, complex (2) had the best capacity to promote the death of the parasite [54].

Aiming to contribute to the development of therapeutic alternatives for neglected diseases and expand our understanding of how coordination compounds affect *T. gondii* growth, we report that the compound (2) $[Fe(HL1)Cl_3]$ exhibited high selectivity for the parasite, with no adverse effects on the host cell. This complex was active against *T. gondii* with an IC_{50} value in the nanomolar range, acting on the plasma membrane, IMC, and cytoplasm, leading tachyzoites to the death within the parasitophorous vacuole.

Materials and methods

***Toxoplasma gondii*.** Tachyzoites used in this study were from the virulent RH strain of *T. gondii*, maintained by intraperitoneal infections of Swiss mice. After 48 h of infection, the parasites were collected by a peritoneal cavity wash with PBS, pH 7.2, and then centrifuged at 1000g for 10 min. The pellet was washed with PBS and Dulbecco's Modified Eagle Medium (DMEM). The parasites were used within 30 - 40 min of their removal from the peritoneal cavity. All animal studies were reviewed and approved by the ethics committee of animal use of the UENF (*Universidade Estadual do Norte Fluminense Darcy Ribeiro*, code: 600).

Culture of cells. LLC-MK2 kidney epithelial cells (Rhesus monkey, *Macaca mulata*) - CCL-7 (ATCC), were grown in 25 cm^2 culture flasks (SPL Life Sciences) containing DMEM (Sigma Aldrich, EUA) supplemented with 10% fetal bovine serum (FBS) at 37 °C in a 5% CO_2

atmosphere. Infection of the cells by the parasite was performed in subconfluent cultures in flasks or on coverslips in 24-well tissue culture plates (SPL Life Sciences).

Iron(III) complex. The mononuclear iron(III) complex [Fe(HL1)Cl_3] was synthesized as previously described by our group [54], and its structure is shown in **Figure 1**. Briefly, the iron(III) complex was obtained by reacting 1 mmol (152 mg) of the ligand HL1 (N-2[(pyridine-2-ylmethyl)amino)ethanol)) with $FeCl_3$. $6H_2O$ (1 mmol, 270 mg) in methanol, under reflux. Light yellow crystals were obtained after a few days. Yield: 87 mg (26%). m.p.: 240 °C. Anal. Calcd for C 8 H 12 Cl 2 FeN 2 O; MW = 314.5 g.mol^{-1}: C, 30.55; H, 3.84; N 8.94. Found: C, 30.53; H, 3.83; N, 8.94. For *in vitro* studies, this complex was dissolved in DMEM at a concentration of 10 mM, sterilized through 0.22 µm filter membranes, and stored at -22 ºC.

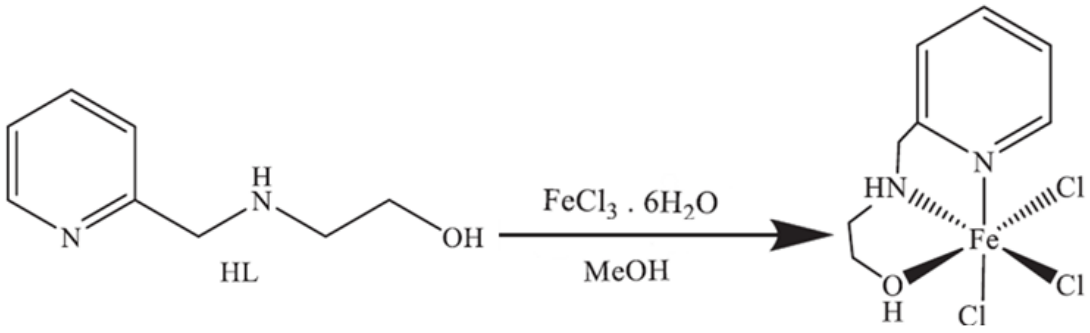

Figure 1. Synthesis of the iron(III) complex based on reference [54].

Cell viability assay. The effect of iron(III) complex on host cells was evaluated based on the reduction of MTT (3-(4,5-dimethylthiazol-2-yl)-2,5-diphenyltetrazolium bromide) and the release of lactate dehydrogenase (LDH). For this assay, 1 x 10^5 cells were seeded per well into 96-well plates and cultured with DMEM supplemented with 5% FBS. After 24 h, the cells were incubated with iron(III) complex (100 µM - 500 µM) in DMEM supplemented with 5% FBS. As a negative control, some cells were also cultured in DMEM supplemented with 5% FBS without the addition of the iron(III) complex. As a positive control, cells were incubated with 10% Triton X-100 in DMEM. After 24 h or 48 h of treatment, the culture supernatant was removed and used for LDH measurement (see below), and 15 µL of MTT (5 mg/mL) supplemented with DMEM was added to each well for 4 h at 37 °C protected from light. The formazan crystals were solubilized by adding 100 µl of dimethyl sulfoxide, and the absorbance was measured in the Versamax microplate reader (Molecular Devices) at 570 nm using the 6.0

SoftMax Pro® software. LDH concentrations were measured in the culture supernatants of the LLC-MK2 cells using the (LDH Liquiform - Labtest) kit with 20 µl of the cultured supernatant, according to the manufacturer's protocol. The data were plotted using the GraphPad Prism 6.0 software. The presented data are representative of the results from three independent experiments.

Anti-proliferative assays. Approximately 2 x 10^5 LLC-MK2 cells were seeded per well onto coverslips in a 24-well plate 1 day before the assay. Cells were infected with parasites using a 5:1 parasite/host cell ratio. Tachyzoites interacted with the host cells for 1 h. Cells were washed with PBS, and the iron(III) complex was added to the cells at different concentrations (12.5 nM – 200 nM) in DMEM supplemented with 10% FBS. After 24 h or 48 h of treatment, cells were fixed with freshly prepared 4% formaldehyde in PBS, stained with Giemsa, and observed by bright field light microscopy (Zeiss Axioplan). Parasite growth was evaluated by direct cell counting on two separate coverslips in at least three independent experiments. The infection index was calculated by multiplying the mean number of internalized *T. gondii* per host cell by the percentage of infected cells. To determine the IC_{50}, the percentage of growth inhibition was plotted as a function of the drug concentration, and the values were fitted to a non-linear curve. Regression analyses were performed using the Sigma Plot 8.0 software. Data were plotted using the GraphPad Prism 6.0® software. Results were represented as the means ± standard deviation of at least three independent experiments. Statistical analysis was performed using one-way ANOVA and two-way ANOVA followed by Tukey´s post hoc test.

Reversibility Test. To verify the reversibility of the effect of iron(III) complex, LLC-MK2 cells were seeded on coverslips in a 24-well plate and infected with *T. gondii* in a 2:1 ratio, parasite-host cell. After 1 h of interaction, cells were washed, and the compounds were added at 12.5 nM and 100 nM with 48 h of treatment. After 48 h, the complex was removed by washing, and the cells were further cultured for an additional 48 h. After this period, the coverslips were fixed in 4% formaldehyde in PBS, and subsequently processed for observation and counting using light microscopy, as previously described.

Transmission electron microscopy. Cells were infected in culture flasks, treated or not, for 24 h and 48 h with 10 nM and 100 nM of the iron(III) complex, and fixed for 1 h in 2.5% glutaraldehyde and 4% recently prepared formaldehyde in 0.1 M sodium cacodylate buffer (pH 7.4). Cells were scraped off the flasks using a rubber policeman, washed with sodium

cacodylate buffer, and post-fixed for 1 h in osmium tetroxide 1% in 0.1 M sodium cacodylate buffer. Cells were washed, dehydrated in acetone, and embedded in Epon. Ultrathin sections were stained with uranyl acetate and lead citrate and observed under a Jeol 1400 Plus transmission electron microscope.

Immunofluorescence assay. LLC-MK2 cells over coverslips were infected with tachyzoites, treated or not for 48 h with 12.5 nM and 100 nM iron(III) complex, washed with PBS, and fixed with 4% freshly prepared formaldehyde in PHEM buffer (60 mM Pipes, 20 mM Hepes, 10 mM EGTA, 5 mM $MgCl_2$, and 70 mM KCl, pH 7.2). After fixation, the cells were washed, permeabilized with 2% Triton X-100 for 10 min, and incubated with 100 mmol/L. NH_4Cl for 30 min and then with PHEM buffer containing 3% bovine serum albumin (PHEM-BSA) for 30 min at room temperature. Cells were incubated for 1 h with the anti-IMC1 mouse monoclonal antibody (1:3000 dilution, kindly provided by Dr. Ward), washed twice with PHEM-BSA, and incubated with rabbit anti-mouse Alexa-488 antibody (1:100 dilution) (Invitrogen). Cells were washed, mounted with the ProLong® Gold antifade reagent (Invitrogen) with 4',6-diamidino-2-phenyl-indole (DAPI), and observed in a confocal laser-scanning microscope (LSM-710, Zeiss).

Interaction with membrane-like structures

Materials. The phospholipids 1,2-dipalmitoyl-sn-glycero-phosphatidylcholine (DPPC), 1,2-dipalmitoyl-sn-glycero-3-phosphoethanolamine (DPPE), 1-palmitoyl-2-oleoyl-sn-glycero-3-phosphocholine (POPC), 1-palmitoyl-2-oleoyl-sn-glycero-3-phospho-L-serine (POPS), 1-palmitoyl-2-oleoyl-sn-glycero-3-phosphoethanolamine (POPE), sphingomyelin (Egg, Chicken – SM), and the spin labels 1-palmitoyl-2-stearoyl(n-doxyl)-sn-glycero-3-phosphocholine (n = 5, 10, and 16 – n-PCSL) and 1,2-dipalmitoyl-sn-glycero-3-phospho(tempo)choline (DPPTC) were purchased from Avanti Polar Lipids, Inc. (Alabaster, AL). Cholesterol (Chol) was obtained from Sigma-Aldrich (St. Louis, MO). All reagents were used without further purification.

Sample preparation. The iron(III) complex stock solution was prepared in milliQ water. The phospholipids and spin labels (DPPTC, 5-PCSL, 10-PCSL, and 16-PCSL) stock solutions were prepared either in chloroform or in chloroform/methanol 1:1 (v/v). Aliquots of phospholipids (2.0 mg for Differential Scanning Calorimetry - DSC - and 0.2 mg for Electron Spin Resonance - ESR) and spin labels (1 mol% for ESR) were mixed in a glass tube, dried under a N_2 flow,

and kept under vacuum for 2 h to remove traces of organic solvent. The lipid film formed was hydrated with either the drug-free buffer (20 mM HEPES, 150 mM NaCl, pH 7.4) or the buffer containing the complex at the desired lipid-to-drug molar ratio of 20:1. The samples were thoroughly vortexed and sonicated in a bath type sonicator for 10 min at 35 ºC for complete hydration. The resulting multilamellar vesicles (MLVs) were then subjected to five freeze-thaw cycles. The final lipid concentration was 10 mg/ml for ESR and 2 mg/ml for DSC.

Differential scanning calorimetry experiments. The thermotropic behavior of various artificial lipid membranes in the absence and presence of iron(III) complex was studied using a NanoDSC (TA Instruments) with a heating rate of 30.0 ºC/h. The lipid types and molar ratios were selected to model membranes based on lipid extracts from *T. gondii* whole cells (WC), the IMC, and LLC-MK2 cells, as described in the literature [58-60]. The lipid compositions and respective molar ratios used were as follows: DPPC, DPPC/Chol 4/1, DPPC/DPPE/POPS/SM 75/10/10/5 (Chol-free WC model), DPPC/DPPE/POPS/SM/Chol 69/9/9/5/10 (WC model), DPPC/DPPE/POPS/SM/Chol 61/8/8/3/20 (IMC model), and DPPC/DPPE/POPS/SM/Chol 45/15/8/12/20 (LLC-MK2 model). Pure DPPC was used as the simplest model because it represents the major phospholipid of the *T. gondii*-enriched membrane fraction [58]. The cholesterol content was capped at 20 mol% to prevent excessive broadening of thermograms. Prior to each measurement, the samples were degassed for 5 min and equilibrated for 10 min at the starting temperature. The resulting thermograms were analyzed using the NanoAnalyze software (TA Instruments).

Electron spin resonance experiments and spectral simulations. Lipid model membranes with compositions similar to those used in the DSC experiments were employed in ESR studies. The compositions and respective molar ratios were as follows: Chol-free WC model – POPC/POPE/POPS/SM 75/10/10/5; WC model – POPC/POPE/POPS/SM/Chol 63/8/8/4/17; IMC model – POPC/POPE/POPS/SM/Chol 53/7/7/3/30; and LLC-MK2 model – POPC/POPE/POPS/SM/Chol 39/13/7/11/30. The inclusion of unsaturated lipids ensured that the membranes remained in the fluid phase at 22 ºC. The chosen lipid compositions were designed to achieve cholesterol/phospholipid molar ratios of 0.2 for the WC model and 0.4 for the IMC and LLC-MK2 models, consistent with values reported in the literature [58-60]. A volume of 20 µL of each lipid mixture/spin label sample was transferred to glass capillaries (1.5 mm I.D.) and set into a quartz tube. The experiments were performed at 22 ºC on a Bruker E-500 spectrometer operating at 9.3 GHz. The following acquisition parameters were used: center

field, 3,360 G; scan width, 120 G; modulation amplitude, 0.5 G for 16-PCSL and 1.0 G for DPPTC, 5-PCSL, and 10-PCSL; modulation frequency, 100 kHz; microwave power, 10 mW; time constant, 128 ms; and acquisition time, 120 s. Nonlinear least-squares fitting of the ESR spectra was performed as previously described [61] using the Multicomponent LabView (National Instruments, Austin, USA) [62], available at http://www.biochemistry.ucla.edu/biochem/Faculty/Hubbell/. The best-fit gyromagnetic-tensor and hyperfine-tensor components are summarized in the Supplementary Table S1.

Results

The toxicity of the iron(III) complex in LLC-MK2 host cells was initially assessed by measuring the reduction of MTT. Following a 24 h treatment, the complex reduced cell viability from 19% to 25% at concentrations of 100 µM to 500 µM. After 48 h, a reduction of approximately 15% in cell viability was observed at concentrations of 500 µM (**Figure 2a**). The LDH assay performed after 48 h of treatment showed that the complex reduced cell viability by up to 12%. However, cell viability remained high (>80%) at all tested concentrations (**Figure 2b**).

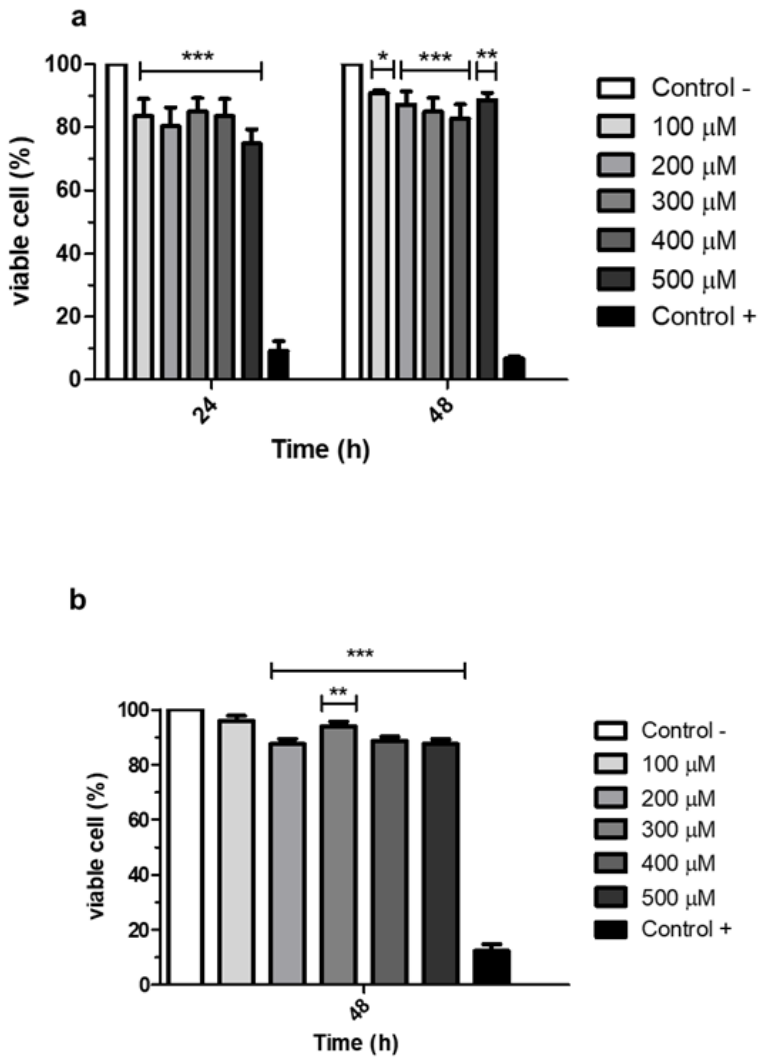

Figure 2. Viability of LLC-MK2 host cells after treatment with iron(III) complex. Host cells were treated with different concentrations of the complex for 24 h and 48 h. **a**. Toxicity of the complex to host cells was evaluated based on the reduction of MTT. **b**. The toxicity of the complex to host cells was also evaluated by the release of lactate dehydrogenase. No significance between variables was found. Negative control: cells cultured in DMEM with FBS without the complex. Positive control: cells cultured with 10% Triton X-100 in DMEM. Mean and standard deviation of three independent experiments. a. * $P < 0.05$, ** $P < 0.01$,*** $P < 0.001$ vs. negative control. b. ** $P < 0.05$, *** $P < 0.05$ vs. negative control, ns: not significant.

The anti-*Toxoplasma* activity of the iron(III) complex was previously evaluated in a study by the group [54]. Based on that work, we tested lower concentrations in LLC-MK2 host cells infected with *T. gondii* to determine the IC_{50}. **Figure 3** shows that the complex induces a dose-dependent inhibition of parasite growth at the concentrations used. After 24 h of treatment,

an IC_{50} of 12.4 nM was obtained. Treatment for 48 h resulted in a significant reduction in the infection index in all tested concentrations of the complex, and the achieved IC_{50} was 56 nM. Compared to the toxicity observed in host cells, the estimated selectivity index of the iron complex on *T. gondii* is higher than 4 x 10^4 and 0.9 x 10^4 for 24 h and 48 h, respectively.

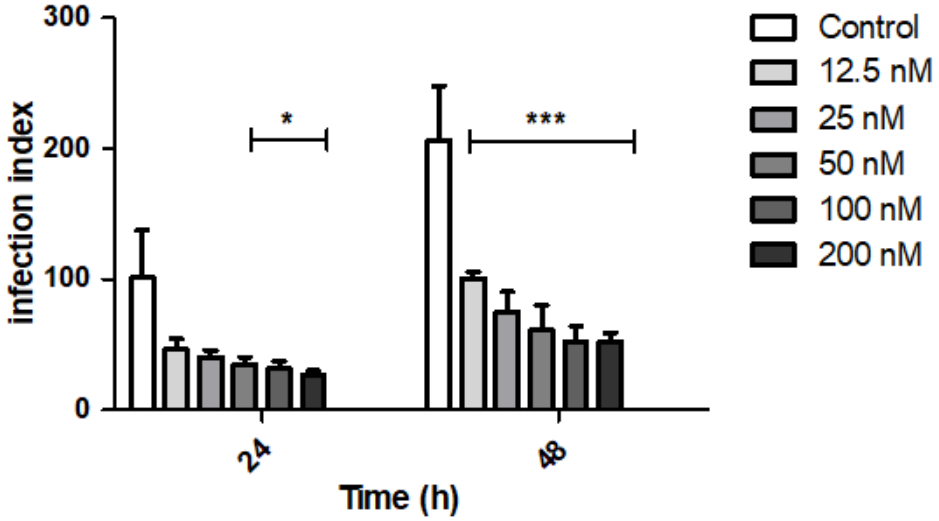

Figure 3. Infection index of *Toxoplasma gondii* in LLC-MK2 host cells for 24 h and 48 h of treatment with different concentrations of the iron(III) complex. Control cells were untreated. Mean and standard deviation of three independent experiments. * $P \leq 0.05$, *** $P \leq 0.001$ vs. control, ns: not significant.

Reversibility of the effect of the iron(III) complex was tested by treating infected cells for 48 h infected cells with the complex (12.5 nM and 100 nM), washing the compound, and further culturing the cells for another 48 h. After removal of the complex, the infection index was reduced and remained constant when 12.5 nM and 100 nM were used, respectively

(**Figure 4**). This result indicates an irreversible effect on the parasites after treatment.

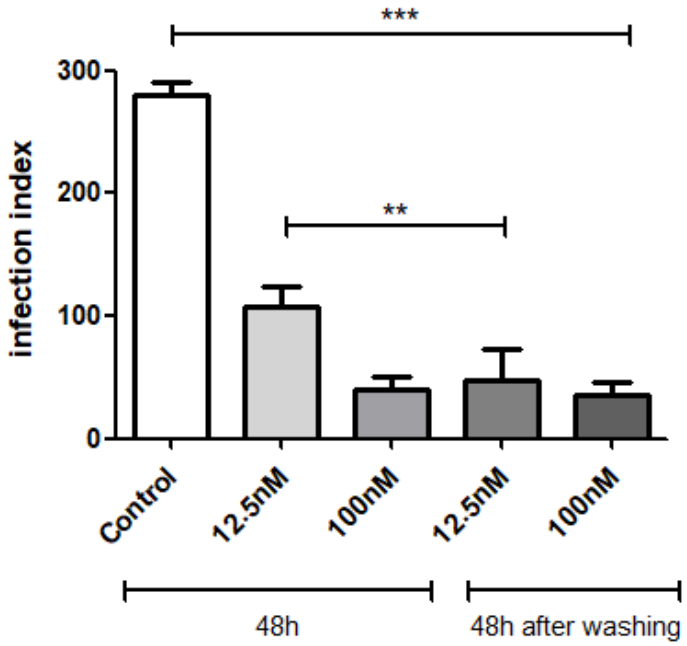

Figure 4. Infection index of LLC-MK2 cells infected with *Toxoplasma gondii* after treatment with the iron(III) complex and removal of the complex (post-wash) and further culture. Possible reversibility of the effect of the complex was tested by treating for 48 h infected cells with the complex (12.5 nM, 100 nM), removing the compound by cell washing, and culturing the cells for an additional 48 h. Parasite growth was evaluated after 48 h and an additional 48 h of culture. Control cells were untreated. Mean and standard deviation of three independent experiments. ***$P \leq 0.05$ vs. control. ** $P \leq 0.05$ in relation to the 12.5 nM treatment without wash.

Light microscopy images were used to evaluate the morphology and arrangement of the parasites inside the parasitophorous vacuoles after 24 h and 48 h of treatment with the iron(III) complex at concentrations of 50 nM and 200 nM (**Figure 5**). Parasites with normal morphology and in large quantities forming rosettes in the parasitophorous vacuoles were observed in infected and untreated host cells (**Figure 5a, b**). After treatment with the complex, there was a reduction in the number of parasites, which presented a round shape (**Figure 5c, d**).

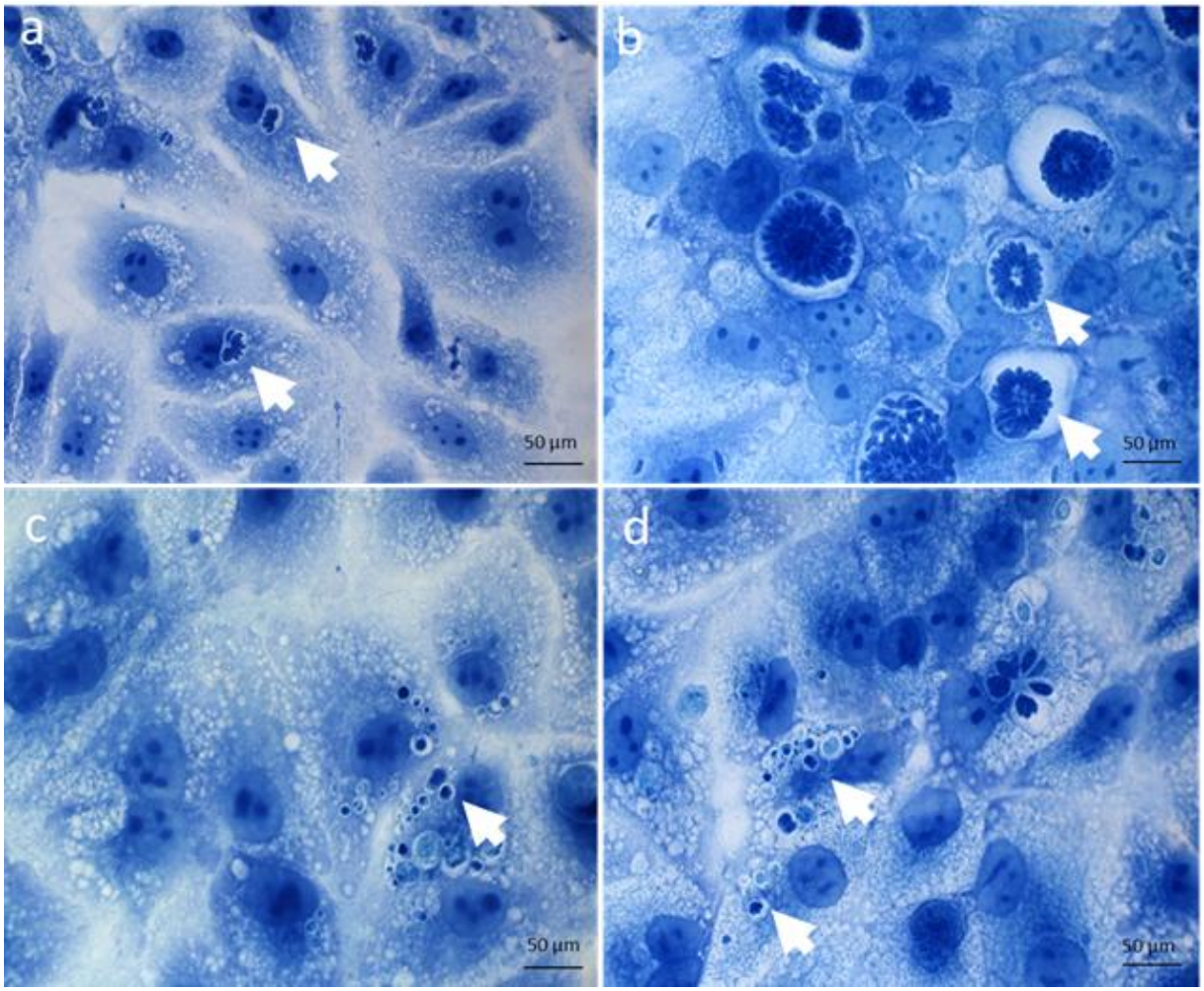

Figure 5. Light microscopy images of Giemsa-stained LLC-MK2 cells infected with *Toxoplasma gondii,* untreated or treated with the iron(III) complex. **a**. Tachyzoites in parasitophorous vacuoles (arrows) after 24 h without treatment. **b.** Tachyzoites forming rosettes (arrow) after 48 h without treatment. **c, d.** LLC-MK2 cells infected with *T. gondii* treated with 50 nM for 24 h and 200 nM for 48 h with the complex, respectively; unusually shaped tachyzoites (arrows) can be seen. Scale bar: 50µm.

Transmission electron microscopy of untreated infected LLC-MK2 host cells showed tachyzoites with well-preserved structures within a parasitophorous vacuole (**Figure 6a, b**). However, 48 h of treatment with the iron(III) complex at 10 nM and 100 nM resulted in the rupture of the plasma membrane and of the IMC of tachyzoites (**Figure 6c, d**). Treated tachyzoites also presented alterations in their cytoplasm, known as clefts, and membrane blebs (**Figure 6e, f**), which are hallmarks of which is a hallmark of apoptosis. Furthermore, parasites were observed with a dead morphology and in the process of degradation inside the parasitophorous vacuole (**Figure 6g, h**).

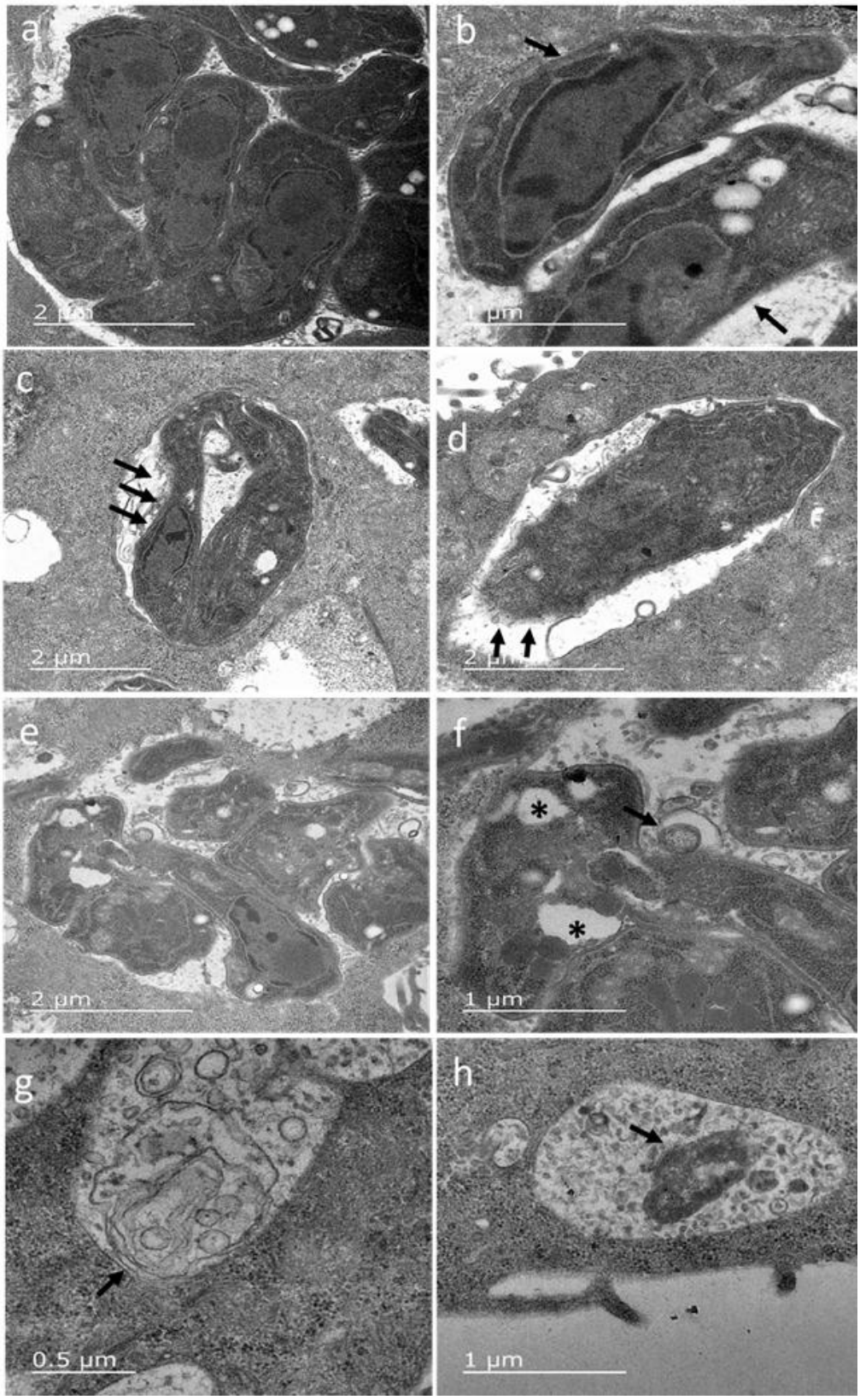

Figure 6. Transmission electron microscopy images of LLC-MK2 cells infected with *Toxoplasma gondii* untreated or treated for 24 h and 48 h with 10 nM and 100 nM of the iron(III) complex. a, b. Tachyzoites inside a parasitophorous vacuole of untreated cell. **b.**

Preserved organelles and an intact inner membrane complex of untreated tachyzoites (arrows) can be seen. **c, d.** Tachyzoites in cells treated with 100 nM of the complex for 48 h exhibit alterations in the plasma membrane and inner membrane complex (arrows).**e, f.** Tachyzoites in cells exposed to 10 nM of complex for 24 h show cytoplasmic changes, known as clefts (*), and the presence of blebs in the plasma membrane (arrow). **g, h.** Dead tachyzoites in cells treated with 100 nM of complex for 48 h are undergoing degradation within the parasitophorous vacuoles (arrow). Bars: 0.5 μm, 1 μm, 2 μm.

T. gondii IMC was labeled with anti-IMC1 antibody to possibly confirm the ultrastructural changes. Confocal laser microscopy images revealed untreated tachyzoites with preserved IMC (**Figure 7a**). In cells treated for 48 h with the iron(III) complex (12.5 nM and 100 nM), small "openings" in the tachyzoite IMC were observed, confirming the disruption of this parasite structure (**Figure 7b, c**).

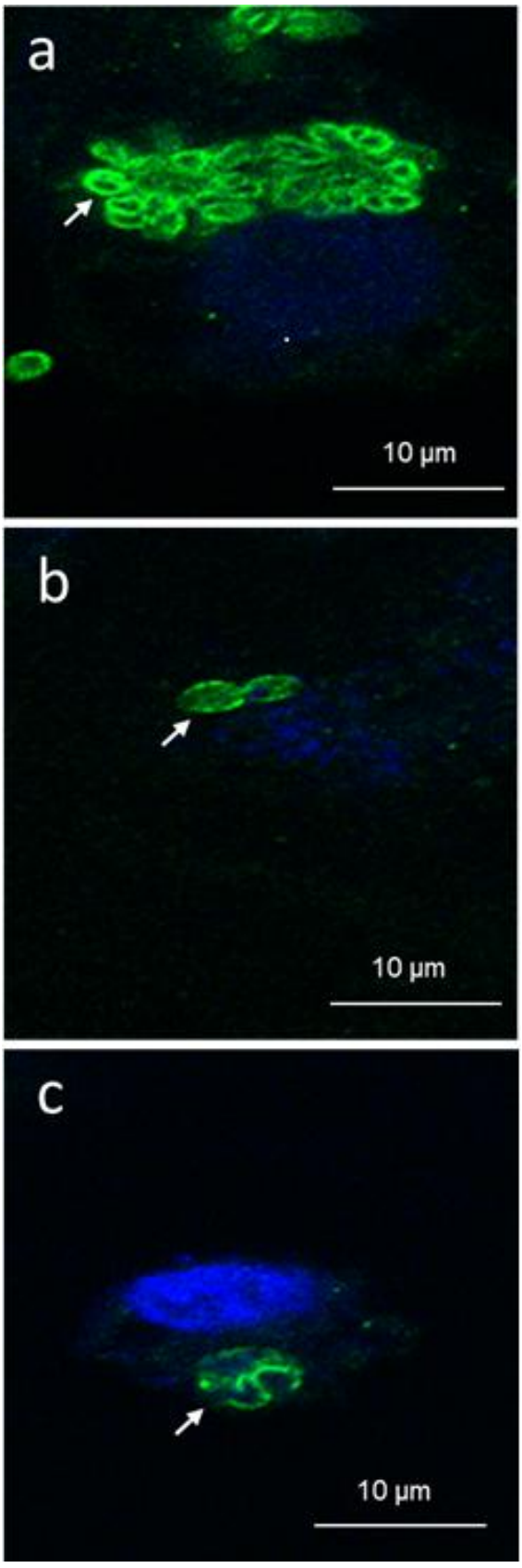

Figure 7. Laser scanning confocal microscopy images of LLC-MK2 cells infected with *Toxoplasma gondii* treated for 48 h with 12.5 nM and 100 nM of the iron(III) complex

labeled with anti-IMC1 and DAPI. **a.** Tachyzoites in untreated host cells showing intact inner membrane complex (green). **b, c.** Tachyzoites in host cells after treatment with the complex showing disruption of the inner membrane complex (arrows). Bars: 10 µm.

Differential scanning calorimetry (DSC) was employed to examine how the iron(III) complex affects the thermal behavior of various lipid model membranes. The thermogram of pure DPPC exhibited a sharp, highly cooperative main phase transition at 41.6 ºC (**Figure 8a**), characteristic of the gel-to-liquid crystalline transition. A distinct pre-transition at 35.5 °C was also observed for pure DPPC. The incorporation of Chol in DPPC bilayers (DPPC/Chol) significantly broadened the main phase transition peak ($\Delta T_{1/2}$ increased from ~ 0.3 ºC to ~ 10 ºC) and abolished the pretransition (**Figure 8b**) [63]. The addition of the complex markedly reduced the half-width of the main phase transition ($\Delta T_{1/2}$) as well as the enthalpy (ΔH) and entropy (ΔS) changes for the DPPC (**Table 1**). Conversely, the complex caused the opposite effect in DPPC/Chol bilayers, increasing ΔH, ΔS, and $\Delta T_{1/2}$ of the transition. More complex membrane models showed broader main phase transitions compared to pure DPPC due to a mixture of lipids displaying different melting temperatures (**Figure 8c-e**), with larger $\Delta T_{1/2}$ values correlating with higher Chol content (**Table 1**). In the Chol-free and Chol-containing whole-cell (WC) membrane models, as well as the IMC model, the complex reduced both ΔH and ΔS, without significantly altering $\Delta T_{1/2}$ (**Figure 8c-e**). Interestingly, in the SM- and phosphatidylethanolamine (PE) -enriched LLC-MK2 membrane model, the complex caused an opposite effect, increasing both ΔH and ΔS of the transition (**Figure 8f**). Notably, in all cases, the melting temperature (T_m) of the lipid systems was only slightly affected by the complex (**Table 1**).

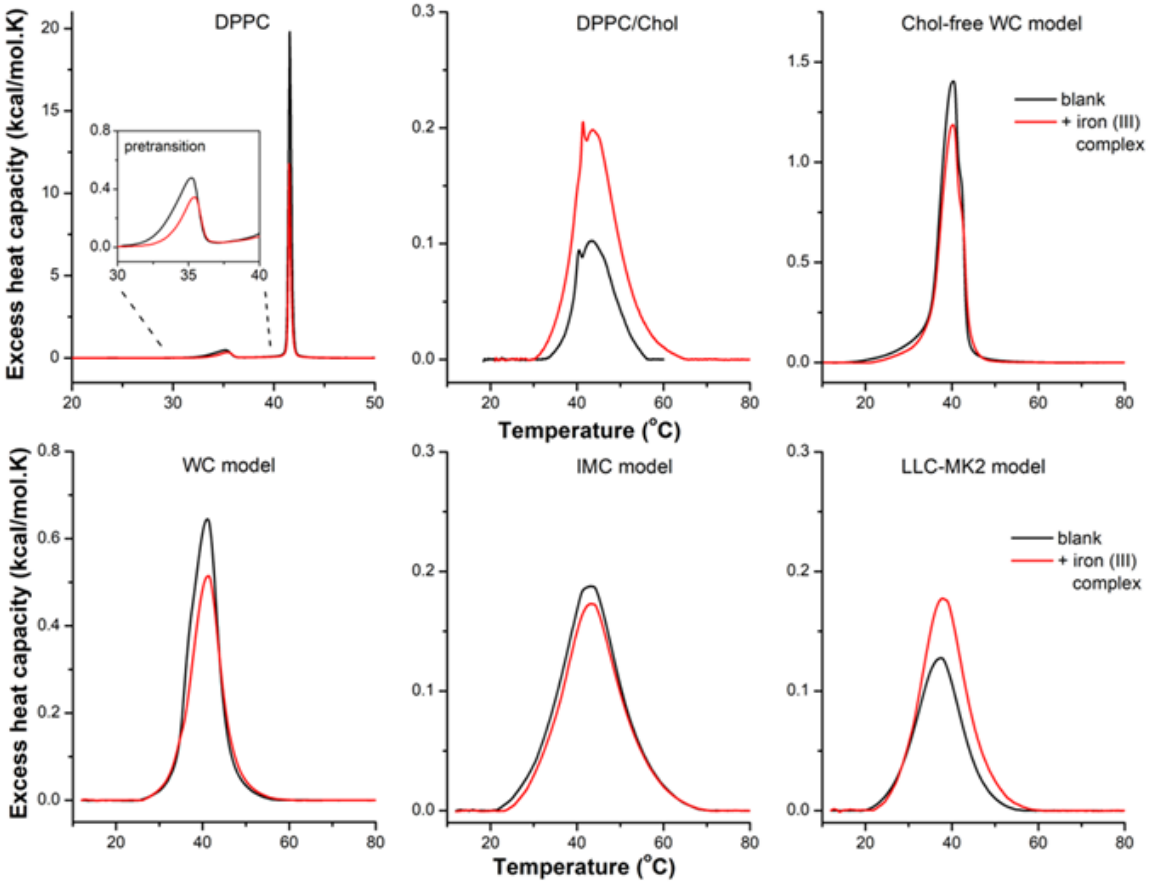

Figure 8. Effect of the iron(III) complex on the thermodynamics of the phase transitions of lipid model membranes. Representative thermograms illustrating the temperature dependence of the excess molar heat capacity of (**a**) DPPC, (**b**) DPPC/cholesterol 4/1, (**c**) DPPC/DPPE/POPS/SM 75/10/10/5 (Chol-free WC model), (**d**) DPPC/DPPE/POPS/SM/Chol 69/9/9/5/10 (WC model), (**e**) DPPC/DPPE/POPS/SM/Chol 61/8/8/3/20 (IMC model) and (**f**) DPPC/DPPE/DPPS/SM/Chol 45/15/8/12/20 (LLC-MK2 model) multilamellar vesicles without (black) and with 5 mol% of iron(III) complex (red). *Inset of panel A*: Zoom in of the DPPC pretransition.

Table 1. Thermodynamics parameters obtained from DSC experiments of lipid membrane phase transitions in the presence and absence of 5 mol% of the iron(III) complex. T_P and T_m stand for the pretransition and main phase transition temperatures, respectively, $\Delta T_{1/2}$ represents the linewidth at half height of the main transition, and ΔH and ΔS represent, respectively, the calorimetric enthalpy change of the whole transition and entropy change at T_m ($\Delta S = \Delta H / T_m$). The samples include DPPC, DPPC/Chol 4/1, DPPC/DPPE/DPPS/SM 75/10/10/5 (Chol-free WC model), DPPC/DPPE/DPPS/SM/Chol 69/9/9/5/10 (WC model), DPPC/DPPE/DPPS/SM/Chol 61/8/8/3/20 (IMC model), and DPPC/DPPE/DPPS/SM/Chol 45/15/8/12/20 (LLC-MK2 model).

Sample	T_P (°C)	ΔH (kcal/mol)	T_m (°C)	$\Delta T_{1/2}$ (°C)	ΔS (cal/mol.K)
DPPC	35.2	8.83	41.6	0.33	28.1
+ iron(III) complex	35.5	5.04	41.5	0.27	16.0
DPPC/Chol	—	1.05	43.6	10.1	3.3
+ iron(III) complex	—	2.65	43.6	11.0	8.4
Chol-free WC model	—	9.16	40.4	5.7	29.2
+ iron(III) complex	—	7.86	40.3	5.9	25.1
WC model	—	5.45	41.2	7.7	17.3
+ iron(III) complex	—	4.75	41.4	7.8	15.1
IMC model	—	3.42	43.2	15.9	10.8
+ iron(III) complex	—	2.99	43.2	15.4	9.5
LLC-MK2 model	—	1.74	37.5	12.1	5.6
+ iron(III) complex	—	2.39	37.8	11.9	7.7

Estimated uncertainties: ΔH (~ 3% at most), T_m (0.1 °C), T_P (0.4 °C), $\Delta T_{1/2}$ (0.02 °C for DPPC, 0.2 °C otherwise).

Electron spin resonance (ESR) was used to investigate whether the iron(III) complex affects the packing and fluidity of artificial model membranes that mimic *T. gondii* (Chol-free WC, WC, and IMC models) and mammalian (LLC-MK2 model) lipid bilayers. Four spin labels were used to monitor structural and dynamic changes at specific membrane regions: DPPTC, 10-PCSL, and 16-PCSL. DPPTC targets the membrane-water interface, while the others probe distinct positions along the acyl chains of the lipid bilayer, from near the bilayer surface to its core [64]. Spectral changes induced by the complex were observed under all conditions, except for 16-PCSL (**Figure 9**), suggesting minimal effect of the complex in the bilayer center.

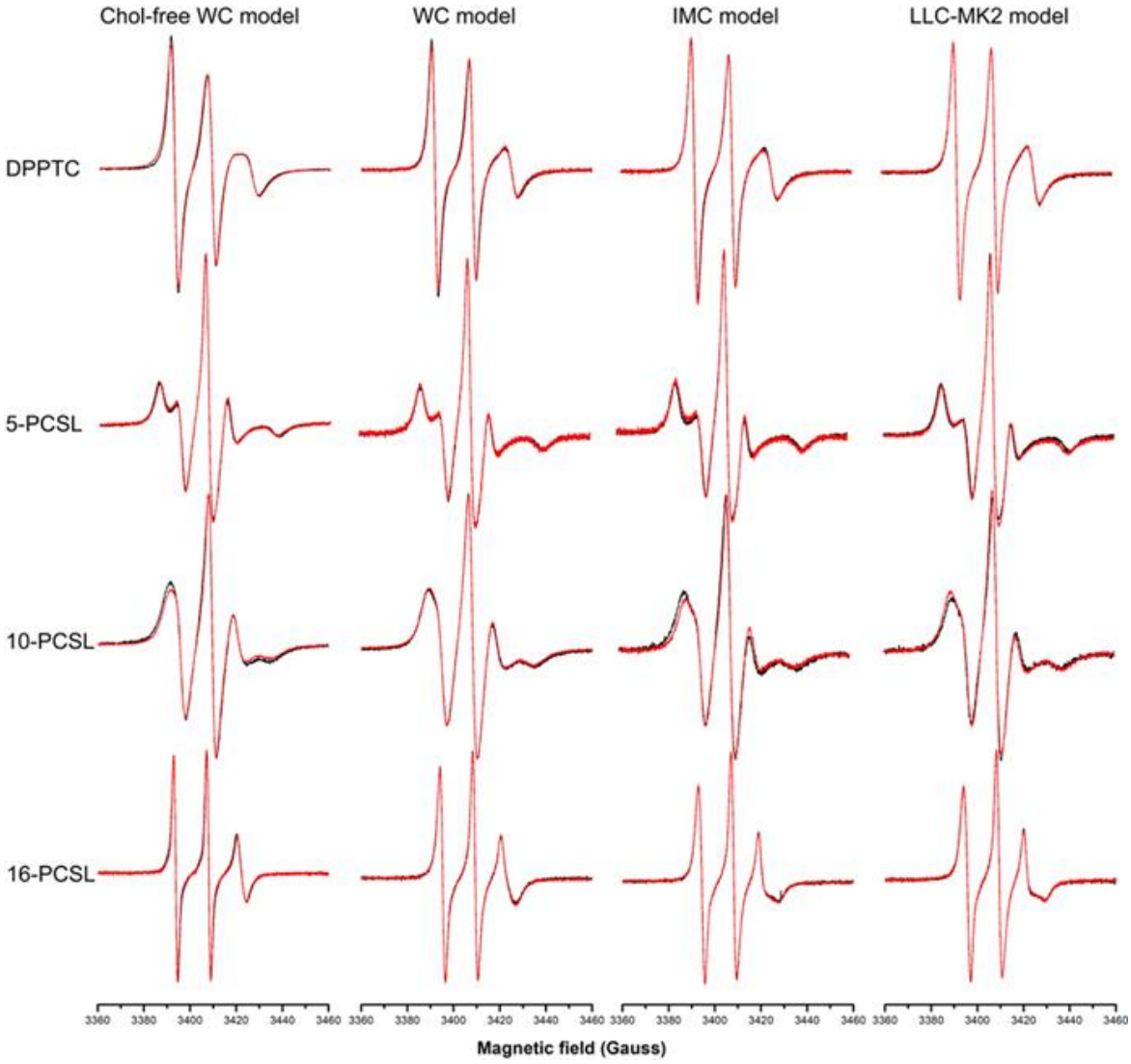

Figure 9. Effect of iron(III) complex on the membrane packing and fluidity. ESR spectra of DPPTC, 5-PCSL, 10-PCSL, and 16-PCSL embedded into 10 mg/mL of multilamellar vesicles of the following lipid model membranes: Chol-free WC, WC, IMC, and LLC-MK2 models. Spectra were acquired at 22 ºC in the absence (black) and presence (red) of the complex at a lipid-to-drug molar ratio of 20 (5 mol%).

Spectral simulations indicate that the complex increases both the order parameter (S_0) and the rotational correlation time (τ) for DPPTC in Chol-free WC and IMC models, while reducing both parameters in the WC model (**Table 2**). In the LLC-MK2 model, the complex caused a minor increase in τ and a negligible change in S_0 for DPPTC, showing minimal impact on headgroup ordering and dynamics. At the upper acyl chain region (5-PCSL), the complex slightly decreased S_0 and τ in all models, reflecting increased fluidity. In the middle acyl chain region (10-PCSL), the complex caused negligible changes in Chol-free and WC models but

increased τ and S_0 in the LLC-MK2 model (**Table 2**), suggesting enhanced ordering deeper in the bilayer.

Table 2. Best-fit rotational correlation time (τ) and order parameter (S_0) obtained from Nonlinear least-squares simulations of the ESR spectra of DPPTC, 5-PCSL, 10-PCSL, and 16-PCSL in multilamellar vesicles at 22 ºC without and with 5 mol% of iron(III) complex. The samples include POPC/POPE/POPS/SM 75/10/10/5 (Chol-free WC model); POPC/POPE/POPS/SM/Chol 63/8/8/4/17 (WC model); POPC/POPE/POPS/SM/Chol 53/7/7/3/30 (IMC model); and POPC/POPE/POPS/SM/Chol 39/13/7/11/30 (LLC-MK2 model).

	Chol-free WC		WC model		IMC model		LLC-MK2 model	
System	**τ (ns)**	**S_0**	**τ (ns)**	**S_0**	**τ (ns)**	**S_0**	**τ (ns)**	**S_0**
DPPTC blank	1.94	0.33	1.43	0.22	1.37	0.17	1.37	0.15
DPPTC + iron(III) complex	2.13	0.35	1.22	0.16	1.58	0.21	1.42	0.16
5-PCSL blank	1.36	0.49	1.45	0.54	1.58	0.60	1.71	0.61
5-PCSL + iron(III) complex	1.27	0.47	1.42	0.52	1.45	0.58	1.61	0.57
10-PCSL blank	2.00	0.20	1.87	0.27	1.89	0.33	1.89	0.29
10-PCSL + iron(III) complex	1.79	0.20	1.81	0.26	1.82	0.30	2.02	0.34
16-PCSL blank	0.28	0.08	0.32	0.12	0.22	0.19	0.20	0.19
16-PCSL + iron(III) complex	0.27	0.07	0.32	0.12	0.23	0.18	0.24	0.19

The uncertainties of the parameters τ and S_0 were estimated in 5% and 0.01, respectively.

Discussion

Current treatment options for toxoplasmosis are limited, and not optimal regarding the harsh profile of side effects and treatment duration (from 4–6 weeks to over 1 year), which may affect compliance [65,66]. In 2021, a study on adverse outcomes associated with the treatment of *T. gondii* infections indicated clindamycin and PYR the most suspicious chemotherapies leading to the death of 23 patients among a total of 102 studied cases [67]. Immunization strategies are currently being studied and developed, however, there is no vaccine available for human administration. Thus, there is an urgent need to develop newer, safer, and more effective treatment alternatives for toxoplasmosis [68]. In the present study, we investigated the anti-*Toxoplasma* activity of the iron(III) complex, whose molecular structure was solved by

monocrystal x-ray diffraction. The data obtained reveals the formation of a mononuclear hexacoordinated iron(III) complex containing a molecule of HL1 ligand and three chloride anions: [Fe(HL)Cl_3] [54].

The viability of the LLC-MK2 host cells after treatment with the iron(III) complex was initially assessed using the MTT reduction assay. After 24 h, the complex slightly reduced cell viability. However, after 48 h, the complex did not affect the host cell viability, as indicated by the MTT (when 500 µM of the complex was used) and by the LDH assays. The tetrazolium salts utilized in the MTT assays measure the mitochondrial metabolic rate and indirectly reflect viable cell numbers in the culture [69]. This suggests that the complex initially affects the mitochondria within the first 24 h, but at a concentration of 500 µM, the complex stabilizes and becomes non-toxic to the cells after 48 h. These findings align with previous studies using the same cell line and two dinuclear µ-oxo iron(III) complexes [49] as well as a dinuclear iron(III) compound [18]. Thus, the iron(III) complex exemplifies another low-toxicity complex for host cells.

A previous study demonstrated that this iron(III) complex has anti-*Toxoplasma* activity at concentrations of 10 µM and 20 µM [54]. Therefore, we tested lower concentrations in LLC-MK2 host cells infected with *T. gondii* and determined the IC_{50}. After 24 h and 48 h of treatment, IC_{50} values of 12.4 nM and 56.0 nM, respectively, were obtained, which were considerably lower than those reported in the literature for clinically used drugs (SDZ, PYR). Our compound demonstrated superior potency at nanomolar concentrations when compared to the lowest IC_{50} values reported for SDZ and PYR. The iron(III) complex was approximately 41 times more effective than SDZ (0.0124 µM vs. 0.512 µM; Trotsko et al., 2019 [24]), and about 26 times more potent than PYR (0.0124 µM vs. 0.326 µM; Trotsko et al., 2019 [24]). These comparisons emphasize the enhanced antiparasitic efficacy of the iron(III|) complex under standard *in vitro* conditions and support its potential as a promising candidate for the treatment of toxoplasmosis.

The IC_{50} values of iron(III) complexes are promising when compared to other coordination compounds reported in the literature. For example, a trithiolato-diruthenium complex conjugated to sulfadoxine inhibited proliferation of *T. gondii* tachyzoites grown in human foreskin fibroblast, with an $IC_{50} < 150$ nM after 3 and 6 days of treatment [70]. Four newly synthesized ferrocene-containing artesunate complexes demonstrated good activity against *T. gondii*, with IC_{50} values in the low micromolar range (0.28 - 1.2 µM) after 24 h and 48 h of treatment [71]. The anti-*Toxoplasma* activity of auranofin was found to depend on the presence of the gold(I) ion and the phosphine ligand, with selected auranofin derivatives (6, 10,

31, and 39) inhibiting parasite growth with IC_{50} values of 0.46 µM, 0.67 µM, 1.41 µM, and 0.59 µM, respectively [72]. Copper(II) and zinc(II) coordination compounds with 5-nitroimidazole-based ligands also showed activity against extracellular *T. gondii* (RH strain) after 1 h of treatment. The copper(II) compounds $[Cu(onz)_2Cl_2]$ and $[Cu(onz)_2Br_2]$ showed IC_{50} values of 8.49 µM and 2.73 µM, respectively, while $[Zn(cenz)_2Br_2]$ exhibited an IC_{50} of 40.0 µM [73]. Non-metallic compounds also showed strong anti-*Toxoplasma* activity, such as ELQ-316 [74-77], FR235222 [78], SW413 [79] with IC_{50} values of 0.007 nM, 9.7 nM, and 20 nM, respectively. Hydroxamate-based compounds also showed IC_{50} near 100 nM [80], while SDZ analogs (1,2,3-triazole-sulfonamide hybrids) exhibited IC_{50} values ranging from 0.01835 µM to 0.07492 µM [81]. Our results indicate that the iron(III) complex effectively inhibited parasite proliferation in the nanomolar range, demonstrating superior activity compared to many other complexes described in the literature. Although a selectivity index was not explicitly calculated – since extremely high concentrations of the iron(III) complex would be required to determine a reasonable IC_{50} for the host cell – it is evident that the compound exhibits high selectivity against *T. gondii* (estimated selectivity index > 4 x 10^4). Therefore, these findings suggest that the iron(III) complex is a promising compound with anti-*Toxoplasma* activity for future *in vivo* studies.

To decipher whether the withdrawal of the iron(III) complex after 48 h of treatment affected the continued growth of tachyzoites, we treated infected cells with the complex for 48 h, removed the compound by washing, and cultured the cells for an additional 48 h. The results showed that the inhibitory effect of the complex persisted even after its withdrawal, indicating an irreversible effect at a concentration of 12.5 nM, with no significant difference observed at 100 nM. Thus, the treated parasites were unable to resume growth in host cells, even 48 h after the compound was removed from the medium. This indicates that the structural and functional changes induced by the treatment irreversibly compromise the viability of the parasite. Notably, this irreversible effect following a short treatment period highlights the potential of the iron (III) complex as a promising anti-*Toxoplasma* agent.

Treatment with the iron(III) complex resulted in morphological and ultrastructural changes in *T. gondii*. Initially, tachyzoites lost their typical shape and became rounded. Transmission electron microscopy revealed alterations in the cytoplasm (clefts) and membrane blebs, the latter being a hallmark of apoptotic cell death [53], ultimately leading to parasite degradation inside the parasitophorous vacuole. These changes may have been triggered by oxidative stress. As previously described, iron(III) can induce the production of free radicals, such as hydroxyl radicals, in biological systems. These reactive species are often associated

with DNA damage, lipid peroxidation, and protein modifications, ultimately leading to cell death [18]. A previous study evaluated whether the stressful conditions induced by iron-based compounds were associated with an oxidative damage. It was found that both *T. gondii*-infected and uninfected host cells exhibited a significant increase in reactive oxygen species (ROS) production only when treated with the compound, suggesting that the treatment altered the intracellular redox balance of the parasites. This disruption may have impaired the parasite's antioxidant defense system, leading to cell death while sparing host cell [18]. Similar effects have been reported for other compounds that generate ROS, disrupting key mitochondrial antioxidant enzymes such as peroxiredoxin, superoxide dismutase, and catalase [82-86]. Given that *T. gondii* is highly sensitive to oxidative stress, even minor disruptions in redox homeostasis can be lethal [87,88], and excessive ROS production has been shown to inhibit or kill the parasite [89].

Another significant ultrastructural change observed after treatment with the iron(III) complex was the rupture of the plasma membrane and the IMC of tachyzoites. The *T. gondii* IMC was stained with anti-IMC1 antibody confirming the disruption of this parasite structure. Apicomplexans exhibit an atypical cytoskeleton organized around a membranous structure, named IMC, which consists of flattened sacs and a meshwork of intermediate filament-like proteins connected to cortical microtubules [57]. The IMC plays a central role in apicomplexan biology, being critical for motility, replication, polarity, and structural integrity [90]. The fast replicating stage of *T. gondii*, the tachyzoite, undergoes endodyogeny, a process in which the IMC provides the scaffold for the formation of two daughter progenies within the mother cell [91]. Therefore, given the observed alterations, it is likely that the iron(III) complex alters the organization and integrity of both the plasma membrane and the IMC of tachyzoites, potentially impairing parasite replication and infection. Similar results were previously reported with other compounds, such as copper complexes, which cause membrane disruption and interfere with the proper arrangement of the IMC, thereby affecting cell division [51]. Additionally, the herbicide oryzalin, a dinitroaniline compound, has been shown to block the formation of the subpellicular microtubules, leading to disruption of the parasite's IMC organization [92]. These findings suggest that the IMC is a highly sensitive structure in the parasite and may represent a key target for antiparasitic compounds.

Understanding the interactions between drugs, including metallopharmaceuticals, and biological membranes is crucial for elucidating molecular mechanisms of action and enhancing therapeutic efficacy. DSC and ESR are pivotal techniques in this regard, offering detailed insights into changes in the physical properties of lipid bilayers induced by drug

interactions [61]. DSC enables the quantification of heat capacity changes in lipid vesicles, shedding light on membrane phase transitions, thermal stability, and structural organization in response to drug incorporation. On the other hand, ESR is a powerful technique for assessing the impact of drugs, peptides, and proteins on the membrane fluidity, packing, and hydration properties [64], which are important to understand their permeability, distribution, and biological activity. This combined approach allowed us to investigate the effect of iron(III) complex on the physical properties of model membranes that mimic the parasite membrane, providing a deep understanding of drug-membrane interactions.

Our DSC results reveal that the iron(III) complex interacts with both simple and complex lipid model membranes, producing opposing effects on the thermodynamic parameters of the membranes' phase transition depending on the lipid composition and Chol content. Specifically, the complex increased the enthalpy and entropy changes of the phase transition in DPPC/Chol and the SM- and PE-enriched LLC-MK2 membrane models. In contrast, it reduced both ΔH and ΔS in Chol-free membranes, as well as in the WC and IMC model membranes. A reduction in ΔH suggests that less energy is required to drive the transition from the ordered to the fluid/disordered phase, indicating that the complex disrupts lipid packing, thereby facilitating the phase transition. Conversely, the increased enthalpy and entropy changes observed in DPPC/Chol and LLC-MK2 membranes suggest that the complex enhances ordering in these bilayers, increasing the energy demand for the phase transition. This behavior points to a more ordered and tightly packed membrane environment in these systems. These findings highlight the differential impact of the complex on membrane stability, which is strongly influenced by the Chol content and overall lipid composition. Moreover, both $\Delta T_{1/2}$ and T_m remained largely unaffected by the complex across all membrane models. The unaltered $\Delta T_{1/2}$ indicates that the cooperativity of the phase transition is not significantly influenced by the complex, while the consistent T_m values suggest that the complex does not substantially shift the gel-to-liquid crystalline transition temperature.

These lipid composition-dependent effects were further explored using ESR spectroscopy, which provided detailed insights into membrane fluidity and packing. The rotational correlation time (τ) and the order parameter (S_0), derived from spectral simulations, offer information on lipid mobility and membrane ordering, respectively. Higher τ values reflect reduced mobility and lower membrane fluidity, while higher S_0 values indicate increased lipid ordering and membrane packing. In parasite-like membranes, the iron(III) complex decreases both S_0 and τ for 5-PCSL and 10-PCSL, indicating reduced lipid packing and enhanced mobility in these regions. Interestingly, in the WC model, the complex increases

S_0 and decreases τ at the membrane-water interface (DPPTC), suggesting tighter packing and reduced mobility of the lipid headgroup region. This behavior contrasts with the Chol-free WC and IMC models, where the complex decreases S_0 and increases mobility at the surface. These findings point to a differential localization of the complex: at the bilayer surface in the WC model but slightly deeper within the bilayer in Chol-free WC and IMC models. The reduced lipid packing and increased dynamics in parasite membranes correlate with the lower energy required for phase transitions observed in DSC, reinforcing the idea that the complex disrupts membrane stability in these systems.

In the mammalian-like LLC-MK2 model, the complex exhibits distinct effects depending on the bilayer region. It decreases S_0 and τ around carbon 5 (5-PCSL), reflecting increased fluidity near the upper acyl chain. In contrast, it increases S_0 and τ at the middle acyl chain region (10-PCSL), indicating enhanced ordering and reduced mobility deeper in the bilayer. The slight increase in τ for 16-PCSL suggests a more restricted lipid mobility at the bilayer core, albeit with minimal changes in S_0. These effects correlate with the higher energy required for phase transitions seen in DSC, suggesting a stabilizing effect of the complex on LLC-MK2 membranes.

The pronounced effects at the membrane-water interface (DPPTC) and upper acyl chain region (5-PCSL), combined with minimal spectral changes in the bilayer core (16-PCSL), confirm that the iron(III) complex predominantly localizes near the bilayer surface, interacting primarily with lipid headgroups and upper chain regions rather than embedding deeply into the membrane.

Taken together, these ESR findings highlight the region-specific and composition-dependent interactions of the iron(III) complex with lipid bilayers. The differential effects observed in parasite and mammalian membrane models suggest that the complex modulates membrane dynamics through selective localization and interaction, likely contributing to its specificity in targeting parasite membranes. These results provide a mechanistic basis for understanding the complex's ability to disrupt parasite membranes while sparing mammalian ones, emphasizing its potential as a selective therapeutic agent.

Conclusion

In conclusion, the iron(III) complex interacts with both *T. gondii* and host cell membranes, but with distinct effects depending on the lipid composition. In parasite-like membranes, the complex induces destabilization, increasing fluidity and reducing lipid packing, which

correlates with irreversible membrane damage and parasite death. In contrast, in mammalian-like membranes, it enhances lipid ordering and restricts mobility, suggesting a stabilizing effect that helps preserve host cell membrane integrity. Its potency at such low concentrations makes this complex a promising candidate for future research in the treatment of toxoplasmosis. Furthermore, its mechanism of action suggests that this complex may serve as a prototype for developing more potent and effective compounds, contributing to the advancement of innovative therapeutic strategies.

Supporting Information

Best-fit hyperfine tensor components and g-tensor components from Nonlinear least-squares simulations of the ESR spectra of multilamellar vesicles without and with iron(III) complex (PDF)

Acknowledgements

Financial support was received from FAPERJ (Fundação Carlos Chagas de Amparo à Pesquisa do Estado do Rio de Janeiro) - Grant numbers 210.778/2021, 211.816/2021, 200.980/2021, 204.136/2024; and CNPq (Conselho Nacional de Desenvolvimento Científico e Tecnológico) - Grant numbers 317528/2021-1, 314305/2023-8. This work was also financed in part by the Coordenação de Aperfeiçoamento de Pessoal de Nível Superior - Brasil (CAPES) - Finance Code 001. IBS thanks CNPq and State University of Northern Rio de Janeiro for the undergraduate scholarship and GVTB thanks Capes for the doctorate fellowship (Grant number 88887.974946/2024-00).

Declaration

Competing Interest The authors declare no competing financial interest.

References

1. Matta S.K., Rinkenberger N., Dunay I.R., Sibley R.D. *Toxoplasma gondii* infection and its implications within the central nervous system. Nat. Rev. Microbiol.19 (2021) 467–80. https://doi.org/10.1038/s41579-021-00518-7.

2. Molan A., Nosaka K., Hunter M., Wang W. Global status of *Toxoplasma gondii* infection: systematic review and prevalence snapshots. Trop. Biom. 36 (2019) 898–925.

3. Montoya J.G., Liesenfeld O. Toxoplasmosis. Lancet 363 (2004) 1965–1976. https://doi.org/10.1016/S0140-6736(04)16412-X.

4. Dubey J.P. Toxoplasmosis- A waterborne zoonosis. Vet. Parasitol. 126 (2004) 57–72. https://doi.org/10.1016/j.vetpar.2004.09.005.

5. Halonen S.K., Weiss L.M. Toxoplasmosis. Handb. Clin. Neurol. 114 (2013) 125–145. https://doi.org/10.1016/B978-0-444-53490-3.00008-X.

6. Black M.W., Boothroyd J.C. Lytic cycle of *Toxoplasma gondii*. Microbiol Mol Biol Rev. 64 (2000) 607–623. https://doi.org/10.1128/MMBR.64.3.607-623.2000.

7. Demar M., Ajzenberg D., Maubon D., Djossou F., Panchoe D., Punwasi W., Valery N., Peneau C., Daigre J.L., Aznar C., Cottrelle B., Terzan L., Darde M.L., Carme B. Fatal outbreak of human toxoplasmosis along the Maroni River: epidemiological, clinical, and parasitological aspects. Clin Infect Dis. 45,7 (2007) 88–95. https://doi.org/10.1086/521246.

8. Wang Z.D., Liu H.H., Ma Z.X., Ma H.Y., LiZ. Y., Yang Z.B., Zhu X.Q., Xu B., Wei F., Liu Q. *Toxoplasma gondii* infection in immunocompromised patients: a systematic review and meta-analysis. Front. Microbiol. 8 (2017) 389.https://doi.org/10.3389/fmicb.2017.00389.

9. Martina M.N., Cervera C., Esforzado N., Linares L., Torregrosa V., Sanclemente G., Hoyo I., Cofan F., Oppenheimer F., Miro J.M., Campistol J.M., Moreno A. *Toxoplasma gondii* primary infection in renal transplant recipients. Two case reports and literature review. Transplant Int. 24 (2011) e6–e12. https://doi.org/10.3389/fmicb.2017.00389.

10. Hampton M.M. Congenital toxoplasmosis: a review. Neonatal Netw. 34,5 (2015) 274–278. https://doi.org/10.1891/0730-0832.34.5.274.

11. Angel S.O., Vanagas L., Ruiz D.M., Cristaldi C., Saldarriaga Cartagena A. M., Sullivan W. J. Jr. Emerging therapeutic targets against *Toxoplasma gondii*: update on DNA repair response inhibitors and genotoxic drugs. Front. Cell. Infection Microbiol. 10 (2020) 289. https://doi.org/10.3389/fcimb.2020.00289.

12. Secrieru A., Costa I.C., O'Neill P.M., Cristiano M.L. Antimalarial agents as Therapeutic Tools Against Toxoplasmosis-A Short Bridge Between Two Distant Illnesses. Molecules. 25,7 (2020) 1574. https://doi.org/10.3390/molecules25071574.

13. Shammaa A.M., Powell T.G., Benmerzouga I. Adverse outcomes associated with the treatment of *Toxoplasma* infections. Sci. Rep. 11 (2021) 1035. https://doi.org/10.1038/s41598-020-80569-7.

14. Dunay I.R., Gajurel K., Dhakal R., Liesenfeld O., Montoya J.G. Treatment of Toxoplasmosis: historical perspective, animal models, and current clinical practice. Clin. Microbiol. Rev. 31 (2018). https://doi.org/10.1128/CMR.00057-17.

15. Montoya J.G., Remington J.S. Management of *Toxoplasma gondii* infection during pregnancy. Clin. Infect. Dis. 47 (2008) 554–566. https://doi.org/10.1086/590149.

16. Alday P.H., Doggett J.S. Drugs in development for toxoplasmosis: Advances, challenges, and current status. Drug Des. Devel. 11 (2017) 273–293. https://doi.org/10.2147/DDDT.S60973.

17. Paquet C., Yudin M.H. Toxoplasmosis in pregnancy: prevention, screening, and treatment. J. Obs. Gynaecol. Can. 35 (2013) 78–81.

18. Portes J.A., Souza T.G., Dos Santos T.A.T., Da Silva L.L.R., Ribeiro T.P., Pereira M.D., Horn Jr A., Fernandes C., Da Matta R.A., de Souza W., Seabra S.H. Reduction of *Toxoplasma gondii* development due to inhibition of parasite antioxidant enzymes by a dinuclear iron (III) compound. Antimicrob. Agents Chemother. 59, 12 (2015) 7374. https://doi.org/10.1128/AAC.00057-15.

19. Jin C., Kaewintajuk K., Jiang J., Jeong W., Kamata M., Kim H., Wataya Y., Park H. *Toxoplasma gondii*: a simple high-throughput assay for drug screening *in vitro*. Exp. Parasitol. 121 (2009) 132–136. https://doi.org/10.1016/j.exppara.2008.10.006.

20. Doliwa C., Escotte-Binet S., Aubert D., Velard F., Schmid A., Geers R., Villena I. Induction of sulfadiazine resistance *in vitro* in *Toxoplasma gondii*. Exp. Parasitol. 133 (2013) 131–136. https://doi.org/10.1016/j.exppara.2012.11.019

21. van der Ven A.J., Schoondermark-van de Ven E.M., Camps W., Melchers W.J., Koopmans P.P., van der Meer J.W., Galama J.M. Antitoxoplasma effect of pyrimethamine, trimethoprim and sulphonamides alone and in combination: implications for therapy. J. Antimicrob. Chemother. 38 (1996) 75–80. https://doi.org/10.1093/jac/38.1.75.

22. Huffman A.M., Ayariga J.A., Napier A., Robertson B.K., Abugri D.A. Inhibition of *Toxoplasma gondii* growth by dihydroquinine and its mechanisms of action. Front Cell Infect Microbiol. 12 (2022) 852–889. https://doi.org/10.3389/fcimb.2022.852889.

23. Węglińska L., Bekier A., Trotsko N., Kaproń B., Plech T., Dzitko K., Paneth A. Inhibition of *Toxoplasma gondii* by 1,2,4-triazole-based compounds: marked improvement in selectivity relative to the standard therapy pyrimethamine and sulfadiazine. Journal of Enzyme Inhibition and Medicinal Chemistry. 37 (2022) 2621–2634. https://doi.org/10.1080/14756366.2022.2112576.

24. Trotsko N., Bekier A., Paneth A., Wujec M., Dzitko K. Synthesis and *in vitro* anti-*Toxoplasma gondii* activity of novel thiazolidin-4-one derivatives. Molecules. 24 (2019) 3029. https://doi.org/10.3390/molecules24173029.

25. Qiu Y., Wang W., Wang Q., Xu J., Dai G., Bai Y., Zhang J. Activity evaluation and mode of action of ICA against *Toxoplasma gondii in vitro*. Biomolecules. 15 (2025) 202. https://doi.org/10.3390/biom15020202.

26. Pearce B.D., Kruszon-Moran D., Jones J.L. The relationship between *Toxoplasma gondii* infection and mood disorders in the third national health and nutrition survey. Biol. Psychiatry 72 (2012) 290–295. https://doi.org/10.1016/j.biopsych.2012.01.003.

27. Heydari P., Yavari M., Adibi P., Asghari G., Ghanadian S.M., Dida G.O., Khamesipour F. Medicinal properties and active constituents of *Dracocephalum kotschyi* and its significance in Iran: a systematic review. Evid. Based Complement. Altern. Med. (2019) 9465309. https://doi.org/10.1155/2019/9465309.

28. Xu Q., Duan Y.Y., Pan M., Jin Q.W., Tao J.P., Huang S.Y. *In vitro* evaluation reveals effect and mechanism of Artemether against *Toxoplasma gondii*. Metabolites.13 (2023) 476. https://doi.org/10.3390/metabo13040476.

29. Wheate N.J., Walker S., Craig G.E., Oun R. The status of platinum anticancer drugs in the clinic and in clinical trials. Dalton Trans. 39 (2010) 8113–8127. https://doi.org/10.1039/C0DT00292E.

30. Oun R., Wheate N.J. Platinum anticancer drugs. In Encyclopedia of Metalloproteins; Kretsinger R.H., Uversky V.N., Permyakov E.A., Eds.; Springer: New York, NY, USA, 2013. https://doi.org/10.1007/978-1-4614-1533-6_525.

31. Dasari S., Tchounwou P.B. Cisplatin in cancer therapy: molecular mechanisms of action. Eur. J. Pharmacol. 740 (2014) 364–378. https://doi.org/10.1016/j.ejphar.2014.07.025.

32. Ghosh S. Cisplatin: the first metal based anticancer drug. Bioorg. Chem. 88 (2019) 102925. https://doi.org/10.1016/j.bioorg.2019.102925.

33. Ndagi U., Mhlongo N., Soliman M.E. Metal complexes in cancer therapy - An update from drug design perspective. Drug Des. Dev. Ther. 11 (2017) 599–616. https://doi.org/10.2147/DDDT.S119488.

34. Gasser G., Ott I., Metzler-Nolte N. Organometallic anticancer compounds. J. Med. Chem. 54 (2011) 3–25. https://doi.org/10.1021/jm100020w.

35. Zhang P., Sadler P.J. Advances in the design of organometallic anticancer complexes. J. Organomet. Chem. 839 (2017) 5–14. https://doi.org/10.1016/j.jorganchem.2017.03.038.

36. Ong Y.C., Gasser G. Organometallic compounds in drug discovery: Past, present and future. Drug Discov. Today Technol. (2019). https;//doi.org/10.16/j.ddtec.2019.06.001.

37. Hartinger C.G., Metzler-Nolte N., Dyson P.J. Challenges and opportunities in the development of organometallic anticancer drugs. Organometallics 31 (2012) 5677–5685. https://doi.org/10.1021/om300373t.

38. Lazarevi´c T., Rilak A., Bugarˇci´c Ž.D. Platinum, palladium, gold and ruthenium complexes as anticancer agents: Current clinical uses, cytotoxicity studies and future perspectives. Eur. J. Med. Chem. 142 (2017) 8–31. https://10.1016/j.ejmech.2017.04.007.

39. Thorp-Greenwood F.L. An introduction to organometallic complexes in fluorescence cell imaging: Current applications and future prospects. Organometallics. 31 (2012) 5686–5692. https://doi.org/10.1021/om3004477.

40. Lo K.K.W., Choia A.W.T., Lawa W.H.T. Applications of luminescent inorganic and organometallic transition metal complexes as biomolecular and cellular probes. Dalton Trans. 41(2012) 6021–6047. https://doi.org/10.1039/C2T11892K.

41. Morais G.R., Paulo A., Santos I. Organometallic complexes for SPECT imaging and/or radionuclide therapy. Organometallics. 31 (2012) 5693–5714. https://doi.org/10.1021/om300501d.

42. Chellan P., Sadler P.J. Enhancing the activity of drugs by conjugation to organometallic fragments. Chem. Eur. J. 26 (2020) 8676–8688. https://doi.org/10.1002/chem.201904699.

43. Ong Y.C., Roy S., Andrews P.C., Gasser G. Metal compounds against neglected tropical diseases. Chem. Rev. 119 (2019) 730–796. https://doi.org/10.1021/acs.chemrer.8b00338.

44. Gambino D., Otero L. Design of prospective antiparasitic metal-based compounds including selected organometallic cores. Inorg. Chim. Acta. 472 (2018) 58–75. https://doi.org/10.1016/j.ica.2017.07.068.

45. Ravera M., Moreno-Viguri E., Paucar R., Perez-Silanes S., Gabano E. Organometallic compounds in the discovery of new agents against kinetoplastid-caused diseases. Eur. J. Med. Chem. 155 (2018) 459–482. https://doi.org/10.1016/j.ejmech.2018.05.044.

46. Frei A., Zuegg J., Elliott A.G., Baker M., Braese, S., Brown C., Chen F., Dowson C.G., Dujardin G., Jung N., King A.P., Mansour A.M., Massi M., Moat J., Mohamed H.A., Renfrew A.K., Ruttedge P.J., Sandler P.J., Todd M.H., Willans C.E., Wilson J.J., Cooper M.A., Blaskovich M.A.T. Metal complexes as a promising source for new antibiotics. Chem. Sci. 11 (2020) 2627–2639. https://doi.org/10.1039/C9SC06460E.

47. Nasiri Sovari S., Zobi F. Recent studies on the antimicrobial activity of transition metal complexes of groups 6–12. Chemistry. 2 (2020) 26. https://doi.org/10.3390/chemistry2020026.

48. Patra M., Gasser G., Metzler-Nolte N. Small organometallic compounds as antibacterial agents. Dalton Trans. 41 (2012) 6350–6358. https://doi.org/10.1039/C2DT12460B.

49. Moreira F.F., Portes J.A., Barros A.N.F., Fernandes C., Horn Jr A., Santiago C.P., Segat B.B., Caramori G.F., Madureira L.M.P., Candela D.R.S., Marques M.M., Lamounier C.R., Jackson A., De Souza W., DaMatta R.A., Seabra S.H. Development of new dinuclear Fe (III) coordination compounds with *in vitro* nanomolar antitrypanosomal activity. Dalton Trans. 50 (2021) 12242–12264. https://doi.org/10.1016/j.molstruc.2022.133380.

50. de Assis V.M., Visentin L.C., de Souza F.S., DaMatta R.A., Horn Jr A., Fernandes C. Synthesis, crystal structure and relevant antiproliferative activity against *Toxoplasma gondii* of a new binuclear Co(II) complex. Inorg. Chem. Commun. 67 (2016) 47. https://doi.org/10.1016/j.inoche.2016.02.017.

51. Portes J.A., Motta C.S., Azeredo N.F., Fernandes C., Horn Jr A., de Souza W., DaMatta R.A., Seabra S.H. *In vitro* treatment of *Toxoplasma gondii* with copper(II) complexes induces apoptosis-like and cellular division alterations. Vet. Parasitol. 245 (2017) 141. https://doi.org/10.1016/j.vetpar.2017.04.002.

52. Batista L.C, de Souza F.S., de Assis V.M., Seabra S.H., Bortoluzzi A.J., Renno M.N., Horn Jr A., DaMatta R.A., Fernandes C. Antiproliferative activity and conversion of tachyzoite to bradyzoite of *Toxoplasma gondii* promoted by new zinc complexes containing sulfadiazine. RSC Adv. 5, 122 (2015) 100606. https://doi.org/10.1039/C5RA17690E.

53. Portes J.A., Azeredo N.F., Siqueira P.G., de Souza T.G., Fernandes C., Horn Jr A., Candela D.R.S., de Souza W., DaMatta R.A., Seabra S.H. A new iron (III) complex-containing sulfadiazine inhibits the proliferation and induces cysto-genesis of *Toxoplasma gondii* . Parasitol. Res. 117, 9 (2018) 2795. https://doi.org/10.1039/C5RA17690E.

54. Cardoso A.P., Madureira L.M.P., Segat B.B., Menezes, J. do N.C., Cargnelutti R., Candela D.R.S., Mariano D.L., Parreira R.L.T., Horn Jr A., Seabra S.H., DaMatta R.A., Moreira F.F., Moreira R.V., Caramori G.F., Fernandes, C. Development, structural, spectroscopic and in silico investigation of new complexes relevant as anti-toxoplasma metallopharmacs. J. of Mol. Struct. 1265 (2022) 133380. https://doi.org/j.molstruc.2022.133380.

55. Harding C.R and Meissner, M. The IMC in *Plasmodium* and *Toxoplasma*. Cell Microbiol. 16 (2014) 632-641. https://doi.org/10.1111/cmi.12285.

56. Cheng ES, Moon AS, Barshop WD, Wohlschlegel JA, Bradley PJ. Function and interactions of a protein bridge between the inner membrane complex and subpellicular microtubules in *Toxoplasma gondii*. (2024). doi:10.1101/2024.05.29.595897.

57. Anderson-White B.R., Ivey F.D., Cheng K., Szatanek T., Lorestani A., Beckers C.J., Ferguson D.J., Sahoo N., Gubbels M.J. A family of intermediate filament-like proteins is

sequentially assembled into the cytoskeleton of *Toxoplasma gondii*. Cell. Microbiol. 13 (2011) 18–31. https://doi.org/10.1111/j.1462-5822.2010.01514.x.

58. Foussard F., Gallois Y., Girault A., Menez J.F. Lipids and fatty acids of tachyzoites and purified pellicles of *Toxoplasma gondii*. Parasitol Res. 77, 6 (1991) 475–477. https://doi.org/10.1007/BF00928412.

59. Hitakarun A., Williamson M.K., Yimpring N., Sornjai W., Wikan N., Arthur C.J., Pompon J., Davidson A.D., Smith D.R. Cell type variability in the incorporation of lipids in the Dengue virus virion. Viruses. 14,11 (2022) 2566. https://doi.org/10.3390/v14112566.

60. Symons J.L., Cho K.J., Chang J.T., Du G., Waxham M.N., Hancock J.F., Levental I., Levental K.R. Lipidomic atlas of mammalian cell membranes reveals hierarchical variation induced by culture conditions, subcellular membranes, and cell lineages. Soft Matter. 17, 2 (2021) 288–297. https://doi.org/10.1039/DOSM00404A.

61. Basso L.G.M., Rodrigues R.Z., Naal R.M.Z.G., Costa-Filho A.J. Effects of the antimalarial drug primaquine on the dynamic structure of lipid model membranes. Bioch. Et Biophy. Acta-Biomemb. 1808 (2011) 55–64. https://doi.org/10.1016/j.bbamem.2010.08.009.

62. Budil D.E.S., Saxena S., Sanghyuk L., Freed H.J. Nonlinear-least-squares analysis of slow-motion EPR spectra in one and two dimensions using a modified Levenberg-Marquardt algorithm. J. of Mag, Res. Series A. 120 (1996) 155–189. https://doi.org/10.1006/jmra.1996.0113.

63. Mannock D.A., Lewis R.N., Mc Elhaney R.N. A calorimetric and spectroscopic comparison of the effects of ergosterol and cholesterol on the thermotropic phase behavior and organization of dipalmitoylphosphatidylcholine bilayer membranes. Biochim. Biophys. Acta. 1798, 3 (2010) 376–388. https://doi.org/10.1016/j.bbamem.2009.09.002.

64. Basso L.G.M., Mendes L.F.S., Costa-Filho A.J. The two sides of a lipid-protein story. Biophys. Rev. 8 (2016) 179–191. https://doi.org/10.1007/s12551-016-0199-5.

65. Alday P.H., Doggett J.S. Drugs in development for toxoplasmosis: Advances, challenges, and current status. Drug Des. Devel. 11 (2017) 273–293. https://doi.org/10.2147/DDDT.S60973.

66. Konstantinovic N., Guegan H., Stäjner T., Belaz S., Robert-Gangneux F. Treatment of toxoplasmosis: current options and future perspectives. Food Waterborne Parasitol. 15 (2019) e00036. https://doi.org/10.1006/j.fawpar.2019.e00036.

67. Shammaa A.M., Powell T.G., Benmerzouga I. Adverse outcomes associated with the treatment of *Toxoplasma* infections. Sci Rep. 11 (2021) 1035. https://doi.org/10.1038/s41598-020-80569-7.

68. Barros M., Teixeira D., Vilanova M., Correia A., Teixeira N., Borges M. Vaccines in congenital toxoplasmosis: advances and perspectives. Front. Immunol. 11 (2021) 3900. https://doi.org/10.3389/fimmu.2020.621997.

69. Rai Y., Pathak R., Kumari N., Sah D.N., Pandey S., Kalra N., Soni R. Dwarakanath B.S., & Bhatt, A.N. Mitochondrial biogenesis and metabolic hyperactivation limits the application of MTT assay in the estimation of radiation induced growth inhibition. Nature – Sci.Rep. 8 (2018) 1531. https://doi.org/10.1038/s41598-018-19930-w.

70. Boubaker G., Bernal A., Vigneswaran A., Imhof D., Ferreira de Sousa M.C., H¨anggeli A.P.K., Haudenschild N., Furrer J., P˘aunescu E., Desiatkina O., Hemphill A. *In vitro* and *in vivo* activities of a trithiolato-diRuthenium complex conjugated with sulfadoxine against the apicomplexan parasite *Toxoplasma gondii*. Int.J.for Parasit: Drugs and Drug Resistance. 25 (2024).100544. https://doi.org/10.1016/j.ijpddr.2024.100544.

71. Munnik B.L., Kaschula C.H., Harding C.R., Chellan P. Investigation of new ferrocenyl-artesunate derivatives as antiparasitics. Dalton Trans. 52 (2023) 15786–15797. https://doi.org/10.1039/D3DT02254D.

72. Ma C.I., Tirtorahardjo J.A., Schweizer S.S., Zhang J., Fang Z., Xing L., Xu M., Herman D.A., Kleinman M.T., McCullough B.S., Barrios A.M., Andrade R.M. Gold(I) ion and the phosphine ligand are necessary for the anti-*Toxoplasma gondii* activity of auranofin. Microbiology. 12 (2024) 2. https://doi.org/10.1128/spectrum.02968-23.

73. Navarro-Penaloza R., Anacleto-Santos J., Rivera-Fernandez N., Sanchez-Bartez F., Gracia-Mora I., Caballero A.B., Gamez P., Barba-Behrens N. Anti-toxoplasma activity and DNA-binding of copper(II) and zinc(II) coordination compounds with 5-nitroimidazole-based ligands. J. of Biol, Inorg, Chem. 29 (2024) 33–49. https://doi.org/10.1007/s00775-023-02029-7.

74. Alday P.H., Bruzual I., Pou S., Nilsen A., Riscoe M.K., Doggett J. Mechanism of action of ELQ-316 against *Toxoplasma gondii*: eEvidence for Qi site inhibition of cytochrome bc1. Open Forum Infect. Dis. 3 (2016) 2249. https://doi.org/10.1093/ofid/ofw172.1797.

75. Alday P.H., Bruzual I., Nilsen A., Pou S., Winter R., Ben Mamoun C., Riscoe M.K., Doggett J.S. Genetic evidence for cytochrome b Qi site inhibition by 4(1H)-Quinolone-3-Diarylethers and Antimycin in *Toxoplasma gondii*. Antimicrob. Agents Chemother. 61 (2017) e01866-16. https://doi.org/10.1128/AAC.01866-16.

76. McConnell E.V., Bruzual I., Pou S., Winter R., Dodean R.A., Smilkstein M.J., Krollenbrock A., Nilsen A., Zakharov L.N., Riscoe M.K., Doggett J.S. Targeted structure-activity analysis of endochin-like quinolones reveals potent Qi and Qo site inhibitors of

Toxoplasma gondii and *Plasmodium falciparum* cytochrome bc(1) and identifies ELQ-400 as a remarkably effective compound against acute experimental Toxoplasmosis. ACS Infect. Dis. 4 (2018) 1574–1584. https://doi.org/10.1021/acsinfecdis.8b00133.

77. Doggett J.S., Nilsen A., Forquer I., Wegmann K.W., Jones-Brando L., Yolken R.H., Bordón C., Charman S.A., Katneni K., Schultz T., Burrows J.N., Hinrichs D.J., Meunier B., Carruthers V.B., Riscoe M.K. Endochin-like quinolones are highly efficacious against acute and latent experimental toxoplasmosis. Proc. Natl. Acad. Sci. USA 109 (2012)15936–15941. https://doi.org/10.1073/pnas.1208069109.

78. Maubon D., Bougdour A., Wong Y.S., Brenier-Pinchart M.P., Curt A., Hakimi M.A., Pelloux H. Activity of the histone deacetylase inhibitor FR235222 on *Toxoplasma gondii*: inhibition of stage conversion of the parasite cyst form and study of new derivative compounds. Antimicrob. Agents Chemother. 54 (2010) 4843–4850. https://doi.org/10.1128/aac.00462-10.

79. Mageed S.N., Cunningham F., Hung A.W., Silvestre H.L., Wen S., Blundell T.L., Abell C., McConkey G.A. Pantothenic acid biosynthesis in the parasite *Toxoplasma gondii*: a target for chemotherapy. Antimicrob. Agents Chemother. 58 (2014) 6345–6353. https://doi.org/10.1128/AAC.02640-14.

80. Boissavy T., Rotili D., Mouveaux T., Roger E., El Aliouat E.M., Pierrot C., Valente S., Mai, A., Gissot M. Hydroxamate-based compounds are potent inhibitors of *Toxoplasma gondii* HDAC biological activity. Antimicr. Agents and Chem. 67, 11 (2023)e0066123. https://doi.org/10.1128/aac.00661-23.

81. Arafa F.M., Osman D.H., Tolba M.M., Rezki N., Aouad M.R., Hagar M., Osman M., Said H. Sulfadiazine analogs: anti-*Toxoplasma in vitro* study of *s*ulfonamide triazoles. Parasit. Res. 122 (2023) 2353–2365. https://doi.org/10.1007/s00436-023-07936-x.

82. Ding M., Clayton C., Soldati D. *Toxoplasma gondii* catalase: are there peroxisomes in toxoplasma? J. Cell Sci. 113 (2000) (Pt 13)2409–2419. https://doi.org/10.1242/jcs.113.13.2409.

83. Miller R.A., Britigan B.E. Role of oxidants in microbial pathophysiology. Clin. Microbiol. Rev. 10 (1997) 1–18. https://doi.org/10.1128/CMR.10.1.1.

84. Ödberg-Ferragut C., Renault J.P., Viscogliosi E., Toursel C., Briche I., Engels A., Lepage G., Morgenstern-Badarau I., Camus D., Tomavo S., Dive D. Molecular cloning, expression analysis and iron metal cofactor characterisation of a superoxide dismutase from *Toxoplasma gondii*. Mol. Biochem. Parasitol. 106 (2000) 121–129. https://doi.org/10.1016/s0166-6851(99)00211-x.

85. Son E.S., Song K.J., Shin J.C., Nam H.W. Molecular cloning and characterization of peroxiredoxin from *Toxoplasma gondii*. Korean J. Parasitol. 39 (2001) 133–141. https://doi.org/10.3347/kjp.2001.39.2.133.

86. Vercesi A.E., Rodrigues C.O., Uyemura S.A., Zhong L., Moreno S.N. Respiration and oxidative phosphorylation in the apicomplexan parasite *Toxoplasma gondii*. J. Biol. Chem. 273 (1998) 31040–31047. https://doi.org/10.1074/jbc.273.47.31040.

87. Akerman S.E., Müller S. Peroxiredoxin-linked detoxification of hydroperoxides in *Toxoplasma gondii*. J. Biol. Chem. 280 (2005) 564–570. https://doi.org/10.1074/jbc.M406367200.

88. Szewczyk-Golec K., Pawłowska M., Wesołowski R., Wróblewski M., Mila-Kierzenkowska C. Oxidative stress as a possible target in the treatment of Toxoplasmosis: perspectives and ambiguities. Int. J. Mol. Sci. 22 (2021) 5705. https://doi.org/10.3390/ijms22115705.

89. Huang M., Cao X., Jiang Y., Shi Y., Ma Y., Hu D., Song X. Evaluation of the combined effect of Artemisinin and Ferroptosis inducer RSL3 against *Toxoplasma gondii*. Int. J. Mol. Sci. 24 (2023) 229. https://doi.org/10.3390/ijms24010229.

90. Mann T., Beckers C. Characterization of the subpellicular network, a filamentous membrane skeletal component in the parasite *Toxoplasma gondii*. Mol Biochem Parasitol. 115 (2001) 257–268. https://doi.org/10.1016/s0166-6851(01)00289-4.

91. Porchet E., Torpier G. Freeze fracture study of *Toxoplasma* and *Sarcocystis* infective stages (Author's transl). Zeitschrift für Parasitenkunde. 54 (1977) 101–124. https://doi.org/10.1007/BF00380795.

92. Stokkermans T.J., Schwartzman J.D., Keenan K., Morrissette N.S., Tilney L.G., Roos D.S. Inhibition of *Toxoplasma gondii* replication by dinitroaniline herbicides. Exp. Parasitol. 84 (1996) 355–370. https://doi.org/10.1006/expr.1996.0124.

4. DISCUSSÃO

Desde a década de 1950, quando a PYR foi introduzida como parte do tratamento para toxoplasmose, a quimioterapia contra *T. gondii* tem se baseado na administração de medicamentos que inibem a replicação do parasito durante a fase aguda (Dunay *et al*., 2018). O tratamento convencional inclui a combinação de PYR e SDZ, que atuam na via do ácido fólico do parasito, com ácido folínico adicionado para mitigar os efeitos adversos no hospedeiro. Embora eficaz, essa terapia está associada a efeitos colaterais significativos. Estes incluem toxicidade hematológica, reações cutâneas como síndrome de Stevens-Johnson e necrólise epidérmica tóxica e intolerância gastrointestinal, que limitam seu uso, particularmente em pacientes crônicos ou imunocomprometidos (Smith *et al*., 2021). Além disso, a PYR tem potencial teratogênico, o que contraindica seu uso durante o primeiro trimestre da gravidez, exigindo a adoção de alternativas terapêuticas mais seguras (Beazley & Egerman, 1998). Nesses casos, a SPI é frequentemente indicada e usada para reduzir o risco de transmissão congênita do parasito (Peyron *et al.*, 1999). Em casos em que a infecção fetal é confirmada ou altamente suspeita, a terapia padrão com PYR pode ser empregada com cautela após 14 semanas de gestação. No entanto, o risco teratogênico continua sendo uma limitação significativa (Bollani *et al*., 2022). Assim, a falta de opções terapêuticas que atendam aos padrões atuais de segurança e eficácia ressalta a necessidade urgente de pesquisa de novos medicamentos tanto para o tratamento de infecções agudas quanto para o manejo de infecções crônicas e potencial reativação (Hajj *et al*., 2021).

Os complexos metálicos emergem como uma classe de compostos promissores para o tratamento de doenças parasitárias, especialmente frente à crescente resistência aos fármacos convencionais (Sánchez-Delgado & Anzellotti, 2004; Chakraborty *et al*., 2024). Sua estrutura versátil permite a modulação de propriedades físico-químicas e farmacocinéticas, além de favorecer a interação seletiva com alvos parasitários, como enzimas essenciais, DNA e componentes de membrana (Drońska *et al*., 2023). Assim, esta abordagem representa uma estratégia inovadora para o desenvolvimento de terapias contra doenças negligenciadas, como leishmaniose, doença de Chagas e toxoplasmose. No presente estudo, avaliou-se o potencial dos complexos metálicos **$[Ni(BPAH)(H_2O)_2].2ClO_4$, $[Cu(HL1)Cl_2]$, $[Fe(HL1)Cl_3]$, $[Zn(HL1)Cl_2]$, $[Zn(HL1)(SDZ)Cl]\cdot 2H_2O$** em modelos *in vitro* como alternativas terapêuticas frente ao *T. gondii*.

No trabalho *A new water-soluble Ni(II) complex as a prototype of metallodrug to treat toxoplasmosis*, ensaios *in vitro* demonstraram que o complexo de níquel(II)

[Ni(BPAH)(H_2O)$_2$].2ClO_4 inibe o crescimento dos taquizoítos com valores de IC_{50} de 0.38 µM em 24 h e 0.36 µM em 48 h, superando complexos metálicos previamente reportados (Portes *et al*., 2015; Portes *et al*., 2017; Portes *et al*., 2018).

Em *Development, structural, spectroscopic and in silico investigation of new complexes relevant as anti-toxoplasma metallopharmacs,* foi conduzido inicialmente um screening *in vitro* para avaliar a atividade anti-*Toxoplasma* dos complexos mononucleares [Cu(HL1)Cl_2], [Fe(HL1)Cl_3], [Zn(HL1)Cl_2] e [Zn(HL1)(SDZ)Cl]·2H_2O. Essa etapa de triagem foi essencial para verificar diferenças de eficácia entre os complexos, permitindo identificar quais apresentavam maior potencial biológico. Destaca-se, nesse contexto, o desempenho do complexo de ferro(III), que apresentou a maior atividade anti-*Toxoplasma* dentre os testados, induzindo redução expressiva do índice de infecção nas concentrações de 10 µM e 20 µM, o que sugere ação direta sobre os taquizoítos. Este resultado direcionou os estudos subsequentes de aprofundamento para o complexo de Fe(III).

Assim, no trabalho *Iron(III) complex impacts Toxoplasma gondii growth by altering the plasma membrane and inner membrane complex* reavaliamos o efeito do complexo mononuclear(III) [Fe(HL1)Cl_3] sobre *T. gondii*. O complexo de ferro(III) apresentou potente atividade *in vitro* com valores de IC_{50} de 12.4 nM e 56 nM após 24 h e 48 h de tratamento, evidenciando eficácia significativamente superior quando comparado ao complexo de níquel(II), cujo IC_{50} se manteve na faixa micromolar. No entanto, ambos se mostraram semelhantes e até mais potentes que os fármacos convencionais, como a PYR e SDZ, cujos valores de IC_{50} variam amplamente entre 0,3 µM e até 7 mM, dependendo da linhagem celular, cepa parasitária e tempo de exposição (Qiu *et al*., 2025; Huffman *et al*., 2022; Węglińska *et al*., 2022; Trotsko *et al*., 2019). Esses resultados são consistentes com estudos anteriores do grupo, que já relataram forte ação antiparasitária de complexos metálicos (Moreira *et al*., 2021; Rocha *et al*., 2023).

Em termos de seletividade e toxicidade, os dois complexos avaliados demonstraram perfis promissores. Ambos apresentaram baixa citotoxicidade para as células hospedeiras LLC-MK2 mesmo em concentrações elevadas, aspecto fundamental no desenvolvimento de novos agentes terapêuticos. O complexo de níquel(II) destacou-se por sua ampla margem de segurança, mantendo mais de 90% de viabilidade celular após 48 h de exposição a 700 µM. Embora esse resultado tenha impedido o cálculo de um índice de seletividade (IS) exato, estimativas indicam um IS > 1800, o que reflete baixa toxicidade frente à célula hospedeira e notável seletividade para o parasito. Por sua vez, o complexo de ferro(III), apesar de apresentar discreta redução na viabilidade celular em concentrações 100 - 500 µM, demonstrou

seletividade ainda mais expressiva (IS > 40.000 em 24 h), associada a uma potência antiparasitária superior, com valores de IC_{50} na escala nanomolar. Esses dados indicam que, embora ambos os compostos sejam seletivos e não tóxicos, o complexo de ferro(III) é consideravelmente mais potente, atuando em concentrações até 30 vezes menores que o complexo de níquel(II). Esse equilíbrio entre alta eficácia frente ao *T. gondii* e baixa citotoxicidade é essencial, sobretudo considerando os efeitos adversos frequentemente associados a fármacos como SDZ e PYR. Estudos clínicos e revisões reportam que a combinação PYR/SDZ causa toxicidade em até 62 % dos pacientes, com interrupção do tratamento em 44 % devido a eventos adversos graves (Alday & Doggett, 2017; Ben-Harari *et al*., 2017; Shamma *et al*., 2021). Além disso, os resultados sugerem que a diferença na composição lipídica das membranas de *T. gondii* e das células hospedeiras pode desempenhar um papel central na seletividade observada, hipótese que será discutida adiante.

Diante dos resultados apresentados acima, tornou-se essencial compreender em maior profundidade o mecanismo de ação dos complexos em *T. gondii*. No caso do complexo de níquel(II), a MET revelou alterações na estrutura da membrana plasmática do parasito e deformação no conóide, estrutura apical fundamental no processo de invasão celular (Koreny *et al*, 2021). Essa alteração comprometeu a capacidade dos taquizoítos de reinfectar novas células hospedeiras, confirmada pelos ensaios de invasão. Esses resultados reforçam o que foi descrito por Hu *et al*. (2002), que demonstraram que a desorganização do conóide ou de seus elementos associados ao IMC inviabiliza a projeção do complexo apical, interrompe a motilidade *gliding* resultando em parasitos incapazes de invadir células hospedeiras e, consequentemente, interrompendo o ciclo infectivo.

No caso do complexo de ferro(III), a MET evidenciou danos ultraestruturais em *T. gondii*, incluindo *clefts* no citoplasma e *blebls* na membrana. Segundo Portes *et al*., 2015 compostos de ferro dinucleares, induzem efeitos citotóxicos em *T. gondii*, levando a alterações ultraestruturais como formação de *blebs* na membrana, além de desencadear outras vias apoptóticas no parasito. A ocorrência simultânea de diferentes tipos de morte celular, como autofagia, apoptose e necrose, também foi descrita em *T. cruzi* por Menna-Barreto *et al*. (2009). Estudos anteriores indicam que complexos de ferro(III) e outros metais de transição podem promover aumento de espécies reativas de oxigênio (ROS), comprometendo o equilíbrio redox do parasito e desencadeando vias de apoptose (Navarro & Visbal., 2014; Portes *et al*., 2015; Britten & Butler, 2022; Casarrubias-Tabarez *et al*., 2023). A presença de *blebs* de membrana, sugere que o complexo de ferro(III) não apenas rompe barreiras estruturais, mas também

interfere no metabolismo oxidativo de *T. gondii*, alvo vulnerável em Apicomplexas (Szewczyk-Golec *et al.*, 2021).

Além disso, através da MET evidenciaram-se rupturas na membrana plasmática e no IMC de *T. gondii.* A ruptura do IMC foi confirmada por imunofluorescência, utilizando anticorpo anti-IMC1, que revelou a fragmentação dessa estrutura. Esse padrão de dano estrutural encontra suporte no estudo de Portes *et al*. (2017) que relatou que o complexo de cobre(II) foi capaz de causar ruptura da membrana plasmática, interferindo na disposição correta do IMC do parasito, afetando a divisão celular. De forma semelhante, Araujo-Silva *et al*. (2021) demonstraram que os inibidores de HDAC Tubastatin A e SAHA comprometeram a montagem e a extensão do IMC de *T. gondii*, além de afetarem a quantidade de α-tubulina, uma proteína-chave do citoesqueleto, possivelmente impactando a integridade dos microtúbulos e a correta segregação nuclear.

Outro ponto relevante é que os ensaios de reversibilidade demonstraram que o tratamento de células infectadas por 48 h seguido da retirada do complexo e cultivo por mais 48 h, o índice de infecção permaneceu reduzido e estável nas concentrações de 12,5 nM e 100 nM, respectivamente. Tal efeito irreversível, alcançado em um curto período de tempo, ressalta o potencial do complexo de ferro(III) como agente anti-*Toxoplasma*, sobretudo quando comparado a fármacos convencionais que geralmente requerem administrações prolongadas para manter níveis terapêuticos e prevenir recidivas (Montoya & Liesenfeld, 2004; Antczak *et al*., 2016).

Os ensaios biofísicos foram fundamentais para elucidar como o complexo de ferro(III) interage seletivamente com modelos de membranas de *T. gondii* e das células hospedeiras, com isso, observou-se que o complexo atua de forma direta na organização lipídica das membranas, modulando parâmetros críticos como empacotamento, fluidez e ordem lipídica. Os dados de DSC mostraram que, em modelos de membranas do parasito, compostas por fosfolipídios como fosfatidilcolina, fosfatidiletanolamina e com baixo teor de colesterol, o complexo de ferro(III) induziu redução na entalpia de transição e na cooperatividade da fase lipídica, sugerindo desorganização da bicamada e maior suscetibilidade a rupturas. Por outro lado, nos modelos de membranas semelhantes às de células de mamíferos, ricas em colesterol e esfingomielina, o complexo apresentou efeito oposto: aumento da ordem lipídica e restrição da fluidez, conferindo estabilidade adicional à membrana hospedeira.

Os resultados de ESR corroboraram esse padrão: em membranas de parasito, os parâmetros S_0 (order parameter) e o tempo de correlação rotacional apresentaram variações indicativas de aumento da fluidez e permeabilidade, enquanto nas membranas modelo de

mamíferos os mesmos parâmetros indicaram maior rigidez. Este perfil é coerente com a hipótese de que os complexos metálicos podem explorar diferenças bioquímicas fundamentais na composição lipídica para exercer uma ação seletiva (Daear *et al*., 2021; Bispo *et al*., 2023; Sule *et al*., 2023). Estudos recentes de Man *et al.* (2023) mostram, via EPR/ESR, que complexos de vanádio alteram significativamente os parâmetros S_0 e τ, aumentando a fluidez em lipossomos modelo de fase líquida. Basso *et al*. (2011) utilizaram ESR spin-label para mostrar que fármacos como a primaquina alteram significativamente os parâmetros S_0 e o tempo de correlação rotacional, indicando aumento de fluidez e desorganização do núcleo lipídico em membranas modelo. Esses achados fortalecem a hipótese de que os complexos metálicos podem explorar diferenças na composição lipídica para provocar alterações seletivas na fluidez de membranas de parasitos versus mamíferos.

A diferença na composição lipídica das membranas é um fator crítico nesse mecanismo de ação. Membranas de parasitos do filo Apicomplexa, como *T. gondii*, apresentam proporções significativamente menores de colesterol e esfingomielina quando comparadas às membranas de células hospedeiras (Welti *et al*., 2007). Essa característica torna as membranas do parasito mais vulneráveis a compostos anfifílicos e redox ativos que desestabilizam a bicamada lipídica, alteram transições térmicas e comprometem sua integridade funcional (Nyonda *et al*., 2022; Zambrano *et al*., 2024).

Os resultados apresentados destacam o potencial dos complexos de níquel(II) e ferro(III) contra *T. gondii*, contribuindo de forma relevante para o entendimento da quimioterapia antiparasitária. A capacidade desses complexos de atuarem em múltiplos alvos diferencia-se das abordagens convencionais com SDZ e PYR, que apresentam limitações em termos de seletividade e eficácia. Nesse contexto, o complexo de ferro(III) destacou-se por sua elevada potência, seletividade e efeito irreversível, abrindo novas perspectivas.

Apesar dos avanços obtidos, este estudo apresenta limitações que devem ser consideradas. Primeiramente, não foram avaliados parâmetros bioquímicos adicionais capazes de esclarecer de forma mais aprofundada os mecanismos moleculares envolvidos na morte do parasito. Além disso, não foram realizados experimentos *in vivo*. Assim, estudos futuros devem contemplar essas abordagens para consolidar o potencial terapêutico do complexo de Fe(III) e avançar em direção à sua aplicação clínica.

5. CONCLUSÕES

- O complexo de níquel(II) apresentou atividade anti-*Toxoplasma* na faixa de micromolar, baixa citotoxicidade para células LLC-MK2 e índice de seletividade elevado. A MET revelou alterações na membrana plasmática e deformação do conóide, resultando na inibição da reinfecção.

- Uma triagem comparativa dos complexos metálicos contra *T. gondii* permitiu destacar o complexo de ferro(III) como o mais promissor.

- O complexo de ferro(III) apresentou atividade anti-*Toxoplasma* na faixa nanomolar e baixa citotoxicidade. Foi observado um efeito irreversível sobre *T. gondii* mesmo após a retirada do composto e cultivo por mais 48 h. Os taquizoítos tratados apresentaram formato arredondado e danos ultraestruturais, como *clefts* no citoplasma, *blebs* de membrana e ruptura do IMC.

- Os complexos de níquel(II) e ferro(III) apresentaram eficácia *in vitro* comparável ou superior à PYR e SDZ contra *T. gondii.*

- As análises biofísicas (DSC e ESR) revelaram que o complexo de ferro(III) desorganiza o empacotamento lipídico de membranas modelo semelhantes às de parasitos, enquanto aumenta a ordenação lipídica em modelos semelhantes às de mamíferos, indicando um mecanismo de seletividade baseado nas diferenças de composição lipídica entre parasito e célula hospedeira.

- Dentre os complexos testados, o complexo de ferro(III) destacou-se por sua elevada potência, seletividade e efeito irreversível, o que reforça o seu potencial para aplicação na quimioterapia antiparasitária e justifica estudos futuros envolvendo modelos *in vivo*.

6. SUGESTÕES PARA TRABALHOS FUTUROS

Estudos *in vitro*:

- Quantificação de espécies reativas de oxigênio (ROS) por DCFH-DA e atividade de enzimas antioxidantes catalase e superóxido dismutase de *T. gondii.*

- Ensaio para detecção de apoptose por TUNEL

- Análise bioenergética, incluindo a atividade de enzimas do ciclo de Krebs (citrato sintase e succinato desidrogenase), o balanço redox ($NADH/NAD^+$) e produção de ATP. O resultado esperado é revelar disfunções metabólicas no parasito, indicando que o complexo possa afetar vias bioenergéticas centrais e, assim, ampliar o entendimento do seu mecanismo de ação multi-alvo.

- Uso de abordagens de proteômica comparativa para identificar alterações em vias metabólicas, estruturais e de sinalização, abrindo novas hipóteses de como esse complexo impacta o parasito em múltiplos níveis. Espera-se identificar proteínas diferencialmente expressas, potenciais alvos secundários e mecanismos de resposta adaptativa de *T. gondii*, fornecendo conhecimento essencial para o desenho de compostos ainda mais potentes e específicos.

Estudos *in vivo*:

- Avaliação da eficácia antiparasitária, sobrevida e análise histopatológica de órgãos-alvo (fígado, baço e cérebro).

- Determinação de parâmetros bioquímicos hepáticos, como ALT, AST, MDA, GSH e SOD - permitirá avaliar possíveis efeitos hepatotóxicos e, ao mesmo tempo, confirmar se o complexo induz ou modula o estresse oxidativo no hospedeiro. O resultado esperado é que o complexo apresente baixo impacto sobre o equilíbrio oxidativo do animal, reforçando o perfil de seletividade e segurança sugerido *in vitro*.

- Investigação dos efeitos imunomodulatórios do complexo. Pretende-se analisar a produção de citocinas pró-inflamatórias (TNF-α, IFN-γ), a ativação de macrófagos e células NK, bem como possíveis efeitos sobre mediadores anti-inflamatórios como IL-10. O resultado esperado é entender se o complexo estimula respostas imunes protetoras, ou seja, se podem atuar como imunomoduladores sinérgicos, algo extremamente promissor para infecções intracelulares persistentes.

7. REFERÊNCIAS

Aerts, R., Mehra, V., Groll, A.H., Martino, R., Lagrou, K., Robin, C., Perruccio, K., Blijlevens, N., Nucci, M., Slavin, M., Bretagne, S., Cordonnier, C., European Conference on Infections in Leukemia group. (2024). Guidelines for the management of *Toxoplasma gondii* infection and disease in patients with hematological malignancies and after hematopoietic stem-cell transplantation: guidelines from the 9th European Conference on Infections in Leukemia, 2022. *Lancet Infect. Dis,* 24(5): e291–e306.

Aguirre, A.A., Longcore, T., Barbieri, M., Dabritz, H., Hill, D., Klein, P.N., Lepczyk, C., Lilly, E.L., McLeod, R., Milcarsky, J., Murphy, C.E., Su, C., VanWormer, E., Yolken, R., Sizemore, G.C. (2019). The One Health Approach to toxoplasmosis: epidemiology, control, and prevention strategies. *EcoHealth*, 16(2): 378–390.

Ajzenberg, D., Bañuls, A.L., Su, C., Dumètre, A., Demar, M., Carme, B., Dardé, M.L. (2004). Genetic diversity, clonality and sexuality in *Toxoplasma gondii*. *Int. J. Parasitol,* 34(10): 1185–1196.

Alday, P.H., Doggett, J.S. (2017). Drugs in development for toxoplasmosis: advances, challenges, and current status. *Drug Des. Devel. Ther,* 11: 273–293.

Amiar, S., Katris, N.J., Berry, L., Dass, S., Duley, S., Arnold, C.S., Shears, M.J., Brunet, C., Touquet, B., McFadden, G.I., Yamaryo-Botté, Y., Botté, C.Y. (2020). Division and adaptation to host environment of apicomplexan parasites depend on apicoplast lipid metabolic plasticity and host organelle remodeling. *Cell Rep,* 30(11): 3778–3792.e9.

Anderson-White, B.R., Ivey, F.D., Cheng, K., Szatanek, T., Lorestani, A., Beckers, C.J., Ferguson, D.J., Sahoo, N., Gubbels, M.J. (2011). A family of intermediate filament-like proteins is sequentially assembled into the cytoskeleton of *Toxoplasma gondii*. *Cell. Microbiol,* 13(1): 18–31.

Antczak, M., Dzitko, K., Długońska, H. (2016). Human toxoplasmosis: Searching for novel chemotherapeutics. *Biomed. Pharmacother,* 82: 677–684.

Araujo-Silva, C.A., De Souza, W., Martins-Duarte, E.S., Vommaro, R.C. (2021). HDAC inhibitors Tubastatin A and SAHA affect parasite cell division and are potential anti-*Toxoplasma gondii* chemotherapeutics. *Int. J. Parasitol. Drugs Drug Resist,* 17: 103–112.

Ardabili, S., Kohl, J., Gül, G., Hodel, M. (2021). What obstetricians should be aware of: serious side effects of antibiotic toxoplasmosis treatment in pregnancy. *BMJ Case Rep,* 14: e240809.

Arquilla, B., Bloem, C., Burguêz, D., Andrioli, G., Dal Ponte, S.T. (2019). Outbreak of toxoplasmosis in the city of Santa Maria, Brazil. *J. Infect. Dis. Prev. Med,* 7(2): 191.

Bahia-Oliveira, L.M., Jones, J.L., Azevedo-Silva, J., Alves, C.C., Oréfice, F., Addiss, D.G. (2003). Highly endemic, waterborne toxoplasmosis in north Rio de Janeiro state, Brazil. *Emerg. Infect. Dis,* 9(1): 55–62.

Basso, L.G.M., Rodrigues, R.Z., Naal, R.M.Z.G., Costa Filho, A.J. (2011). Effects of the antimalarial drug primaquine on the dynamic structure of lipid model membranes. *Biochim. Biophys. Acta – Biomembr,* 1808(1): 55–64.

Batista, L.C., de Souza, F.S., de Assis, V.M., Seabra, S.H., Bortoluzzi, A.J., Rennó, M.N., Horn Jr., A., DaMatta, R.A., Fernandes, C. (2015). Antiproliferative activity and conversion of tachyzoite to bradyzoite of *Toxoplasma gondii* promoted by new zinc complexes containing sulfadiazine. *RSC Adv,* 5: 100606–100617.

Beazley, D.M., Egerman, R.S. (1998). Toxoplasmosis. *Semin. Perinatol,* 22(4): 332–338.

Ben Chaabene, R., Lentini, G., Soldati-Favre, D. (2021). Biogenesis and discharge of the rhoptries: Key organelles for entry and hijack of host cells by the Apicomplexa. *Mol. Microbiol,* 115(3): 453–465.

Ben-Harari, R.R., Goodwin, E., Casoy, J. (2017). Adverse event profile of pyrimethamine-based therapy in toxoplasmosis: A systematic review. *Drugs R&D*, 17(4): 523–544.

Besteiro, S., Dubremetz, J.F., Lebrun, M. (2011). The moving junction of apicomplexan parasites: A key structure for invasion. *Cell. Microbiol,* 13(6): 797–805.

Bigna, J.J., Tochie, J.N., Tounouga, D.N., Bekolo, A.O., Ymele, N.S., Youda, E.L., Sime, P.S., Nansseu, J.R. (2020). Global, regional, and country seroprevalence of *Toxoplasma gondii* in pregnant women: A systematic review, modeling and meta-analysis. *Sci. Rep,* 10(1): 12102.

Bisio, H., Soldati-Favre, D. (2019). Signaling cascades governing entry into and exit from host cells by *Toxoplasma gondii*. *Annu. Rev. Microbiol,* 73: 579–599.

Bisio, H., Krishnan, A., Marq, J.B., Soldati-Favre, D. (2022). *Toxoplasma gondii* phosphatidylserine flippase complex ATP2B–CDC50.4 critically participates in microneme exocytosis. *PLoS Pathog,* 18(3): e1010438.

Bispo, D.S.C., Correia, M., Carneiro, T.J., Martins, A.S., Reis, A.A.N., Carvalho, A.L.M.B.d., Marques, M.P.M., Gil, A.M. (2023). Impact of Conventional and Potential New Metal-Based Drugs on Lipid Metabolism in Osteosarcoma MG-63 Cells. *Int. J. Mol. Sci,* 24: 17556.

Blume, M., Seeber, F. (2018). Metabolic interactions between *Toxoplasma gondii* and its host. *F1000Res,* 7: F1000 Faculty Rev-1719.

Bollani, L., Auriti, C., Achille, C., Garofoli, F., De Rose, D.U., Meroni, V., Salvatori, G., Tzialla, C. (2022). Congenital toxoplasmosis: The state of the art. *Front. Pediatr,* 10: 894573.

Brito, R.M.M., de Lima Bessa, G., Bastilho, A.L., Dantas-Torres, F., de Andrade-Neto, V.F., Bueno, L.L., Fujiwara, R.T., Magalhães, L.M.D. (2023). Genetic diversity of *Toxoplasma gondii* in South America: Occurrence, immunity, and fate of infection. *Parasites Vectors*, 16(1): 461.

Britten, N.S., Butler, J.A. (2022). Ruthenium metallotherapeutics: Novel approaches to combatting parasitic infections. *Curr. Med. Chem,* 29(31): 5159–5178.

Bruijnincx, P.C., Sadler, P.J. (2010). New trends for metal complexes with anticancer activity. *Curr. Opin. Chem. Biol,* 12(2): 197–206.

Caballero, A.B., Marín, C., Rodríguez-Diéguez, A., Ramírez-Macías, I., Barea, E., Sánchez-Moreno, M., Salas, J.M. (2011). *In vitro* and *in vivo* antiparasitic activity against *Trypanosoma cruzi* of three novel 5-methyl-1,2,4-triazolo[1,5-a]pyrimidin-7(4H)-one-based complexes. *J. Inorg. Biochem,* 105(6): 770–776.

Caldas, L.A., Attias, M., de Souza, W. (2018). A structural analysis of the natural egress of *Toxoplasma gondii*. *Microbes Infect,* 20(1): 57–62.

Camossi, L.G., Greca-Júnior, H., Corrêa, A.P., Richini-Pereira, V.B., Silva, R.C., Da Silva, A.V., Langoni, H. (2011). Detection of *Toxoplasma gondii* DNA in the milk of naturally infected ewes. *Vet. Parasitol,* 177(3–4): 256–261.

Carey, K.L., Westwood, N.J., Mitchison, T.J., Ward, G.E. (2004). A small-molecule approach to studying invasive mechanisms of *Toxoplasma gondii*. *Proc. Natl. Acad. Sci. USA*, 101(19): 743.

Cardoso, A.P., Madureira, L.M.P., Segat, B.B., Menezes, J.N.C., Cargnelutti, R., Candela, D.R.S., Mariano, D.L., Parreira, R.L.T., Horn Jr, A., Seabra, S.H., DaMatta, R.A., Moreira, F.F., Moreira, R.V., Caramori, G.F., Fernandes, C. (2022). Development, structural, spectroscopic and in silico investigation of new complexes relevant as anti-toxoplasma metallopharmacs. *J. Mol. Struct,* 1265: 133380.

Carruthers, V.B., Giddings, O.K., Sibley, L.D. (1999). Secretion of micronemal proteins is associated with *Toxoplasma* invasion of host cells. *Cell. Microbiol,* 1: 225–235.

Carruthers, V.B., Sherman, G.D., Sibley, L.D. (2000). The *Toxoplasma* adhesive protein MIC2 is proteolytically processed at multiple sites by two parasite-derived proteases. *J. Biol. Chem,* 275(19): 14346–14353.

Carruthers, V.B., Tomley, F.M. (2008). Microneme proteins in apicomplexans. *Subcell. Biochem,* 47: 33–45.

Carruthers, V., Boothroyd, J.C. (2007). Pulling together: An integrated model of *Toxoplasma* cell invasion. *Curr. Opin. Microbiol,* 10(1): 83–89.

Carver, P.L. (2019). Metals in medicine: The therapeutic use of metal ions in the clinic. *Met. Ions Life Sci,* 19.

Casarrubias-Tabarez, B., Rivera-Fernández, N., Rojas-Lemus, M., López-Valdez, N., Fortoul, T. (2023). Vanadium compounds as antiparasitic agents: An approach to their mechanisms of action. *J. Trace Elem. Med. Biol,* 78: 127201.

Cassini, A. (2012). Chemical biology of anticancer metallodrugs. In: Sigel, A., Sigel, H., Sigel, R.K.O. (eds.), *Metal Ions in Life Sciences: Interplay between Metal Ions and Nucleic Acids*. Vol. 10. Dordrecht: Springer. p. 295–332.

Cerutti, A., Blanchard, N., Besteiro, S. (2020). The bradyzoite: A key developmental stage for the persistence and pathogenesis of toxoplasmosis. *Pathogens*, 9(3): 234.

Chakraborty, S., Ghosh, S., Dalui, S., Dey, A. (2024). A review on the anti-parasitic activity of ruthenium compounds. *J. Basic Appl. Zool,* 85: 17.

Charital, S., Thomas, N., Singh, R., Banerjee, A., Dubey, J.P., Sullivan, W.J. Jr. (2024). *Toxoplasma gondii* acyl-CoA synthetase TgACS1 is required for fatty acid salvage under nutrient stress conditions. *mBio*, 15(2): e00427–24.

Charron, A.J., Sibley, L.D. (2002). Host cells: Mobilizable lipid resources for the intracellular parasite *Toxoplasma gondii*. *J. Cell Sci,* 115(Pt 15): 3049–3059.

Charron, A.J., Sibley, L.D. (2004). Molecular partitioning during host cell penetration by *Toxoplasma gondii*: membrane dynamics at the moving junction. *Traffic*, 5(11): 855–867.

Chen, K., Huang, X., Distler, U., Tenzer, S., Günay-Esiyok, Ö., Gupta, N. (2023). Apically-located P4-ATPase1–Lem1 complex internalizes phosphatidylserine and regulates motility-dependent invasion and egress in *Toxoplasma gondii*. *Comput. Struct. Biotechnol. J,* 21: 1893–1906.

Chiari, C.A., Neves, D.P. (1984). Toxoplasmose humana adquirida através da ingestão de leite de cabra. *Mem. Inst. Oswaldo Cruz*, 79(3): 337–340.

Coppens, I., Romano, J.D. (2018). Hostile intruder: *Toxoplasma* holds host organelles captive. *PLoS Pathog.*, 14(3): e1006893. Erratum in: *PLoS Pathog,* 14(4): e1007018.

da Costa, M.A., Pinto-Ferreira, F., de Almeida, R.P.A., Martins, F.D.C., Pires, A.L., Mareze, M., Mitsuka-Breganó, R., Freire, R.L., da Rocha Moreira, R.V., Borges, J.M., Navarro, I.T. (2020). Artisan fresh cheese from raw cow's milk as a possible route of transmission in a toxoplasmosis outbreak in Brazil. Zoonoses Public Health. Mar, 67(2):122-129.

Daear, W., Mundle, R., Sule, K., & Prenner, E. J. (2021). The degree and position of phosphorylation determine the impact of toxic and trace metals on phosphoinositide-containing model membranes. 1: 100021.

Dasari, S., & Tchounwou, P. B. (2014). Cisplatin in cancer therapy: molecular mechanisms of action. *European Journal of Pharmacology*, 740: 364–378.

Dass, S., Sharma, A., Gupta, N. (2024). The acyl-CoA synthetase TgACS3 is crucial for fatty acid utilization and membrane biogenesis in *Toxoplasma gondii*. *J. Lipid Res,* 65(4): 100381.

Demar, M., Hommel, D., Djossou, F., Peneau, C., Boukhari, R., Louvel, D., Bourbigot, A.M., Nasser, V., Ajzenberg, D., Dardé, M.L., Carme, B. (2012). Acute toxoplasmoses in immunocompetent patients hospitalized in an intensive care unit in French Guiana. *Clin. Microbiol. Infect,* 18(7): E221–E231.

Deng, H., Huang, X., Jin, C.M., Jin, C.M., Quan, Z.S. (2019). Synthesis, *in vitro* and *in vivo* biological evaluation of dihydroartemisinin derivatives with potential anti-*Toxoplasma gondii* agents. *Bioorg. Chem,* 94: 103467.

Docampo, R., Jimenez, V., King-Keller, S., Li, Z.H., Moreno, S.N. (2011). The role of acidocalcisomes in the stress response of *Trypanosoma cruzi*. *Adv. Parasitol,* 75: 307–324.

Doliwa, C., Escotte-Binet, S., Aubert, D., Sauvage, V., Velard, F., Schmid, A., Villena, I. (2013). Sulfadiazine resistance in *Toxoplasma gondii*: no involvement of overexpression or polymorphisms in genes of therapeutic targets and ABC transporters. *Parasite*, 20: 19.

dos Santos, B.M., Ribeiro, E.L.S., Lima, M.S. (2023). Toxoplasmose gestacional: um estudo epidemiológico. *Rev. JRG Estud. Acadêmicos*, 6(13): 674–687.

de Moura, L., Bahia-Oliveira, L.M., Wada, M.Y., Jones, J.L., Tuboi, S.H., Carmo, E.H., Ramalho, W.M., Camargo, N.J., Trevisan, R., Graça, R.M., da Silva, A.J., Moura, I., Dubey, J.P., Garrett, D.O. (2006).Waterborne toxoplasmosis, Brazil, from field to gene. *Emerg Infect Dis*, 12(2):326–329.

dos Santos, R.M., Silveira, L.M.G., Vommaro, R.C. (2020). Ultrastructural organization of the conoid complex in *Toxoplasma gondii*: evidence for conserved features among Apicomplexa. *Parasitol. Int,* 76: 102045.

Drońska, D., Talarek, S., Włoch, A. (2023). Metal-based drugs as promising therapeutic agents against parasitic diseases: Opportunities and challenges. *Coord. Chem. Ver,* 478: 214978.

Dubey, J.P., Frenkel, J.K. (1973). Experimental *Toxoplasma* infection in mice with strains producing oocysts. *J. Parasitol,* 59(3): 505–512.

Dubey, J.P., Frenkel, J.K. (1976). Feline toxoplasmosis from acutely infected mice and the development of *Toxoplasma* cysts. *J. Protozool,* 23(4): 537–546.

Dubey, J.P., Lindsay, D.S., Speer, C.A. (1998). Structures of *Toxoplasma gondii* tachyzoites, bradyzoites, and sporozoites and biology and development of tissue cysts. *Clin. Microbiol. Ver.,* 11(2): 267–299.

Dubey, J.P., Thulliez, P. (1993). Persistence of tissue cysts in edible tissues of cattle fed *Toxoplasma gondii* oocysts. *Am. J. Vet. Res,* 54(2): 270–273.

Dubey, J.P. (2008). The history of *Toxoplasma gondii*—the first 100 years. *Vet. Parasitol,* 163(3): 184–195.

Dubremetz, J.F. (1998). Host cell invasion by *Toxoplasma gondii*. *Trends Microbiol,* 6(1): 27–30.

Dubois, D.J., Soldati-Favre, D. (2019). Biogenesis and secretion of micronemes in *Toxoplasma gondii*. *Cell Microbiol,* 21(5): e13018.

Dunay, I.R., Gajurel, K., Dhakal, R., Liesenfeld, O., Montoya, J.G. (2018). Treatment of toxoplasmosis: Historical perspective, animal models, and current clinical practice. *Clin. Microbiol. Ver,* 31(4): e00057–17.

Elsheikha, H.M., Marra, C.M., Zhu, X.Q. (2020). Epidemiology, pathophysiology, diagnosis, and management of cerebral toxoplasmosis. *Clin. Microbiol. Ver,* 34(1): e00115–19.

Ferguson, D.J. (2004). Use of molecular and ultrastructural markers to evaluate stage conversion of *Toxoplasma gondii* in both the intermediate and definitive host. *Int. J. Parasitol,* 34(3): 347–360.

Ferguson, D.J. (2009). *Toxoplasma gondii*: 1908-2008, homage to Nicolle, Manceaux and Splendore. Mem Inst Oswaldo Cruz104(2):133-48..

Fraser, M., Matuschewski, K., Maier, A.G. (2023). The enemy within: lipid asymmetry in intracellular parasite-host interactions. *Emerg. Top. Life Sci,* 7(1): 67–79.

Frénal, K., Dubremetz, J.F., Lebrun, M., Soldati-Favre, D. (2017). Gliding motility powers invasion and egress in Apicomplexa. *Nat. Rev. Microbiol,* 15(11): 645–660.

Gallois, Y., Foussard, F., Girault, A., Hodbert, J., Tricaud, A., Mauras, G., Motta, C. (1988). Membrane fluidity of *Toxoplasma gondii*: a fluorescence polarization study. *Biol. Cell*, 62(1): 11–15.

Gilbert, R.E., Freeman, K., Lago, E.G., Bahia-Oliveira, L.M.G., Tan, H.K., Wallon, M., Buffolano, W., Stanford, M.R., Petersen, E. (2008). Sequelas oculares da toxoplasmose congênita no Brasil em comparação com a Europa. *PLoS Negl. Trop. Dis,* 2: e277.

Gold, D.A., Kaplan, A.D., Lis, A., Bett, G.C.L., Rosowski, E.E., Cirelli, K.M., Bougdour, A., Sidik, S.M., Beck, J.R., Lourido, S., Egea, P.F., Bradley, P.J., Hakimi, M.A., Rasmusson, R.L.,

Saeij, J.P.J. (2015). The *Toxoplasma* dense granule proteins GRA17 and GRA23 mediate the movement of small molecules between the host and the parasitophorous vacuole. *Cell Host Microbe*, 17(5): 642–652.

Gould, S.B., Tham, W.H., Cowman, A.F., McFadden, G.I. (2008). Alveolins, a new family of cortical proteins that define the protist infrakingdom Alveolata. *Mol. Biol. Evol,* 25(12): 2629–2639.

Grigg, M.E., Ganatra, J., Boothroyd, J.C., Margolis, T.P. (2001). Unusual abundance of atypical strains associated with human ocular toxoplasmosis. *J. Infect. Dis,* 184(5): 633–639.

Guerra, W., Azevedo, E.A., Monteiro, A.R.S., Bucciarelli-Rodriguez, M., Chartone-Souza, E., Nascimento, A.M.A., Fontes, A.P.S., Le Moyec, L., Pereira-Maia, E.C. (2005). Synthesis, characterization, and antibacterial activity of three palladium(II) complexes of tetracyclines. *J. Inorg. Biochem,* 99: 2348–2354.

Hajj, R.E., Tawk, L., Itani, S., Hamie, M., Ezzeddine, J., El Sabban, M., El Hajj, H. (2021). Toxoplasmosis: Current and emerging parasite druggable targets. *Microorganisms*, 9(12): 2531.

Harding, C.R., Meissner, M. (2014). The IMC in *Plasmodium* and *Toxoplasma*. *Cell. Microbiol,* 16: 632–641.

Harding, C.R., Gow, M., Kang, J.H., Shortt, E., Manalis, S.R., Meissner, M., Lourido, S. (2019). Alveolar proteins stabilize cortical microtubules in *Toxoplasma gondii*. *Nat. Commun,* 10: 401.

Haas, T.A., Plow, E.F. (1994). Integrin-ligand interactions: a year in review. *Curr. Opin. Cell Biol,* 6(5): 656–662.

He, T.Y., Li, Y.T., Liu, Z.D., Cheng, H., Bao, Y.F., Zhang, J.L. (2024). Lipid metabolism: the potential targets for toxoplasmosis treatment. *Parasites Vectors*, 17: 111.

Heaslip, A.T., Nelson, S.R., Warshaw, D.M. (2016). Dense granule trafficking in *Toxoplasma gondii* requires a unique class 27 myosin and actin filaments. *Mol. Biol. Cell*, 27(13): 2080–2089.

Heintzelman, M.B. (2006). Cellular and molecular mechanics of gliding locomotion in eukaryotes. In: *International Review of Cytology*, Vol. 251. San Diego: Academic Press. p. 79–129.

Hill, D., Dubey, J.P. (2002). *Toxoplasma gondii*: transmission, diagnosis and prevention. *Clin. Microbiol. Infect,* 8: 634–640.

Howe, D.K., Sibley, L.D. (1995). *Toxoplasma gondii* comprises three clonal lineages: correlation of parasite genotype with human disease. *J. Infect. Dis,* 172(6): 1561–1566.

Hu, K., Roos, D.S., Murray, J.M. (2002). A novel polymer of tubulin forms the conoid of *Toxoplasma gondii*. *J. Cell Biol,* 156(6): 1039–1050.

Hu, K., Johnson, J., Florens, L., Fraunholz, M., Suravajjala, S., DiLullo, C., Yates, J., Roos, D.S., Murray, J.M. (2006). Cytoskeletal components of an invasion machine—the apical complex of *Toxoplasma gondii*. *PLoS Pathog,* 2(2): e13.

Huffman, A.M., Ayariga, J.A., Napier, A., Robertson, B.K., Abugri, D.A. (2022). Inhibition of *Toxoplasma gondii* growth by dihydroquinine and its mechanisms of action. *Front. Cell Infect. Microbiol,* 12: 852–889.

Hunter, C.A., Sibley, L.D. (2012). Modulation of innate immunity by *Toxoplasma gondii* virulence effectors. *Nat. Rev. Microbiol,* 10(11): 766–778.

Jia, Y., Marq, J.B., Bisio, H., Jacot, D., Mueller, C., Yu, L., Choudhary, J., Brochet, M., Soldati-Favre D. (2017). Crosstalk between PKA and PKG controls pH-dependent host cell egress of *Toxoplasma gondii*. *EMBO J,* 36(21): 3250–3267.

Jin, C., Kaewintajuk, K., Jiang, J., Jeong, W., Kamata, M., Kim, H., Wataya, Y., Park, H. (2009). *Toxoplasma gondii*: a simple high-throughput assay for drug screening *in vitro*. *Exp. Parasitol,* 121: 132–136.

Jones, J., Dubey, J.P. (2014). Comments on "Detection of *Toxoplasma gondii* in raw caprine, ovine, bovine, and camel milk using cell cultivation, cat bioassay, capture ELISA, and PCR methods in Iran". *Foodborne Pathog. Dis,* 11(6): 500–501.

Jones, E., Dimmock, P.W., Spencer, S.A. (2001). A randomized controlled trial to compare methods of milk expression after preterm delivery. *Arch. Dis. Child Fetal Neonatal Ed,* 85(2): F91–F95.

Katlama, C., De Wit, S., O'Doherty, E., Van Glabeke, M., Clumeck, N. (1996). Pyrimethamine-clindamycin vs. pyrimethamine-sulfadiazine as acute and long-term therapy for toxoplasmic encephalitis in patients with AIDS. *Clin. Infect. Dis,* 22(2): 268–275.

Kessler, H., Herm Götz, A., Hegge, S., Rauch, M., Soldati-Favre, D., Frischknecht, F., Meissner, M. (2008). Microneme protein 8—a new essential invasion factor in *Toxoplasma gondii*. *J. Cell Sci,* 121(Pt 7): 947–956.

Konstantinović, N., Guegan, H., Stäjner, T., Belaz, S., Robert-Gangneux, F. (2019). Treatment of toxoplasmosis: Current options and future perspectives. *Food Waterborne Parasitol,* 15: e00036.

Koreny, L., Zeeshan, M., Barylyuk, K., Tromer, E.C., van Hooff, J.J.E., Brady, D., et al. (2021). Molecular characterization of the conoid complex in *Toxoplasma* reveals its conservation in all apicomplexans, including *Plasmodium* species. *PLoS Biol,* 19(3): e3001081.

Lalita Chopra, A.S., Diotima Bose, M., Singh Chauhan, A., Alhadrawi, M., Chauhan, A., & Kumar, D. (2024). Application of cisplatin and other platinum-containing drugs in cancer therapy: Comprehensive review. *E3S Web of Conferences*, 588: 02015.

Layton, J., Theiopoulou, D.C., Rutenberg, D., Elshereye, A., Zhang, Y., Sinnott, J., Kim, K., Montoya, J.G., Contopoulos-Ioannidis, D.G. (2023). Clinical spectrum, radiological findings, and outcomes of severe toxoplasmosis in immunocompetent hosts: A systematic review. *Pathogens*, 12: 543.

Liu, Y., Tang, Y., Tang, X., Wu, M., Hou, S., Liu, X., Li, J., Deng, M., Huang, S., Jiang, L. (2021). Anti-*Toxoplasma gondii* effects of a novel spider peptide XYP1 *in vitro* and *in vivo*. *Biomedicines*, 10(5): 1176.

Maenz, M., Schlüter, D., Liesenfeld, O., Schares, G., Gross, U., Pleyer, U. (2014). Ocular toxoplasmosis: Past, present, and new aspects of an old disease. *Prog. Retin. Eye Res,* 39: 77–106.

Man, D., Pytel, B., Białek, M. (2023). Impact of vanadium complexes with tetradentate Schiff base ligands on the DPPC and EYL liposome membranes: EPR studies. *Appl. Sci.*, 13: 3272.

Masur, H., Jones, T.C., Lempert, J.A., Cherubini, T.D. (1978). Outbreak of toxoplasmosis in a family and documentation of acquired retinochoroiditis. *Am. J. Med,* 64(3): 396–402.

Matta, S.K., Rinkenberger, N., Dunay, I.R., Sibley, L.D. (2021). *Toxoplasma gondii* infection and its implications within the central nervous system. *Nat. Rev. Microbiol,* 19(7): 467–480.

McAuley, J.B. (2014). Congenital toxoplasmosis. *J. Pediatric Infect. Dis. Soc,* 3(Suppl 1): S30–S35.

Mele, A., Paterson, P.J., Prentice, H.G., Leoni, P., Kibbler, C.C. (2002). Toxoplasmosis in bone marrow transplantation: a report of two cases and systematic review of the literature. *Bone Marrow Transplant,* 29(8): 6.

Melo, E.J., Attias, M., De Souza, W. (2000). The single mitochondrion of tachyzoites of *Toxoplasma gondii*. *J. Struct. Biol,* 130(1): 27–33.

Menna-Barreto, R.F.S., Corrêa, J.R., Cascabulho, C.M., Fernandes M.C., Pinto A V; Soares M. J; De Castro, S. L. (2009). Naphthoimidazoles promote different death phenotypes in *Trypanosoma cruzi*. *Parasitology*, 136(5): 499–510.

Mercier, C., Cesbron-Delauw, M.F. (2015). *Toxoplasma* secretory granules: One population or more. *Trends Parasitol,* 31(2): 60–71.

Milewska Bobula, B., Lipka, B., Gołąb, E., Dębski, R., Marczyńska, M., Paul, M., Panasiuk, A., Seroczyńska, M., Mazela, J., Dunin Wąsowicz, D. (2015). Recommended management of

Toxoplasma gondii infection in pregnant women and their children. *Przegl. Epidemiol,* 69: 291–298.

Molan, A., Nosaka, K., Hunter, M., Wang, W. (2019). Global status of *Toxoplasma gondii* infection: Systematic review and prevalence snapshots. *Trop. Biomed,* 36(4): 898–925.

Montazeri, M., Mehrzadi, S., Sharif, M., Sarvi, S., Tanzifi, A., Aghayan, S.A., Daryani, A. (2018). Drug resistance in *Toxoplasma gondii*. *Front. Microbiol,* 9: 2587.

Montoya, J.G., Liesenfeld, O. (2004). Toxoplasmosis. *Lancet*, 363(9425): 1965–1976.

Montoya, J.G., Remington, J.S. (2008). Management of *Toxoplasma gondii* infection during pregnancy. *Clin. Infect. Dis,* 47(4): 554–566.

Mordue, D.G., Håkansson, S., Niesman, I., Sibley, L.D. (1999). *Toxoplasma gondii* resides in a vacuole that avoids fusion with host cell endocytic and exocytic vesicular trafficking pathways. *Exp. Parasitol,* 92(2): 87–99.

Moreira, F.F., Portes, J.A., Azeredo, N.F.B., Fernandes, C., Horn Jr., A., Santiago, C.P., Segat, B.B., Caramori, G.F., Madureira, L.M.P., Sanchez Candela, D.R., Marques, M.M., Resende, J.A.L.C., de Souza, W., DaMatta, R.A., Seabra, S.H. (2021). Development of new dinuclear Fe(III) coordination compounds with *in vitro* nanomolar antitrypanosomal activity. *Dalton Trans,* 50: 12242–12259.

Moudy, R., Manning, T.J., Beckers, C.J. (2001). The loss of cytoplasmic potassium upon host cell breakdown triggers egress of *Toxoplasma gondii*. *J. Biol. Chem,* 276(44): 41492–41501.

Navarro, M., Visbal, G. (2015). Metal-based antiparasitic therapeutics. In: Nriagu, J.O., Skaar, E.P. (eds.), *Trace Metals and Infectious Diseases*. Cambridge (MA): MIT Press. Chapter 10.

Nicolle, C., Manceaux, L. (1908). Sur un protozoaire nouveau du gondi (*Ctenodactylus gondii*). *C. R. Acad. Sci. Paris*, 147: 763–766.

Nolan, S.J., Romano, J.D., Coppens, I. (2017). Host lipid droplets: An important source of lipids salvaged by the intracellular parasite *Toxoplasma gondii*. *PLoS Pathog,* 13(6): e1006362.

Nyonda, M.A., Kloehn, J., Sosnowski, P., Krishnan, A., Lentini, G., Maco, B., Marq, J.B., Hannich, J.T., Hopfgartner, G., Soldati-Favre, D. (2022). Ceramide biosynthesis is critical for the establishment of the intracellular niche of *Toxoplasma gondii*. *Cell Rep,* 40(7): 111224.

Ortega-Barria, E., Boothroyd, J.C. (1999). A *Toxoplasma* lectin-like activity specific for sulfated polysaccharides is involved in host cell infection. *J. Biol. Chem,* 274(3): 1267–1276.

Ouologuem, D.T., Roos, D.S. (2014). Dynamics of the *Toxoplasma gondii* inner membrane complex. *J. Cell Sci,* 127(Pt 15): 3320–3330.

Ovciarikova, J., Lemgruber, L., Stilger, K.L., Sullivan, W.J., Sheiner, L. (2017). Mitochondrial behaviour throughout the lytic cycle of *Toxoplasma gondii*. *Sci. Rep,* 7: 42746.

Paquet, C., Yudin, M.H. (2018). No. 285-Toxoplasmosis in Pregnancy: Prevention, Screening, and Treatment. *J Obstet Gynaecol Can*, 40(8):e687–e693.

Pernas, L., Adomako-Ankomah, Y., Shastri, A.J., Ewald, S.E., Treeck, M., Boyle, J.P., Boothroyd, J.C. (2014). Toxoplasma effector MAF1 mediates recruitment of host mitochondria and impacts the host response. *PLoS Biol,* 12(4):e1001845.

Peyron, F., Wallon, M., Liou, C., Garner, P. (1999). Treatments for toxoplasmosis in pregnancy. *Cochrane Database Syst Ver,* (3): CD001684.

Pinto-Ferreira, F., Caldart, E.T., Pasquali, A.K.S., Mitsuka-Breganó, R., Freire, R.L., Navarro, I.T. (2019). Patterns of Transmission and Sources of Infection in Outbreaks of Human Toxoplasmosis. *Emerg Infect Dis,* 25(12):2177–2182.

Pomares, C., Ajzenberg, D., Bornard, L., Bernardin, G., Hasseine, L., Darde, M.L., Marty, P. (2011). Toxoplasmose e carne de cavalo, França. *Emerg Infect Dis,* 17:1327–1328.

Porter, S.B., Sande, M.A. (1992). Toxoplasmosis of the central nervous system in the acquired immunodeficiency syndrome. *N Engl J Med,* 327(23):1643-1648.

Portes, J.A., Souza, T.G., Dos Santos, T.A.T., Da Silva, L.L.R., Ribeiro, T.P., Pereira, M.D., Horn, Jr A., Fernandes, C., Da Matta, R.A., de Souza, W., Seabra, S.H. (2015). Reduction of *Toxoplasma gondii* development due to inhibition of parasite antioxidant enzymes by a dinuclear iron (III) compound. *Antimicrob Agents Chemother,* 59(12):7374.

Portes, J.A., Motta, C.S., Azeredo, N.F., Fernandes, C., Horn Jr, A., de Souza, W., DaMatta, R.A., Seabra, S.H. (2017). *In vitro* treatment of *Toxoplasma gondii* with copper(II) complexes induces apoptosis-like and cellular division alterations. *Vet Parasitol,* 245:141.

Portes, J.A., Azeredo, N.F., Siqueira, P.G., de Souza, T.G., Fernandes, C., Horn Jr, A., Candela, D.R.S., de Souza, W., DaMatta, R.A., Seabra, S.H. (2018). A new iron (III) complex-containing sulfadiazine inhibits the proliferation and induces cystogenesis of *Toxoplasma gondii*. *Parasitol Res,* 117(9):2795.

Prata, B.J., Prado, S.L., Nascimento, G.M., Fontes, G.H.S., Santos, A.C.F.S., Ferreira, L.M.A., Araujo, I.O. (2023). Análise da incidência epidemiológica de toxoplasmose congênita nas regiões brasileiras durante os anos de 2019 a 2022. *Braz J Infect Dis,* 27: 103498.

Pratt, S., Wansadhipathi-Kannangara, N.K., Bruce, C.R., Mina, J.G., Shams-Eldin, H., Casas, J., Hanada, K., Schwarz, R.T., Sonda, S., Denny, P.W. (2013). Sphingolipid synthesis and scavenging in the intracellular apicomplexan parasite, *Toxoplasma gondii*. *Mol Biochem Parasitol,*187(1–2):43–51.

Qiu, Y., Wang, W., Wang, Q., Xu, J., Dai, G., Bai, Y., Zhang, J. (2025). Activity evaluation and mode of action of ICA against *Toxoplasma gondii in vitro*. *Biomolecules,*15:202.

Radke, J.R., Guerini, M.N., Jerome, M., White, M.W. (2001). Uma alteração no período pré-mitótico do ciclo celular está associada à diferenciação de bradizoítos em *Toxoplasma gondii*. *Mol Biochem Parasitol,* 131:119–127.

Rajapakse, S., Weeratunga, P., Rodrigo, C., de Silva, N.L., Fernando, S.D. (2017). Prophylaxis of human toxoplasmosis: a systematic review. *Pathog Glob Health.* 111(7):333-342.

Ramírez-Macías, I., Marín, C., Salas, J.M., Caballero, A., Rosales, M.J., Villegas, N., Rodríguez-Díez, A., Barea, E., Sánchez-Moreno, M. (2011). Biological activity of three novel complexes with the ligand 5-methyl-1,2,4-triazolo[1,5-a]pyrimidin-7(4H)-one against *Leishmania* spp. *J Antimicrob Chemother,* 66(4):813–819.

Rastogi, S., Cygan, A.M., Boothroyd, J.C. (2019). Translocation of effector proteins into host cells by *Toxoplasma gondii*. *Curr Opin Microbiol,* 52:130-138.

Rauwolf, K.K., Floeth, M., Kerl, K., Schaumburg, F., Groll, A.H. (2021). Toxoplasmosis after allogeneic haematopoietic cell transplantation disease burden and approaches to diagnosis, prevention and management in adults and children. *Clin Microbiol Infect,* 27(3):378–388.

Reingold, A.L. (1998). Outbreak investigations—a perspective. *Emerg Infect Dis,* 4(1):21-27.

Luft, B.J., Remington, J.S. (1992). Toxoplasmic encephalitis in AIDS. *Clin Infect Dis,* 15(2):211-222.

Ribeiro, E., Ramalho, A.L.R., Costa, A.O., Nascimento, D.E.A., Souza, F.P., Higuchi, M.O., Kriger, C.S.G., Oliveira, V.S. (2025). Toxoplasmose na gestação: risco e complicações. *Braz J Health Ver,* 8(2):e79297.

Robert-Gangneux, F., Dardé, M.L. (2012). Epidemiology of and diagnostic strategies for toxoplasmosis. *Clin Microbiol Rev,* 25(2):264-296.

Robert-Gangneux, F., Meroni, V., Dupont, D., Botterel, F., Garcia, J.M.A., Brenier-Pinchart, MP, et al. (2018). Toxoplasmosis in transplant recipients, Europe, 2010–2014. *Emerg Infect Dis,* 24(8):1497–1504.

Rocha, S.M., Horn, Jr A., Terra, A.R.M.L., Rezende, L.M., Moreira, F.F., DaMatta, R.A., et al. (2023). *In vitro* anti-*Leishmania* activity of new isomeric cobalt(II) complexes and in silico insights: Mitochondria impairment and apoptosis-like cell death of the parasite. *J Inorg Biochem,* 240:112088.

Romano, J.D., Sonda, S., Bergbower, E., Smith, M.E., Coppens, I. (2013). *Toxoplasma gondii* salvages sphingolipids from the host Golgi through the rerouting of selected Rab vesicles to the parasitophorous vacuole. *Mol Biol Cell,* 24(12):1974–1995.

Ronconi, L, Sadler, P.J. (2007). Using coordination chemistry to design new medicines. *Coord Chem Ver,* 251(13-14):1633–1648.

Saeij, J.P., Boyle, J.P., Boothroyd J.C. (2005). Differences among the three major strains of *Toxoplasma gondii* and their specific interactions with the infected host. *Trends Parasitol,* 21(10):476–481.

Saeij, J.P., Boyle, J.P., Coller, S., Taylor, S., Sibley, L.D., Brooke-Powell, E.T. et al.(2006). Polymorphic secreted kinases are key virulence factors in toxoplasmosis. *Science,* 314(5806):1780–1783.

Salari, N., Lotfi, F., Abdolmaleki, A., Heidarian, P., Rasoulpoor, S., Fazeli, J., et al. (2025). The global prevalence of mild cognitive impairment in geriatric population with emphasis on influential factors: a systematic review and meta-analysis. *BMC Geriatr,* 25(1):313.

Sánchez-Delgado, R.A., Anzellotti, A. (2004). Metal complexes as chemotherapeutic agents against tropical diseases: trypanosomiasis, malaria, and leishmaniasis. *Mini Rev Med Chem,* 4(1):23–30.

Sanchez, S.G., Besteiro, S. (2021). The pathogenicity and virulence of *Toxoplasma gondii*. *Virulence,* 12(1):3095–3114.

Shammaa, A.M., Powell, T.G., Benmerzouga, I. (2021). Adverse outcomes associated with the treatment of *Toxoplasma gondii* infections in real-world data. *Sci Rep,* 11:1035.

Sheiner, L., Vaidya, A.B., McFadden, G.I. (2013). The metabolic roles of the endosymbiotic organelles of *Toxoplasma* and *Plasmodium* spp. *Curr Opin Microbiol,* 16(4):452–458.

Shunmugam, S., Arnold, C.S., Dass, S., Katris, N.J., Botté, C.Y. (2022). The flexibility of Apicomplexa parasites in lipid metabolism. *PLoS Pathog,* 18(3):e1010313.

Sibley, L.D., Boothroyd, J.C. (1992). Virulent strains of *Toxoplasma gondii* comprise a single clonal lineage. *Nature.* 359(6390):82–85.

Sibley, L.D. (1995). Invasion of vertebrate cells by *Toxoplasma gondii* occurs by active penetration of the host cell. *J Cell Sci,* 108(6):2457–2464.

Sibley, L.D. (2010). How apicomplexan parasites move in and out of cells. *Curr Opin Biotechnol,* 21(5):592–598.

Silva, L.A., Andrade, R.O., Carneiro, A.C.A.V., Vitor, R.W.A. (2014). Overlapping *Toxoplasma gondii* genotypes circulating in domestic animals and humans in southeastern Brazil. *PLoS ONE,* 9(2):e90237.

Silva, J.L.M., Costa, J.T.R., dos Santos, T.C.S., Viana, A.C., Lopes, R.S., Ferreira e Souza, T.T, et al. (2019). Drug resistance and variable susceptibility of *Toxoplasma gondii* strains to

pyrimethamine and sulfadiazine in Brazilian congenital toxoplasmosis cases. *Acta Trop,* 197:105083.

Smith, N.C., Goulart, C., Hayward, J.A., Kupz, A., Miller, C.M., van Dooren, G.G. (2021). Control of human toxoplasmosis. *Int J Parasitol,* 51(2–3):95–121.

Sparvoli, D., Lebrun, M. (2021). Unraveling the Elusive Rhoptry Exocytic Mechanism of Apicomplexa. *Trends Parasitol,* 37(7):622–637.

Stramba-Badiale, M., Nador, F., Porta, N., Guffanti, S., Frediani, M., Colnaghi, C., et al. (1997). QT interval prolongation and risk of life-threatening arrhythmias during toxoplasmosis prophylaxis with spiramycin in neonates. *Am Heart J,* 133(1):108–111.

Sule, K., Anikovskiy, M., & Prenner, E. J. (2023). Lipid Structure Determines the Differential Impact of Single Metal Additions and Binary Mixtures of Manganese, Calcium, and Magnesium on Membrane Fluidity and Liposome Size. *International Journal of Molecular Sciences*, *24*(2): 1066.

Szewczyk-Golec, K., Pawłowska, M., Wesołowski, R., Wróblewski, M., Mila-Kierzenkowska, C. (2021). Oxidative stress as a possible target in the treatment of toxoplasmosis: perspectives and ambiguities. *Int J Mol Sci,* 22:5705.

Taylor, S., Barragan, A., Su, C., Fux, B., Fentress, S.J., Tang, K., et al.(2006). A secreted serine-threonine kinase determines virulence in the eukaryotic pathogen *Toxoplasma gondii*. *Science,* 314(5806):1776–1780.

Tell i Puig, A., Soldati-Favre, D. (2024). Roles of the tubulin-based cytoskeleton in the *Toxoplasma gondii* apical complex. *Trends Parasitol,* 40(5):401–415.

Tosetti, N., Dos Santos, Pacheco N., Soldati-Favre, D., Jacot D. (2019). Three F-actin assembly centers regulate organelle inheritance, cell-cell communication, and motility in *Toxoplasma gondii*. *Elife,* 8:e42669.

Trotsko, N., Bekier, A., Paneth, A., Wujec, M., Dzitko, K. (2019). Synthesis and *in vitro* anti-*Toxoplasma gondii* activity of novel thiazolidin-4-one derivatives. *Molecules,* 24:3029.

van Dooren, G.G., Striepen, B. (2013). The algal past and parasite present of the apicoplast. *Annu Rev Microbiol,* 67:271–289.

Vella, S.A., Moore, C.A., Li, Z.H., et al. (2021). The role of potassium and host calcium signaling in *Toxoplasma gondii* egress. *Cell Calcium,* 94:102337.

van der Vem, AJ., Schoondermark-van de Vem, E.M., Camps, W., Melchers, W.J., Koopmans, P.P., van der Meer, J.W., et al. (1996). Antitoxoplasma effect of pyrimethamine, trimethoprim and sulphonamides alone and in combination: implications for therapy. *J Antimicrob Chemother,* 38:75–80.

Venkatasubramaniam, A., Rajappa, S. (2025). Metal complexes of antidiabetic drugs: a new horizon in therapeutic applications. *J Inorg Biochem,* 245:112507.

Vidal, J.E. (2019). HIV-related cerebral toxoplasmosis revisited: current concepts and controversies of an old disease. *J Int Assoc Provid AIDS Care,* 18:2325958219867315.

Welti, R., Seymour, S.L., Weng, J., Li J., Baldwin, J., Dixon, J.E., Lambeth, J.D. (2007). Lipidomic analysis reveals that *Toxoplasma gondii* contains phosphatidylthreonine, a novel phospholipid. *Eukaryot Cell,* 6(3):442–458.

Węglińska L., Bekier A., Trotsko N., Kaproń B., Plech T., Dzitko K., Paneth A. (2022). Inhibition of *Toxoplasma gondii* by 1,2,4-triazole-based compounds: marked improvement in selectivity relative to the standard therapy, pyrimethamine and sulfadiazine. *Journal of Enzyme Inhibition and Medicinal Chemistry,* 37: 2621–2634.

Wong, S.Y., Remington, J.S. (1994). Toxoplasmosis in pregnancy. *Clin Infect Dis,* 18(6):853–861.

Whitelaw, J.A., Latorre-Barragan, F., Gras, S., Pall, G.S., Leung, J.M., Heaslip, A., et al. (2017). Surface attachment, promoted by the actomyosin system of *Toxoplasma gondii*, is important for efficient gliding motility and invasion. *BMC Biol,* 15:1.

Ybañez, R.H.D., Ybañez, A.P., Nishikawa, Y. (2020). Review of the current trends of toxoplasmosis serodiagnosis in humans. *Front Cell Infect Microbiol,* 10:204.

Zambrano, P., Manrique-Moreno, M., Petit, K., Colina, J. R., Jemiola-Rzeminska, M., Suwalsky, M., & Strzalka, K. (2024). Differential Scanning Calorimetry in drug–membrane interactions. *Biochemical and Biophysical Research Communications*, 709: 149806.

Zhu, W., Li, J., Pappoe, F., Shen, J., Yu, L. (2019). Strategies developed by *Toxoplasma gondii* to survive in the host. *Front Microbiol,* 10:899.